TAMPEREEN TEKNILLINEN YLIOPISTO
TAMPERE UNIVERSITY OF TECHNOLOGY

Ville Syrjälä

Analysis and Mitigation of Oscillator Impairments in Modern Receiver Architectures

Julkaisu 1047 • Publication 1047

Tampere 2012

Tampereen teknillinen yliopisto. Julkaisu 1047
Tampere University of Technology. Publication 1047

Ville Syrjälä

Analysis and Mitigation of Oscillator Impairments in Modern Receiver Architectures

Thesis for the degree of Doctor of Science in Technology to be presented with due permission for public examination and criticism in Tietotalo Building, Auditorium TB111, at Tampere University of Technology, on the 29th of June 2012, at 12 noon.

Tampereen teknillinen yliopisto - Tampere University of Technology
Tampere 2012

Thesis Supervisor:

Mikko Valkama, Professor, Doctor of Technology
Department of Communications Engineering
Tampere University of Technology
Tampere, Finland

Pre-examiners:

Lars Lundheim, Professor, Doktor Ingeniør
Department of Electronics and Telecommunications
Norwegian University of Science and Technology
Trondheim, Norway

Oscar Gustafsson, Associate Professor, Doctor of Philosophy
Department of Electrical Engineering
Linköping University
Linköping, Sweden

Opponent:

Timo Rahkonen, Professor, Doctor of Technology
Electronics Laboratory
University of Oulu
Oulu, Finland

ISBN 978-952-15-2832-3 (printed)
ISBN 978-952-15-2855-2 (PDF)
ISSN 1459-2045

Abstract

The ever-increasing complexity of radio devices is phenomenon fed by the ever-growing demands of users for higher data rates and more services from a single device. Today, advanced cellular phones have transceivers for reception of multiple different kinds of communications signals. Moreover, even reception of signals from a single communications system might require multiple transceivers, when the system utilizes multiple antennas or multiple frequency bands for transmission. At the same time, communications waveforms are getting more complex since more and more data should be transmitted in the same bandwidth. These highly dynamic signals set very tight demands for the quality of transceiver electronics. The above aspects are, on the other hand, in contradiction with the other strong demands of utilizing smaller, cheaper and less power consuming radio transceivers.

From the point-of-view of communications receiver design, the above demands are mapped to challenges of designing very simple receivers with high-quality output, or receivers that are very flexible to process many different signals at the same time but that are still relatively simple. One solution to the design of simple receivers with high-quality output is moving the complexity of devices from the analogue side to the digital side. This means using very simple receiver architecture, possibly with low-cost components, and using digital signal processing to compensate for the impairments caused by the simple design and the low-cost electronics. On the other hand, a solution to obtain a flexible and simple receiver is moving the sampling and analogue-to-digital interface as near to the antenna as possible, and processing the reception of wide spectrum in a single receiver. Naturally, this is also moving the complexity from the analogue side to the digital side. All this is also partially motivated by the well-known Moore's law.

This thesis focuses on the both of the scenarios proposed above from the point-of-view of oscillator impairments in two modern receiver architectures, namely direct-conversion receiver architecture and direct-RF-sampling receiver architecture. Special emphasis is given to Orthogonal frequency division multiplexing (OFDM) signals since they are very vulnerable to phase-noise like effects and are very widely used nowadays. The direct-conversion receiver architecture is based on direct downconversion of signals from radio frequencies to baseband. The phase noise of the downconverting oscillator naturally causes errors to the signal in the downconversion process. In this thesis, the effects of the phase noise are analysed in OFDM communications link using downconverting oscillator with arbitrary phase-noise spectral

shape. Also, existing algorithms for phase-noise mitigation in OFDM are reviewed and four new iterative digital-signal-processing based mitigation algorithms are proposed. The first algorithm is fairly simple, stemming from the idea of using linear interpolation between two common-phase-error estimates to obtain an estimate of the underlying time-varying phase characteristics. The second algorithm on the other hand is an extension to existing intercarrier-interference estimation method. Simply put, the idea is to improve the phase-noise estimates given by the existing algorithm with interpolation near the boundaries of OFDM symbols. The last two of the algorithms work in time-domain and are stand-alone algorithms. In both of them, an estimate of the received time-domain waveform is reconstructed after initial symbol detection, and the time-varying phase noise process is estimated from the received signal with the aid of the reconstructed waveform with various digital-signal-processing methods. The proposed algorithms are compared to the state-of-the-art algorithms in different scenarios with both transmitter and receiver phase noises present. In general, the proposed algorithms offer significant performance improvement over the state-of-the-art algorithms in the literature.

The contributions from the point-of-view of direct-RF-sampling receiver are in the modelling of sampling-jitter phenomenon in voltage sampling based and charge sampling based direct-RF-sampling receivers. Based on the analysis of the voltage-sampling based direct-RF-sampling receiver, OFDM phase-noise mitigation algorithms are proposed to be used in sampling-jitter mitigation. Furthermore, one reference tone based sampling-jitter mitigation algorithm is proposed. The proposed techniques are also compared to the state-of-the-art techniques, and the results show that clear performance improvements can be attained with the proposed techniques. Simulations are also carried out in the challenging case where nearby interferers are also considered present in the sampled signal, as is practical because of challenging implementation of RF filtering in high-frequency sampling. The results show that the proposed algorithms still manage to provide relatively good performance when interference level is reasonable. In addition to sampling-jitter mitigation algorithms, the analysis of charge-sampling based direct-RF-sampling receiver showed interesting filtering phenomenon in the spectrum of the error caused by the sampling jitter in some of the charge-sampler implementations. The phenomenon is so powerful that it should be taken into account in receiver design.

Preface

The research work related to this doctoral thesis was carried out during years 2007-2011 at the Department of Communications Engineering, Tampere University of Technology, Tampere, Finland. The research work was financially supported by the graduate school of the president of Tampere University of Technology, the Academy of Finland, the Finnish Funding Agency for Technology and Innovation, Jenny and Antti Wihuri Foundation, HPY Research Foundation, Finnish Foundation for Technology Promotion, Ulla Tuominen Foundation, Tuula and Yrjö Neuvo Foundation and Tampere Doctoral Programme in Information Science and Engineering. I am grateful for all the support and interest my research has obtained.

I would like to thank my thesis supervisor Prof. Mikko Valkama for his efforts to guide me in my research all the way from my M.Sc. thesis work in 2006-2007 to the end of my doctoral studies in 2012. I would also like to express my thanks to Prof. Markku Renfors for his guidance in the initial phases of my research during my M.Sc. thesis work. I am also thankful to my thesis pre-examiners Prof. Lars Lundheim and Assoc. Prof. Oscar Gustafsson for their kind examination. I would also like to thank my opponent Prof. Timo Rahkonen for agreeing to act as my opponent in the public defence of my dissertation.

I would like to thank all the co-workers for peaceful, very warm and friendly atmosphere at the department. I would also like to thank all my friends. I would specially like to thank, without intention to forget anyone, Markus Allén, Dr. Lauri Anttila, Lei Chen, Sener Dikmese, Ahmet Gökceoglu, Tero Isotalo, Vesa Lehtinen, Toni Levanen, Petri Mantere, Jaakko Marttila, Tuomas Peltola, Tuukka Peltola, Jukka Rinne, Dr. Ali Shahed, Muhammad Usman Sheikh, Dr. Danai Skournetou, Jukka Talvitie, Nikolay N. Tchamov, Jussi Turkka, Tuomo Tuunanen and Dr. Yaning Zou for their help and friendship during the thesis work.

Finally, I would like to express my warmest thanks to my parents Esko and Rauni Syrjälä, my brother and sister Mikko and Anniina Syrjälä, and to my grandmother and late grandfather Terttu and Erkki Syrjälä for their love and invaluable support during my life and studies. Last but not least, I thank Masoumeh Hasani for her love and caring.

Lapua, May 2012.

Ville Syrjälä

Contents

List of Publications

The following publications form the basis of this thesis:

[P1] V. Syrjälä, M. Valkama, N. N. Tchamov, and J. Rinne, "Phase noise modelling and mitigation techniques in OFDM communications systems," in *Proc. Wireless Telecommunications Symposium 2009* (*WTS'09*), IEEE, Prague, Czech Republic, April 2009.

[P2] V. Syrjälä and M. Valkama, "Jitter mitigation in high-frequency bandpass-sampling OFDM radios," in *Proc. IEEE Wireless Communications & Networking Conference 2009* (*IEEE WCNC'09*), Budapest, Hungary, April 2009.

[P3] V. Syrjälä and M. Valkama, "Sampling jitter estimation and mitigation in direct RF sub-sampling receiver architecture," in *Proc. Sixth International Symposium on Wireless Communication Systems 2009* (*ISWCS'09*), IEEE, Siena-Tuscany, Italy, September 2009.

[P4] V. Syrjälä and M. Valkama, "Sampling jitter cancellation in direct-sampling radio," in *Proc. IEEE Wireless Communications & Networking Conference 2010* (*IEEE WCNC'10*), Sydney, Australia, April 2010.

[P5] V. Syrjälä and M. Valkama, "Analysis and mitigation of phase noise and sampling jitter in OFDM radio receivers," *International Journal of Microwave and Wireless Technologies*, Vol. 2, No.2, pp. 193-202, April 2010.

[P6] V. Syrjälä, M. Valkama, Y. Zou, N. N. Tchamov, and J. Rinne, "On OFDM link performance under receiver phase noise with arbitrary spectral shape," in *Proc. IEEE Wireless Communications & Networking Conference 2011* (*IEEE WCNC'11*), Cancun, Quintana-Roo, Mexico, March 2011.

[P7] V. Syrjälä and M. Valkama, "Receiver DSP for OFDM systems impaired by transmitter and receiver phase noise," in *Proc. IEEE International Conference on Communications 2011* (*IEEE ICC'11*), Kyoto, Japan, June 2011.

[P8] N. N. Tchamov, V. Syrjälä, J. Rinne, M. Valkama, Y. Zou, and M. Renfors, "System- and circuit-level optimization of PLL designs for DVB-T/H receivers," *Analog Integrated Circuits and Signal Processing Journal*, January 2012, 10.1007/s10470-011-9823-2.

[P9] V. Syrjälä, V. Lehtinen, and M. Valkama, "Sampling jitter in charge sampling radio," in *Proc. IEEE Wireless Communications & Networking Conference 2012 Workshops* (*IEEE WCNCW'12*), Paris, France, April 2012.

[P10] V. Syrjälä and M. Valkama, "Iterative receiver signal processing for joint mitigation of transmitter and receiver phase noise in OFDM-based cognitive radio link," in *Proc. International ICST Conference on Cognitive Radio Oriented Wireless Networks* (*CROWNCOM'12*), Stockholm, Sweden, June 2012.

List of Abbreviations

16QAM	16-quadrature-amplitude-modulation
3GPP	3rd Generation Partnership Project
ACE	advanced channel estimation
ADC	analogue-to-digital converter
AM	amplitude modulation
AWGN	additive white Gaussian noise
CPE	common phase error
CO	crystal oscillator
CS	charge sampling
DC	direct current
DCR	direct-conversion receiver
DFT	discrete Fourier transform
FRO	free-running oscillator
GPRS	General Packet Radio Service
GSM	Global System for Mobile Communications
I	in-phase
I/Q	in-phase/quadrature
ICI	intercarrier interference
IDFT	inverse discrete Fourier transform
IF	intermediate frequency
ITU-R	International Telecommunication Union – Radiocommunication Sector
LNA	low-noise amplifier

LO	local oscillator
LS	least squares
LTE	Long Term Evolution
LTE-A	Long Term Evolution – Advanced
MMSE	minimum mean-square error
NMT	Nordic Mobile Telephone
OFDM	Orthogonal frequency division multiplexing
OFDMA	orthogonal frequency division multiple access
PCI	perfect channel information
PLL	phase-locked loop
PSD	power spectral density
Q	quadrature
QAM	Quadrature amplitude modulation
RF	radio frequency
RMS	root mean square
S/H	sample-and-hold
SER	symbol-error rate
SHF	super-high frequency
SHR	superheterodyne receiver
SINR	signal-to-interference+noise ratio
SNR	signal-to-noise ratio
SIR	signal-to-interference ratio
TCE	traditional channel estimation
UHF	ultra-high frequency
UMTS	Universal Mobile Telecommunications System
VCO	voltage-controlled oscillator
VS	voltage sampling

List of Principal Symbols and Notations

α	first subcarrier index of the current channel
β	3-dB bandwidth of the phase noise
β_{ang}	3-dB bandwidth of the phase noise (in angular frequency)
γ	overall signal-to-interference+noise ratio
γ_c	frequency at which phase noise PSD deviates from nominal $1/f$ slope
γ_k	signal-to-intereference+noise ratio for k th subcarrier in OFDM symbol
$\delta_{n,1}$	sampling jitter at the beginning of integration interval in charge sampling
$\delta_{n,2}$	sampling jitter at the end of integration interval in charge sampling
$\Delta\omega$	frequency offset from the nominal oscillation frequency
$\Delta\omega_f$	offset from the carrier at which flicker noise effect is dominating
$\Delta\omega_w$	offset from the carrier at which white noise effect is dominating
ε	a very small number
ζ_n	sampling-jitter realization at n th sample in voltage sampling
θ_m	estimate vector of transmitter and receiver phase-noise complex exponential
κ	last subcarrier index of the current channel
λ_k	spectral mask of phase noise at k th subcarrier
μ	expectation value
π	mathematical constant pi, 3.14159265358979323846264338327 9...
ρ	received signal-to-noise ratio
σ	standard deviation
σ^2	variance

σ_{ϕ}^2	variance of the phase noise
σ_{adj}^2	average power of the sent subcarrier symbols at adjacent channels
σ_h^2	average magnitude response of the channel
σ_w^2	variance of white Gaussian noise
σ_x^2	average power of the sent subcarrier symbols
σ_z^2	average power of the additive noise
τ	time offset (in seconds)
υ_k	additive noise and ICI due to extra spectral component of the phase noise
$\phi(t)$	phase noise at time moment t
ϕ_m^{CPE}	common phase error at m th OFDM symbol
ϕ_n	phase noise at time nT_s
$\boldsymbol{\phi}_m$	vector of combined transmitter and receiver phase noise samples
$\boldsymbol{\phi}_{m,R}$	vector of receiver phase-noise samples for m th OFDM symbol
$\boldsymbol{\phi}_{m,T}$	vector of transmitter phase-noise samples for m th OFDM symbol
Φ_k	DFT of sampled phase-noise
ψ_k	power of the phase noise around the k th subcarrier
ω	angular frequency
ω_c	angular centre or carrier frequency
ω_{IF}	intermediate frequency of useful signals
ω_{ref}	frequency of reference tone
$\omega_{ref,IF}$	intermediate frequency of reference tone
A	amplitude of an oscillating signal
A_c	amplitude of transmitted tone
A_{ref}	amplitude of reference tone
arg(·)	argument of the complex exponential
$B(t)$	standard Brownian motion at time t
B_n	standard Brownian motion at time nT_s

c	diffusion rate
diag(·)	operator which creates diagonal matrix from input vector
D	maximum delay spread of multipath channel in samples
e	Napier's constant, 2.71828182845904523536028747135 2...
$\mathbf{e}_n$	unit vector of lenth N and unity as its n th element
e^{jx}	complex exponential function with argument x
e_n^{jit}	error caused by sampling jitter to n th sample in charge sampling
$\mathrm{E}\{\cdot\}$	statistical expectation operator
f	frequency (in Herz)
f_c	centre frequency
f_{IF}	intermediate frequency
F_s	sampling rate or sampling frequency $(1/T_s)$
G	number of samples in guard interval/cyclic prefix
$\mathbf{h}_m$	channel impulse-response vector for m th OFDM symbol
$H(\omega)$	transfer function of a digital filter
$H_k(m)$	k th frequency bin of the channel transfer function for m th OFDM symbol
$\mathbf{H}_m$	circulant channel convolution matrix
j	imaginary unit
J_k	k th spectral component phase-noise complex exponential
k	subcarrier index in an OFDM symbol
$L(\Delta\omega)$	one-sided-PSD phase-noise measurement at offset $\Delta\omega$ from the carrier
$\mathrm{LPF}\{\cdot\}$	ideal lowpass filter operator
m	OFDM symbol index
n	generic sample index
N	number of subcarriers in an OFDM symbol
N_a	number of active subcarriers in an OFDM symbol
$\mathcal{N}(\mu,\sigma^2)$	normal distribution with expected value μ and variance σ^2

$\mathbf{p}$	permutation matrix
$\widehat{\mathbf{P}}$	discrete Fourier transforms of permutation matrices
$\mathbf{P}_m$	vector of pilot subcarrier values at m th OFDM symbol
$\mathbf{q}_m$	scaling vector
$r(t)$	real I/Q modulated signal
r_n	real sampled I/Q modulated signal
$\mathbf{r}_m$	time-domain received signal vector from m th OFDM symbol
$r_{n,CS}$	charge-samples I/Q modulated signal
$r_{n,CS}^{jit}$	charge-samples I/Q modulated signal with sampling jitter
$R_k(m)$	k th DFT sample of the received signal from m th OFDM symbol
$R_{vv}(t, t-\tau)$	autocorrelation with timing offset τ
$s(t)$	baseband complex signal
$s_I(t)$	in-phase component of the baseband complex signal
$s_Q(t)$	quadrature component of the baseband complex signal
$S_{a,ss}(\omega)$	single-sided power-spectral-density of the VCO at ω
$S_{a,ss,CO}(\omega)$	single-sided power-spectral-density of the CO at ω
$S_f(\omega)$	power spectral density of the flicker noise at ω
$S_v(\omega)$	power spectral density of $v(t)$ at frequency ω
$S_{v,ss}(\omega)$	single-sided power spectral density of $v(t)$ at frequency ω
S_p	set of pilot subcarrier indices
t	time (in seconds)
t_n	sampling moments nT_s
$t_{n,1}^{jit}$	sampling moments at the beginning of integration interval with jitter
$t_{n,2}^{jit}$	sampling moments at the end of integration interval with jitter
T_i	integration interval in charge sampling
T_s	sampling interval $(1/F_s)$
u	number of significant spectral component of phase noise

$v(t)$	real oscillator signal
$v_c(t)$	complex oscillator signal
$x(t)$	arbitrary example signal
$x_n(m)$	n th sample of m th OFDM symbol
$X_k(m)$	k th subcarrier symbol at m th OFDM symbol
$\mathbf{z}_m$	additive white Gaussian noise vector for m th OFDM symbol
$Z_k(m)$	frequency domain noise at k th subcarrier symbol of m th OFDM symbol
$[a,b]$	set with all integer numbers between a and b including the a and b
∞	infinity
$\lvert\cdot\rvert$	absolute value operator
$\cup$	union of two sets
$*$	circular convolution operator
$\hat{x}$	estimate of x
x^y	y th power of x
$\frac{dy(x)}{dx}$	derivative of $y(x)$ in respect to x
$\int_a^b y(x)dx$	definite integral of $y(x)$ in respect to x from a to b
$\sum_{x=a}^{b} y(x)$	sum of $y(x)$ values with integer x values from a to b

Chapter 1

Introduction

1.1. Background and Motivation

Wireless communications has been a part of people's lives throughout the ages. Beginning from simple speech, shout and shout chains, people have invented ways to communicate over larger and larger distances. Fire and smoke signals were the first ways to increase the communication distance by no longer relying only on the voice communications. Then, with the help of amplification by telescopes, the distances increased further, and also information could be delivered at higher rate, because more sophisticated signals could be delivered, e.g., by means of optical telegraphs. Already in the beginning of the 19th century, there were vast optical telegraph networks in use.

In the mid-19th-century began a strong era of wired communications with electric telegraph services followed by phone services in the 1870s [30]. Wired communications increased the reliability, distance and information rate of the communications greatly. However, wireless communications has always had its place in many applications, since wired communications is always limited by wires. In the end of the 19th century, wireless telegraph services became available after the invention of radio [39]. After that, in the mid-1910s, the first audio radio transmissions were made and already in the beginning of the 1920s many broadcasting radio stations were on the air [30]. Still, wired communications had a powerful grip on all-around communications, since the radio spectrum was limited, and wired communications simply offered high signalling rates with high reliability over long distances relatively cheaply. Also, people were used to communicate within the limits set by wires, so there was no real need for new, expensive and complex wireless communications devices in general, only for some special purposes.

Great advances in transmission techniques and electronic circuits since the first radios from the turn of the 19th and the 20th centuries have little by little allowed also the wireless communications to reach the point where signalling rates are high enough for many attractive

applications. Therefore, wired communications has lost most of its edge over wireless communications. Compared to their wired counterparts, wireless services offer the possibility to communicate independent of location, which always gives a certain edge in the competition. At first, because of costs and complexity of radio devices, radio communications was mainly used in broadcasting and military solutions. It was not until the 1980s, when the first vast analogue cellular networks were established using, e.g., Nordic Mobile Telephone (NMT) system. Then already in the beginning of the 1990s, first vast digital cellular networks using Global System for Mobile Communications (GSM) were built. This allowed more secure and higher quality communications and services. Shortly after that, because of decreasing prices of mobile devices and rising interest in wireless freedom, mobile telephones got their places in the pockets of most of the people in the developed countries, and later even in the developing countries.

Currently, the focus of wireless development is on getting higher and higher data rates for mobile users. Already with the early 3G systems, such as Universal Mobile Telecommunications System (UMTS), data rates have been high enough for every-day use of the internet. However, for more enjoyable and advanced use of the networks (e.g., use of high definition video, television, games, video calls etc.), the more advanced 3G system, 3rd Generation Partnership Project (3GPP) Long Term Evolution (LTE), has been proposed, and is already in use in many countries. It offers great advances in data rates, but utilizes Orthogonal frequency division multiplexing (OFDM) [28], [46], [68] in the downlink, which is very demanding for the used mobile transceivers. Furthermore, the emerging 4G system will most likely be based on 3GPP LTE-Advanced (LTE-A) which is also utilizing OFDM as the core transmission technique.

OFDM is the transmission technique which the research in this thesis mainly focuses on. OFDM has lots of benefits compared to many alternative transmission methods. It can, e.g., efficiently combat intersymbol interference due to multipath propagation and supports practical multiantenna communications. However, OFDM imposes high quality-demands for transceiver components [2], [23], [28], [51], [57]. Good examples of such challenges are sensitivity to different oscillator impairments, like carrier frequency offset and phase noise. This is a demanding situation for designers of mobile devices since using high-quality components practically means either higher power consumption and size or high cost of the transceiver. Naturally this is very critical from the mobile device design point of view, as the main properties over which manufacturers of mobile devices compete are small size, relatively low costs and long-lasting battery. Especially the last property has recently been much overlooked by many manufacturers of cellular phones, and thus users are dependent on having an outside power source available even multiple times per day. This heavily limits the main advance of having a mobile device in the first place, the mobility.

Huge advancements in signal-processor implementation techniques and other digital platforms in the recent decades have allowed very powerful computing units to be included in very small devices, such as cellular phones, without remarkable increase in power consumption. Because of this, the use of enhancing digital-signal-processing algorithms has become very attractive in the reception and transmission of signals [23]. With digital signal processing, many hardware-level algorithms can be implemented in digital domain after sampling. This is beneficial, because usually complicated analogue components cannot be integrated efficiently into silicon, thus making the transceiver design very challenging, as bulky analogue components consume much power and are relatively expensive. With digital signal processing, very advanced algorithms can be implemented, e.g., to improve the quality of received or transmitted signals. This on the other hand allows increases in data-rates and/or allows picking up less powerful signals, and thus allows decreasing the level of signalling in overall networks. Such digital signal processing has been classically used at the receivers, e.g., in mitigating or equalizing the radio channel effects. In the recent years however it has also been demonstrated to be a feasible solution in mitigating the imperfections of RF components. Good examples are mitigations of receiver nonlinearities [57], [58], [70] and receiver in-phase/quadrature imbalance [2], [3], [4] based on digital-signal-processing. In this thesis, such approach is taken to suppress the effects of oscillator impairments.

1.2. Scope of the Thesis

The scope of this thesis is to study ways for mobile transceiver manufacturers to design transceivers with lower power consumption, size and costs than currently possible. To achieve this, the thesis proposes ways to move the complexity of transceivers from the analogue-component side to the digital-signal-processing side. This can be done in two ways. One, by implementing digital-signal-processing algorithms to mitigate impairments in transceivers in order to relax the quality-of-operation requirements for the transceiver components or, two, by moving the sampling in the receivers as near to the antenna as possible, which minimizes the amount of analogue components and thus potentially results in a very flexible, small and low-power receiver. Both of these goals are based on moving the complexity to the digital side (and also to analogue-to-digital interface) of the transceiver, which is also partially motivated by the well-known Moore's law.

In this thesis, the transceiver-impairment mitigation with digital-signal-processing algorithms focuses mainly on the oscillator phase-noise. The topic was chosen, even though much literature was already available on the topic, because the full understanding of the phase noise effects on OFDM systems has been gained only recently [54]. Also, OFDM became very interesting topic not until recently, so even though high-quality contributions for the phase-noise mitigation in OFDM were available, e.g., in [9] and [45], there was still much

potential left in the study area to develop better algorithms and deepen the general understanding of the phase-noise effects.

The effect of sampling-jitter on direct radio-frequency (RF) sampling receivers has been receiving surprisingly little attention in the recent literature. The studies about sampling jitter in direct-RF-sampling were mostly done for positioning receivers, since the effect was relatively easy to analyse, and sampling jitter was considered generally either a minor problem or very simple to analyse for many of the other applications. However, as this thesis demonstrates, the sampling jitter in direct-RF-sampling receiver is an especially big problem if OFDM signal are received, as the effect is similar to that of the phase noise in direct conversion receivers. From the sampling-jitter mitigation point-of-view, only some very special case algorithms have been proposed earlier. In this thesis also this is fixed. A general algorithm for sampling-jitter mitigation is proposed, but also some specific algorithms for sampling-jitter mitigation for OFDM signals are proposed. Furthermore, sampling jitter effect had also received only minor attention in charge-sampling based direct-RF-sampling receivers. This thesis also tries to widen the understanding of the sampling-jitter effect on the charge sampling receivers, by the means of the analysis of the error.

1.3. Outline and Main Contributions of the Thesis

After this chapter, the thesis is structured as follows. The second chapter shortly describes the modern receiver architectures, and discusses about benefits and downsides concerning their implementation. Then, in the third chapter, phase-noise effects on general communications signals and especially on OFDM signals are analysed. The signal-to-interference+noise ratio (SINR) analysis for the OFDM link, presented in the third chapter, is one of the main contributions of this thesis, and was first published in [P6] and [P8]. Furthermore, the generalized oscillator model first proposed in [P6] is one of the minor contributions of the thesis. In the fourth chapter, sampling jitter is studied in the direct-RF-sampling receiver architecture, in both voltage sampling and charge sampling cases. The contributions of the chapter are the idea of mapping sampling jitter as phase noise, which was first published in [P2], and the analysis of the spectral shape of the sampling jitter in charge-sampling receiver first published in [P9]. The fifth chapter is then the most remarkable contribution of this thesis. First, state-of-the-art phase-noise mitigation algorithms are reviewed, followed by the presentation of several contributing algorithms first presented in [P1], [P5], [P7] and [P10], whose performance exceed the state-of-the-art. Another chapter with contributions to digital-signal-processing techniques is the sixth chapter. There, state-of-the-art in sampling-jitter mitigation in direct-RF-sampling is first presented. One of the contributions is then the proposal to use phase-noise mitigation algorithms for sampling jitter mitigation in OFDM signals received with direct-RF-sampling receiver that was first proposed in [P2]. Another contribution is general-use algorithm for sampling-jitter mitigation in direct-RF-sampling

receivers published in [P3] and [P4]. Then the work is concluded in the seventh chapter. In the last, eighth chapter, the publications included in the thesis are shortly summarized and the author's contributions to the publications are described in detail.

Chapter 2

Modern Receiver Architectures

Radio communications is based on sending information as electromagnetic radiation from transmitter to receiver. The information is transmitted by modulating a relatively high-frequency carrier signal with a signal carrying the information. In early days, when spark-gap transmitters were used in wireless telegraphy, the carrier signals were very high bandwidth signals. This restricted the efficient use of the radio spectrum. However, later when people started to use oscillators and amplitude modulation (AM), the carrier signal modulated by the information waveform was neatly around the designated carrier frequency. This allowed deploying many different communications signals near to each other, so that they did not strongly disturb each other. At this point, more complicated receiver architectures became a very important research topic, because of the challenging task of separating different signals from each other. Receiver architecture basically tells how the receiver does its main tasks, namely amplification of the signal to compensate for propagation losses, selectivity to separate the useful signal from the rest of the signals, and tunability to select the desired channel.

At first, the passive AM radios based on crystal detector only had little selectivity. The aim of the radio design was more to gain sensitivity than signal quality. Later with the invention of vacuum tubes for signal amplification, also the signal quality started to gain more attention. After the invention of the superheterodyne receiver (SHR) architecture [52], even higher signal quality was achievable.

In the SHR architecture, the signal is downconverted from RF to some intermediate frequency (IF) for filtering and amplification. Then, the downconverted signal is further downconverted to even lower frequencies (either to second IF and/or finally to the baseband) for further processing. The approach sets relatively relaxed requirements for most of the analogue components in the receiver. However, SHR architecture suffers from image

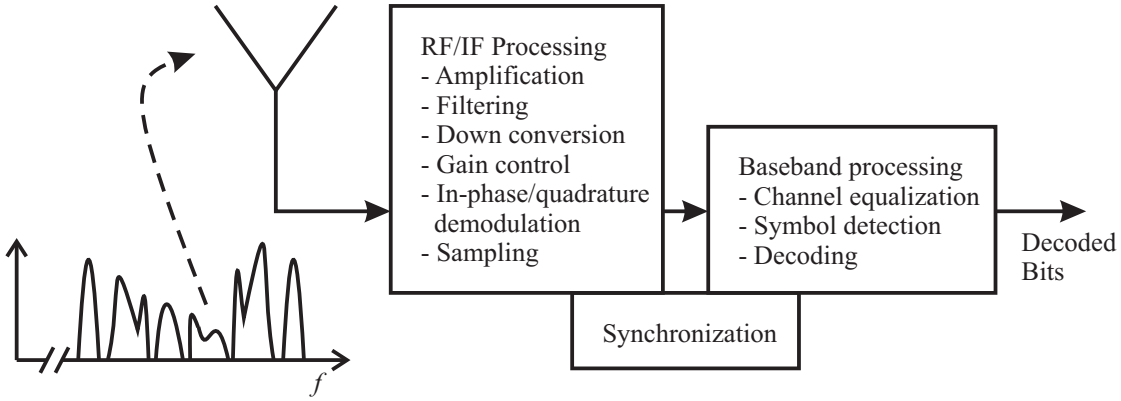

Figure 2-1: Principal receiver structure consisting of radio frequency (RF)/intermediate frequency (IF) processing, synchronization and baseband processing blocks. Some of the main tasks of the blocks are mentioned.

frequency problems, because filter at the RF should filter out the image frequency (which is two times the IF away from the useful signal), so that it does not interfere the downmixed signal at the IF [49]. However, it is very demanding to build selective filters at RF, which dictates that the IF should be high enough that the image frequency is far enough away from the useful signal. This on the other hand makes the filtering of the IF signal more difficult, namely the IF filter should be relatively selective [49]. As a result, requirements for the both filters are relatively tight, which makes the integration of the SHR to a single circuit very demanding or even impossible. Furthermore, another problem is the need for huge amount of analogue components. Because of overall problems, the SHRs are power consuming, bulky and expensive. However, the SHR architecture is still used in many radios, and some of the modern receiver architectures are still based on the same idea.

In modern receiver architectures, the main goal is to design flexible and as heavily integrated receiver as possible by minimizing the number of analogue components, and thus the power consumption, size and cost of the receiver. A modern receiver has also various additional tasks not discussed above, such as sampling, channel equalization, symbol detection due to digital modulation, and of course decoding of the transmitted bits. Principal structure of a modern receiver is depicted in Figure 2-1.

2.1. Direct-Conversion Receiver Architecture

The oldest and currently the most used of the modern receiver architectures is the very well-known direct-conversion receiver (DCR) architecture [49] depicted in Figure 2-2. Even though it (or at least the basic idea of it) was already invented in the 1920s, the DCR architecture can be considered modern, because its practical implementation has not until in recent years become feasible in commercial wireless devices.

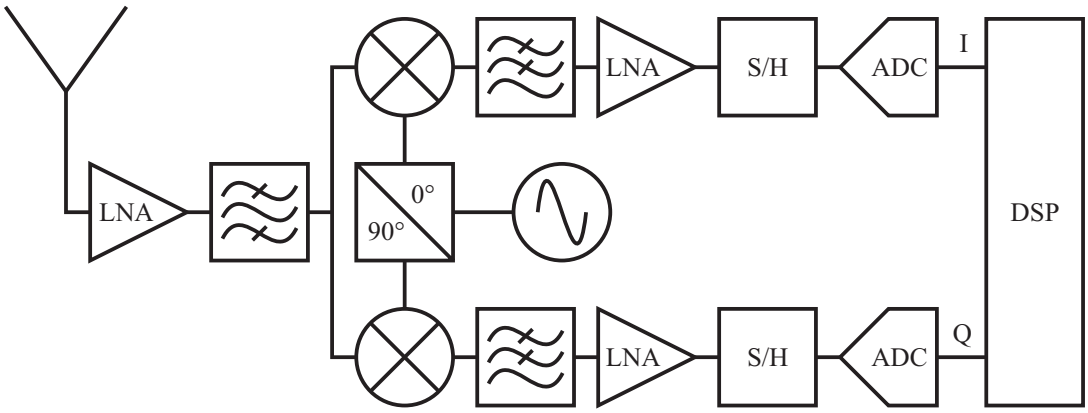

Figure 2-2: Direct-conversion receiver architecture, where upper branch is for the in-phase component and lower branch is for quadrature component of the signal.

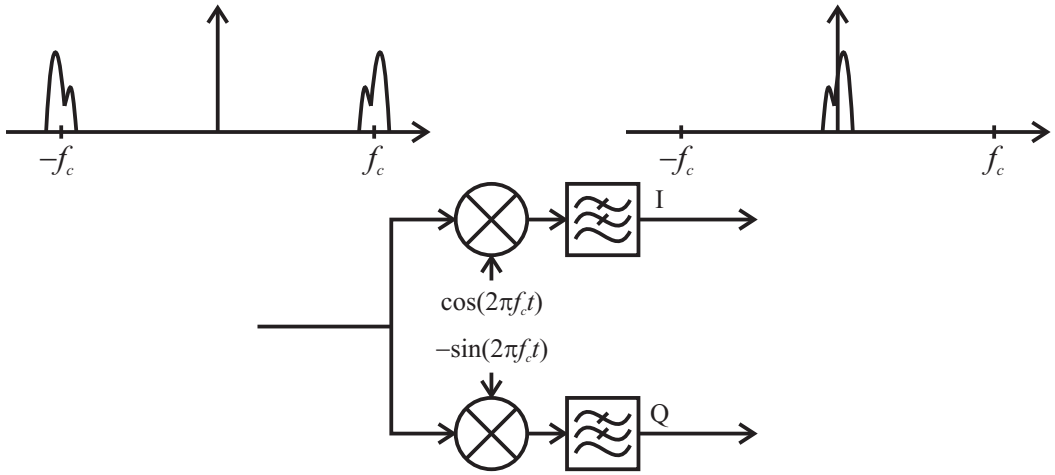

Figure 2-3: Principle spectra at the input and output of I/Q demodulator. I/Q signal is downconverted from the centre frequency f_c to the baseband.

Operating Principle

Unlike SHR, DCR downconverts the received signal directly from the RF to the baseband frequencies [49]. As demonstrated in Figure 2-2, in DCR architecture signal is first amplified with low-noise amplifier (LNA) and then bandpass filtered. Then the signal is downconverted directly to the baseband with complex mixing. The in-phase (I) and quadrature (Q) components of the complex signal are then separately lowpass filtered, amplified and finally sampled, e.g., with sample-and-hold (S/H) circuit. The principle spectrum example for the in-phase/quadrature (I/Q) downconversion process is depicted in Figure 2-3. The structure is very simple and does not have the image problems like SHR architecture has. The requirements for the filters in the structure are relatively relaxed, allowing the filter to be integrated into same circuit with the other receiver components [49]. Furthermore, when the signal is downconverted to the baseband as soon as possible, as in DCR, the components after the downmixing can be very simple at the baseband frequencies while still having good properties. For multichannel communications systems, DCR must have also a tunable

oscillator and maybe a tunable RF filter (depending on the overall design), so it can select which channel it downconverts. Another possibility is to downconvert the channels to around the baseband, and to apply the final selectivity and downconversion in digital domain for the sampled signal. This can be thought to be wideband DCR, but it can also be considered to be so-called low-IF receiver architecture.

Architectural Problems

Even though the structure of DCR is very simple, there are reasons why this very old idea has just become applicable in recent years. Actually, there are many problems that arise when using DCR architecture. The main problems are direct-current (DC) offset, I/Q imbalance and second order intermodulation.

DC offset is one big problem in DCR [49]. The DC-offset problem exists because the local oscillator (LO) signal is at the same frequency as the carrier of the desired signal. When the LO signal leaks from its mixer input to the second mixer input, the LO signal mixes with itself, effectively downconverting itself as DC [49]. Even worse, the LO signal can leak to the input of the amplifier prior the mixer. This way the leaked LO signal gets amplified, making the DC offset problem worse. DC offset can also occur when amplified received signal leaks from its mixer port to the mixer port of the LO signal [49]. This is not a problem if the received signal does not have high-power interferers, since the useful signal power is usually relatively low. However, when high-power interferers exist, as they usually do, they can mix themselves to DC when they leak to the LO port of the mixer. The self-mixing of the interferers generates DC offset that rapidly changes as a function of time, whereas the LO self-mixing results into much more predictable DC offset. Thus self-mixing of the interferers is potentially more burdensome problem to mitigate. In addition to the leaking problem, DC offsets can also be generated by $1/f$ noise of the components after the downmixer [49]. This is because the very low power desired signal is already at the baseband at this point.

I/Q imbalance is another well-known problem of DCR architecture. The structure depicted in Figure 2-2 works ideally only when I and Q branches after the complex mixing have exactly 90 degrees phase difference and the frequency responses of both of the branches are exactly the same. This is however impossible to achieve in a real world receiver, and the existing mismatch between the branches is called I/Q imbalance. Ideally, the complex mixer downconverts the desired signal from positive (or negative) frequencies to the baseband. However, with the I/Q imbalance problem, also the signals from negative (or positive) frequencies are mixed to the baseband on top of the desired signal. The signals do not combine constructively, so they interfere with each other. Some advanced mitigation approaches are proposed, e.g., in [2], [3], [4]. In [3] circularity based relatively simple but efficient technique is proposed.

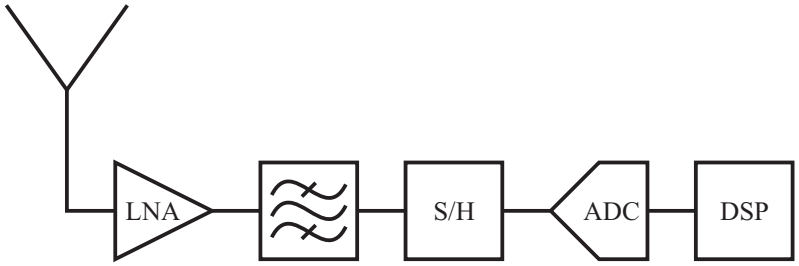

Figure 2-4: Voltage-sampling based direct-RF-sampling receiver architecture, real subsampling version.

DCR is also sensitive to second order intermodulation. For example, when high-power interferers near the useful signal are amplified with the LNA at the receiver, the nonlinearity of the LNA generates even order distortion at around the baseband frequencies [57]. This distortion is of course then mixed with the mixer, but in reality the mixer also passes directly through small portion of the signal [49]. This distortion can therefore, after the mixer, appear at the same frequencies as the useful signal. Some mitigation aspects are available, e.g., in [70]. Also, the LNA generates the even order distortion to twice the frequencies of the interferers. These are not yet a problem, but since mixer also has nonlinear amplification stage in it, the intermodulation components at high frequencies can eventually be visible at the baseband after the mixing [57].

Other not so critical problems include, e.g., LO signal leakage to the antenna (and thus to the environment of the receiver) [49].

All these problems already have many solutions available today, and DCR architecture is used in many mobile receivers for many different kinds of communications systems. In this thesis, none of these architectural problems are considered in more detail. However, phase noise of the downconverting oscillator is one of the main themes of this thesis, which is also one of the problems in direct conversion receiver architecture.

2.2. Direct-RF-Sampling Receiver Architecture Using Voltage Sampling

In voltage-sampling (VS) direct-RF-sampling receiver architecture [52], the idea is to take samples from the signal as early in the receiver as possible using traditional sample-and-hold sampler. The earliest stage to take the samples is naturally after the signal is received by the antenna. However, to lower the requirements set for the sampling process, usually signal is first amplified and filtered as depicted in Figure 2-4. The sampling can be done so that the signal bands of interest are directly sampled without aliasing. This approach, however, requires very high sampling frequencies. Another approach is to subsample the signal so that it aliases to certain IF. The principle spectra at the input and at the output of direct-RF-sampling receiver using real subsampling are depicted in Figure 2-5. The principle received spectrum in this case however is highly simplified, since many different signal bands alias on top of each other around the same IF. Therefore, the subsampling increases the filtering

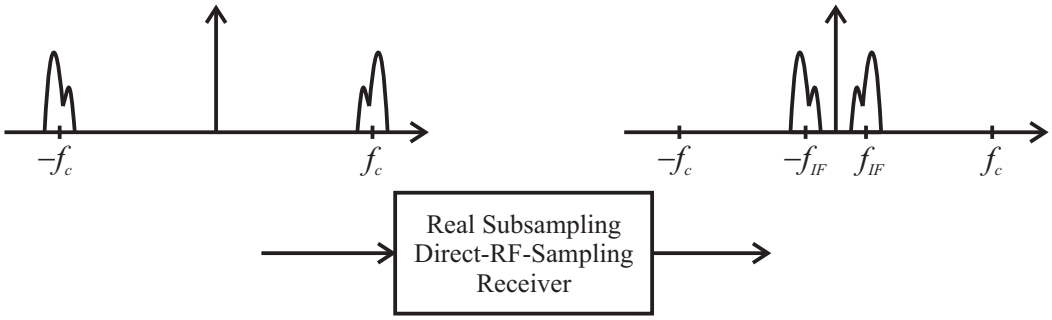

Figure 2-5: Principle spectra at the input and output of real subsampling direct-RF-sampling receiver. Controlled aliasing is used to downconvert the desired signal band from centre frequency f_c to intermediate frequency f_{IF}.

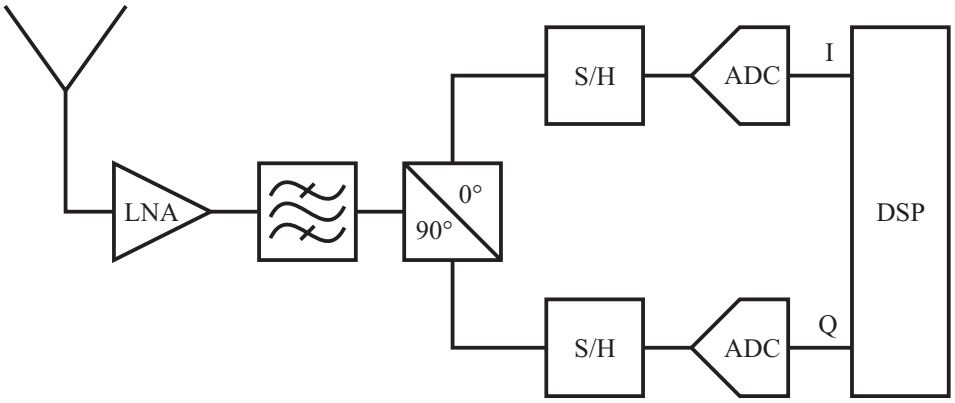

Figure 2-6: Voltage-sampling based direct-RF-sampling receiver architecture, I/Q subsampling version. Upper sampling branch is for in-phase component and lower sampling branch is for quadrature component of the signal.

requirements prior the sampling process. Yet another version is so-called I/Q version, in which the signal and its 90 degrees phase delayed version are sampled separately. The I and Q components of the signal can then be I/Q demodulated with digital signal processing. The structure is illustrated in Figure 2-6. As depicted in the figure, it needs two sampling branches to sample the in-phase and quadrature components of the I/Q signal separately. The principle spectra at the input and output are similar to the case in Figure 2-3. Now, the controlled aliasing during sampling moves the desired signal band from the RF frequencies to some IF frequencies. Then, the needed filtering on the signal is made in the digital domain, and the I/Q signal are attained. As with the real subsampling case, also the I/Q subsampling case has very high filtering requirements due to aliasing of the unwanted signals on top of the desired signals.

The structure is very simple and it potentially minimizes the power consumption, size and cost of the receiver, and because it also minimizes the amount of bulky analogue components, it can be efficiently integrated into silicon. Furthermore, the architecture is very flexible, since the signal selectivity can mostly be implemented in the digital domain after the sampling. However, the architecture imposes very high demands for the speed and the accuracy of the sampling circuitry. Since very wide RF band is sampled, in addition to high dynamicity

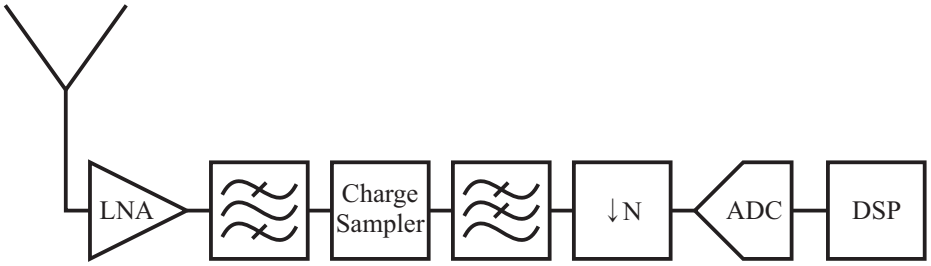

Figure 2-7: Charge-sampling based direct-RF-sampling receiver architecture, real version.

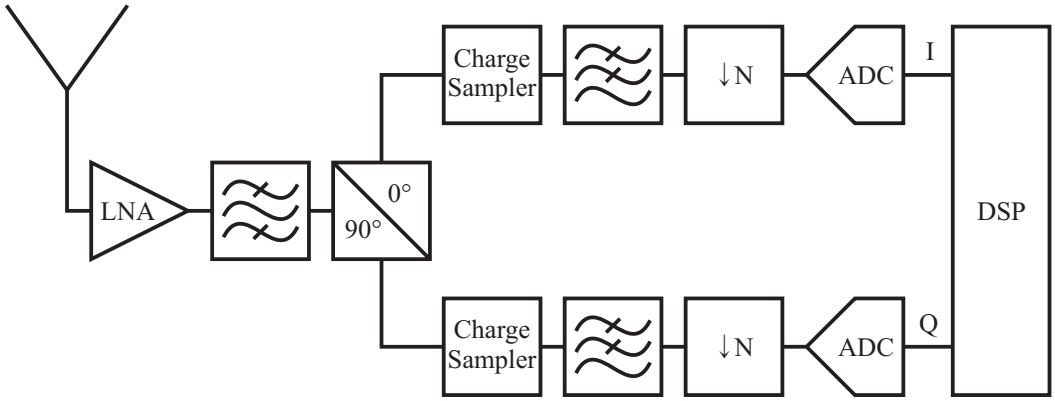

Figure 2-8: Charge-sampling based direct-RF-sampling receiver architecture, I/Q version. Upper sampling branch is for in-phase component and lower sampling branch is for quadrature component of the signal.

requirements, relatively high sampling frequency is required, even when using bandpass sampling. And of course, always when ultra-high-frequency (UHF) and/or super-high-frequency (SHF) signal are directly sampled, the timing requirements for the sampling process are very strict. In effect, in direct-RF-sampling mobile-receivers sampling jitter is a huge problem [5], [44], [60], [P3], [P4], [62], [63].

2.3. Direct-RF-Sampling Receiver Architecture Using Charge Sampling

The fundamental idea of the charge-sampling (CS) direct-RF-sampling receiver architecture [1] is the same as that of the VS direct-RF-sampling receiver, but with minor differences. The idea is still to sample the signal as early stage of the receiver as possible to simplify the receiver structure. However, instead of using VS (namely sample-and-hold circuit), CS is used. In CS, the samples are attained by collecting the signal current to capacitors, from which the sample values are then read after the current is collected for a long enough time. This is essentially building coarse filtering to the incoming signal. In CS, the advantage is having potentially lower power consumption and higher sampling rates, in addition to easily implementable built-in frequency-selectivity [1], [7], [29], [31], [33], [40], [41]. The build-in frequency selectivity relaxes the high filtering requirements typical for subsampling direct-RF-sampling receivers. Example structures of CS direct-RF-sampling receivers are depicted in Figure 2-7 and Figure 2-8, the former being the version with real processing and the latter being the I/Q version, as discussed in Section 2.2. As an example, practical receiver

implementations for Bluetooth and GSM/General Packet Radio Service (GPRS) have been reported in [41].

Even though the sampling process in CS direct-RF-sampling receivers is different from that of the VS direct-RF-sampling receivers, some of the same bottle necks still remain in the architecture, because still UHF and/or SHF signals are sampled with help of inaccurate sampling clock. Therefore, also CS direct-RF-sampling receivers are very vulnerable to sampling jitter. Studying the sampling jitter effect on charge-sampling direct-RF-sampling receiver architecture is one of the topics of this thesis.

Chapter 3

Phase Noise in Direct Conversion Receivers

Because DCR architecture is used in most of the advanced commercial mobile devices of today, also impairments that are not so tightly considered architectural weaknesses are interesting. One of the most interesting impairments in this context is phase noise [23]. Its effect on DCR is especially interesting since phase noise is a very big problem in mobile OFDM receivers, in which DCR is usually used. Furthermore, emerging mobile standard like 3GPP LTE and LTE-A use OFDM.

First, this chapter gives a very short introduction to phase noise modelling. Then effect of the phase noise on general I/Q signal in DCR is discussed. After that the chapter centres on phase noise effect on OFDM in general level, followed by SINR analysis of the OFDM radio link impaired by receiver phase noise. The SINR analysis part is one of the significant contributions of this thesis.

3.1. Phase Noise Modelling

Even though phase noise modelling is not directly related to DCR architecture, it is shortly presented here for completeness of the study. This section is based on the phase noise modelling and analysis given in [20], [21], [22], [54], [65], [P6] and [P8], and shortly summarized in [P1]. The generalized oscillator model is also one of the contributions of this thesis.

There are many non-idealities that are related to oscillators, such as carrier frequency offset and phase offset. However, the most complex of the non-idealities is the time varying phase noise denoted here by $\phi(t)$. Ideal real oscillator-generated signal with phase noise can be written as

$$v(t) = A\cos\left(\omega_c t + \phi(t)\right). \tag{3.1}$$

Here, A is the amplitude of the oscillating signal and ω_c is the nominal angular oscillation frequency (carrier frequency in context of DCR). The phase noise modelling focuses on the modelling of the time-varying phase noise component $\phi(t)$. The modelling in this thesis is typically based on simple mathematical free-running oscillator (FRO) model, but also on more complex phase-locked-loop (PLL) oscillator model, since in practice PLL oscillators are used in many communications devices.

Free-Running Oscillator

The free-running oscillator (FRO) model is simple and easy to use in simulations and mathematical analysis. It is based on the assumption that phase-noise process is a so called Brownian motion process (also known as Wiener process or random-walk process). It can be written as

$$\phi(t) = \sqrt{c}\, B(t), \tag{3.2}$$

where $B(t)$ is time varying standard Brownian motion [42] and c is the diffusion rate that is basically the inverse of relative oscillator quality. What makes FRO easy to use in discrete-time simulations, is the simple generation of the sampled version of (3.2), which in effect can be written as

$$\phi_n = \sqrt{c}\, B(nT_s) \triangleq \sqrt{c}\, B_n \ , \tag{3.3}$$

where T_s is the sampling interval. From the definition of the standard Brownian motion, $B(nT_s) - B((n+1)T_s) \sim \mathcal{N}(0, T_s)$, where $\mathcal{N}(\mu, \sigma^2)$ denotes the normal distribution with expectation value μ and variance σ^2. This effectively means that the sampled FRO process can be generated as cumulative sum of normal distributed random realizations with zero mean and variance cT_s. This on the other hand means, that we are able to characterize the whole phase noise process with just a single parameter c. It is easy to see that since the variance of the process increases as a function of time, the phase process of FRO is non-stationary.

To map the parameter c to more easily measureable and interpretable parameter, let us study the power spectral density (PSD) of the FRO. This is because the decay of the oscillator PSD is commonly used to characterize the oscillator phase-noise properties [45], [54]. Specifically 3-dB bandwidth is used in this context, and it can be calculated as a point where the PSD has decayed to half of its maximum. PSD of the oscillator signal in (3.1) can be easily calculated by calculating the Fourier transform of its autocorrelation. The autocorrelation for real signal $v(t)$ is given by

$$R_{vv}(t, t+\tau) = \mathrm{E}\{v(t)v(t+\tau)\} = \mathrm{E}\left\{\cos[\omega_c t + \phi(t)]\cos[\omega_c(t+\tau) + \phi(t+\tau)]\right\} = \frac{e^{-\frac{1}{2}c|\tau|}}{2}\cos(\omega_c \tau). \tag{3.4}$$

Here, $\mathrm{E}\{\cdot\}$ is the statistical expectation operator and $|\cdot|$ is absolute value operator. Also, value A in (3.1) is fixed to unity. From this it is easy to see that even though $\phi(t)$ is non-stationary process, the oscillator process $v(t)$ is second-order stationary (since autocorrelation function is independent of t and mean is always zero [17]). From (3.4) it is relatively easy to derive the PSD of $v(t)$ by taking the Fourier transform

$$S_v(\omega) = \int_{-\infty}^{\infty} R_{vv}(t, t+\tau)\cos(\omega\tau)\,d\tau = \frac{1}{2}\frac{c/2}{(c/2)^2 + (\omega+\omega_c)^2} + \frac{1}{2}\frac{c/2}{(c/2)^2 + (\omega-\omega_c)^2}. \quad (3.5)$$

Now, if we assume that the oscillation frequency ω_c is relatively large and that the diffusion rate c is relatively small (which they are in practice), we can approximate the one-sided PSD of the noisy oscillator signal as

$$S_{v,ss}(\Delta\omega) \approx \frac{c/2}{(c/2)^2 + (\Delta\omega)^2}. \quad (3.6)$$

Here, $\Delta\omega = \omega - \omega_c$ is the frequency difference from the nominal oscillation frequency. This corresponds to the well-known Lorentzian spectrum [54]. From this, it is simple to calculate the 3-dB bandwidth of the oscillator process (3.1) as

$$\beta = \frac{c}{4\pi} \quad (3.7)$$

or $\beta_{ang} = c/2$ in angular frequency. Now, instead of characterizing the phase-noise process with c, we can use the 3-dB bandwidth of the oscillator, which is more tangible quantity. The 3-dB bandwidth is naturally the same for the corresponding complex oscillator $v_c(t) = A\left[\cos(\omega_c t + \phi(t)) + j\sin(\omega_c t + \phi(t))\right] = Ae^{j(\omega_c t + \phi(t))}$ [54].

Phase-Locked-Loop Oscillator

There are various ways to model PLL oscillator. In this thesis, the model introduced in [65] and [P8] is used. It models a PLL oscillator that takes into account white and flicker ($1/f$) noises [15] in its free-running voltage-controlled oscillator (VCO) and only white noise in its free-running crystal oscillator (CO). The VCO model is based on work done in [20] and [21]. In the oscillator model, first, one-sided PSD of a baseband equivalent VCO is derived according to [21] as

$$S_{a,ss}(\Delta\omega) = \frac{c_w + c_f S_f(\Delta\omega)}{\left(\frac{c_w + c_f S_f(\Delta\omega)}{2}\right)^2 + (\Delta\omega)^2}. \quad (3.8)$$

Here, PSD of the flicker noise is

$$S_f(\Delta\omega) = \frac{2\pi}{|\Delta\omega|} - \frac{4}{\Delta\omega}\tan^{-1}\left(\frac{\gamma_c}{\Delta\omega}\right), \tag{3.9}$$

$$c_w = \frac{2\pi}{\Delta\omega_f - \Delta\omega_w}\left[\Delta\omega_f^3 10^{\frac{L(\Delta\omega_f)}{10}} - \Delta\omega_w^3 10^{\frac{L(\Delta\omega_w)}{10}}\right], \tag{3.10}$$

and

$$c_f = \frac{2\pi\left(\Delta\omega_w - \Delta\omega_f\right)}{\Delta\omega_w\Delta\omega_f}\left[\Delta\omega_f^2 10^{\frac{L(\Delta\omega_f)}{10}} - \Delta\omega_w^2 10^{\frac{L(\Delta\omega_w)}{10}}\right]. \tag{3.11}$$

On these, γ_c is a frequency at which the flicker noise PSD deviates from the nominal $1/f$ slope, and $\Delta\omega_w$, $\Delta\omega_f$, $L(\Delta\omega_w)$ and $L(\Delta\omega_f)$ can be attained from circuit simulator or one-sided-PSD spot measurements of VCO oscillator. $L(\Delta\omega_w)$ is a measurement at white noise dominated region of the oscillator spectrum at offset $\Delta\omega_w$ from the nominal oscillation frequency, and $L(\Delta\omega_f)$ is a measurement at flicker noise dominated region of the oscillator spectrum at offset $\Delta\omega_f$ from the nominal oscillation frequency. The corresponding PSD of the CO is generated also with (3.8), but without flicker noise. The equation for PSD of the CO can thus be simply written as

$$S_{a,ss,CO}(\Delta\omega) = \frac{c_{w,CO}}{\left(\frac{c_{w,CO}}{2}\right)^2 + (\Delta\omega)^2}. \tag{3.12}$$

Here, $c_{w,CO}$ is given by (3.10), but naturally from the corresponding measurements of the CO. The equation (3.12) resembles closely the PSD of the FRO model in (3.6), because the used CO is a high-quality FRO with relatively low nominal oscillation frequency. However, (3.12) is the PSD for baseband equivalent oscillator and, furthermore, maps the oscillator measurements to PSD through measurement parameter $c_{w,CO}$. Now, to generate the actual PSD of the complex PLL-oscillator $v_c(t) = Ae^{j(\omega_c t + \phi(t))}$ actually needed in the baseband simulations, we need to combine the PSD of the CO and VCO. In this work, combination is done according to the work done in [P8].

Now, we know that the PSD of the complex exponential of the phase noise approximately equals to the PSD of the actual phase noise $\phi(t)$ at frequencies higher than the 3-dB bandwidth of the oscillator [20]. For details refer to [20]. In our PLL model, the approximation can be used in general as justified in [P8]. We can thus generate the phase noise by shaping spectrum of white Gaussian noise to correspond the baseband equivalent version of $S_{a,ss}(\Delta\omega)$, namely $S_{a,ss}(\omega)$. Example CO, VCO and PLL PSDs are depicted in

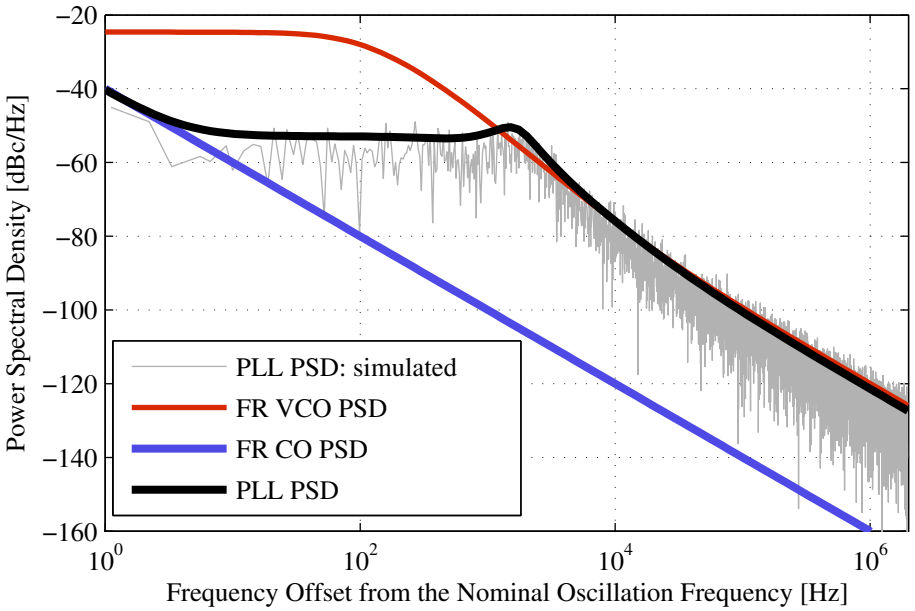

Figure 3-1: Example PSDs of free-running CO and VCO used in the design of a PLL. Theoretical and simulated PSDs of the resulting PLL are also depicted.

Figure 3-1 with parameters $L(\Delta\omega_w) = -120$ dBc/Hz at $\Delta\omega_w = 1$ MHz, $L(\Delta\omega_f) = -76$ dBc/Hz at $\Delta\omega_f = 10$ kHz, $L_{CO}(\Delta\omega_{w,CO}) = -160$ at $\Delta\omega_{w,CO} = 1$ MHz, and $\gamma_c = 2.15$ kHz. For more details and discussion refer to [20], [21], [65] and [P8].

Generalized Oscillator

To generalize the oscillator model even further, the non-constrained form of the given PLL oscillator model first proposed in [P6] is presented. We generate the phase noise in same way with the help of spectral mask, but now without any constraints on the oscillator phase-noise spectrum. Practically this means that we generate white-Gaussian-noise, transfer it to frequency domain with the discrete Fourier transform (DFT), then filter the signal with an arbitrary phase-noise spectral-mask, and the filtered result is then finally transformed back to the time domain with the inverse discrete Fourier transform (IDFT). Naturally in this model, phase noise is generated in blocks since we cannot have infinite length DFT/IDFT pair. The actual spectral mask can be obtained, e.g., directly from circuit simulator or from measurements of an oscillator.

For purposes of later analysis, let us next derive a connection between the phase-noise spectral-mask and average powers of the spectral components of the phase noise complex exponential. The spectral components can be calculated easily with DFT. N -point DFT of the phase noise complex exponential is

$$J_k(m) = \frac{1}{\sqrt{N}} \sum_{n=0}^{N-1} e^{j\phi_n(m)} e^{-j2\pi nk/N} . \tag{3.13}$$

Here, $k \in [0, N-1]$ is the index of the spectral component (corresponds later to the index of one of the subcarriers in OFDM, out of total of N subcarriers) and m is the index of the spectral DFT block (corresponds later to the index of the OFDM symbol in OFDM case). Furthermore $\phi_n(m)$ is the phase noise realization at n th sample of m th spectral block (or at n th sample of m th OFDM symbol in OFDM case). With small phase approximation, i.e., $e^{j\phi_n(m)} \approx 1 + j\phi_n(m)$, and when keeping unit variance we can write

$$e^{j\phi_n(m)} \approx \frac{1 + j\phi_n(m)}{\sqrt{1+\sigma_\phi^2}}, \tag{3.14}$$

where σ_ϕ^2 is the average power of the phase noise $\phi_n(m)$, which can be derived from the spectral mask as [P6]

$$\sigma_\phi^2 = \frac{\sigma_w^2}{N}\sum_{k=0}^{N-1}\lambda_k^2 . \tag{3.15}$$

Here, σ_w^2 is the variance of the time-domain white Gaussian noise from which the phase noise is generated and λ_k is the spectral mask multiplier for the k th spectral component. Now by combining (3.13) and (3.14), we can write

$$J_k(m) \approx \frac{1}{\sqrt{N\left(1+\sigma_\phi^2\right)}}\sum_{n=0}^{N-1}\left[1 + j\phi_n(m)\right]e^{-j2\pi nk/N} . \tag{3.16}$$

When $k \neq 0$, we can write

$$J_k(m) \approx \frac{j}{\sqrt{N\left(1+\sigma_\phi^2\right)}}\sum_{n=0}^{N-1}\phi_n(m)e^{-j2\pi nk/N} = \frac{j\Phi_k(m)}{\sqrt{1+\sigma_\phi^2}}, \tag{3.17}$$

where $\Phi_k(m)$ is the k th frequency bin of N -point Fourier transform of $\phi_n(m)$. So finally

$$k \neq 0: \quad \mathrm{E}\left[\left|J_k(m)\right|^2\right] \approx \frac{\sigma_w^2\lambda_k^2}{1+\sigma_\phi^2} = \frac{\sigma_w^2\lambda_0^2}{1+\frac{\sigma_w^2}{N}\sum_{k=0}^{N-1}\lambda_k^2} \triangleq \frac{\psi_k^2}{1+\frac{1}{N}\sum_{k'=0}^{N-1}\psi_{k'}^2}, \tag{3.18}$$

and when $k = 0$, (3.16) can be written as

$$J_0(m) \approx \frac{N + j\sum_{n=0}^{N-1}\phi_n(m)}{\sqrt{N\left(1+\sigma_\phi^2\right)}} = \frac{\sqrt{N} + j\Phi_0(m)}{\sqrt{1+\sigma_\phi^2}}, \tag{3.19}$$

so we have

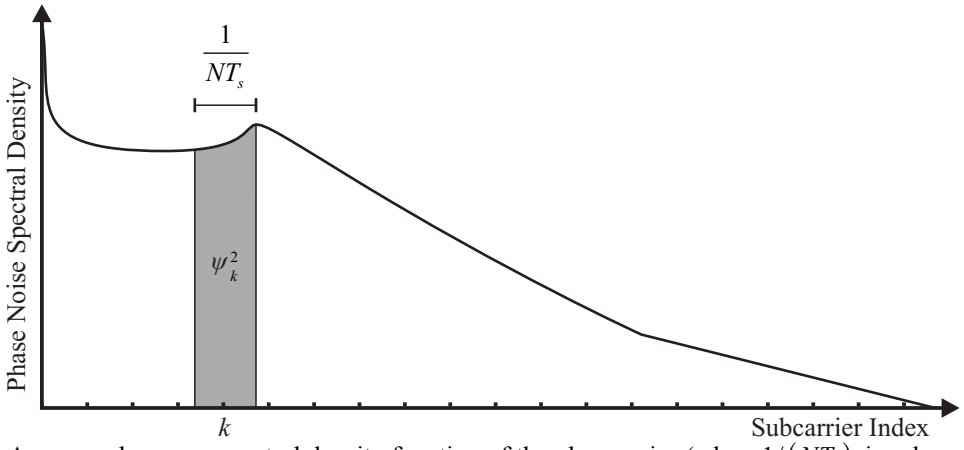

Figure 3-2: An example power spectral density function of the phase noise (where $1/(NT_s)$ is subcarrier spacing in OFDM case).

$$k=0:\quad \mathrm{E}\left[\left|J_0(m)\right|^2\right]\approx\frac{N+\sigma_w^2\lambda_k^2}{1+\sigma_\phi^2}=\frac{N+\sigma_w^2\lambda_0^2}{1+\frac{\sigma_w^2}{N}\sum_{k=0}^{N-1}\lambda_k^2}\triangleq\frac{N+\psi_0^2}{1+\frac{1}{N}\sum_{k=0}^{N-1}\psi_k^2}. \tag{3.20}$$

Here, $\psi_k^2=\sigma_w^2\lambda_k^2$ is the power of the phase noise around the k th frequency bin (or around the k th subcarrier as depicted in Figure 3-2.) For OFDM case, quantity ψ_k^2 can be simply connected to the practical oscillator PSD measurements by

$$\psi_k^2=\sigma_w^2\lambda_k^2\approx\mathrm{PSD}_\phi\left(k\frac{1}{NT_s}\right)\frac{1}{NT_s}. \tag{3.21}$$

Here, PSD_ϕ is the PSD of the phase noise process at the frequency given by the argument and $1/(NT_s)$ is OFDM subcarrier spacing (For general case $1/(NT_s)$ is frequency resolution in the discrete Fourier transform.) Equation (3.21) connects the powers of the spectral components of the phase-noise complex exponential to the more tangible PSD values.

3.2. *Effect of Phase Noise on General I/Q Signal*

General complex signal, i.e. I/Q signal, consists of two real signals. The real signals are called the in-phase (I) and the quadrature (Q) components of the complex signal [46]. If $s(t)$ is the I/Q signal, it is separated to its I and Q components as follows

$$s(t)=s_I(t)+js_Q(t), \tag{3.22}$$

where $s_I(t)$ and $s_Q(t)$ are the I component and the Q component of complex signal $s(t)$, respectively. I/Q modulation is a modulation technique in which a carrier signal is modulated by a complex signal so that the I and Q components are orthogonal to each other and thus separable at the receiver. The general I/Q modulated signal can be written as

$$r(t)=s_I(t)\cos(\omega_c t)-s_Q(t)\sin(\omega_c t). \tag{3.23}$$

Ideal DCR demodulates the I/Q modulated signal back to its I and Q components. For example, if the structure in Figure 2-2 would be used to receive the signal in (3.23), the demodulated I component would be sampled at the upper branch and the demodulated Q component would be sampled in the lower branch of the structure.

Now, when the phase noise is present in the oscillator, the upper branch signal (the I component) after the mixing and the lowpass filter can be written as

$$\hat{s}_I(t) = \mathrm{LPF}\left\{r(t)\cos\left(\omega_c t + \phi(t)\right)\right\} = \frac{s_I(t)\cos\left(\phi(t)\right) + s_Q(t)\sin\left(\phi(t)\right)}{2}, \tag{3.24}$$

where $\phi(t)$ is the phase noise and $\mathrm{LPF}\{\cdot\}$ is an ideal lowpass filter with cutoff frequency of, e.g., ω_c. The corresponding Q component is then

$$\hat{s}_Q(t) = \mathrm{LPF}\left\{r(t)\left[-\sin\left(\omega_c t + \phi(t)\right)\right]\right\} = \frac{s_Q(t)\cos\left(\phi(t)\right) - s_I(t)\sin\left(\phi(t)\right)}{2}. \tag{3.25}$$

Now, since we have the I and Q components of the complex signal at the receiver output, we can write the received complex signal with phase-noise effect according to (3.22) as

$$\begin{aligned}\hat{s}(t) &= \hat{s}_I(t) + j\hat{s}_Q(t) = s_I(t)\left[\cos\left(\phi(t)\right) - j\sin\left(\phi(t)\right)\right] + js_Q(t)\left[\cos\left(\phi(t)\right) - j\sin\left(\phi(t)\right)\right] \\ &= s_I(t)e^{-j\phi(t)} + js_Q(t)e^{-j\phi(t)} = s(t)e^{-j\phi(t)}.\end{aligned} \tag{3.26}$$

Therefore, in I/Q downconversion (and therefore in DCR) the phase noise effect on the signal waveform (namely the baseband equivalent effect of phase noise) can be seen as a multiplication with a complex exponential that has negative phase-noise sequence as its argument. Of course, after the sampling, the signal with phase noise is

$$\hat{s}_n = s(nT_s)e^{-j\phi_n}, \tag{3.27}$$

where T_s is the sampling interval, n is the sample index and $\phi_n = \phi(nT_s)$. From now on in analysis, the negative phase in the complex oscillator model is substituted with positive phase. This is done merely for better appearance, and can be done since the sign of the phase noise does not have any effect on the statistics of the complex oscillator.

3.3. *Effect of Phase Noise on OFDM Signals*

It is easy to see from (3.27), that the effect of the phase noise on the constellation of a single carrier, e.g. 16-quadrature-amplitude-modulated (16QAM), [35] signal is time-varying phase rotation of the constellation as depicted in Figure 3-3 (a). Such effect, if small, is relatively easily compensated by constellation derotation. Also, small phase error in single carrier signal has only a minor effect on the signal quality with reasonable modulation. In effect, the phase

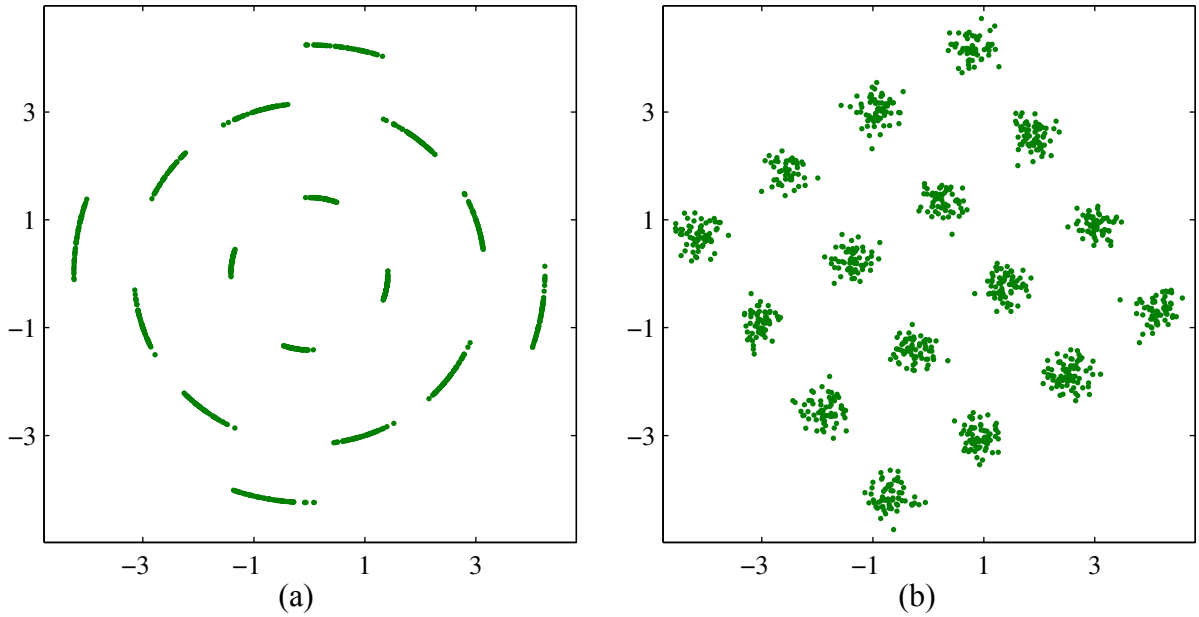

Figure 3-3: Single-carrier 16QAM signal (1024 symbols) with phase noise in (a) and OFDM with 16QAM subcarrier modulation (1024 subcarriers) with phase noise in (b). In both cases FRO phase-noise with 3-dB bandwidth of 100 Hz is assumed. I and Q components of the signals are presented in horizontal and vertical axis, respectively. The bandwidths of the total signals are approximately the same.

noise has mostly been a problem because of interchannel interference caused by the signal spread and the spread of high-power interferers on top of the useful signal. However, for multicarrier signals, the effect of the phase noise is much more complex and severe as depicted in Figure 3-3 (b) for OFDM using 16QAM subcarrier modulation. This is because in frequency domain, the effect of phase noise can be seen as spread of the spectral contents of the received signals. Therefore, since OFDM signal has many subcarriers overlapping each other, in addition that every OFDM symbol is phase rotated similarly as single carrier symbols, also the subcarriers spread on top of each other causing intercarrier interference [6], [51], [67]. In a constellation, the effect is seen as spread around the ideal rotated constellation points. The effects of the phase noise on OFDM signals have been studied and analysed, e.g., in [34], [38], [51], [54], [55] and [74]. In addition to these inband effects, also OFDM suffers from the spread of the out-of-band interferers on top of the useful signal due to phase noise. In this thesis, also the out-of-band interferer case is studied analytically, but the phase noise mitigation algorithms are built keeping only the inband effect in mind. The illustration of the inband case is depicted in Figure 3-4 and the case with adjacent channels (strictly speaking orthogonal frequency division multiple access (OFDMA) case since the adjacent channels are in the same OFDM signal) is depicted in Figure 3-5.

Signal Model for OFDM Radio Link Corrupted by Phase Noise

For OFDM configuration with N subcarriers $k = 0, 1, \ldots, N-1$, the m th OFDM symbol is

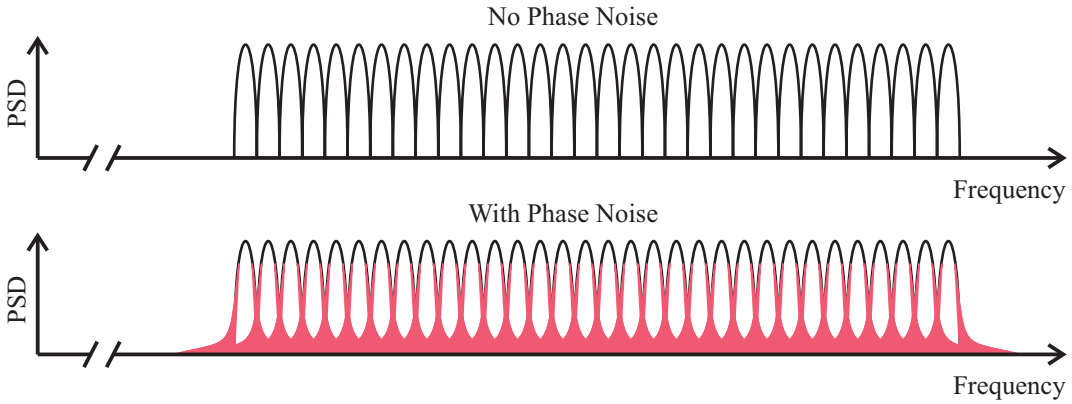

Figure 3-4: Illustration of phase noise induced spectrum spread of an OFDM signal with 32 subcarriers. Phase noise spread is denoted by filled area.

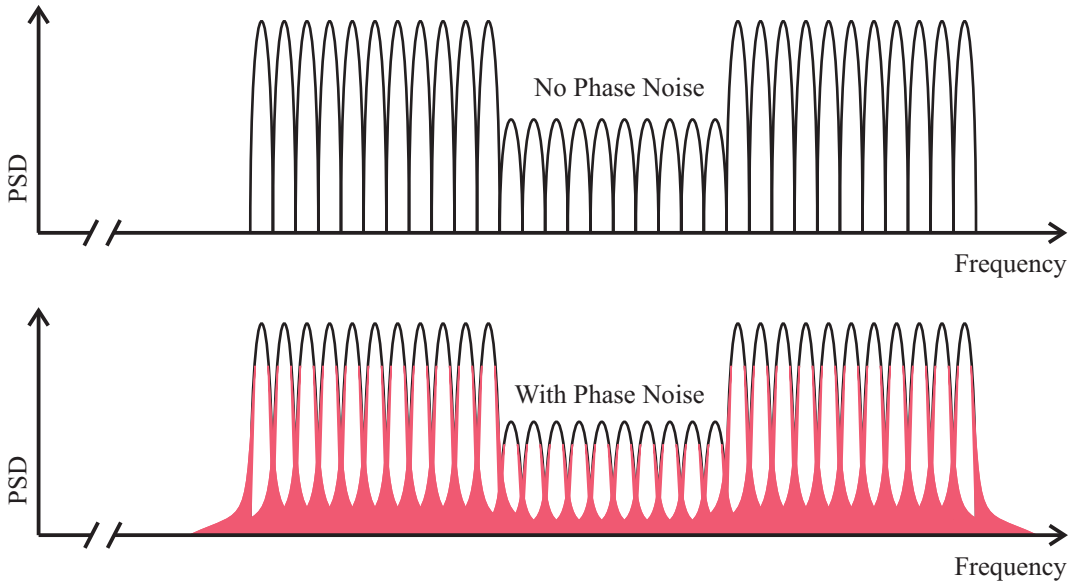

Figure 3-5: Illustration of phase noise induced spectrum spread of an OFDM signal with 32 subcarriers divided to 3 channels. A lower powered channel suffers from the spread of the adjacent more powerful channels. Phase noise spread is denoted by filled area.

generated from subcarrier symbols $X_k(m)$ with the help of N-point IDFT [68]. The nth sample of such OFDM symbol can be written as

$$x_n(m) = \frac{1}{\sqrt{N}} \sum_{k=0}^{N-1} X_k(m)\, e^{j2\pi kn/N}, \tag{3.28}$$

where sampling index $n = [0, N-1]$. Now with subcarrier spacing $1/(NT_s)$ (sampling interval is T_s and sampling frequency $F_s = 1/T_s$), the OFDM-symbol length in seconds is NT_s. In practice also cyclic prefix is implemented to exploit relatively long symbol duration of OFDM symbols. This is done by reconstructing the OFDM symbol so that the last G samples of each OFDM symbol are copied so that they precede the actual OFDM-symbols samples. This lengthens the OFDM symbol to $N+G$ samples, which in seconds is

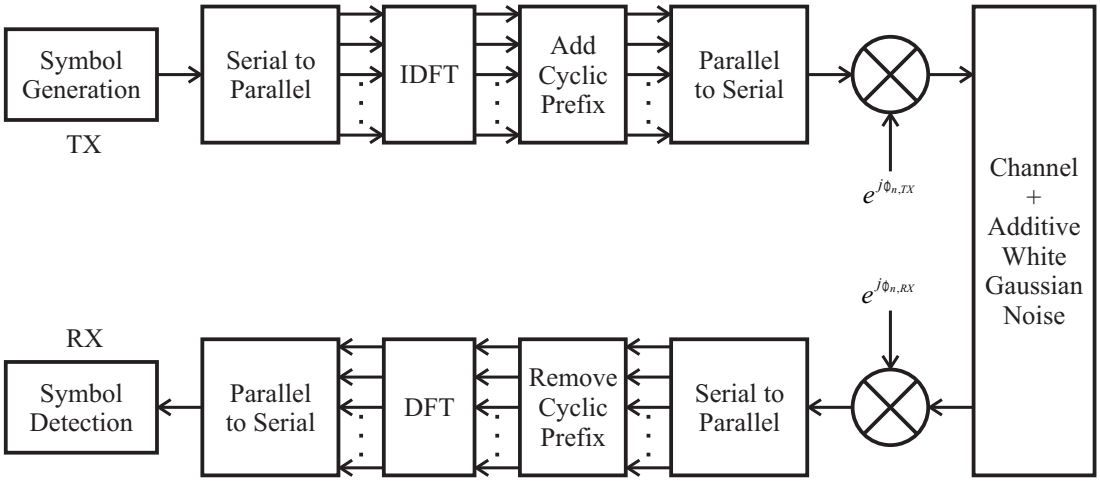

Figure 3-6: Illustration of the OFDM link model.

$(N+G)T_s$. The cyclic prefix effectively makes the OFDM signal immune to intersymbol interference, if the length of the cyclic prefix is longer than the maximum delay spread of the communications channel. In this case, after ideal upconversion at the transmitter, time-invariant multipath channel, ideal downconversion and removal of the cyclic prefix at the receiver, the m th received OFDM symbol can be written as

$$\mathbf{r}_m = (\mathbf{h}_m * \mathbf{x}_m) + \mathbf{z}_m, \tag{3.29}$$

where $\mathbf{h}_m$ is $(D \times 1)$ multipath channel impulse response vector so that $D < G$, $\mathbf{x}_m = [x_0(m), x_1(m), \ldots, x_{N-1}(m)]^T$, operator $*$ denotes circular convolution between the elements of the operated vectors, and $\mathbf{z}_m$ is $(N \times 1)$ vector of white Gaussian noise samples. Now the expression in (3.29) can be simplified with the help of circulant convolution matrix [24] as

$$\mathbf{r}_m = \mathbf{H}_m \mathbf{x}_m + \mathbf{z}_m, \tag{3.30}$$

where $\mathbf{H}_m$ is $(N \times N)$ circulant convolution matrix corresponding to the channel impulse response vector $\mathbf{h}_m$. With phase noise in upconverting and downconverting oscillators in the transmitter and the receiver, respectively (so that the overall link is as depicted in Figure 3-6), we can write the received signal as

$$\begin{aligned} \mathbf{r}_m &\approx \operatorname{diag}\left(e^{j\boldsymbol{\phi}_{m,R}}\right) \mathbf{H}_m \operatorname{diag}\left(e^{j\boldsymbol{\phi}_{m,T}}\right) \mathbf{x}_m + \mathbf{z}_m \\ &= \operatorname{diag}\left(e^{j\boldsymbol{\phi}_{m,R}}\right) \operatorname{diag}\left(e^{j\boldsymbol{\phi}_{m,T}}\right) \mathbf{H}_m \mathbf{x}_m + \mathbf{z}_m \\ &= \mathbf{H}_m \operatorname{diag}\left(e^{j\boldsymbol{\phi}_{m,R}}\right) \operatorname{diag}\left(e^{j\boldsymbol{\phi}_{m,T}}\right) \mathbf{x}_m + \mathbf{z}_m . \end{aligned} \tag{3.31}$$

Here, $\operatorname{diag}(\cdot)$ is a function which creates a diagonal matrix out from its input vector, and $\boldsymbol{\phi}_{m,T}$ and $\boldsymbol{\phi}_{m,R}$ vectors consist of transmitter and receiver phase noise samples $\phi_{n,X}(m)$, $X \in \{T, R\}$, respectively, so that $\boldsymbol{\phi}_{m,X} = [\phi_{0,X}(m), \phi_{1,X}(m), \ldots, \phi_{N-1,X}(m)]^T$, $X \in \{T, R\}$. The equation (3.31)

is only approximation because transmitter phase noise is always different in the cyclic prefix part of the signal and in the part of the signal that the cyclic prefix is copied from. Therefore (3.31) is not accurately true, because the cyclic prefix does not work as intended. However, the accuracy of (3.31) is enough for the phase-noise estimation algorithms later developed in this thesis, as will be proven with simulations. The second and the third form of (3.31) stem from the fact that circulant matrices are commutative, and that $\mathbf{H}_m$ is indeed circulant as are the diagonal matrices. We are therefore able to change the order of the diagonal phase noise matrices and the channel matrix in (3.31). So, we are able to approximately model all the phase noise as either transmitter or receiver phase-noise and mark the combined phase noise term as $\phi_m = \phi_{m,T} + \phi_{m,R}$ [38], [45], [54].

3.4. Contributions to OFDM-Link Performance Analysis under Phase Noise

The signal model in (3.31) for the received signal after the DFT in the receiver without transmitter phase noise can be written as

$$R_k(m) = X_k(m)H_k(m)J_0(m) + \sum_{l=0,\, l\neq k}^{N-1} X_l(m)H_l(m)J_{k-l}(m) + \sqrt{N}\,Z_k(m)\,, \tag{3.32}$$

where $H_k(m)$ is channel transfer function, $J_k(m)$ is the frequency-domain phase-noise complex exponential defined in (3.13), and $Z_k(m)$ is frequency-domain additive white Gaussian-noise. $Z_k(m)$ is multiplied with $\sqrt{N}$, because with the scaling of the DFT used in (3.13) and (3.28), the ideal oscillator response is amplitude multiplication by $\sqrt{N}$. The scaling used in (3.13) is used for the phase noise also here. The equation (3.32) shows the two fundamentally different effects of the phase noise on OFDM signal separately. The left-hand side has the signal component multiplied by the DC-bin of the phase-noise complex exponential. This effect is called common phase error (CPE) and it is the same rotation that all the subcarrier symbols within one OFDM symbol experience. The right term is the additive noise term, which is error from the spread of the adjacent subcarriers on top of the k th one. This phase-noise effect is called intercarrier interference (ICI). Now if we assume that CPE is easily mitigated (as is in practice the case) and the ICI is the only remaining error due to phase noise, we can define signal-to-interference+noise ratio (SINR) into form [P6]

$$\gamma_k = \frac{\mathrm{E}\left[\left|X_k(m)H_k(m)J_0(m)\right|^2\right]}{\mathrm{E}\left[\left|\sum_{l=0,\, l\neq k}^{N-1} X_l(m)H_l(m)J_{k-l}(m) + \sqrt{N}\,Z_k(m)\right|^2\right]}. \tag{3.33}$$

Now, if we make natural assumptions 1) that $X_k(m)$, $H_k(m)$, $J_k(m)$ and $Z_k(m)$ are mutually statistically independent and stationary, 2) that for $\forall k$: $X_k(m)$ are independent of each other and 3) that $\mathrm{E}\left[X_k(m)\right] = 0$, we can rewrite (3.33) as

$$\gamma_k = \frac{\mathrm{E}\left[\left|X_k(m)\right|^2\right]\mathrm{E}\left[\left|H_k(m)\right|^2\right]\mathrm{E}\left[\left|J_0(m)\right|^2\right]}{\sum_{l=0,\,l\neq k}^{N-1}\mathrm{E}\left[\left|X_l(m)\right|^2\right]\mathrm{E}\left[\left|H_l(m)\right|^2\right]\mathrm{E}\left[\left|J_{k-l}(m)\right|^2\right]+N\,\mathrm{E}\left[\left|Z_k(m)\right|^2\right]}. \tag{3.34}$$

Now, with assumption that the average noise power, average channel power response and average transmitted signal power are subcarrier independent, namely

$$\forall k: \quad \mathrm{E}\left[\left|Z_k(m)\right|^2\right]=\sigma_z^2, \tag{3.35}$$

$$\forall k: \quad \mathrm{E}\left[\left|H_k(m)\right|^2\right]=\sigma_h^2, \tag{3.36}$$

and

$$\forall k: \quad \mathrm{E}\left[\left|X_k(m)\right|^2\right]=\sigma_x^2, \tag{3.37}$$

we can simplify (3.34) into form

$$\gamma_k = \frac{\sigma_x^2\sigma_h^2\,\mathrm{E}\left[\left|J_0(m)\right|^2\right]}{\sigma_x^2\sigma_h^2\sum_{l=1}^{N-1}\mathrm{E}\left[\left|J_l(m)\right|^2\right]+N\sigma_z^2}=\frac{\mathrm{E}\left[\left|J_0(m)\right|^2\right]}{\sum_{l=1}^{N-1}\mathrm{E}\left[\left|J_l(m)\right|^2\right]+\frac{N\sigma_z^2}{\sigma_x^2\sigma_h^2}}=\frac{\mathrm{E}\left[\left|J_0(m)\right|^2\right]}{\sum_{l=1}^{N-1}\mathrm{E}\left[\left|J_l(m)\right|^2\right]+\frac{N}{\rho}}. \tag{3.38}$$

Here $\rho=\sigma_x^2\sigma_h^2/\sigma_z^2$ is the average received signal-to-noise ratio (SNR). Now from Parseval's theorem and linearity of the expectation value operator it stems that

$$\sum_{k=0}^{N-1}\mathrm{E}\left[\left|J_k(m)\right|^2\right]=N. \tag{3.39}$$

Now by using (3.39), we can rewrite (3.38) into simpler form as

$$\gamma_k=\gamma=\frac{\mathrm{E}\left[\left|J_0(m)\right|^2\right]}{N-\mathrm{E}\left[\left|J_0(m)\right|^2\right]+\frac{N}{\rho}}, \tag{3.40}$$

which is subcarrier independent and only depends on the second-order statistics of the CPE term. Now by using (3.20), we can approximate (3.40) as

$$\gamma\approx\frac{N+\psi_0^2}{\sum_{k=1}^{N-1}\psi_k^2+\frac{1}{\rho}\sum_{k=0}^{N-1}\psi_k^2+\frac{N}{\rho}}. \tag{3.41}$$

This is relatively simple formula for SINR, taking into account that it is for general OFDM signal with arbitrary oscillator. Furthermore, it is relatively easy to expand this for the case with adjacent channel interference as shown in [P8]. It can be done, e.g., by defining

subcarriers from index α to κ ($\alpha \le \kappa$) to belong to the interesting channel and the other subcarriers to belong to adjacent channels. Since the indexing of the DFT is always circular, we can change the k dependent sums in the analysis to be from $-N/2$ to $N/2-1$ instead of original interval from 0 to $N-1$. This selection is done, so that the channel selection with α and κ corresponds to the indexing of OFDM subcarriers which starts from $-N/2$ and ends to $N/2-1$ so that the DC bin is indexed as frequency-bin number 0. This results in more illustrative presentation. Thus, instead of definition in (3.37), we define

$$k \in [\alpha, \kappa]: \quad \mathrm{E}\left[|X_k(m)|^2 \right] = \sigma_x^2, \tag{3.42}$$

$$k \in [-N/2, \alpha-1] \cup [\kappa+1, N/2-1]: \quad \mathrm{E}\left[|X_k(m)|^2 \right] = \sigma_{adj}^2. \tag{3.43}$$

So here, for simplicity, we assume that all subcarriers that belong to adjacent channels have the same power σ_{adj}^2. Then, with assumptions (3.35), (3.36), (3.42) and (3.43), we can write (3.34) into form

$$\begin{aligned} k \in [\alpha, \kappa]: \quad \gamma_k &= \frac{\sigma_x^2 \sigma_h^2 \, \mathrm{E}\left[|J_0(m)|^2 \right]}{\sigma_x^2 \sigma_h^2 \sum\limits_{l=\alpha, l\neq k}^{\kappa} \mathrm{E}\left[|J_{k-l}(m)|^2 \right] + \sigma_{adj}^2 \sigma_h^2 \sum\limits_{l=-N/2, l\notin[\alpha,\kappa]}^{N/2-1} \mathrm{E}\left[|J_{k-l}(m)|^2 \right] + N\sigma_z^2} \\ &= \frac{\mathrm{E}\left[|J_0(m)|^2 \right]}{\sum\limits_{l=k-\kappa, l\neq 0}^{k-\alpha} \mathrm{E}\left[|J_l(m)|^2 \right] + \frac{\sigma_{adj}^2}{\sigma_x^2} \sum\limits_{l=k-\alpha+1}^{k-\kappa-1+N} \mathrm{E}\left[|J_l(m)|^2 \right] + \frac{N}{\rho}} \end{aligned}. \tag{3.44}$$

Note that here spectral mask values ψ_k are also circularly indexed, once again for the sake of simpler presentation of the result. Above, SINR is only calculated for $k \in [\alpha, \kappa]$ for simpler formulation of the resulting equation. To calculate SINR for adjacent channel subcarriers, σ_x^2 in the numerator of the first form of (3.44) should just simply be replaced with corresponding subcarrier dependent value. Now, by using (3.18) and (3.20), we can approximate

$$k \in [\alpha, \kappa]: \quad \gamma_k \approx \frac{N + \psi_0^2}{\sum\limits_{l=k-\kappa, l\neq 0}^{k-\alpha} \psi_l^2 + \frac{\sigma_{adj}^2}{\sigma_x^2} \sum\limits_{l=k-\alpha+1}^{k-\kappa-1+N} \psi_l^2 + \frac{1}{\rho} \sum\limits_{l=0}^{N-1} \psi_l^2 + \frac{N}{\rho}}. \tag{3.45}$$

Logically, compared to case without adjacent channels, (3.45) only has an extra additive interference term due to the adjacent channels.

In Figure 3-7 (a), the results given by the theoretical formula (3.41) are compared to results given by simulator for case without adjacent channel. In Figure 3-7 (b), then, the results given by the theoretical formula (3.45) are compared to those given by the simulator for the case with adjacent channels. In both cases, OFDM signal with 1024 subcarriers, 15 kHz subcarrier

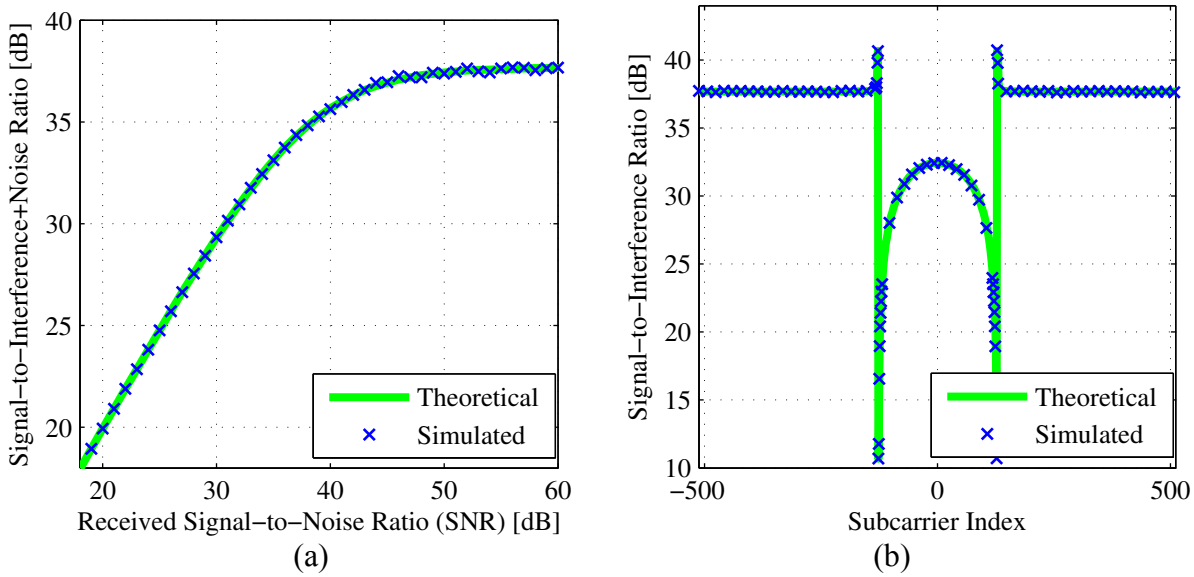

Figure 3-7: OFDM system (1024 subcarriers) performance under phase noise from PLL type oscillator with parameters $L(\Delta\omega_w) = -120$ dBc/Hz at $\Delta\omega_w = 1$ MHz, $L(\Delta\omega_f) = -76$ dBc/Hz at $\Delta\omega_f = 10$ kHz, $L_{CO}(\Delta\omega_{w,CO}) = -120$ at $\Delta\omega_{w,CO} = 1$ MHz, and $\gamma_c = 2.15$ kHz. In (a), no adjacent channels are assumed and therefore (3.41) is used, and SINR is given as a function of received SNR. In (b), adjacent channels are assumed present, and therefore (3.45) is used, and SIR (no additive noise) is given as a function of subcarrier index.

spacing, and cyclic prefix of length 63 samples is generated. For the case without adjacent channels all the subcarriers have the same power. For the case with adjacent channels, the subcarriers with indices from -128 to 127 have unity power. The powers of the other subcarriers are 30 dB higher, and they act as adjacent channels. In the simulator, after signal generation, the signal is passed through Extended ITU-R Vechicular A multipath channel [61]. Then, additive noise is added (for the case without adjacent channels), and downconverting oscillator with PLL phase-noise in the receiver is modelled. Then, after removal of the cyclic prefix and DFT, SINR (SIR) is calculated for the case without (with) adjacent channel. The additive noise is omitted from the adjacent channel case in this example merely for simpler presentation. As is clearly visible in Figure 3-7, the performances calculated with formulas (3.41) and (3.45) correspond almost perfectly to the performances given by the numerical computations carried out by the simulator.

The resulting formulas (3.41) and (3.45) can, e.g., be used to optimize the design of oscillator for use in up/downconversion of OFDM signals with certain parameters. The formulas are also useable in determining the allowable phase-noise spectral-density for given OFDM signal parameterization and dynamics of the received signals, such that the received signal quality stays above target SINR.

Chapter 4

Sampling Jitter in Direct-RF-Sampling Receivers

Direct-RF-sampling receiver can be based on either very high-frequency sampling to prevent aliasing effect in the sampling or on subsampling where the desired signal is downconverted to around lower centre frequency with the help of the aliasing effect [37], [59]. Use of very low-frequency sampler is not feasible in compact and inexpensive devices even when aliasing effect is exploited, because it is very challenging to clear the other non-interesting signal bands that would also alias on top of the desired signal. Also, to build a multi-system receiver, possibility of which is naturally one of the main benefits in the direct-RF-sampling receiver architecture, relative high sampling frequencies are required. This inherently makes the sampling circuit relatively large, expensive and power consuming. Compromise must thus be made between the properties and quality requirements of the sampling circuitry. One of the quality factors of a sampler, sampling jitter, has serious effects on the performance of devices that sample high-frequency signals, such as direct-RF-sampling receivers [32], [60]. Timing errors in the sampling process cause higher errors to high-frequency signals than to low-frequency signals. This stems directly from the fact that the value of a higher-frequency signal varies more aggressively versus time than the value of a lower-frequency signal. In addition of the inband effects, sampling jitter causes spread also in the interferers that are partly sampled, because of challenging implementation of the RF filtering in direct-RF-sampling receivers. The spread of high-power interferers can cause significant deterioration of the quality of the useful signal [P3], [P4]. The sampling jitter is thus a very bad problem in every system in which high-frequency signals are sampled [32], [44], [60]. In the traditional VS scheme, it is well established that the spectral shape of the error due to timing jitter resembles closely the spectrum of the timing jitter process itself. However, as this thesis shows, that is not necessary the case with CS.

In this chapter, sampling jitter effect is studied in more detail for VS and CS direct-RF-sampling receiver architectures.

4.1. Contributions to the Modelling of Sampling Jitter in Voltage Sampling

Some of the traditional sampling jitter models or approximations are not either accurate enough or otherwise useable for sampling jitter mitigation in direct-RF-sampling receivers. For example, widely used approximation [59], of sampling signal $x(t)$,

$$x(nT_s + \zeta_n) \approx x(nT_s) + \zeta_n \left.\frac{dx(t)}{dt}\right|_{t=nT_s} \tag{4.1}$$

is a general sampling model and is very awkward to use in direct-RF-sampling receiver context in general. Especially the widely used classical model of modelling sampling jitter as additive white noise (which stems from (4.1) when the sampling jitter is white noise) is very inaccurate, also in general, since white noise assumption does not hold in practice. In this section, sampling jitter model designed especially for direct-RF-sampling receiver architecture is proposed. It is designed to make the simulation (and analysis) simple when sampling jitter is present in sampled high-frequency but relatively narrowband (in relation to the centre frequency) signals, while being very accurate [64].

A general I/Q modulated signal

$$r(t) = s_I(t)\cos(\omega_c t) - s_Q(t)\sin(\omega_c t) \tag{4.2}$$

can, after sampling with ideal VS direct-RF-sampling receiver, be written as

$$r_n \triangleq r(nT_s) = s_I(nT_s)\cos(\omega_c nT_s) - s_Q(nT_s)\sin(\omega_c nT_s). \tag{4.3}$$

When sampling jitter is present at the sampler, instead of the ideal sampling moments $t_n = nT_s$, the sampling moments are $t_n = nT_s + \zeta_n$, so the signal at the VS direct-RF-sampling receiver with sampling jitter can be written into form

$$\begin{aligned}\tilde{r}_n &\triangleq r(nT_s + \zeta_n) = s_I(nT_s + \zeta_n)\cos(\omega_c(nT_s + \zeta_n)) - s_Q(nT_s + \zeta_n)\sin(\omega_c(nT_s + \zeta_n)) \\ &= s_I(nT_s + \zeta_n)\cos(\omega_{IF} nT_s + \omega_c \zeta_n) - s_Q(nT_s + \zeta_n)\sin(\omega_{IF} nT_s + \omega_c \zeta_n)\end{aligned}. \tag{4.4}$$

Here ζ_n is the n th sample of the time-varying sampling-jitter process taken at a time moment nT_s, and ω_{IF} is the centre frequency of the signal after aliasing due to possible subsampling. In case of controlled aliasing $\omega_{IF} < \omega_c$ and in case without aliasing $\omega_{IF} = \omega_c$. After the digital I/Q downconversion, the signal in (4.4) can be written as

$$\tilde{s}_n = \mathrm{LPF}\left\{\tilde{r}_n\, e^{-j\omega_{IF} nT_s}\right\} = s(nT_s + \zeta_n)e^{j\omega_c \zeta_n}. \tag{4.5}$$

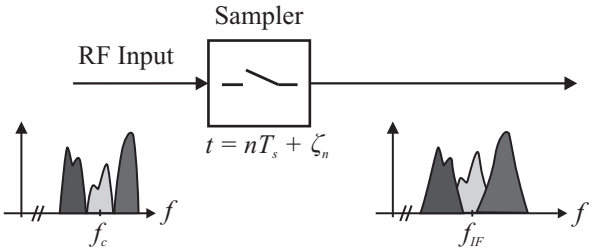

Figure 4-1: Spectrum of the sampled signal is spread by the sampling jitter.

So the actual sampling-jitter corrupted signal is the useful signal sampled with the sampling jitter multiplied by a complex exponential with $\omega_c\zeta_n$ as its argument. The effect is very similar to the effect of the phase noise in DCR as was seen in (3.27). And actually since in (4.4) the frequency of the carrier components (cosine and sine waves) is much higher than the bandwidth of the I and Q components (our original, and reasonable, assumption), the inaccuracy of the sampling process (namely the sampling-jitter effect) is dominating in the carrier components [64]. This is why we are able to approximate (4.5) as

$$\tilde{s}_n \approx s(nT_s)e^{j\omega_c\zeta_n}. \tag{4.6}$$

With this approximation, we are therefore able to model the sampling jitter in VS direct-RF-sampling receiver similarly as we modelled phase noise in DCR. Now instead of sampled phase noise process ϕ_n, the argument of the multiplying complex exponential is $\omega_c\zeta_n$. The result is illustrated in Figure 4-1. The model is very accurate in sampling jitter modelling in direct-RF-sampling receivers [64]. This result and its use in mitigation of the sampling jitter were first published in [P2].

When practical RF filtering is considered, also some adjacent channels or other high-power interferers may find their way into the input of the sampler, namely to the signal $s(t)$. In such case, the only difference is basically in the bandwidth of the modelled signal. Therefore also in this case, the model (4.5) is accurate. However, in the model (4.6) relatively small bandwidth was assumed in respect to the centre frequency. Anyway, since centre frequencies tend to be very high, the model (4.6) is relatively accurate with an assumption of realistic RF filtering. This is also discussed later in this thesis, and the model is proven to be applicable for relatively high-bandwidth signals.

4.2. Sampling of High-Frequency Signals in Charge-Sampling Receiver

In charge-sampling receiver, received voltage-signal is transformed to a current-signal by a transconductance amplifier. The current-signal is then integrated by capacitor(s) for duration T_i to get the sample. The nth sample of ideal charge-sampled I/Q-modulated signal can thus be written as

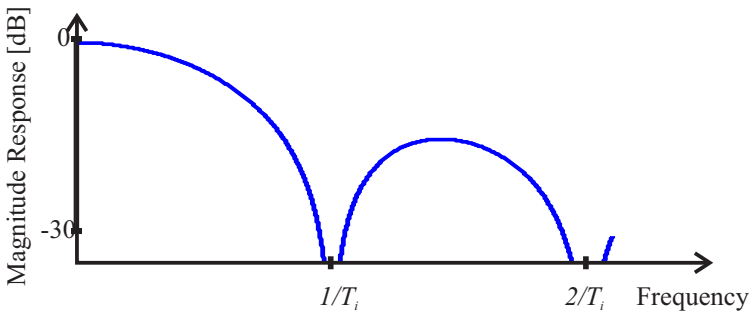

Figure 4-2: Ideal amplitude response of charge-sampling receiver.

$$\begin{aligned} r_{n,CS} &= \int_{nT_s-T_i/2}^{nT_s+T_i/2} \left[r(t) \right] dt = \int_{nT_s-T_i/2}^{nT_s+T_i/2} \left[s_I(t)\cos\left(\omega_c t\right) - s_Q(t)\sin\left(\omega_c t\right) \right] dt \\ &= \int_{t-T_i/2}^{t+T_i/2} \left[s_I(\tilde{t})\cos\left(\omega_c \tilde{t}\right) - s_Q(\tilde{t})\sin\left(\omega_c \tilde{t}\right) \right] d\tilde{t} \Bigg|_{t=nT_s} . \end{aligned} \tag{4.7}$$

Here, T_s is the sampling interval ($T_s \geq T_i$). Since the samples are taken by integrating, the signal spectrum is shaped with transfer function

$$H(\omega) = c\,\mathrm{sinc}\left(T_i\omega/2\right) \triangleq \frac{c\sin\left(T_i\omega/2\right)}{T_i\omega/2}, \tag{4.8}$$

where c is a sampling-circuit dependent constant [16]. The corresponding amplitude response (for a circuit with $c = 0$) is depicted in Figure 4-2. It is thus natural that in the charge sampler the integration duration T_i should be carefully selected, so that the desired signal does not get too attenuated. Note that already the second lobe in the magnitude response is very low compared to the first one, so also the sampling frequency should be relatively high compared to the centre frequency of the signal band. For example the works in [31] and [33] propose also embedded filtering functions into the charge-sampling circuit. This is done by using higher rate integration than is the desired useful sampling frequency. The short charges are integrated at very high rate to multiple capacitors. The charges are weighted, and when the actual sample is taken, it consists of multiple filtered short charges, which approximately corresponds to digital filtering. The basic block diagram of such charge-sampling radio is depicted in Figure 2-7. There the filtering and undersampling blocks refer to the filtering and bandpass sampling that the filtering charge sampler does. This advanced case is not studied further in this thesis, but the same sampling-jitter considerations apply to that case as well. From now on, just a simple sinc-type filtering response given in (4.8) is assumed for the useful signal in the rest of this thesis.

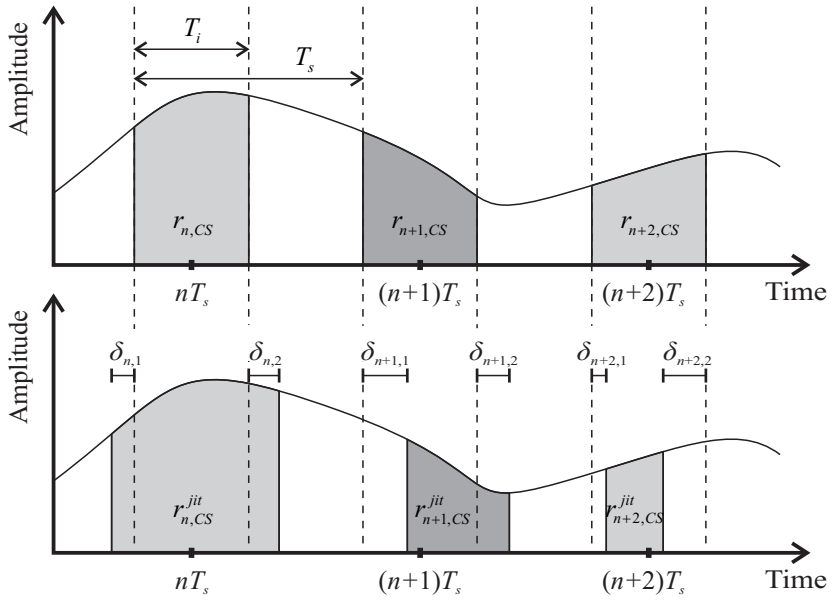

Figure 4-3: Illustration of the general charge-sampling without (upper figure) and with (lower figure) sampling jitter.

4.3. Contributions to Sampling-Jitter Analysis in Charge-Sampling Receiver

In VS, it is very well established that the spectral shape of the sampling-jitter caused error follows closely the spectral shape of the sampling jitter process itself [P3]. However, this is not necessary the case in CS, since the sampling does not mean only taking samples at certain moments of time. Instead, it means integrating the signal for certain duration. The sampling jitter causes uncertainty on the moment when the integration interval begins and ends. To make things more complex, the sampling jitter realizations at the beginning and at end of different integration periods behave differently depending on the structure of the sampler. The general case is depicted in Figure 4-3. The analysis of the spectral shape of the sampling-jitter induced noise for charge-sampling radio is one of the contributions of this thesis, and it is presented in this section. The analysis was first presented in [P9].

Sampling-Jitter Caused Error in Charge-Sampling Receiver

The charge sampled I/Q-modulated signal (4.7) with sampling jitter can be written as

$$r^{jit}_{n,CS} = \int_{nT_s - T_i/2 + \delta_{n,1}}^{nT_s + T_i/2 + \delta_{n,2}} \left[s_I(t)\cos\left(\omega_c t\right) - s_Q(t)\sin\left(\omega_c t\right) \right] dt \,, \tag{4.9}$$

where $\delta_{n,1}$ and $\delta_{n,2}$ are the sampling jitters at the beginning and at the end of the integration interval, respectively. From now on, the jittered integration intervals are written, for the sake of simplified notation, as $t^{jit}_{n,1} = nT_s - T_i/2 + \delta_{n,1}$ and $t^{jit}_{n,2} = nT_s + T_i/2 + \delta_{n,2}$. Therefore, the result of the integration in (4.9) can be written as

$$r_{n,CS}^{jit} = \frac{1}{\omega_c}\Big[s_I(t_{n,2}^{jit})\sin\left(\omega_c t_{n,2}^{jit}\right) + s_Q(t_{n,2}^{jit})\cos\left(\omega_c t_{n,2}^{jit}\right) - s_I(t_{n,1}^{jit})\sin\left(\omega_c t_{n,1}^{jit}\right) - s_Q(t_{n,1}^{jit})\cos\left(\omega_c t_{n,1}^{jit}\right)\Big] - \frac{1}{\omega_c}\int_{t_{n,1}^{jit}}^{t_{n,2}^{jit}}\left[\frac{ds_I(t)}{dt}\sin\left(\omega_c t\right) + \frac{ds_Q(t)}{dt}\cos\left(\omega_c t\right)\right]dt\,, \tag{4.10}$$

where notation dy/dt refers to derivative of y with respect to t. Now since the rate of change in the lowpass signals $s_I(t)$ and $s_Q(t)$ is relatively small compared to the rate of change in the sine and cosine components of the signal, and because the integral term of (4.10) would still result on something divided by a very high value (ω_c), we can approximate (4.10) as

$$r_{n,CS}^{jit} \approx \frac{1}{\omega_c}\Big[s_I(t_{n,2}^{jit})\sin\left(\omega_c t_{n,2}^{jit}\right) + s_Q(t_{n,2}^{jit})\cos\left(\omega_c t_{n,2}^{jit}\right) - s_I(t_{n,1}^{jit})\sin\left(\omega_c t_{n,1}^{jit}\right) - s_Q(t_{n,1}^{jit})\cos\left(\omega_c t_{n,1}^{jit}\right)\Big]. \tag{4.11}$$

Once again, the sine and cosine signals vary much more rapidly than the corresponding I and Q component signals, because from that we know that the small timing error in the overall signal has dominating effect on the sine and cosine terms compared to the effect on the I and Q components of the signal [64]. Therefore, (4.11) can be approximated as

$$r_{n,CS}^{jit} \approx \frac{1}{\omega_c}\Big[s_I(t_{n,2})\sin\left(\omega_c t_{n,2}^{jit}\right) + s_Q(t_{n,2})\cos\left(\omega_c t_{n,2}^{jit}\right) - s_I(t_{n,1})\sin\left(\omega_c t_{n,1}^{jit}\right) - s_Q(t_{n,1})\cos\left(\omega_c t_{n,1}^{jit}\right)\Big]. \tag{4.12}$$

Here, $t_{n,1} = nT_s - T_i/2$ and $t_{n,2} = nT_s + T_i/2$, so the jitter effect was removed from the low-frequency lowpass-signals. Now with the trigonometric identity for sum of angles and well-known small phase approximation ($\varepsilon \ll 1 : \sin(\varepsilon) \approx \varepsilon, \cos(\varepsilon) \approx 1$), (4.12) can be rewritten as

$$\begin{aligned} r_{n,CS}^{jit} \approx \frac{1}{\omega_c}\Big\{ & s_I(t_{n,2})\Big[\sin\left(\omega_c t_{n,2}\right) + \omega_c \delta_{n,2}\cos\left(\omega_c t_{n,2}\right)\Big] \\ & + s_Q(t_{n,2})\Big[\cos\left(\omega_c t_{n,2}\right) - \omega_c \delta_{n,2}\sin\left(\omega_c t_{n,2}\right)\Big] \\ & - s_I(t_{n,1})\Big[\sin\left(\omega_c t_{n,1}\right) + \omega_c \delta_{n,1}\cos\left(\omega_c t_{n,1}\right)\Big] \\ & - s_Q(t_{n,1})\Big[\cos\left(\omega_c t_{n,1}\right) - \omega_c \delta_{n,1}\sin\left(\omega_c t_{n,1}\right)\Big]\Big\}. \end{aligned} \tag{4.13}$$

Now, if we want to analyse the error of the jitter, the ideal sampled waveform $r_{n,CS}$ in (4.7) should be subtracted from the signal with sampling jitter $r_{n,CS}^{jit}$ in (4.13). By following the same procedure as used when attaining (4.11) from (4.9), the $r_{n,CS}$ in (4.7) can be first approximated as

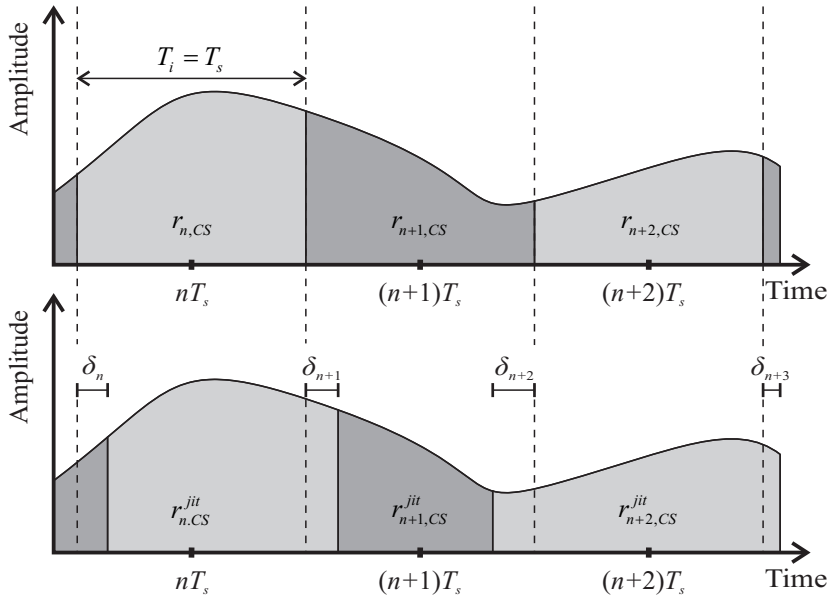

Figure 4-4: Illustration of the charge-sampling without (upper figure) and with (lower figure) sampling jitter in the case where the next integration interval begins immediately after the previous one ends.

$$r_{n,CS} \approx \frac{1}{\omega_c}\Big[s_I(t_{n,2})\sin\left(\omega_c t_{n,2}\right) + s_Q(t_{n,2})\cos\left(\omega_c t_{n,2}\right) - s_I(t_{n,1})\sin\left(\omega_c t_{n,1}\right) + s_Q(t_{n,1})\cos\left(\omega_c t_{n,1}\right)\Big]. \tag{4.14}$$

Therefore, since the approximations of $r_{n,CS}$ in (4.14) and $r^{jit}_{n,CS}$ in (4.13) have many of the same terms, the approximate error due to sampling jitter can simply be written as

$$\begin{aligned} e^{jit}_{n,CS} &= r^{jit}_{n,CS} - r_{n,CS} \\ &\approx \frac{1}{\omega_c}\Big\{\omega_c\delta_{n,2}\Big[s_I(t_{n,2})\cos\left(\omega_c t_{n,2}\right) - s_Q(t_{n,2})\sin\left(\omega_c t_{n,2}\right)\Big] \\ &\quad -\omega_c\delta_{n,1}\Big[s_I(t_{n,1})\cos\left(\omega_c t_{n,1}\right) - s_Q(t_{n,1})\sin\left(\omega_c t_{n,1}\right)\Big]\Big\} \\ &= \delta_{n,2} r(t_{n,2}) - \delta_{n,1} r(t_{n,1}). \end{aligned} \tag{4.15}$$

So the error is the sum of $\delta_{n,2} r(t_{n,2})$ and $-\delta_{n,1} r(t_{n,1})$, which are the products of the sampling jitter realization and the value of the I/Q signal at different points of time. This is the additive effect of the sampling jitter in general charge-sampling receiver.

Case Study of the Attained Error

The approximate error $e^{jit}_{n,CS}$ derived above depends on the properties of and the relationship between variables $\delta_{n,1}$ and $\delta_{n,2}$, and on the value of function r (I/Q signal) at time moments $t_{n,1}$ and $t_{n,2}$. These on the other hand depend on the implementation of the charge-sampling circuit of the charge-sampling receiver. One way to implement the sampling circuit is proposed, e.g., in [29]. They propose a charge sampling scheme depicted in Figure 4-4,

namely integration interval always begins at the same time that the previous sampling interval ends. This basically means that the integration interval length is the same as the length of the sampling interval, and that the timing of the integration is controlled with a single clock. In this case, since according to Figure 4-4, $\delta_{n,2} = \delta_{n+1,1} \triangleq \delta_{n+1}$ and $r(t_{n,2}) = r(t_{n+1,1}) \triangleq r(t_{n+1})$, the error due to sampling jitter can be rewritten for this special case as

$$e_{n,case}^{jit} \approx \delta_{n+1} r(t_{n+1}) - \delta_n r(t_n) . \tag{4.16}$$

The error at n th sample is thus the sum between $\delta_{n+1} r(t_{n+1})$ and its delayed additive inverse $-\delta_n r(t_n)$. This directly corresponds to the filtering of the signal $\delta_{n+1} r(t_{n+1})$ with digital filter with transfer function $H(z) = 1 - z^{-1}$. In effect, the error is highpass filtered product of the sampling jitter sequence and the corresponding I/Q signal realizations. The filtering effect happens because of the implementation of the sampling circuit, so the filtering effect is not dependent on the properties of the signal or on the properties of the sampling jitter sequence in any way. This case is referred as "case study" from now on.

Analysis of the Attained Error in General

Even though the above case study is one of the logical ways to design the timing of the charge sampling circuit, it is worth to analyse the error due to sampling jitter also in more general case, as there are many ways to implement such circuits [1], [7], [29], [40], [41]. The above mentioned filtering of the spectrum of the error happens only if $\delta_{n,2} = \delta_{n+1,1}$ and $r(t_{n,2}) = r(t_{n+1,1})$. In general case, the error of the sampling jitter is given by (4.15), and the timing process of general charge-sampling receiver is depicted in Figure 4-3.

In general, the most prominent note of the properties of the error caused by the timing jitter is that it is just a sum between $\delta_{n,2} r(t_{n,2})$ and $-\delta_{n,1} r(t_{n,1})$. This, in effect, means that the spectral shape of the error in general strongly depends on the spectral shape of the signal $r(t)$ and the sampling jitter. For example, the discussed filtering effect can still be mildly visible when $\delta_{n,2}$ and $\delta_{n+1,1}$, and $r(t_{n,2})$ and $r(t_{n+1,1})$ correlate with each other. Since sampling frequency is usually assumed relatively high in the direct-RF-sampling receivers utilizing charge sampling, there probably is heavy correlation between values $r(t_{n,2})$ and $r(t_{n+1,1})$. Also, the correlation between $\delta_{n,2}$ and $\delta_{n+1,1}$ exists if the sampling-clock signal is generated with some sophisticated method such as PLL, which would cause clear dependence between subsequent sampling jitter realizations. It should be noted however, that if the sampling jitter is plain white Gaussian noise, the resulting spectrum of the sampling jitter is approximately merely that of the white Gaussian noise itself, no matter what are the properties of the sampled signal. This is trivial to show by studying the autocorrelation of the jitter error $R_{e,jit}(n,k) = \mathrm{E}\left[e_{n,CS}^{jit} \, e_{k,CS}^{jit} \right]$, which can be approximately written as

$$\begin{aligned} R_{e,jit}(n,k) &= \mathrm{E}\left[e_{n,CS}^{jit}\, e_{k,CS}^{jit} \right] \approx \mathrm{E}\left\{ \left[\delta_{n,2} r(t_{n,2}) - \delta_{n,1} r(t_{n,1}) \right] \left[\delta_{k,2} r(t_{k,2}) - \delta_{k,1} r(t_{k,1}) \right] \right\} \\ &= \mathrm{E}\left[\delta_{n,2} r(t_{n,2}) \delta_{k,2} r(t_{k,2}) \right] - \mathrm{E}\left[\delta_{n,2} r(t_{n,2}) \delta_{k,1} r(t_{k,1}) \right] \\ &\quad - \mathrm{E}\left[\delta_{n,1} r(t_{n,1}) \delta_{k,2} r(t_{k,2}) \right] + \mathrm{E}\left[\delta_{n,1} r(t_{n,1}) \delta_{k,1} r(t_{k,1}) \right] \\ &= \mathrm{E}\left[\delta_{n,2} \delta_{k,2} \right] \mathrm{E}\left[r(t_{n,2}) r(t_{k,2}) \right] - \mathrm{E}\left[\delta_{n,2} \delta_{k,1} \right] \mathrm{E}\left[r(t_{n,2}) r(t_{k,1}) \right] \\ &\quad - \mathrm{E}\left[\delta_{n,1} \delta_{k,2} \right] \mathrm{E}\left[r(t_{n,1}) r(t_{k,2}) \right] + \mathrm{E}\left[\delta_{n,1} \delta_{k,1} \right] \mathrm{E}\left[r(t_{n,1}) r(t_{k,1}) \right], \end{aligned} \tag{4.17}$$

and when $n \neq k$ and the sampling jitter terms are white Gaussian noise, (4.17) can be rewritten and calculated as

$$\begin{aligned} R_{e,jit}(n,k) &= \mathrm{E}\left[\delta_{n,2} \delta_{k,2} \right] \mathrm{E}\left[r(t_{n,2}) r(t_{k,2}) \right] - \mathrm{E}\left[\delta_{n,2} \delta_{k,1} \right] \mathrm{E}\left[r(t_{n,2}) r(t_{k,1}) \right] \\ &\quad - \mathrm{E}\left[\delta_{n,1} \delta_{k,2} \right] \mathrm{E}\left[r(t_{n,1}) r(t_{k,2}) \right] + \mathrm{E}\left[\delta_{n,1} \delta_{k,1} \right] \mathrm{E}\left[r(t_{n,1}) r(t_{k,1}) \right] \\ &= 0 . \end{aligned} \tag{4.18}$$

Therefore, the properties of the error caused by the sampling jitter heavily depend on the design of the timing of the charge sampler, and not only on the properties of the sampling jitter as in the voltage sampling case.

Simulations and Simulation Analysis

The previous results are verified here with simulations. In the simulations, 3GPP-LTE downlink like OFDM signal with bandwidth of 15.36 MHz is generated. First, the signal is 2^{18} times oversampled for the charge-sampling modelling purposes resulting in simulator sampling frequency of 4.0265 THz, and the baseband signal is then I/Q modulated around a carrier frequency of 867.5 MHz. The selected carrier frequency is the 3GPP-LTE downlink frequency-band number 18. Now since in this study only the properties of the sampling jitter after the charge-sampling reception are interesting, at this point already, the charge-sampling receiver with sampling jitter is modelled. The charge-sampling receiver is modelled so that the modelled sampling frequency of the receiver is 3932.16 MHz, which provides 256 times oversampling for the OFDM waveform, but still allows us to model the charge sampler and its sampling jitter with the remaining 1024 times oversampling (from the original 2^{18}). Furthermore, linear interpolation is used in addition to oversampling, to model the sampling-jitter impaired waveform accurately. The simulations are run for simulated case (in which whole receiver is simulated) and for semianalytic case. The semianalytic case is based on simulated signals and sampling jitter realizations, but the resulting sampling-jitter error is generated simply by using (4.15). Also, in the results for the case study, scaled amplitude spectrum of the expected filtering effect $H(z) = 1 - z^{-1}$ is also depicted in the figures. The used sampling-jitter models are white-Gaussian-noise type jitter and sampling jitter generated

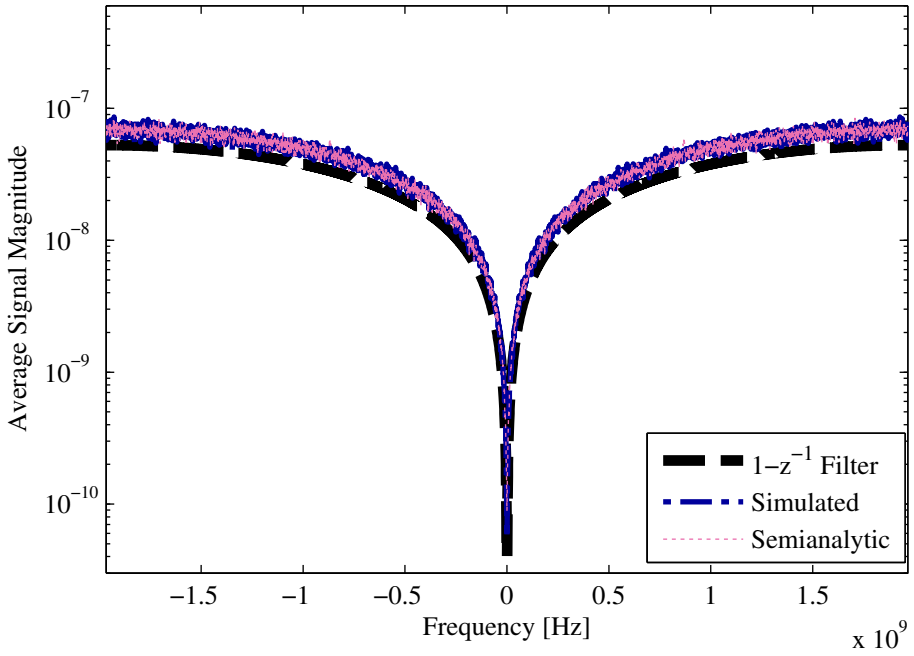

Figure 4-5: Spectrum of the error due to white-Gaussian-noise sampling-jitter with 20 ps RMS value. In case with $T_s = T_i$ for the case study.

by PLL oscillator with the presented oscillator model of [P8]. Model of very low-quality PLL oscillator (with parameters $L(\Delta\omega_w)$ = −60 dBc/Hz at $\Delta\omega_w$ = 1 MHz, $L(\Delta\omega_f)$ = −35 dBc/Hz at $\Delta\omega_f$ = 10 kHz, $L_{CO}(\Delta\omega_{w,CO})$ = −120 at $\Delta\omega_{w,CO}$ = 1 MHz, and γ_c = 57.6 kHz.) is used so that the results are easier to depict with spectral plots (of reasonable accuracy.)

The first thing that meet the eye in the simulations, from Figure 4-5 to Figure 4-9, is that the simulated and semianalytic results are in every figure on top of each other, so the simulations verify the derived formula (4.15) for the sampling-jitter error. The Figure 4-5 and Figure 4-6 depict the results for the case study. As expected, the filtering effect is clearly visible in both of the figures, namely in case with white-Gaussian-noise type sampling jitter and in case of PLL-generated sampling jitter. From Figure 4-5, we see how the originalally white-Gaussian-noise like spectrum is now closely following the scaled amplitude-response of the filter. From Figure 4-6 on the other hand, we see the same effect on the PLL-generated sampling jitter error. Figure 4-7 depicts the case in which the timing signal is generated by PLL for beginnings and ends of the sampling intervals independently when $T_s = T_i$. Now, we see that there is no filtering effect what-so-ever. We see approximately the same spectrum shape of the error that we have in case of voltage sampling, when in VS the timing of the sampling is controlled by the similar PLL. In Figure 4-8 and Figure 4-9 the sampling jitter is generated with single PLL for the whole sampling process, meaning that there is clear

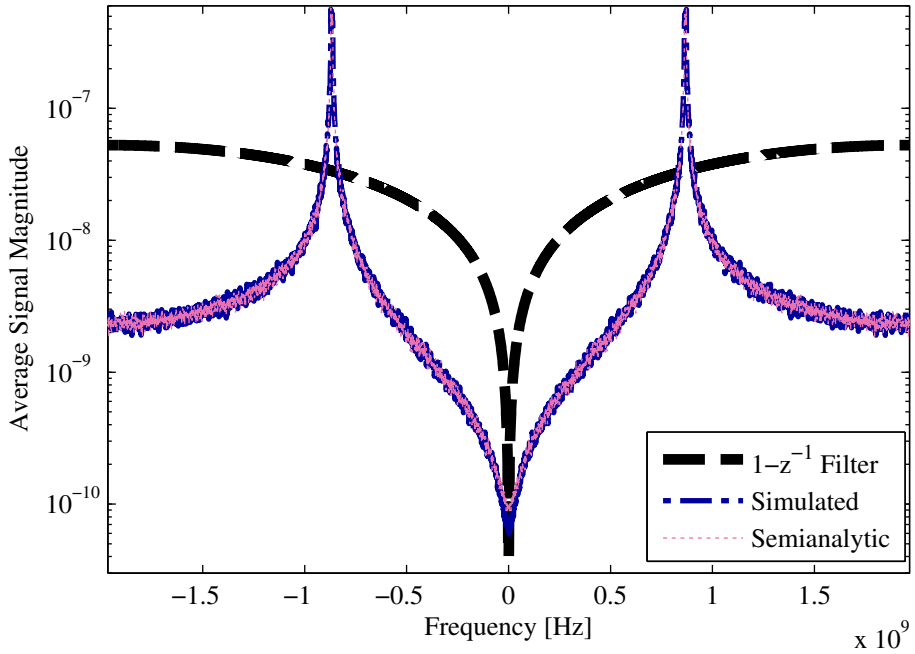

Figure 4-6: Spectrum of the error due to PLL-generated sampling-jitter with 20 ps RMS value. In case with $T_s = T_i$ for the case study.

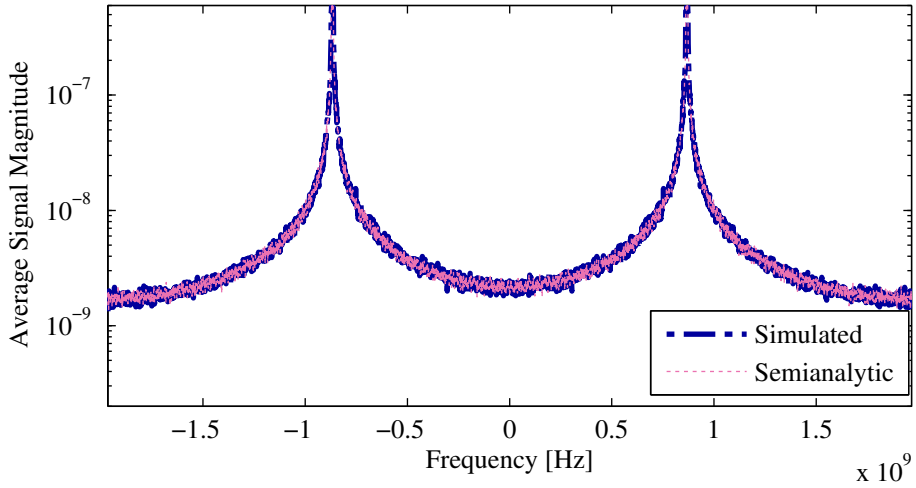

Figure 4-7: Spectrum of the error due to PLL-generated sampling-jitter with 20 ps RMS value. In case with $T_s = T_i$, but the sampling jitter at the beginnings and ends of the integrations intervals are generated independently of each other.

correlation between the end of the previous and the beginning of the current integration intervals. From Figure 4-8 we see the case when $T_s = 2T_i$. The filtering effect is still clearly visible, when comparing the centre and edge parts of the spectrum to those of the Figure 4-7, where no filtering effect is present. In case with $T_s = 4T_i$ depicted in Figure 4-9, the filtering effect is hardly visible anymore, because the distance between the edges of the subsequent integration intervals increases, and the correlation between the integration boundaries gets smaller.

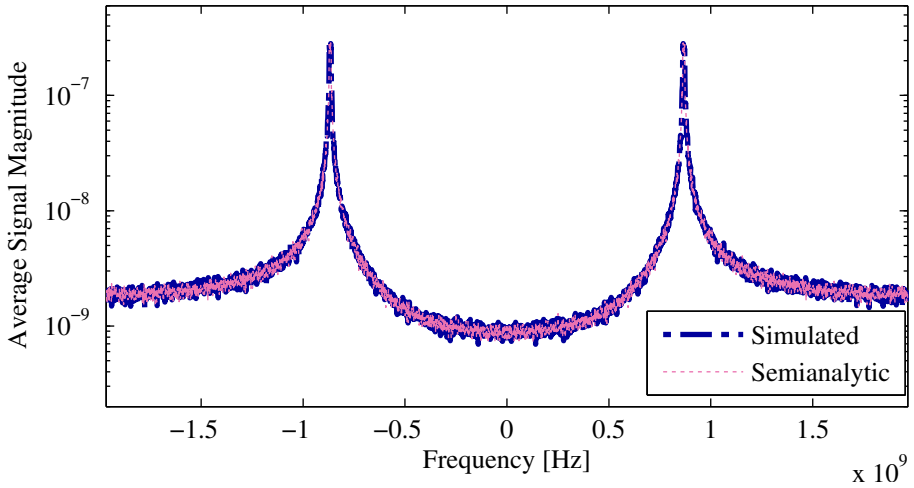

Figure 4-8: Spectrum of the error due to single PLL-generated sampling-jitter process with 20 ps RMS value in case with $T_s = 2T_i$.

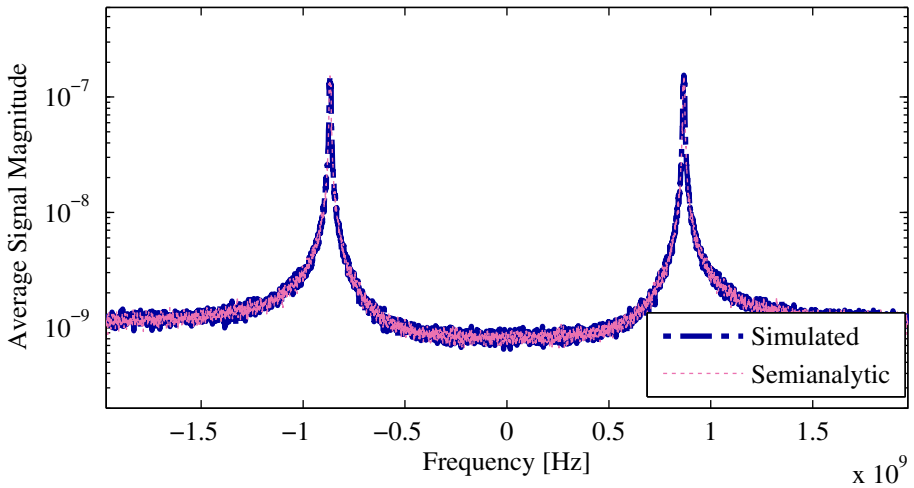

Figure 4-9: Spectrum of the error due to single PLL-generated sampling-jitter process with 20 ps RMS value in case with $T_s = 4T_i$.

Further Thoughts on the Results and Application to Receiver Dimensioning

A good example how the results can be used in receiver design is visualized in Figure 4-10. There, the signal filtering due to basic charge sampling is depicted with the response of the sampling-jitter noise in the case study. The signal-to-jitter-noise density gain curve then gives the gain due to shaping of the sampling-jitter error in comparison to the case without the shaping. Also signal-to-noise density ratio due to additive noise (signal-to-noise ratio is 40 dB prior sampling) and sampling jitter (white-Gaussian-noise with power 30 dB below the useful signal level) is depicted in the figure. Basically of all the curves, the signal-to-jitter density gain curve is most valuable for general purposes from the sampling-jitter analysis point-of-view, since it gives directly the gain of the analysed error shaping. It can be seen that some gain due to spectral shaping of the sampling-jitter error can be achieved, but only when

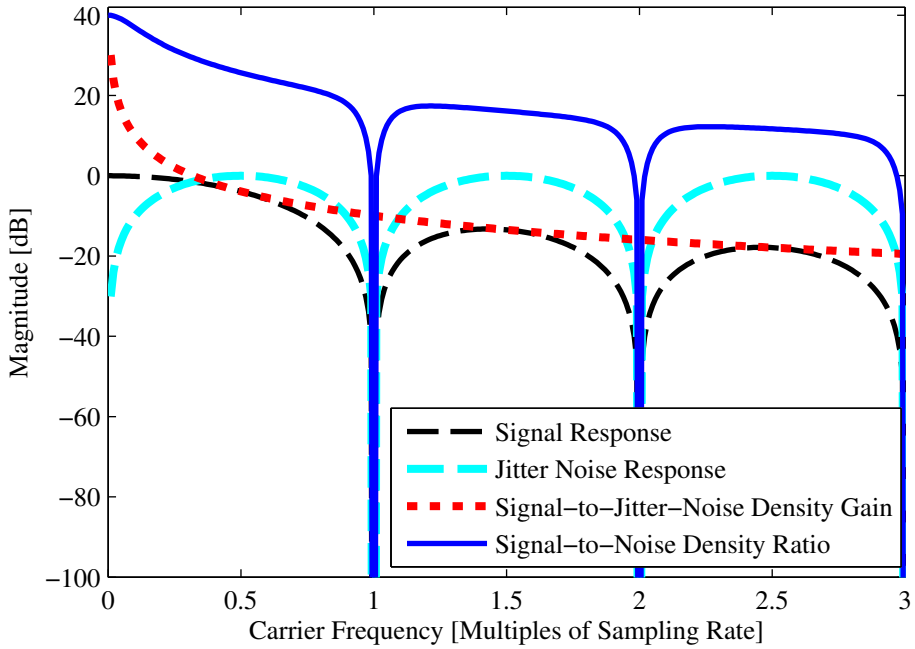

Figure 4-10: Filtering responses of the signal and the corresponding sampling jitter noise in the case study. Also the gain given by the shaping of the sampling-jitter caused error compared to no-shaping case is depicted. Furthermore, the corresponding signal-to-noise density ratio due to additive noise and sampling-jitter noise is given when signal-to-noise ratio is 40 dB is prior the sampling and the white-Gaussian-noise sampling-jitter is 30 dB under the signal level.

oversampling ratio is very high, namely when the centre frequency of the sampled signal is less than 1/3 of the sampling frequency. In direct-RF sampling, this might mean sampling frequency in order of 3-6 GHz when centre frequencies in the order of 1-2 GHz are considered. When these levels of sampling frequencies are not achievable, the results support not using the same timer for the beginning and for the end of the integration intervals.

Chapter 5

Phase Noise Mitigation in OFDM Receivers

The task of phase-noise estimation and mitigation in OFDM radios is one of the main topics of this thesis. Phase-noise effect on OFDM signals is very severe and complicated of nature, so there has not been very good algorithms to get rid of the phase-noise effects from OFDM signals until recently. In the literature, first, only CPE mitigation was considered, e.g., in [51]. This was natural approach as CPE has potentially very serious effect on the OFDM signal if free-running oscillator is used. However, CPE is hardly a problem in wireless communications link, since in conventional channel estimation techniques also the effect of the CPE is usually estimated as a part of the channel. Furthermore, if the phase noise is just jitter around the nominal phase, as is the case, e.g., in PLL oscillator, the CPE alone is merely a minor problem, because the strength of the CPE caused constellation rotation depends on the average phase error from the nominal phase during the duration of one OFDM symbol. However, if multipath communications channel is assumed not present, like e.g. with additive white-Gaussian-noise channel assumption, the CPE estimation is interesting because it is simpler than doing the channel estimation. Furthermore, if channel is assumed known, CPE estimation is interesting for the analysis of ICI mitigation algorithms.

The mitigation of the ICI part of the phase noise has also received extensive attention in the literature. In [73], general phase noise mitigation technique mitigating CPE and ICI has been considered. More advanced iterative algorithm for phase noise mitigation, where also the lowpass nature of the phase noise process was taken into account, was proposed in [45]. The iterative part of the technique was further improved in [9] by coding, and the actual phase noise compensation part was further improved in [10].

This thesis proposes some new algorithms for phase-noise mitigation. The first algorithm is computationally efficient way to estimate ICI with simple linear interpolation of CPE estimates first proposed in [P1]. The idea is to interpolate the CPE estimates from the middle

sample of one OFDM symbol to the middle samples of the adjacent OFDM symbols. The idea works surprisingly well and performs almost as good as much more complex algorithms in the literature. Another idea is proposed in [P1] and [P5], and is based on the same problem setting as the technique proposed in [10], but was invented independently during the publication process of [10] and gives much better performance. The idea is relatively simple. During simulations, the author noticed that the algorithm in [45] provided very bad phase noise estimates at the beginning and at the end of each OFDM symbol. Due to continuous nature of the phase noise, the phase noise estimates can however be interpolated over the interval in which the estimates are poor. This algorithm provided better performance than the algorithms existing in the literature at the time of publication.

The thesis also proposes two new ideas for phase-noise mitigation. They are iterative time-domain phase-noise mitigation algorithms, which have first been published in [P7] and [P10]. The idea in both is to detect the received signal after only the CPE of the phase noise is mitigated, and then to reconstruct the phase-noise-free received signal. This signal is then used for phase noise estimation by comparing it to the actually received signal with phase noise still present. The obtained phase-noise estimate is used to clean the original received signal after which it is detected again, and the whole process is iterated. Both algorithms give significant performance improvement compared to the existing algorithms in the literature.

In the rest of this chapter, selected state-of-the-art phase-noise mitigation algorithms for OFDM are shortly presented. Then, the proposed algorithms are presented in detail, and their performance is compared to the performance of the state-of-the-art algorithms. Also, practical channel estimation aspects are shortly discussed from the phase noise mitigation perspective.

5.1. State of the Art in Phase Noise Estimation and Mitigation

This section presents the state of the art in phase-noise mitigation algorithms prior the algorithms proposed in this thesis. First, simple CPE mitigation technique proposed in [72] is presented as it is usually needed in more advanced iterative ICI mitigation techniques to get the initial detection result. Then, more advanced algorithm, namely the ICI mitigation algorithm proposed in [45], is presented in detail, followed by the detailed presentation of the improvement to the algorithm proposed in [10]. The method in [10] was developed parallel, and independently, to the algorithms of [P1] proposed in this thesis.

CPE Estimation and Mitigation

CPE is a multiplication by the same complex number that all the subcarrier symbols within an OFDM symbol experience [54], [67]. CPE estimation techniques therefore merely estimate the common complex multiplier for all the subcarriers of an OFDM symbol. Such estimation techniques have been proposed, e.g., in [51], [56], [69] and [72]. The techniques are usually similar, and basically just solve the problem of CPE estimation with averaging the estimated

CPE values at pilot subcarriers using least squares (LS) estimation. So directly from [72], the LS solution for CPE during m th OFDM symbol can be written as

$$\hat{J}_0(m) = \frac{\sum_{k \in S_p} R_k(m) X_k^*(m) H_k^*(m)}{\sum_{k \in S_p} \left| X_k(m) H_k(m) \right|^2}. \quad (5.1)$$

Where the notations follow the basic signal modelling presented in (3.28)-(3.32). Here, S_p is a set of pilot subcarriers. In this thesis, LS estimate in (5.1) is always used for the CPE estimation, because of its computational simplicity. After computing the LS estimate for the individual OFDM symbols, the mitigation of the CPE is very simple. Just division of the received subcarrier symbol values with the corresponding CPE estimate is required.

ICI Estimation and Mitigation

The ICI is the more complex part of the phase noise effect, and thus also its estimation is more complex than the estimation of the CPE. When CPE is mitigated from the signal, the remaining time-domain phase noise contribution for individual OFDM symbols is just the same as the original with only one exception: the mean of the remaining phase noise is approximately zero. The zero-mean phase noise causes the ICI. The problem of estimating and mitigating the ICI has been widely studied in the literature. Some examples are the studies in [8], [9], [10], [11], [12], [13], [14], [18], [19], [25], [26], [27], [36] [43], [45], [47], [48], [50], [73] and [75]. Of these, in [19], [48], [50] and [75] the phase noise is compensated jointly with either channel and/or other transceiver impairments, such as I/Q imbalance. Joint phase-noise mitigation and data-detection algorithms are proposed, in [36], and the improvements to the ideas are proposed in [25], [26] and [27]. Examples of time-domain phase-noise mitigation algorithms are given, e.g., in [18] and [75]. The algorithm in [18] is based on estimating the most dominant discrete-cosine-transform terms of the phase noise. The algorithm is then enhanced in [14] by iteratively using the non-pilot symbols in the phase-noise estimation process. Another time-domain algorithm based on Kalman tracking is proposed in [8]. The frequency-domain ICI-mitigation algorithm proposed in [45] is based on two simple but significant ideas, i.e., iterative estimation of the phase noise and exploiting the knowledge that most information of the phase noise can be recovered from the first few terms of its discrete Fourier transform. Its performance is improved in [9] and [10], by means of improving the estimation algorithm and exploiting the information given by coding, respectively. Also, relatively low-complexity non-iterative algorithm with frequency-domain phase-noise mitigation is presented in [47]. It also exploits the idea of estimating only few of the most dominant terms of the Fourier transform of the phase noise. In the paper, the other presented technique, which is based on interpolation, is almost identical to the CPE interpolation technique proposed by the author of this thesis previously in [P1] (it is also one

of the contributions of this thesis). Also, in [71], they propose similar algorithm. It should be noted that the publications [47] and [71] were published in late 2010 and 2011, respectively, whereas the author's algorithm was published in [P1] already in early 2009.

From all the available ICI mitigation algorithms, the algorithm of [45] with its expansion in [10] are presented as the state-of-the-art algorithms in more detail, because they provide excellent performance with reasonable complexity. Another reason is the fact that the algorithm of [45] is easily modified without noticeable performance loss to a LS-based algorithm, which does not require prior knowledge about the statistics of the phase noise. The idea is based on the frequency-domain signal model presented in (3.32). By modelling the signal, while keeping in mind the assumption that most of the ICI effect of the phase noise is indeed in its first u spectral components on the both sides of the DC bin, we are able to rewrite (3.32) as

$$R_k(m) = \sum_{l=-u}^{u} X_{k-l}(m)H_{k-l}(m)J_l(m) + \upsilon_k(m) = \sum_{l=-u}^{u} A_{k-l}(m)J_l(m) + \upsilon_k(m), \tag{5.2}$$

where for simplicity we have substituted $X_k(m)H_k(m)$ with $A_k(m)$, and $\upsilon_k(m)$ denotes the term with combined effect of additive noise and the ICI contribution outside the spectral components range $[-u, u]$. Now if this equation is written only for subcarriers $k \in \{l_1, l_2, \ldots, l_P\}$, where $P \geq 2(u+1)$, we can write a solvable matrix equation as

$$\begin{bmatrix} R_{l_1}(m) \\ R_{l_2}(m) \\ \vdots \\ R_{l_P}(m) \end{bmatrix} = \begin{bmatrix} A_{l_1+u}(m) & A_{l_1+u-1}(m) & \cdots & A_{l_1-u}(m) \\ A_{l_2+u}(m) & \ddots & \ddots & \vdots \\ \vdots & \ddots & \ddots & \vdots \\ A_{l_P+u}(m) & \cdots & \cdots & A_{l_P-u}(m) \end{bmatrix} \begin{bmatrix} J_{-u}(m) \\ J_{-u+1}(m) \\ \vdots \\ J_u(m) \end{bmatrix} + \begin{bmatrix} \upsilon_{l_1}(m) \\ \upsilon_{l_2}(m) \\ \vdots \\ \upsilon_{l_P}(m) \end{bmatrix}. \tag{5.3}$$

This can be written compactly as $\mathbf{R}_{m,P} = \mathbf{A}_{m,u}\mathbf{J}_{m,u} + \boldsymbol{\Upsilon}_{m,P}$, where $\mathbf{R}_{m,P}$ and $\boldsymbol{\Upsilon}_{m,P}$ are $(P \times 1)$ vectors, $\mathbf{J}_{m,u}$ is $(2u+1 \times 1)$ vector and $\mathbf{A}_{m,u}$ is $(P \times 2u+1)$ matrix. From this it is easy to estimate the most prominent ICI components $\mathbf{J}_{m,u}$ with LS estimation as

$$\hat{\mathbf{J}}_{m,u} = \left(\mathbf{A}_{m,u}^H \mathbf{A}_{m,u}\right)^{-1} \mathbf{A}_{m,u}^H \mathbf{R}_{m,P}. \tag{5.4}$$

In order to compute the above estimate, $\mathbf{A}_{m,u}$ needs to be known. In the algorithm, the detection results after the CPE mitigation are used, and then for the next iteration the detection result from the previous iterations are used. Channel estimates or prior channel knowledge are also needed for the computation of the estimate. Instead of the above LS solution, we could also use, e.g., minimum mean-square error (MMSE) estimation, but we would then also need to know more about the statistics of the phase-noise process in order to use it. Furthermore, the simulations by the author showed that the performance improvements are almost non-existent. This is why in this thesis only the LS version of the estimation

algorithm is used as a reference technique. Another reason is that the algorithms proposed in this thesis do not require any prior information about the statistics of the phase noise process, so for fairness that should be the case also with the reference algorithms.

After the estimation of the most prominent spectral components of the phase noise, the actual mitigation can simply be done by taking deconvolution between the received signal after the DFT and the estimated truncated-DFT of the phase noise in (5.4). The signal can then be detected, put through further iterations, or just further processed with different algorithms, as seen necessary.

Modified ICI Estimation

Using heavily truncated Fourier transform to estimate a non-periodic signal, such as the phase noise sequence, is a problem, because strictly speaking DFT assumes that the time-domain signal is periodic, while phase noise in general is a nonperiodic process. That is not a problem with non-truncated version of the DFT, but truncating DFT makes the periodicity assumption very prominent in the corresponding time-domain signal [10], [P1].

In [10], they discuss and propose a solution to the problem that arises from using truncated DFT in the ICI estimation algorithm of [45]. The proposed solution is very simple, and is based on mapping the received time-domain signal vector so that the edge parts of an OFDM symbol are mapped to the centre part of the vector. The mapping can be done with time-domain multiplication with permutation matrices of the form

$$\begin{aligned} \mathbf{p}_r &= \left[\mathbf{e}_{N/2+1}, \mathbf{e}_{N/2+2}, \ldots, \mathbf{e}_N, \mathbf{e}_{N-1}, \ldots, \mathbf{e}_{N/2}\right]^T, \\ \mathbf{p}_l &= \left[\mathbf{e}_{N/2}, \mathbf{e}_{N/2-1}, \ldots, \mathbf{e}_1, \mathbf{e}_2, \ldots, \mathbf{e}_{N/2+1}\right]^T. \end{aligned} \tag{5.5}$$

Here, $\mathbf{p}_r$ and $\mathbf{p}_l$ are the size ($N \times N$) permutation matrices for the right and left edge, respectively. $\mathbf{e}_n$ is a unit vector of length N, which has unity as its nth element and other elements are zeros. This kind of a mapping in time domain finally corresponds to mapping the truncated frequency-domain phase-noise estimate with discrete Fourier transforms $\widehat{\mathbf{P}}_r$ and $\widehat{\mathbf{P}}_l$ of the permutation matrices $\mathbf{p}_r$ and $\mathbf{p}_l$. So what we actually need to do is to multiply the truncated phase noise estimate $\hat{\mathbf{J}}_{m,u}$ (filled with zeros to be size $N \times 1$) with $\widehat{\mathbf{P}}_r$ and $\widehat{\mathbf{P}}_l$. When calculating the matrix multiplication in the receiver, naturally only non-zero elements of the $\hat{\mathbf{J}}_{m,u}$ are interesting, so $\widehat{\mathbf{P}}_r$ and $\widehat{\mathbf{P}}_l$ can be modified smaller accordingly, and full matrix multiplication does not need to be done. The resulting sequence is then transformed to the time domain, and the samples corresponding the estimated phase noise at the edges are picked and used as new phase-noise estimates, instead of using the estimates provided by $\hat{\mathbf{J}}_{m,u}$. In [10], the edge substation window on the both sides was proposed to be around 6 % of the OFDM symbol length, which also gave the best results in the simulations done by the author [P1].

Compared to the algorithm of [45], the complexity is increased because we need some extra computations. Most burdensome of the needed extra computations result from the fact that the signal needs to be processed in the time-domain, so the signal needs to be transformed to the frequency-domain again. Depending on the receiver implementation, this results to at least one extra DFT.

5.2. Contributions to Phase Noise Estimation and Mitigation

In this section, all the phase noise mitigation algorithms proposed in this thesis work are presented and summarized. First, a very simple technique to improve the CPE estimates with linear interpolation is presented. This is followed by the presentation of the technique to improve the performance of the state-of-the-art technique of [45]. Both of these techniques were first published in [P1]. Then, two iterative time-domain phase-noise mitigation techniques are presented. These were first published in [P7] and [P10].

ICI Estimation Technique Using CPE Interpolation (LI-CPE) [P1]

The idea of the first ICI estimation technique proposed in this thesis, called LI-CPE, is very simple [P1]. It is based on the fact that the CPE estimate for an OFDM symbol is approximately the mean of the phase noise sequence during that symbol. Because of this, the CPE corresponds to the exact value of the phase noise most likely in the middle of the OFDM symbol. Then, if we interpolate between the CPE values of adjacent OFDM symbols, from middle of one OFDM symbol to the middle of the adjacent OFDM symbols, we have a crude estimate of the phase noise with CPE and ICI taken into account. To improve the estimate a little, we also scale the interpolation result by replacing the DC bin of the attained phase noise estimate with the original CPE estimate. This is logical since CPE estimates are relatively reliable. Interpolation on the other hand has changed the CPE estimate, so replacing it with more reliable one, gives improved estimate. Illustration of the technique is given in Figure 5-1. In the figure, the small hops at the OFDM symbol boundaries are resulting from the CPE replacement.

The interpolation in this technique can be done in various ways. In this thesis, however, only simple linear interpolation is used. The reason for this choice is not only the fact that linear interpolation is very simple to do, but also the fact that if we interpolate between two points of random walk (Wiener) process, the linear interpolation is actually approximately the optimum way to do the interpolation [75].

It should be noted that using this technique imposes a delay of one OFDM symbol, since we cannot get the full interpolation result before the estimation of the CPE of the next symbol has been done.

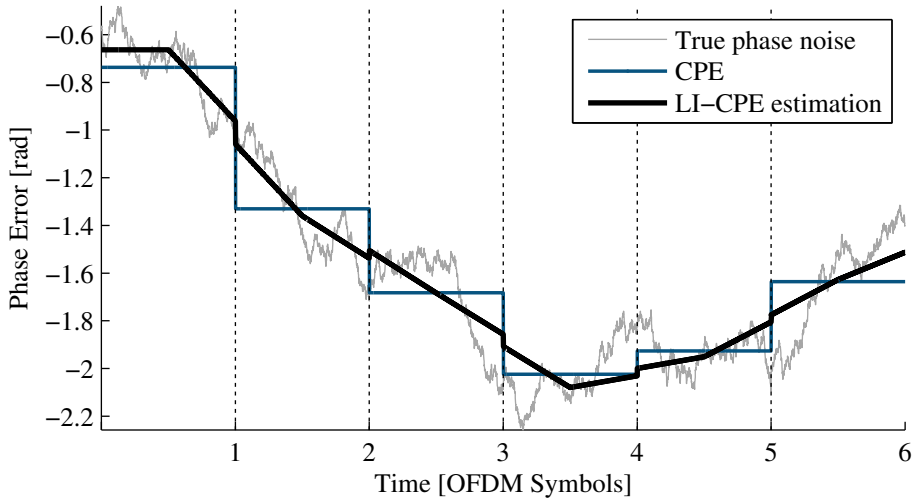

Figure 5-1: Illustration of the phase noise sequence, the corresponding CPE estimate and the estimation result given by the LI-CPE technique.

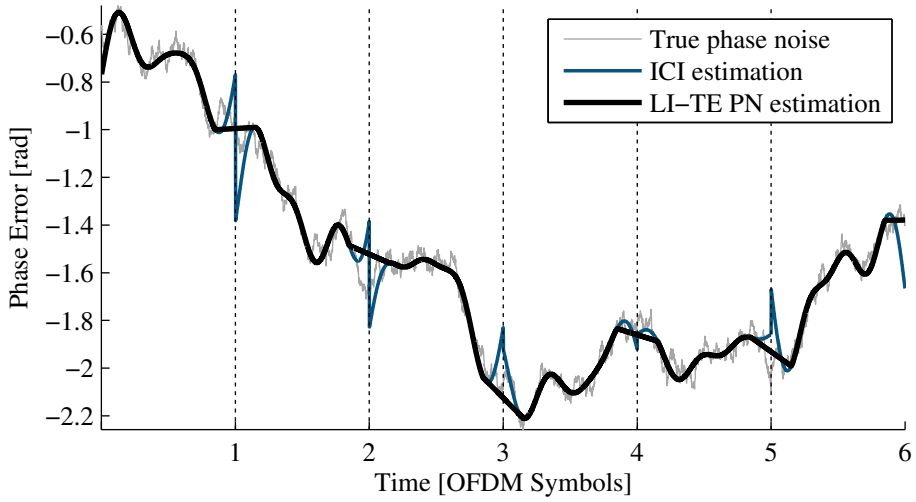

Figure 5-2: Illustration of the phase noise sequence and the corresponding ICI estimation result given by algorithm of [45] and by the proposed LI-TE technique.

Iterative ICI Estimation Technique Using Tail Interpolation (LI-TE) [P1]

The second ICI estimation technique is based on the ICI estimation algorithm of [45]. Before having access to [10], also the author of this thesis noticed the poor performance of the algorithm of [45] at the OFDM symbol boundaries. The poorness was clear when plotting the time-domain phase-noise estimate versus the actual phase-noise sequence. This comparison is depicted in Figure 5-2. The peaks at the OFDM symbol boundaries are very clear and relatively wide, and the values of the estimates during these peaks differ from the underlying phase noise sequence relatively much. Mathematically the effect results from the truncation of the DFT done in the algorithm of [45].

To effectively combat the peaking effect of the algorithm of [45], this thesis proposes a new technique, called LI-TE, for improving the estimates at the OFDM symbol boundaries.

The author's simulation showed that already continuing the last reliable estimate of the phase noise to the edge of the OFDM symbol gives very impressive performance improvement. However, to further improve the estimate, once again, interpolation is proposed. In LI-TE technique, interpolation is done from the last reliable phase-noise estimate of the previous OFDM symbol to the first reliable estimate of the phase noise of the current OFDM symbol. So once again the idea is very simple, and like with LI-CPE, only the very simple linear interpolation is used in this thesis. According to empirical analysis, the optimal interpolation window is around 15 % of the total OFDM symbol length at the both edges of the OFDM symbol. In this empirical analysis, cyclic prefix length was assumed 6.15 % of the total OFDM symbol length.

It should be noted that, like LI-CPE, also LI-TE imposes a delay to the system. LI-TE needs the ICI estimation results given by the algorithm of [45] for the previous and the next OFDM symbol, so the first iteration imposes a delay of one OFDM symbol. The delay increases when the number of iterations is increased, if the LI-TE is also used to the next OFDM symbol prior to interpolation. This is not necessary, because the interpolation can be done based on the non-optimal phase-noise estimate of the next OFDM symbol as well. However, the best performance is obtained if LI-TE is done for the next OFDM symbol as well in the iteration loops. This results in one extra delay of one OFDM symbol per iteration. In most cases, already two or three iterations give performance very near to the maximum the technique is capable of [P1], [P5], [P7], so the needed number of iterations is not high. Also, being relatively computationally complex, using many iterations is not so feasible anyway. The technique is around the same class in complexity as the technique in [10].

Channel Estimation Aspects in the Proposed Techniques [P5]

Both the proposed techniques, LI-CPE and LI-TE, rely on the interpolation of phase noise estimates between adjacent OFDM symbols. However, if the channel estimation is done in the conventional way OFDM symbol by OFDM symbol, the CPE is also estimated at the same time, and when channel equalization is done, also the CPE information is lost. CPE information is vital for LI-CPE technique. Also LI-TE needs the CPE information to work optimally, but it still manages to cut the bad peaks in the ICI estimates at the symbol boundaries even when the CPE information is lost. Here, a channel estimation technique which retains the CPE information is proposed. It works with quasistatic channel, and it was first proposed in [P5].

In the proposed channel-estimation algorithm, we first need the channel estimates at the pilot subcarriers. These are usually attained, by using zero-forcing principle as

$$\hat{\mathbf{H}}_{m,pilots} = \mathbf{R}_{m,pilots} \circ / \mathbf{P}_m . \tag{5.6}$$

Here, $\circ/$ is a point-by-point division operator. $\hat{\mathbf{H}}_{m,pilots}$ is a $(P\times 1)$ vector (P is the number of pilots) consisting of the estimate of the channel frequency responses at the pilot subcarriers. $\mathbf{P}_m$ is $(P\times 1)$ vector of sent pilot symbols at the pilot subcarriers. $\mathbf{R}_{m,pilots}$ is $(P\times 1)$ vector of received subcarrier symbols corresponding to the pilot subcarriers. Now if we assume that the channel is quasistatic for the duration of K OFDM symbols, we know that when there is no CPE present, the partial channel estimates $\hat{\mathbf{H}}_{m,pilots}$ should be the estimates of the same channel for the current and the adjacent $K-1$ OFDM symbols. Using this, it is trivial to estimate the relative CPE from the partial channel estimates. The relative CPE in l th OFDM symbol in respect to the CPE in m th OFDM symbol can then be written as

$$\hat{\mathbf{J}}_{l,0,rel} = \hat{\mathbf{H}}_{l,pilots} \circ / \hat{\mathbf{H}}_{m,pilots} . \tag{5.7}$$

As said, this is the relative CPE, which is computed for every OFDM symbol within the quasistatic duration of the channel in respect to m th OFDM symbol. We are actually not interested in the actual CPE value before channel equalization, but we are indeed interested in the relative CPE value, so the interpolation in the phase-noise estimation techniques works as intended. This is because the ICI estimation methods LI-CPE and LI-TE rely on the relative CPE information. We have now P estimates of the relative CPE for each OFDM symbol within the quasistatic duration of the channel in vectors $\hat{\mathbf{J}}_{l,0,rel}$, so to get the final CPE estimate for l th OFDM symbol we can take the mean of the all P CPE estimates within one OFDM symbol as

$$\hat{J}_{0,rel}(m) = \overline{\hat{\mathbf{J}}}_{l,0,rel} , \tag{5.8}$$

where $\overline{\mathbf{x}}$ denotes taking the mean of the elements of vector $\mathbf{x}$. The CPE can then be taken out from the channel estimates before the channel equalization to retain the CPE information in the OFDM symbols. This approach also allows averaging of the channel estimates within the quasistatic windows, which is not directly possible otherwise in the presence of the phase noise. Naturally, if the channel can be assumed to be static during the K OFDM symbols, it is beneficial to average the channel estimates. However, this would not be possible if the relative CPE is not removed first from the channel estimates. After averaging, the partial channel estimates can be used however seen fit in the channel estimation. In this thesis, the total channel estimate is constructed just by using linear interpolation between the adjacent pilot subcarriers.

It should be noted that for LI-CPE and LI-TE algorithms, already the minimum quasistatic case ($K = 3$) is sufficient to make them work very well.

Iterative Time-Domain Phase-Noise Mitigation Algorithm [P7]

The first time-domain algorithm (called here Syrjälä algorithm for consistency, because the

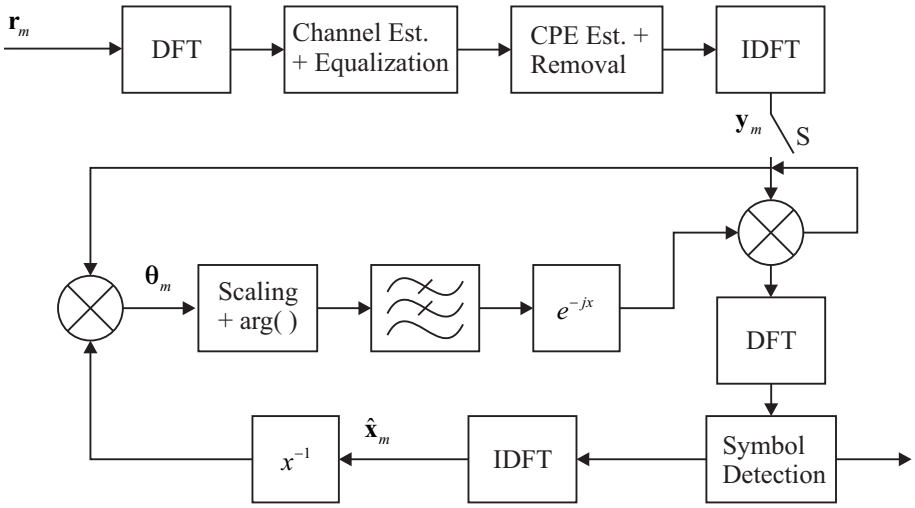

Figure 5-3: Illustration of the first proposed time-domain phase-noise mitigation algorithm (Syrjälä). The switch S passes through the OFDM symbol and then opens. It is open until all the iterations have been completed and the next OFDM symbol is taken in.

author did not name the algorithm in the original publication [P7]) proposed in this thesis was first introduced in [P7], and is depicted in Figure 5-3. The idea is to use time-domain signal, which is reconstructed from the detection results and which therefore is without phase noise and additive noise, and compare that reconstructed signal to the time-domain signal which still has the phase noise present ($\mathbf{y}_m$ in the figure.).

So let us start from the received time-domain signal (3.31) which is corrupted by the noisy oscillator at the transmitter, channel and the noisy oscillators at the receiver. Now as already discussed, (3.31) can be rewritten as

$$\mathbf{r}_m \approx \mathbf{H}_m \,\mathrm{diag}\left(e^{j\boldsymbol{\phi}_m}\right)\mathbf{x}_m + \mathbf{z}_m \,. \tag{5.9}$$

Here, all the phase noise is modelled as transmitter phase noise because it is beneficial in the derivation of the algorithm. After DFT, channel equalization, CPE mitigation and IDFT, (5.9) can be written as

$$\begin{aligned} \mathbf{y}_m &\approx \left(\hat{\mathbf{H}}_{m,CPE}\right)^{-1}\left[\mathbf{H}_m \,\mathrm{diag}\left(e^{j\boldsymbol{\phi}_m}\right)\mathbf{x}_m + \mathbf{z}_m\right] \\ &\approx \mathrm{diag}\left(e^{j\left(\boldsymbol{\phi}_m - \hat{\phi}_{m,CPE}\right)}\right)\mathbf{x}_m + \left(\hat{\mathbf{H}}_{m,CPE}\right)^{-1}\mathbf{z}_m \,. \end{aligned} \tag{5.10}$$

Here, $\hat{\mathbf{H}}_{m,CPE}$ is $(N \times N)$ circulant convolution matrix of the channel estimates which also includes the CPE estimate $\hat{\phi}_{m,CPE}$. Already before the IDFT we are able to do symbol detection for the first iteration of the algorithm, so Figure 5-3 is a little misleading on this part. After the symbols are detected, an estimate of the time-domain OFDM waveform $\hat{\mathbf{x}}_m$ is constructed from the detected symbols with IDFT. This symbol is approximately the input signal of the iterative part of the algorithm, $\mathbf{y}_m$, without phase noise and additive noise

effects. The signal $\mathbf{y}_m$ is then divided by the signal $\hat{\mathbf{x}}_m$, and the result is very crude estimate of the phase noise term given as

$$\begin{aligned}\boldsymbol{\theta}_m &\approx \mathrm{diag}^{-1}\left(\hat{\mathbf{x}}_m\right)\left[\mathrm{diag}\left(e^{j\left(\boldsymbol{\phi}_m-\hat{\phi}_{m,CPE}\right)}\right)\mathbf{x}_m+\left(\hat{\mathbf{H}}_{m,CPE}\right)^{-1}\mathbf{z}_m\right] \\ &\approx e^{j\left(\boldsymbol{\phi}_m-\hat{\phi}_{m,CPE}\right)}+\mathrm{diag}^{-1}\left(\hat{\mathbf{x}}_m\right)\left(\hat{\mathbf{H}}_{m,CPE}\right)^{-1}\mathbf{z}_m\,.\end{aligned} \tag{5.11}$$

Here we take the inverses of elements of vector $\hat{\mathbf{x}}_m$, which can however have zero elements. If there are zero elements, the resulting value from the inverse operation is set to zero. This selection is done, because it forces the estimation algorithm to ignore zero values of the $\hat{\mathbf{x}}_m$. If $\mathbf{x}_m$ would have zero values, they would anyway be affected very heavily by the additive noise, so it is better to totally ignore them in the estimation process. At this point, we use the knowledge that phase-noise complex-exponential and the actual phase-noise sequences are steep lowpass processes, so we filter signal $\boldsymbol{\theta}_m$ with lowpass filter to improve the estimate. Prior to filtering however, we scale the signal and take its argument. The scaling is done to give more weight for the samples that have more likely higher amplitudes. This is beneficial because the additive noise affects the low-amplitude samples very heavily and has only mild effect on high-amplitude samples. The dynamics of the signal is very high, because OFDM signal is well-known to have high peak-to-average-power ratio. The scaling is done according to the amplitudes in the reconstructed signal, and can be, e.g. done as

$$\mathbf{q}_m=\frac{\sqrt{2}\left|\hat{\mathbf{x}}_m\right|^2}{N_a/N}\,. \tag{5.12}$$

This is a $(N\times 1)$ vector of scaling factors. $\left|\hat{\mathbf{x}}_m\right|^2$ is a vector consisting of squared absolute values of the elements of the vector $\hat{\mathbf{x}}_m$. N_a is number of active subcarriers. With this scaling, it is assumed that the average power of each active subcarrier is unity and that the channel magnitude response is also unity. The scaling indeed gives exponentially more weight to the higher-amplitude samples of the signal. After scaling, taking an argument and lowpass filtering, the estimate of the phase noise (without the already estimated part of the CPE) can be written as

$$\mathrm{LPF}\left\{\mathrm{diag}\left(\mathbf{q}\right)\arg\left(\boldsymbol{\theta}_m\right)\right\}\approx\boldsymbol{\phi}_m-\hat{\phi}_{m,CPE}\,. \tag{5.13}$$

Here, $\arg(\cdot)$ function gives the argument of the complex exponential. This result is then used as an argument of inverse complex exponential function, and the time-domain input signal of the algorithm, $\mathbf{y}_m$, is sample by sample multiplied by corresponding samples of this. The result is then discrete Fourier transformed and the symbols are detected. The algorithm can then be used iteratively by using these now much improved symbol detection results as a basis of reconstructing a new time-domain reference signal $\hat{\mathbf{x}}_m$.

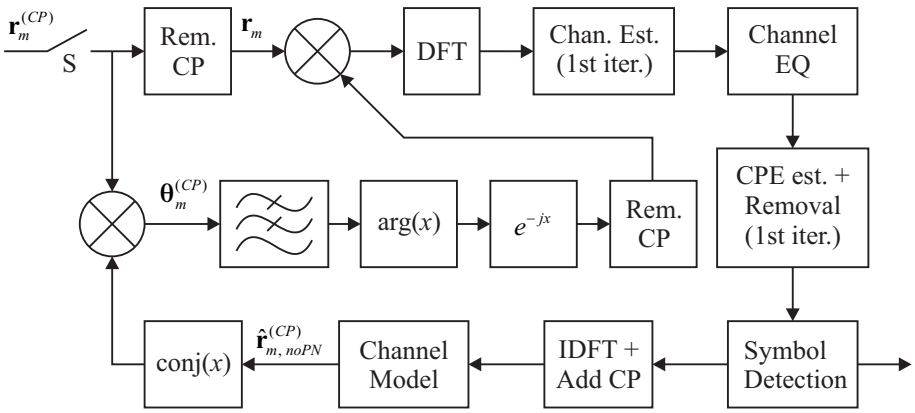

Figure 5-4: Illustration of the second proposed time-domain phase-noise mitigation algorithm (SyrjäläMOD). The switch S passes through the OFDM symbol and then opens. It is open until all the iterations have been completed and the next OFDM symbol is taken in.

Improved Iterative Time-Domain Phase-Noise Mitigation Algorithm [P10]

The second time-domain algorithm (called here SyrjäläMOD, again, for consistency because the author did not name the algorithms in the original publication) proposed in this thesis was first introduced in [P10], and is depicted in Figure 5-4. It is improved and polished version of the Syrjälä algorithm of [P7], so it is based on the same idea, i.e., to reconstruct the input signal without phase noise and to use this reconstructed signal to estimate the phase noise in the input signal. As can be seen from Figure 5-4, the algorithm has around the same level of complexity that the Syrjälä algorithm has. It also has an option to estimate the channel and the CPE again in the later iterations. Unlike the Syrjälä algorithm, this algorithm is derived from the case where the transmitter and receiver phase noises are both mapped as receiver phase noise. This is natural for the algorithm because, the phase noise compensation is done already after the cyclic prefix removal at the receiver, prior to channel estimation. The received signal without cyclic prefix is then

$$\mathbf{r}_m \approx \mathrm{diag}\left(e^{j\boldsymbol{\phi}_m}\right)\mathbf{H}_m\mathbf{x}_m + \mathbf{z}_m . \tag{5.14}$$

Prior the first iteration of the actual phase-noise estimation part, in addition to the cyclic prefix removal, the signal is discrete Fourier transformed, the channel is estimated and equalized, CPE is estimated and removed, and finally the symbols are detected. From this signal, the approximate of the received signal without phase noise is reconstructed with IDFT, and in this algorithm also the cyclic prefix is added. Then the channel is modelled according to the channel estimation result. This is approximately the received signal without phase noise $\hat{\mathbf{r}}_{m,noPN}^{(CP)}$. Complex conjugate of this signal is then taken and it is multiplied with the received signal $\mathbf{r}_m^{(CP)}$. The signal resulting from this multiplication (only for illustration purposes without cyclic prefix) can be written as

$$\begin{aligned}\boldsymbol{\theta}_m &\approx \mathrm{diag}\left(\hat{\mathbf{H}}_m^* \hat{\mathbf{x}}_m^*\right)\left[\mathrm{diag}\left(e^{j\boldsymbol{\phi}_m}\right)\mathbf{H}_m \mathbf{x}_m\right] \\ &\approx \mathrm{diag}\left(\left|\hat{\mathbf{H}}_{m,CPE}\hat{\mathbf{x}}_m\right|^2\right)e^{j\boldsymbol{\phi}_m} + \mathrm{diag}\left(\hat{\mathbf{H}}_m^* \hat{\mathbf{x}}_m^*\right)\mathbf{z}_m \,.\end{aligned} \tag{5.15}$$

This is actually already approximately the phase-noise complex exponential, the samples of which are also multiplied with the power of the corresponding subcarrier with channel contribution. The resulting multiplication is actually a good thing, since it scales the signal as done separately in the Syrjälä algorithm. Here, the scaling is build-in since we use complex conjugate instead of division as in the Syrjälä algorithm. The improved version of the estimate can be achieved with steep lowpass filtering as in the Syrjälä algorithm, and the estimate at this point can be written as (again, without cyclic prefix)

$$\mathrm{LPF}\{\boldsymbol{\theta}_m\} \approx \mathrm{diag}(\mathbf{a}_m)e^{j\boldsymbol{\phi}_m} \,. \tag{5.16}$$

Here, $\mathbf{a}_m$ is the $(N \times 1)$ vector with erroneous non-unity amplitudes in the estimates. The lowpass filtering is then followed by taking the argument of the signal and then the inverse of the complex exponential with that argument. This effectively allows us to get rid of the non-unity amplitude of the estimate of the phase-noise complex exponential. Then, finally the cyclic prefix is removed from the signal and the phase noise is compensated from the received signal after cyclic prefix removal by multiplication by the computed inverse of the estimate. After this the signal goes through the same process until the symbol detection, and if more iterations are wanted, the newly detected symbols are used to build more reliable estimate of the received signal, and the phase noise estimation and mitigation are done again.

5.3. *Performances of the Algorithms*

This section shortly describes the simulator and presents the simulation results with analysis of the results.

Parameters of Simulated System and Simulation Routine

To compare the performances of the reviewed and the proposed phase-noise mitigation algorithms, symbol-error rate (SER) simulations are run with the following simulation routine. First, 3GPP-LTE downlink type OFDM-signal with 1024 subcarriers is created with 15 kHz subcarrier spacing. 600 of the subcarriers, 300 on the both sides of the centre subcarrier, are active and carry 16QAM modulated data, and the rest of the subcarriers are null. After the signal creation the cyclic prefix of length 63 samples is added to the OFDM symbols. The transmitter phase noise is then modelled to the signal. After this, the signal is put through channel, which is depending on a case either additive white Gaussian noise (AWGN) channel or extended International-Telecommunication-Union – Radiocommunication-Section (ITU-R) Vehicular A multipath-channel described in [61]. The multipath channel is assumed to be quasistatic for duration of 12 OFDM symbols. After the

channel, receiver phase noise is modelled. The free-running phase noise model is used in the modelling of the transmitter and receiver phase noises. The reported simulated phase noise 3-dB bandwidths are the sums of the bandwidths of the transmitter and receivers phase noise processes. After phase noise, the cyclic prefix is removed and the OFDM signal is discrete Fourier transformed. Then, channel and CPE are estimated and equalized. In the channel estimation, three cases are simulated: 1) perfect channel information is assumed, 2) traditional pilot subcarrier based LS algorithm is used and the missing channel frequency response is estimated with linear interpolation, and 3) the advanced channel estimation scheme proposed in this thesis and [P5] is used. For the perfect channel information case, only 16 subcarriers are considered as pilots (for CPE estimation), and for practical channel estimation cases 66 equally-spaced pilot subcarriers per OFDM symbol are used. The channel and CPE equalizations are then followed by the ICI-mitigation algorithms presented and proposed. It should be noted that even though in all the algorithm derivations only either transmitter or receiver phase noises were assumed present, in the simulations both, transmitter and receiver, phase noises are assumed present.

All the iterative ICI-mitigation algorithms are iterated 3 times. For Petrovic algorithm [45], and thus for Bittner [10] and LI-TE algorithms, parameter $u = 3$. For Bittner algorithm 70 samples and for LI-TE algorithms 155 samples at the both edges of the OFDM symbol are used for tail estimation. For Syrjälä and SyrjäläMOD algorithms, the used lowpass filters to separate the phase-noise estimate from the noise are designed with the Remez algorithm and are of order 200 and 350, for AWGN channel and extended ITU-R Vehicular A channel, respectively.

Simulation Results and Analysis

The simulation results are given from Figure 5-5 to Figure 5-13. In the figures, the compared algorithms are CPE estimation, LI-CPE, Petrovic, Bittner, LI-TE, Syrjälä, SyrjäläMOD from [72], [P1], [45], [10], [P1], [P7] and [P10], respectively. In Figure 5-5 and Figure 5-6, SER is given in AWGN channel case. The proposed algorithms perform very well. LI-CPE algorithm gives fair performance improvement over the performance of plain CPE estimation, and it even matches the performance of Petrovic algorithm with high phase noise 3-dB bandwidths. Furhermore, LI-TE technique improves the performance clearly over the performances of the state-of-the-art ICI-mitigation algorithms. Then, Syrjälä and SyrjäläMOD algorithms yet outperform LI-TE technique clearly. The same result is visible when studying the performance as a function of phase noise 3-dB bandwidth and SNR. In Figure 5-7 and Figure 5-8, the same results are given but for extended ITU-R Vehicular A multipath channel. Perfect channel knowledge is assumed. Now, LI-CPE gets very near to the performance of Petrovic technique all-around, and even manages to outperform it with higher phase-noise

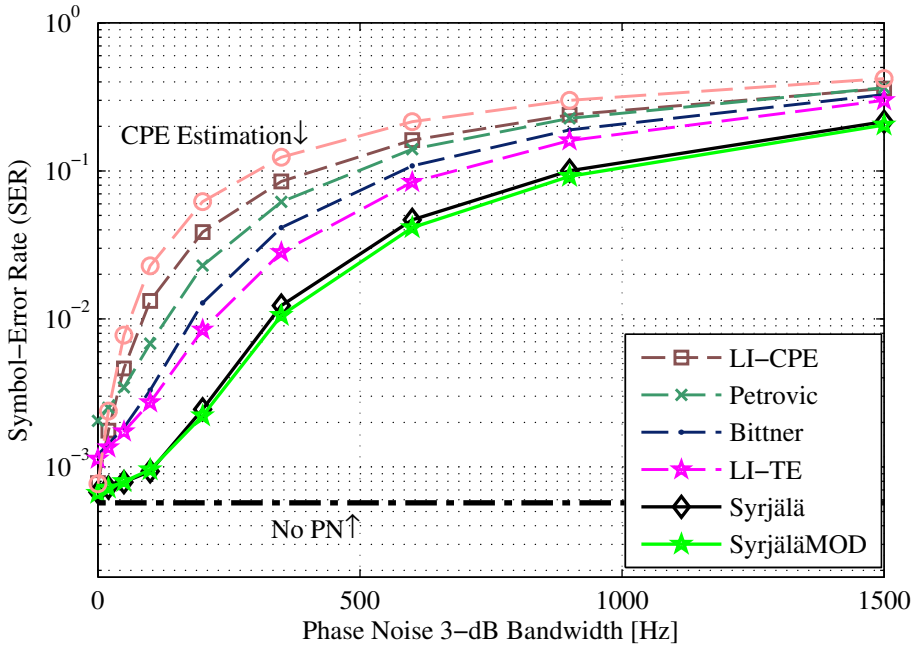

Figure 5-5: Simulated SER as a function of phase noise 3-dB bandwidth (β) in AWGN channel with received SNR fixed to 18 dB.

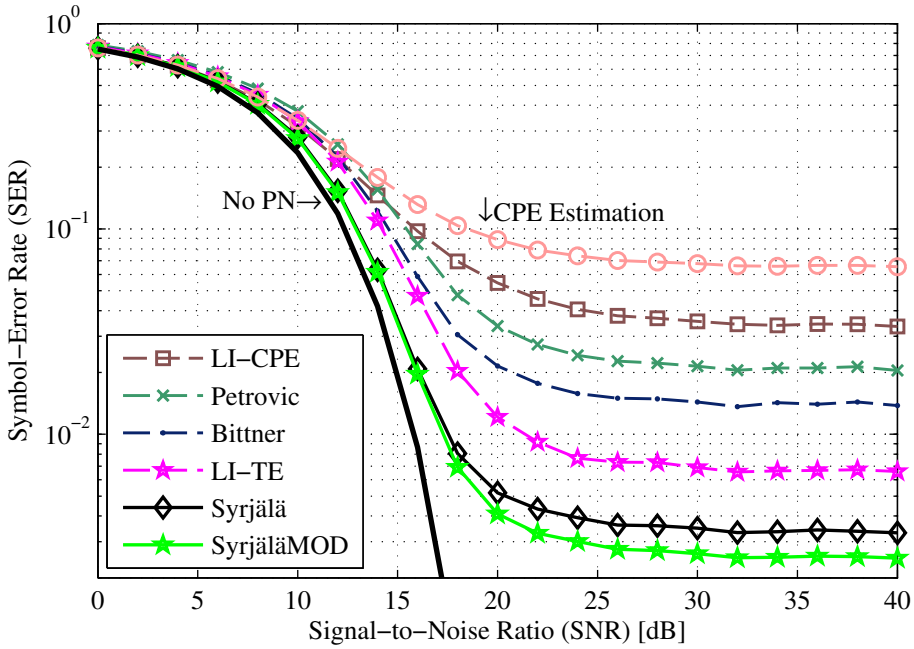

Figure 5-6: Simulated SER as a function of received SNR in AWGN channel. Phase noise 3-dB bandwidth (β) is fixed to 300 Hz.

3-dB bandwidths. In this case too, the proposed techniques LI-TE, Syrjälä and SyrjäläMOD give fair improvement over the state-of-the-art algorithms. It should be especially noted that SyrjäläMOD algorithm manages to give huge performance improvement even over Syrjälä algorithm, especially at higher signal-to-noise ratio region. Results for PLL-oscillator generated phase noise with parameters $L(\Delta\omega_w) = -110$ dBc/Hz at $\Delta\omega_w = 1$ MHz,

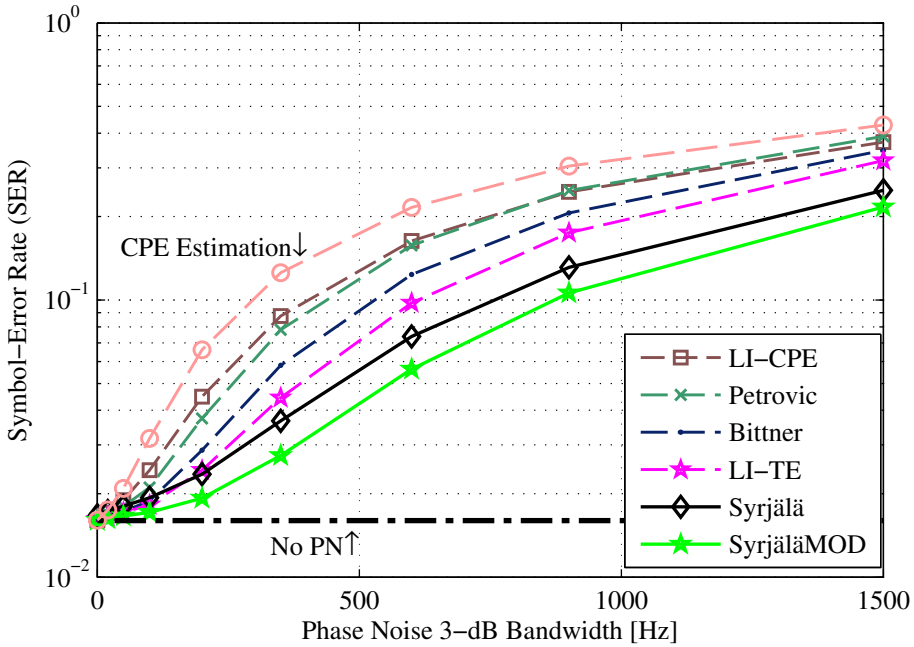

Figure 5-7: Simulated SER as a function of phase noise 3-dB bandwidth (β) in extended ITU-R Vehicular A multipath channel with received SNR fixed to 26 dB.

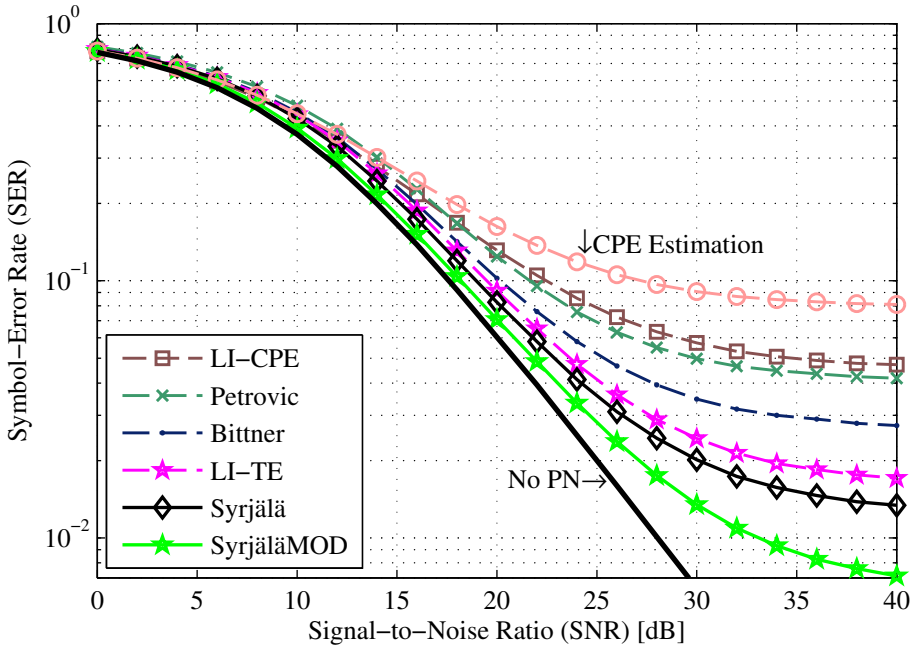

Figure 5-8: Simulated SER as a function of received SNR in extended ITU-R Vehicular A multipath channel. Phase noise 3-dB bandwidth (β) is fixed to 300 Hz.

$L(\Delta\omega_f) = -75$ dBc/Hz at $\Delta\omega_f = 30$ kHz, $L_{CO}(\Delta\omega_{w,CO}) = -90$ at $\Delta\omega_{w,CO} = 100$ Hz, and $\gamma_c = 20.384$ kHz in AWGN channel environment are depicted in Figure 5-9.

When also different channel estimation techniques are considered, the performance differences between the algorithms change only a little as is depicted in Figure 5-10 and Figure 5-11. However, it is worth noticing that with advanced channel estimation case,

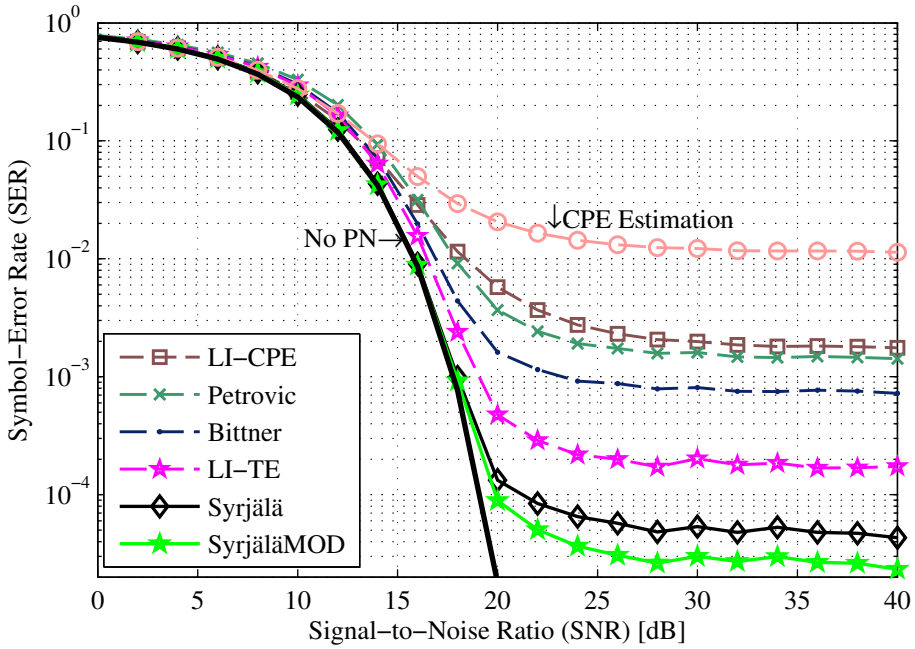

Figure 5-9: Simulated SER as a function of received SNR in AWGN channel. Phase noise is generated by PLL oscillator with parameters $L(\Delta\omega_w) = -110$ dBc/Hz at $\Delta\omega_w = 1$ MHz, $L(\Delta\omega_f) = -75$ dBc/Hz at $\Delta\omega_f = 30$ kHz, $L_{CO}(\Delta\omega_{w,CO}) = -90$ at $\Delta\omega_{w,CO} = 100$ Hz, and $\gamma_c = 20.384$ kHz.

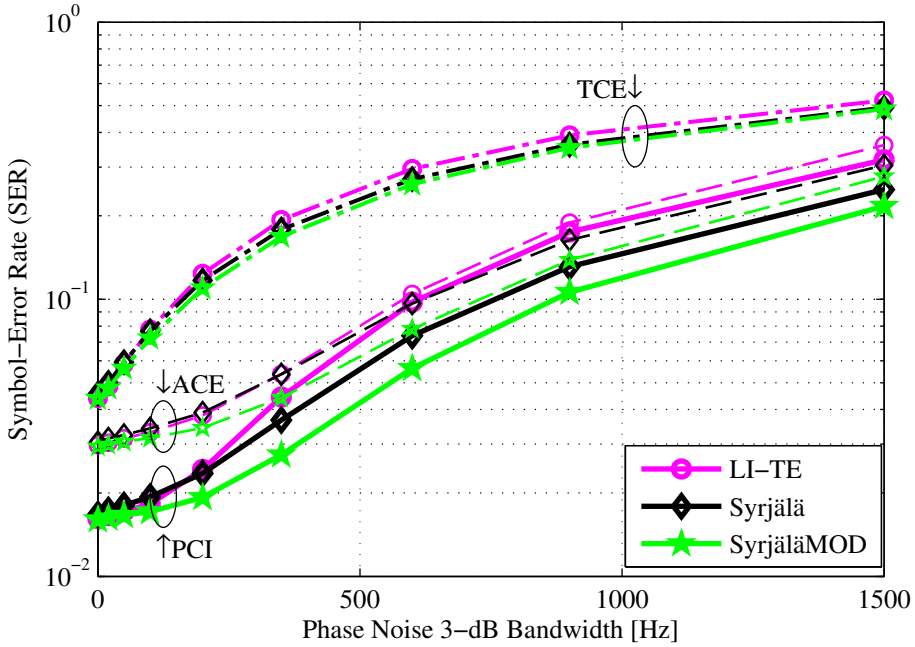

Figure 5-10: Simulated SER as a function of phase noise 3-dB bandwidth (β) in extended ITU-R Vehicular A multipath channel with received SNR fixed to 26 dB. Simulations are run with different levels of channel knowledge. The curve groups denoted by TCE, ACE and PCI are with traditional channel estimation, advanced channel estimation and perfect channel information, respectively.

SyrjäläMOD algorithm manages to attain almost the performance of Syrjälä algorithm with perfect channel information in higher phase noise 3-dB bandwidth regions. The performances of the algorithms overall with the advanced channel estimation are convincing. However, with

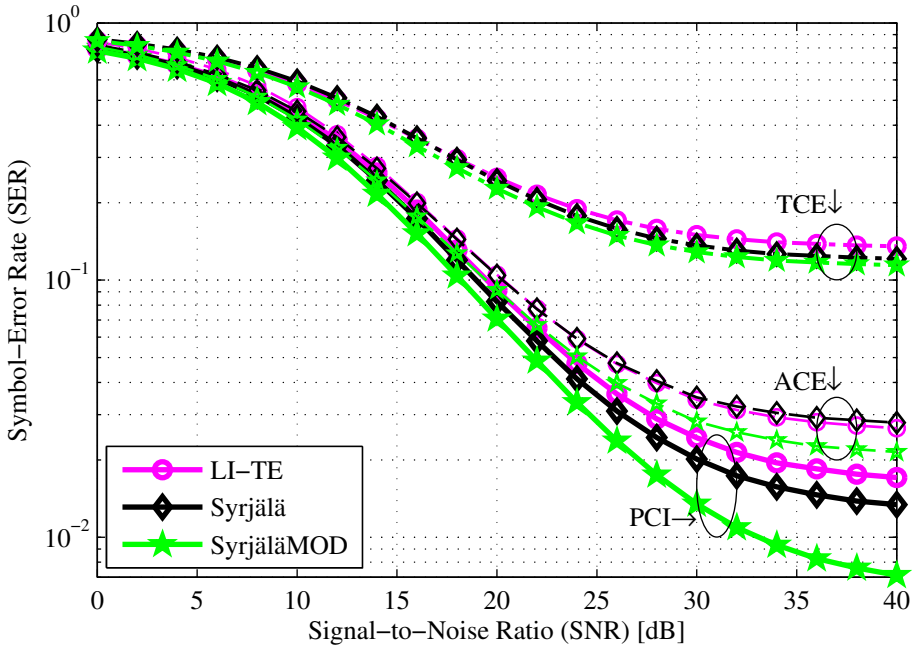

Figure 5-11: Simulated SER as a function of received SNR in extended ITU-R Vehicular A multipath channel. Phase noise 3-dB bandwidth (β) is fixed to 300 Hz. Simulations are run with different levels of channel knowledge. The curve groups denoted by TCE, ACE and PCI are with traditional channel estimation, advanced channel estimation and perfect channel information, respectively.

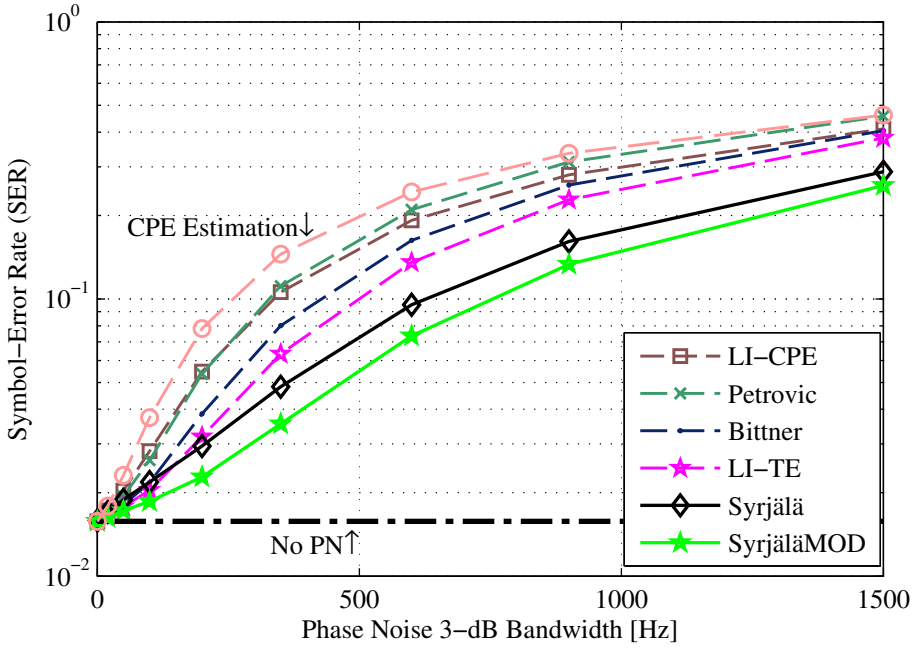

Figure 5-12: Simulated SER as a function of phase noise 3-dB bandwidth (β) in extended ITU-R Vehicular A multipath channel with received SNR fixed to 26 dB. This is OFDMA case where 150 edge subcarriers with 10 dB higher average signal power on both sides are considered to belong to another user.

traditional channel estimation rather poor performance is attained, but that is mainly because of relatively poor channel estimates. But even then, the proposed algorithms outperform the state-of-the-art algorithms.

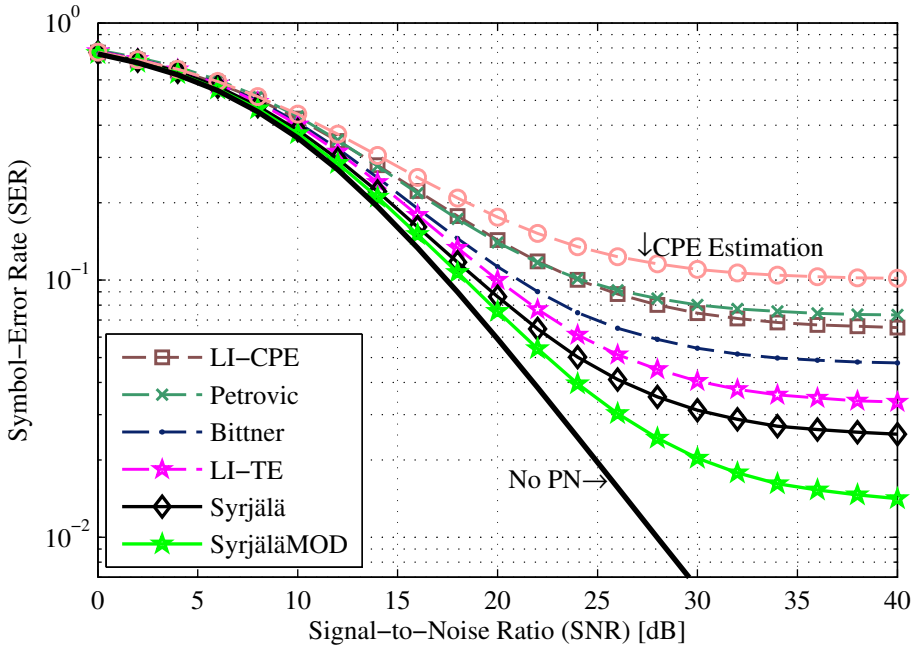

Figure 5-13: Simulated SER as a function of received SNR in extended ITU-R Vehicular A multipath channel. Phase noise 3-dB bandwidth (β) is fixed to 300 Hz. This is OFDMA case where 150 edge subcarriers with 10 dB higher signal power on both sides are considered to belong to another user.

Also simulation results for OFDMA case are depicted in Figure 5-12 and Figure 5-13. Compared to earlier discussion the only two differences are that 1) the 150 edge subcarriers on both sides of the current user's 300 subcarrier in the middle are at 10 dB higher power level, and 2) the 150 edge subcarriers are considered to belong to another user, so they are not considered when SER is calculated. In this simulation all the subcarriers are detected at the receiver, since the received signal must anyway be fully received and discrete Fourier transformed. The high-power adjacent user signals are beneficial in iterative phase noise mitigation algorithms, but on the other hand also spread on top of the current user's subcarriers relatively heavily. As the figures depict, the relative performance differences between the algorithms stay the same compared to the case without other users' signals, with one exception. The LI-CPE algorithm seems to perform relatively better. It outperforms the Petrovic algorithm with reasonable phase-noise 3-dB bandwidths, and even the Bittner algorithm for higher 3-dB bandwidths. Overall performance drops a little at higher phase-noise 3-dB bandwidth region because of the adjacent signal spread also depicted in Figure 3-5. In the simulations, the reported signal-to-noise ratios refer to the signal-to-noise ratios of the current user.

For detailed performance analysis about how the algorithms scale with increasing number of iterations, refer to [P7] and [P10].

Chapter 6

Sampling Jitter Mitigation in Direct-RF-Sampling Receivers

The second estimation and mitigation topic of this thesis is sampling jitter mitigation in VS direct-RF-sampling receivers based on digital signal processing. In the literature, sampling jitter mitigation in direct-RF-sampling receiver has not received wide attention. However, it is a very interesting study topic, since sampling jitter is one of the biggest obstacles that prevents the use of direct-RF-sampling receiver architecture in mobile receivers [37], [59], [60]. This chapter also shows that the sampling jitter is especially serious problem in direct-RF-sampling receivers receiving OFDM signals.

The structure of this chapter is as follows. First, the state-of-the-art of the sampling-jitter mitigation in direct-RF sampling is discussed. Then, the proposed algorithms first published in [P2], [P3], [P4] and [P5] are presented. Finally, the performances of all of the presented algorithms are compared.

6.1. State of the Art in Sampling Jitter Estimation and Mitigation

To the author's best knowledge, there are no real contributions in the literature for sampling jitter mitigation in direct-RF-sampling receivers, although for other applications, sampling-jitter mitigation techniques have been proposed, e.g., in [53] and [66]. This is why we present technique of [53] here as a reference technique. It is designed for narrow-band signals and it was not designed for direct-RF-sampling. Therefore, the use of the technique of [53] in sampling jitter estimation in direct-RF-sampling receiver can be considered a minor contribution of this thesis. The algorithm is presented here trying to follow the original presentation of [53] with only minor changes, while however adding changes that are related to the new application of sampling jitter mitigation in direct-RF-sampling receivers. The technique works in this context surprisingly well. Simply put, the idea is to insert a reference

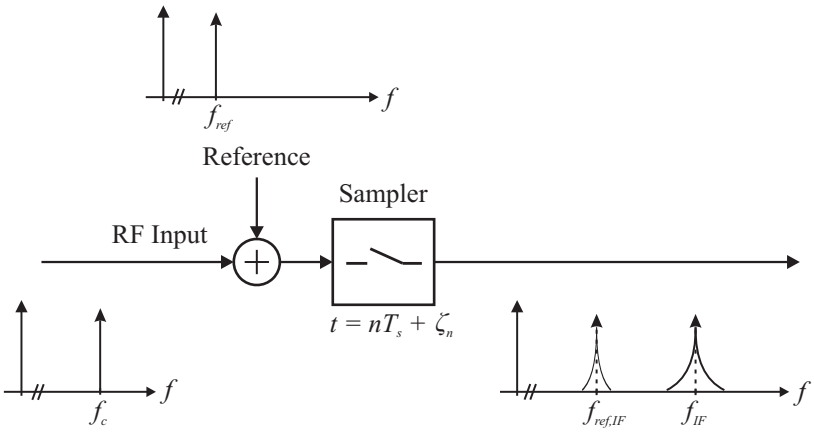

Figure 6-1: Demonstration of the spectra of the signals prior and after the sampling process. Higher frequency useful signal is more spread by the sampling jitter than the lower frequency reference signal.

tone to the signal prior the sampling, to separate the sampling-jitter effect from that tone after the sampling, and to use the separated sampling-jitter effect to get rid of the sampling jitter from the sampled useful signal.

So the idea is to add a reference tone (at frequency ω_{ref} and with amplitude A_{ref})

$$r_{ref}(t) = A_{ref}\cos\left(\omega_{ref}t\right) \tag{6.1}$$

to the narrowband signal (actually to a sinusoid with amplitude A_c and frequency ω_c)

$$r_{cos}(t) = A_c\cos\left(\omega_c t\right) \tag{6.2}$$

prior to the sampling. The frequency ω_{ref} is selected so that it is not in the useful signal band and the frequency and its surroundings are as clear as possible from interference. Now, when the sum signal is sampled with jitter (at $t = nT_s + \zeta_n$), the signal can be written as

$$\begin{aligned}\tilde{r}_{n,cos+ref} &= A_c\cos\left(\omega_c nT_s + \omega_c\zeta_n\right) + A_{ref}\cos\left(\omega_{ref}nT_s + \omega_{ref}\zeta_n\right)\\ &= A_c\cos\left(\omega_{IF}nT_s + \omega_c\zeta_n\right) + A_{ref}\cos\left(\omega_{ref,IF}nT_s + \omega_{ref}\zeta_n\right).\end{aligned} \tag{6.3}$$

The sampled sum signal is also depicted in Figure 6-1. The second form of (6.3) takes into account the aliasing of the message signal to the IF band ω_{IF}. Depending on the ω_{ref} also the reference tone might alias around its IF band $\omega_{ref,IF}$. It should be however noted that $\omega_{IF} = \omega_c$ and/or $\omega_{ref,IF} = \omega_{ref}$ if sampling frequency is high enough that the aliasing does not happen. From now on, even though both presentations are mathematically identical for corresponding sampling frequencies, we will use the aliased versions of the frequencies when applicable for completeness of the presentation. Now, after using small phase approximation on the signal in (6.3), we can write

$$\begin{aligned}\tilde{r}_{n,cos+ref} \approx\ & A_c\cos\left(\omega_{IF}nT_s\right) - A_c\omega_c\zeta_n\sin\left(\omega_{IF}nT_s\right)\\ &+ A_{ref}\cos\left(\omega_{ref,IF}nT_s\right) - A_{ref}\omega_{ref}\zeta_n\sin\left(\omega_{ref,IF}nT_s\right).\end{aligned} \tag{6.4}$$

Now, after digital complex downconversion of the reference tone and lowpass filtering, the resulting signal can be written as

$$\mathrm{LPF}\left\{\tilde{r}_{n,cos+ref}\, e^{-j\omega_{ref,IF}nT_s}\right\} = \tilde{s}_{n,ref} \approx \frac{A_{ref} + j\, A_{ref}\omega_{ref}\zeta_n}{2}. \tag{6.5}$$

Then, the direct current component can be removed either by knowing the amplitude A_{ref} and removing the corresponding voltage from the signal $\tilde{s}_{n,ref}$ or by lowpass filtering the signal to find the direct current component and then removing it from the signal. The signal after this removal can be written as

$$\breve{s}_{n,ref} \approx \frac{j\, A_{ref}\omega_{ref}\zeta_n}{2}. \tag{6.6}$$

Now, after separation of the useful signal with digital complex downconversion and lowpass filtering, the signal in (6.4) can be written as

$$\mathrm{LPF}\left\{\tilde{r}_{n,cos+ref}\, e^{-j\omega_{IF}nT_s}\right\} = \tilde{s}_n \approx \frac{A_c + j\, A_c\omega_c\zeta_n}{2} = A_c\,\frac{1+j\,\omega_c\zeta_n}{2}. \tag{6.7}$$

From this form we can see that the signal at this point resembles much the signal $\breve{s}_{n,ref}$ in (6.6) above. Actually since the interesting signal was a tone with amplitude A_c, the useful signal is merely the DC A_c and the jitter effect can be seen as a multiplier of A_c in the final form of (6.7). We can thus use signal $\breve{s}_{n,ref}$ to get rid of the jitter term in (6.7). Now if we scale the signal $\breve{s}_{n,ref}$ by ω_c/ω_{ref}, add already removed $A_{ref}/2$ back to it, and finally scale the result with $1/A_{ref}$, we arrive in to form

$$\frac{1}{A_{ref}}\left(\frac{A_{ref}}{2} + \frac{\omega_c}{\omega_{ref}}\breve{s}_{n,ref}\right) \approx \frac{1}{A_{ref}}\left(\frac{A_{ref}}{2} + \frac{\omega_c}{\omega_{ref}}\frac{j\omega_{ref}\zeta_n A_{ref}}{2}\right) = \frac{1+j\omega_c\zeta_n}{2}. \tag{6.8}$$

This is exactly the jitter caused multiplier to the pure message tone when using the small phase approximation. After dividing the signal at the sampler output after digital I/Q downconversion and lowpass filtering with signal in (6.8), the sampling jitter is mitigated.

6.2. Contributions to Sampling Jitter Estimation and Mitigation

In this section, all the sampling jitter mitigation algorithms proposed in this thesis are presented. First, a technique first published in [P3] and [P4] is given. Then the use of already proposed phase noise mitigation techniques in sampling jitter mitigation is discussed.

Sampling Jitter Estimation and Mitigation Using Injected Reference Tone

The first proposed algorithm is partially building on one of the ideas presented in [53], namely on the idea to use reference tone in sampling jitter mitigation. In [53], the reference

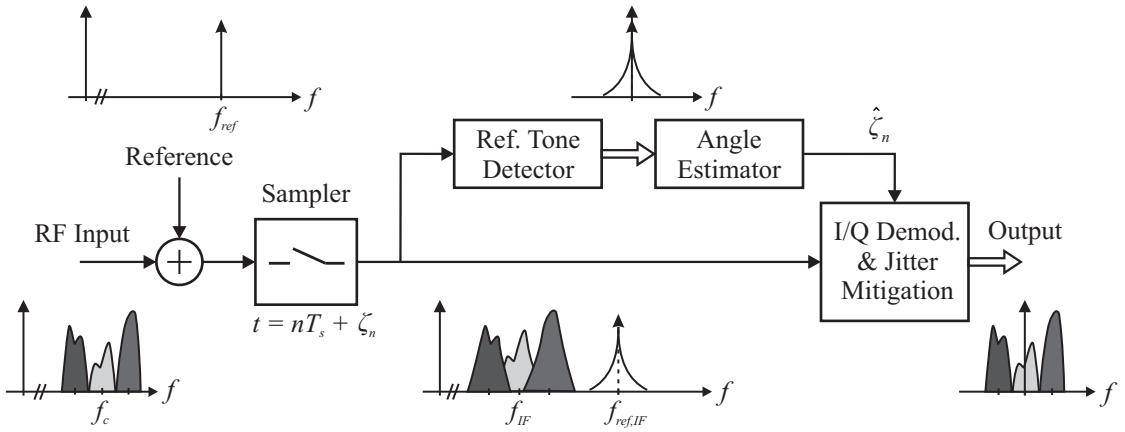

Figure 6-2: Illustration of the proposed reference tone based sampling-jitter estimation and mitigation technique. Frequencies f_{IF} and $f_{ref,IF}$ are the IF bands in which the corresponding signals alias because of subsampling. $f_{IF} = f_c$ and $f_{ref,IF} = f_{ref}$ if aliasing does not happen because of high enough sampling frequency.

tone was used to construct the multiplicative effect of the phase noise for narrow band signal. In the proposed sampling jitter estimation algorithm however, the reference tone is used to estimate the values of the sampling jitter process ζ_n for all the samples, and then the estimate of the sampling jitter process is used for sampling-jitter mitigation. The algorithm is easier to use and understand, than the algorithm of [53] and it is also designed to work well also with wideband signals. Furthermore, in its derivation, we do not need to use small phase approximation. The algorithm is illustrated in Figure 6-2.

The starting point is the sampled I/Q signal model given in (4.4). After adding the reference tone in (6.1) to the signal, the total sampled signal can be written as

$$\begin{aligned}\tilde{r}_{n,s+r} &= s_I(nT_s+\zeta_n)\cos\left(\omega_c nT_s+\omega_c\zeta_n\right) - s_Q(nT_s+\zeta_n)\sin\left(\omega_c nT_s+\omega_c\zeta_n\right)\\ &\quad + A_{ref}\cos\left(\omega_{ref}nT_s+\omega_{ref}\zeta_n\right)\\ &= \mathrm{Re}\left\{\left[s_I(nT_s+\zeta_n)+js_Q(nT_s+\zeta_n)\right]e^{j\omega_c nT_s}e^{j\omega_c\zeta_n} + A_{ref}e^{j\omega_{ref}nT_s}e^{j\omega_{ref}\zeta_n}\right\}\\ &= \mathrm{Re}\left\{s(nT_s+\zeta_n)e^{j\omega_c nT_s}e^{j\omega_c\zeta_n} + A_{ref}e^{j\omega_{ref}nT_s}e^{j\omega_{ref}\zeta_n}\right\}\\ &= \mathrm{Re}\left\{s(nT_s+\zeta_n)e^{j\omega_{IF}nT_s}e^{j\omega_c\zeta_n} + A_{ref}e^{j\omega_{ref,IF}nT_s}e^{j\omega_{ref}\zeta_n}\right\}.\end{aligned} \tag{6.9}$$

The last form takes into account the aliasing as explained when explaining algorithm of [53] previously in Section 6.1. Now, to use the reference tone, we use complex digital mixing to downconvert the reference tone, followed by a lowpass filter, to separate the reference tone from the other signals. The signal after downconversion and lowpass filter can be written as

$$\tilde{s}_{n,ref} = \mathrm{LPF}\left(\tilde{r}_{n,s+r}\, e^{-j\omega_{ref}nT_s}\right) \approx A_{ref}e^{j\omega_{ref}\zeta_n}. \tag{6.10}$$

This holds only approximately even when ideal LPF is considered since sampling jitter spreads the present signals. Anyway, after we take the argument of the complex exponential $\tilde{s}_{n,ref}$, and divide the result by ω_{ref}, we get relatively good estimate of the sampling jitter

$$\hat{\zeta}_n = \frac{\arg\left(\tilde{s}_{n,ref}\right)}{\omega_{ref}}. \tag{6.11}$$

Now to use the estimated sampling jitter in mitigation from the actual received signal perspective, we start again from $\tilde{r}_{n,s+r}$ in (6.9), and this time downconvert the useful signal to the baseband. After downconversion and lowpass filtering, the signal can be written as

$$\tilde{s}_{n,sig} = \mathrm{LPF}\left(\tilde{r}_{n,s+r}\, e^{-j\omega_c nT_s}\right) \approx s(nT_s + \zeta_n) e^{j\omega_c \zeta_n}. \tag{6.12}$$

We can then mitigate the sampling-jitter effect by multiplying the signal $\tilde{s}_{n,sig}$ by signal $\exp\left(-j\omega_c \hat{\zeta}_n\right)$, which results into signal

$$\tilde{s}_{n,sig} \exp\left(-j\omega_c \hat{\zeta}_n\right) \approx s(nT_s + \zeta_n) e^{j\left(\omega_c \zeta_n - \omega_c \hat{\zeta}_n\right)} \approx s(nT_s + \zeta_n) \tag{6.13}$$

and then using interpolation for the remaining signal according to the sampling jitter estimates $\hat{\zeta}_n$. However, the interpolation is not necessary needed. Therefore we can approximate $\tilde{s}_{n,sig}$ as [64]

$$\tilde{s}_{n,sig} \approx s(nT_s) e^{j\omega_c \zeta_n}, \tag{6.14}$$

and after multiplication by signal $\exp\left(-j\omega_c \hat{\zeta}_n\right)$, we have approximately the desired waveform $s(nT_s)$. The interpolation can be left undone because timing errors have much higher (dominating) effect on the high-frequency carrier components than on the low-frequency signal components [60], [64]. This basically means that already very good jitter mitigation is attained by multiplying the signal $\tilde{s}_{n,sig}$ by $\exp\left(-j\omega_c \hat{\zeta}_n\right)$.

Thoughts about Neighbouring Channels and Nearby Interferers

Above discussion did not make any assumption of the information signal $s(t)$. Ideally it would have only the desired signal components in it. However, this is naturally not realistic, as building selective RF filtering in a direct-RF-sampling receiver is very challenging, or even impossible in mobile devices due to tight size and cost restrictions. Now if we still assume that the reference tone is relative pure from the interference from the other signals (since the selection of the reference tone frequency is relatively free), we can assume that the sampling jitter estimation can be done similarly as above even when adjacent channel interferers are present near the useful signal. However, now due the imperfect RF-filtering, at the sampler input there are interfering signals $s_{i,1}(t)$ and $s_{i,2}(t)$ at the both sides of the useful signal at centre frequencies $\omega_{i,1} < \omega_c$ and $\omega_{i,2} > \omega_c$, respectively. If $\omega_{i,1,IF}$ and $\omega_{i,2,IF}$ are the possibly aliased centre frequencies from the original centre frequencies $\omega_{i,1}$ and $\omega_{i,2}$, then after sampling, the overall signal without the reference tone can be written (without and with aliasing) as

$$\begin{aligned}\tilde{r}_{n,s+i} &= \mathrm{Re}\Big\{ s(nT_s+\zeta_n)e^{j\omega_c nT_s}e^{j\omega_c\zeta_n} \\ &\quad + s_{i,1}(nT_s+\zeta_n)e^{j\omega_{i,1}nT_s}e^{j\omega_{i,1}\zeta_n} + s_{i,2}(nT_s+\zeta_n)e^{j\omega_{i,2}nT_s}e^{j\omega_{i,2}\zeta_n}\Big\} \\ &= \mathrm{Re}\Big\{ s(nT_s+\zeta_n)e^{j\omega_{IF}nT_s}e^{j\omega_c\zeta_n} \\ &\quad + s_{i,1}(nT_s+\zeta_n)e^{j\omega_{i,1,IF}nT_s}e^{j\omega_{i,1}\zeta_n} + s_{i,2}(nT_s+\zeta_n)e^{j\omega_{i,2,IF}nT_s}e^{j\omega_{i,2}\zeta_n}\Big\}.\end{aligned} \tag{6.15}$$

Now, when the jitter is compensated with the proposed method from the I/Q downconverted version of (6.15), the resulting signal can be written as

$$\begin{aligned}\tilde{r}_{n,s+i,comp} &= e^{-j\omega_c\hat{\zeta}_n}\Big[s(nT_s+\zeta_n)e^{j\omega_c\zeta_n} + s_{i,1}(nT_s+\zeta_n)e^{j(\omega_{i,1,IF}-\omega_{IF})nT_s}e^{j\omega_{i,1}\zeta_n} \\ &\quad + s_{i,2}(nT_s+\zeta_n)e^{j(\omega_{i,2,IF}-\omega_{IF})nT_s}e^{j\omega_{i,2}\zeta_n}\Big] \\ &\approx s(nT_s+\zeta_n) + s_{i,1}(nT_s+\zeta_n)e^{j(\omega_{i,1,IF}-\omega_{IF})nT_s}e^{j(\omega_{i,1}-\omega_c)\zeta_n} \\ &\quad + s_{i,2}(nT_s+\zeta_n)e^{j(\omega_{i,2,IF}-\omega_{IF})nT_s}e^{j(\omega_{i,2}-\omega_c)\zeta_n}.\end{aligned} \tag{6.16}$$

This can be further approximated, because interferers and the useful signal vary very slowly in relation to the jitter values (bandwidths of around few megahertz and sampling-jitter RMS value around picoseconds range), into form

$$\tilde{r}_{n,s+i,comp} \approx s(nT_s) + s_{i,1}(nT_s)e^{j(\omega_{i,1,IF}-\omega_{IF})nT_s}e^{j(\omega_{i,1}-\omega_c)\zeta_n} + s_{i,2}(nT_s)e^{j(\omega_{i,2,IF}-\omega_{IF})nT_s}e^{j(\omega_{i,2}-\omega_c)\zeta_n}. \tag{6.17}$$

Now, in the approximation, the only effect of the sampling jitter left is the multiplication by the complex exponentials $\exp\left(j\left(\omega_{i,1}-\omega_c\right)\zeta_n\right)$ and $\exp\left(j\left(\omega_{i,2}-\omega_c\right)\zeta_n\right)$ of the interferer signals. Since both frequencies $\omega_{i,1}$ and $\omega_{i,2}$ are frequencies near the ω_c, their effect of spreading the spectrum of the interferers is vanishingly small. Therefore, based on (6.17), with the proposed sampling-jitter mitigation, also the jitter from the nearby interferers is mostly mitigated. Therefore, it can be said that the proposed sampling-jitter mitigation technique works also in the more practical case with adjacent channel interferers.

Use of Phase Noise Mitigation Techniques in Sampling Jitter Mitigation

As already mentioned, sampling jitter in direct-RF-sampling receivers has very similar effect on the actual communications signal as the phase noise has in case of direct-conversion receiver. We thus propose the use of the already presented OFDM phase-noise mitigation algorithms in jitter mitigation in OFDM direct-RF-sampling receivers. It should be noted, that the above algorithm is derived for general communications link, but the OFDM phase-noise mitigation algorithms can only be used for OFDM. In effect, we exploit the signal model (4.6) in sampling-jitter estimation and mitigation. This idea was first published in [P2]. It should be noted that according to the same idea, also some general phase noise mitigation algorithms can be used for sampling-jitter mitigation for non-OFDM signals in direct-RF-sampling receivers.

6.3. Performances of the Algorithms

Simulation parameters, simulated system, and the phase-noise mitigation algorithm parameters are selected the same as in Section 5.3. The simulations are carried out as follows. First, OFDM transmitter is modelled and the output OFDM-signal with 15 kHz subcarrier spacing and 1024 subcarriers (of which 600 are active 16QAM modulated, 300 on both side of the centre subcarrier) at 2.6 GHz carrier frequency is put through AWGN channel. At the receiver, first, reference tone at 36 MHz is added to the received signal so that the average PSD of the tone is about 40 dB over the average PSD of the received signal. Then direct-RF-sampling receiver using subsampling is modelled with oversampling factor of 16, namely subsampling at frequency 245.76 MHz ($16\times1024\times15$ kHz). The useful signal thus experiences controlled aliasing and the centre frequency changes to 103.36 MHz ($-2.6\,\text{GHz}+11F_s$). The sampling jitter is generated with the PLL model with parameters $L(\Delta\omega_w)$ = −110 dBc/Hz at $\Delta\omega_w$ = 1 MHz , $L(\Delta\omega_f)$ = −69 dBc/Hz at $\Delta\omega_f$ = 10 kHz, $L_{CO}(\Delta\omega_{w\_CO})$ = −160 at $\Delta\omega_{w\_CO}$ = 1 MHz, and γ_c = 1.86 kHz. After the PLL phase-noise generation the sampling jitter is got by scaling the sequence to RMS value of the jitter. The sampling jitter is modelled to the carrier components accurately, and to the lowpass signal separately by 3rd order (cubic) spline interpolation. After sampling-jitter modelling, the "Rutten" algorithm (presented in [53] and reviewed in Section 6.1) and "Inject" algorithm proposed in Section 6.2 are implemented for sampling-jitter mitigation. Then, the reference tone is removed from the signal after the digital signal downconversion. Finally signal is resampled at the original OFDM sampling frequency 15.36 MHz. Alternatively, instead of the sampling-jitter mitigation algorithms, phase-noise mitigation techniques are implemented for sampling-jitter mitigation in their correct place at the receiver chain (as explained in Chapter 5). We use the same techniques with the same names that were used in Section 5.3. Then, the signal is detected and SER is computed for each used sampling-jitter mitigation technique.

The simulations are also carried out for a case where OFDM signal is sampled with powerful nearby interfering signals. The interfering signals are three sinusoids on the left side of the useful signal (at 7.495 MHz, 7.5 MHz and 7.505 MHz offsets from the carrier frequency) and bandpass noise with bandwidth of 4.5 MHz on the right side of the useful signal with 9.5 MHz offset from the carrier frequency. The case is depicted in Figure 6-3. The PSDs of the interfering signals are on average about 40 dB higher than the PSD of the useful OFDM signal.

The simulation results are depicted in Figure 6-4, Figure 6-5, Figure 6-6 and Figure 6-7. Only AWGN channel case was considered since the relationship between the different channel cases were similar to the results already discussed with the phase noise mitigation in Chapter 5. The Figure 6-4 depicts the results for fixed received SNR of 18 dB as a function of RMS value of the sampling jitter. The curve of the Syrjälä algorithm was omitted for the sake

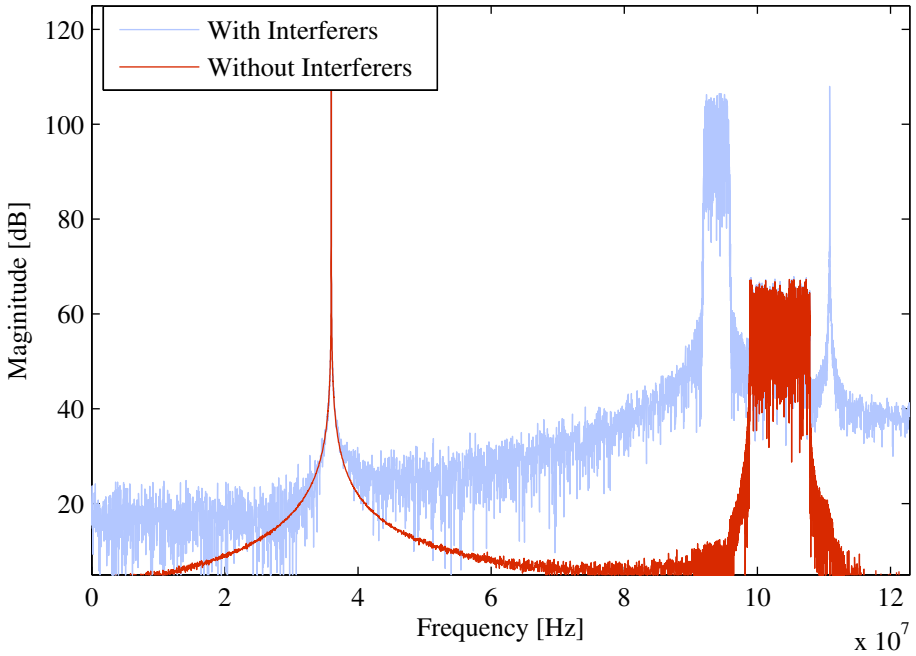

Figure 6-3: OFDM signal and the reference tone with and without the nearby interferers that are about 40 dB higher power level compared to the OFDM signal.

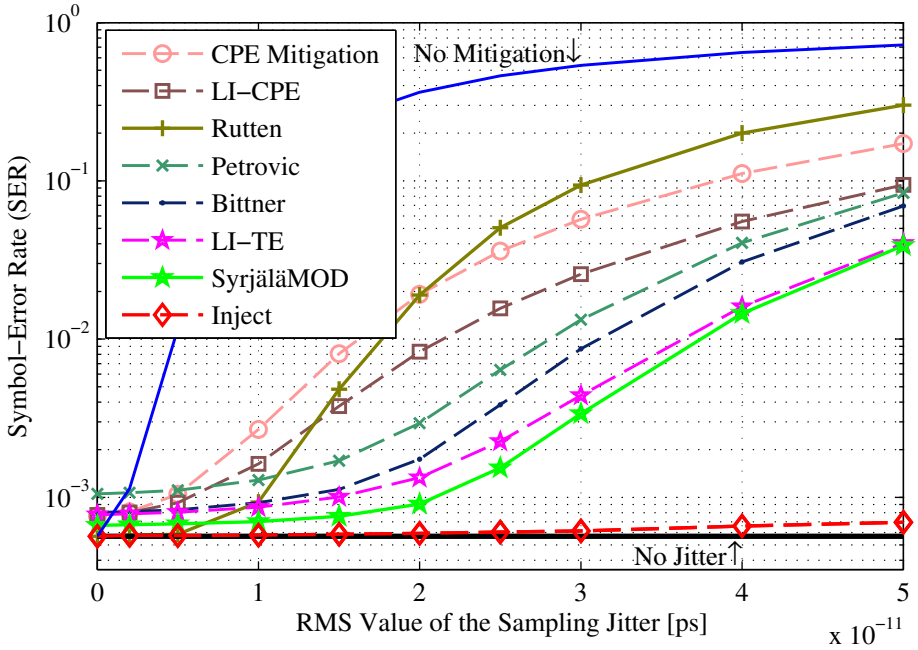

Figure 6-4: Simulated SER as a function of sampling jitter RMS value in AWGN channel with received SNR fixed to 18 dB. Syrjälä algorithm is omitted for the sake of readability.

of readability. It was very close to the curve of the SyrjäläMOD algorithm. As can be seen from the figure, the phase noise mitigation algorithms perform pretty well in sampling jitter mitigation as well. With higher than 20 ps RMS jitter, all the sampling-jitter mitigation techniques clearly outperform the reference sampling-jitter mitigation algorithm (Rutten), and still with lower RMS jitter values good phase-noise mitigation algorithms manage to match or

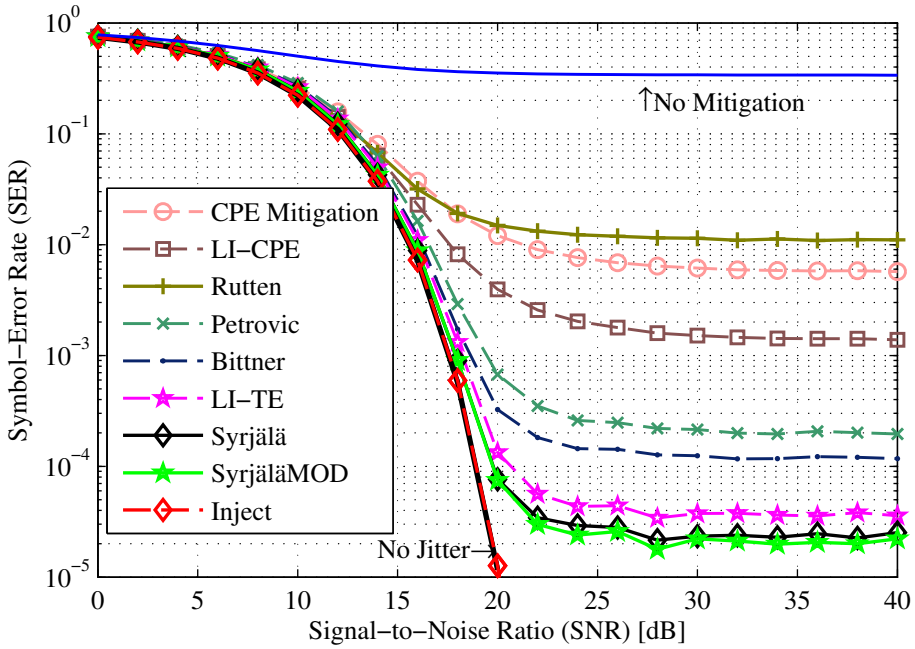

Figure 6-5: Simulated SER as a function of received SNR in AWGN channel. Sampling jitter RMS value is fixed to 20 ps.

improve the performance. However, the proposed Inject algorithm outperforms every other algorithm clearly with all levels of sampling jitter, and manages to stay very near the performance attained without sampling jitter. The mutual performance differences between the phase-noise mitigation algorithms stay approximately the same as in phase-noise mitigation. In Figure 6-5, the simulated SER is given as a function of received SNR for fixed 20 ps RMS value of the sampling jitter. From the curves we can see, that the phase-noise mitigation algorithms once again manage to achieve very good performance compared to the Rutten algorithm, but once again, the Inject algorithm gives superior performance. The figure was not continued to lower SERs for better readability, but the Inject algorithm followed closely the no-phase-noise curve until the simulation accuracy was not sufficient anymore. In the Figure 6-6 and Figure 6-7 the same results are given but with nearby interfering signals present. The relative performances of the algorithms stay almost the same. However, the algorithms dependent on the reference tone suffer more heavily because also the reference tone gets corrupted by the spread of the interferers due to sampling jitter. Results from Syrjälä algorithm are omitted from both of the figures for the sake of readability of the figures. Its performance is almost the same as the performance of SyrjäläMOD algorithm because the AWGN case is studied.

Even though the Inject algorithm gave very good performance and is relatively simple, it requires the reference tone to be injected prior the sampling, and the reference tone should be relatively pure signal. This might be too high requirement for many applications, especially since in direct-RF-sampling many time the objective is to minimize the number of analogue

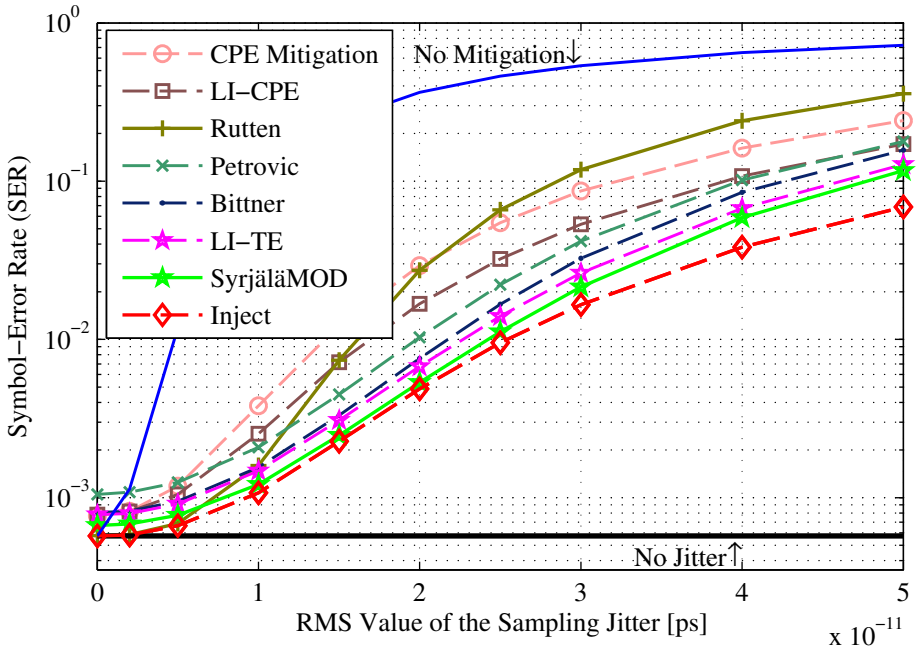

Figure 6-6: Simulated SER as a function of sampling jitter RMS value in AWGN channel with received SNR fixed to 18 dB and with nearby interferers.

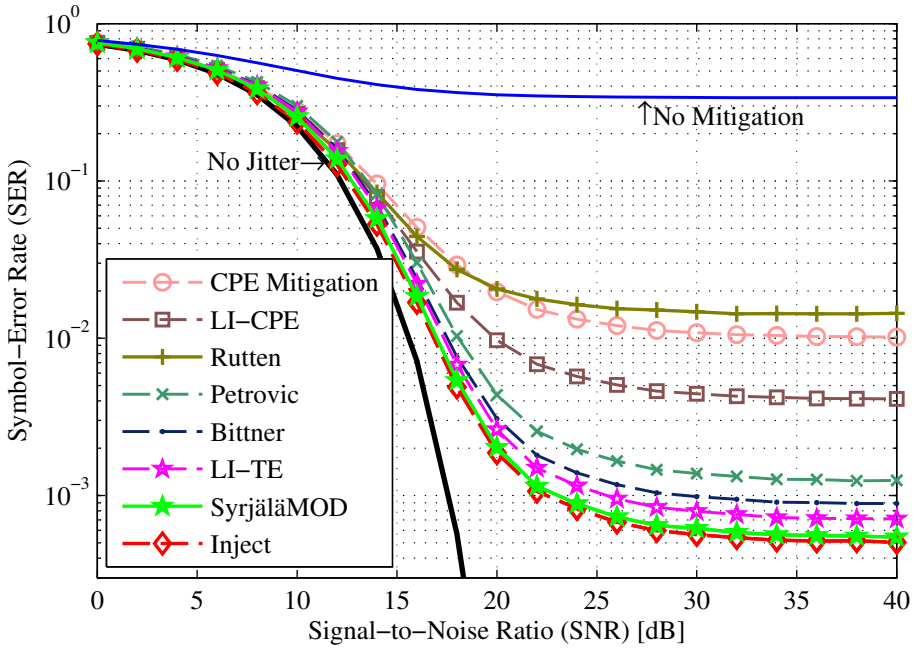

Figure 6-7: Simulated SER as a function of received SNR in AWGN channel. Sampling jitter RMS value is fixed to 20 ps and with nearby interferers.

components in the receiver. Therefore, if OFDM signals are received, the phase-noise mitigation algorithms offer very good mitigation performance without the need for the reference tone. Also, then the oversampling ratio at the sampler does not have to be high for the sake of reference tone, but the phase-noise mitigation algorithms work at the base sampling rate of the OFDM system (namely at $N \times$ subcarrier spacing).

Chapter 7

Conclusions

Oscillator impairments have a huge effect on the performance of radio communications transceivers, and therefore on the performances of the corresponding radio link and radio network. Phase noise is very tedious problem in modern communications transceivers, such as direct-conversion and super-heterodyne OFDM-radios, and sampling jitter on the other hand is a big problem in direct-RF-sampling receivers.

In this thesis, the effect of the phase noise generated by oscillator with arbitrary phase-noise spectral shape was analysed in OFDM signal case. Also, adjacent channel users were considered. Closed form solution for signal-to-interference+noise ratio was derived for OFDM link having single user, but also for the case with adjacent channel users present. Sampling-jitter effect was also analysed in voltage-sampling and charge-sampling based direct-RF-sampling receivers. In voltage sampling case, it was seen that the effect of the sampling jitter resembles closely that of the phase noise in direct-conversion receivers. In charge sampling case, we showed that the effect of the sampling jitter depends heavily on the implementation of the charge-sampling circuitry. We proved that the spectrum of the error caused by the sampling jitter experiences very heavy filtering effect in some implementation scenarios, which in turn has direct implications to the receiver dimensioning in terms of the chosen sampling rate and sampling interval relative to the RF centre-frequency.

In the thesis, we also proposed new digital-signal-processing algorithms for phase noise and sampling jitter mitigation in OFDM direct-conversion receivers and in general (and OFDM) voltage-sampling direct-RF-sampling receivers, respectively. Four algorithms were proposed for OFDM direct-conversion receivers. The first one is computationally efficient way to estimate the time-varying phase noise based on interpolating common-phase-error estimates over adjacent OFDM symbols. The second algorithm improves the performance of existing phase-noise mitigation algorithm by decreasing the estimation error at the boundary parts of each OFDM symbol. The last two are based on reconstruction of the transmitted time-

domain waveform from the initial symbol decisions at the receiver, and using the reconstructed signal to estimate the phase-noise complex exponential. All of the proposed algorithms can be used iteratively. These algorithms were also proposed for use in OFDM direct-RF-sampling receivers for sampling-jitter mitigation. Also, an algorithm for sampling jitter mitigation in general direct-RF-sampling receiver was proposed. The algorithm was based on injecting a reference tone to the sampler input and using it to estimate the sampling jitter for each taken sample. The performances of the proposed algorithms were then compared to those of the state-of-the-art algorithms from the literature. All of the phase-noise mitigation algorithms provided clear performance improvement over the existing algorithms in the literature of around the similar level of complexity. Also adjacent channel OFDMA case was considered. When adjacent channels had reasonably higher power levels, only small overall performance drop was observed. The phase-noise mitigation algorithms still provided very good performance. The proposed time-domain algorithms scaled very well when the number of iteration was increased, unlike any existing algorithm in the literature. The obtained performance improvements using the proposed sampling-jitter mitigation algorithms were significant. The same conclusion was reached for the case with high-power nearby interfering signals present at the sampler input. Even though higher sampling jitter levels severely damaged the performance of the overall simulated radio link, the sampling jitter mitigation algorithms were still able to provide very good performance improvement, especially when sampling jitter was at reasonable levels.

Chapter 8

Summary of Publications and the Author's Contributions

This chapter shortly summarizes the most significant ideas in the papers attached to this thesis from this thesis point-of-view. Also, the author's contribution to the papers is described in detail.

8.1. Summary of Publications

The phase-noise estimation and mitigation algorithms are proposed in [P1], [P5], [P7] and [P10]. In [P1] and [P5], LI-CPE and LI-TE techniques are developed to improve the performances of existing plain CPE and ICI mitigation algorithms, respectively. In [P7], time-domain phase-noise estimation and mitigation algorithm is presented. It is based on time-domain comparison of the received signal with phase noise and reconstructed phase-noise-free signal. The structure provides very high performance especially in additive white-Gaussian-noise channel. A modified and improved version of the algorithm of [P7] is presented in [P10]. A few of the weaknesses of the original algorithm of [P7] are addressed by including also the cyclic prefix in the phase-noise estimation, and moving the phase-noise mitigation part to right after the signal sampling, before the channel estimation. This provides improved all-around performance compared to the performance of the algorithm of [P7], and very nice performance gain in multipath channel conditions. Also channel estimation aspects are considered in [P5].

In [P2], [P3], [P5] and [P4], the sampling-jitter estimation and mitigation algorithms are proposed for voltage-sampling based direct-RF-sampling receiver. In [P2] and [P5], the sampling jitter in direct-RF-sampling receiver is proved to have approximately same effect on the signal as the phase noise has on direct-conversion receiver. Therefore, the presented OFDM phase-noise mitigation techniques are proposed to be used in the sampling-jitter mitigation in direct-RF-sampling receivers. The phase-noise mitigation algorithms provide very good performance in the sampling-jitter mitigation. In [P3] and [P4], injection of a

reference tone at the sampler input, and using that as a base for sampling-jitter estimation and mitigation, is proposed. The idea gives very high quality estimates, and the mitigation performance is even higher than that of the phase-noise mitigation algorithms.

SINR performance analysis for OFDM signal under receiver phase noise generated by oscillator with arbitrary phase-noise spectral shape is given in [P6]. The analysis is based on the phase noise model in which white-Gaussian-noise is shaped to match a generated spectral mask of the phase noise. The analysis is expanded to the case with adjacent channels in [P8]. Other technical content, other than the SIR analysis, developed and reported in [P8] are outside this thesis work.

Publication [P9] gives analysis of the error caused by the sampling jitter in charge-sampling direct-RF-sampling receiver. The work is based on small-phase approximation, but also on the approximation that sampling-jitter effect on high-frequency carrier components of the signal is dominant over the effect the timing jitter has on the low-frequency information signals. The paper shows that the error spectrum due to sampling jitter is heavily shaped in some charge-sampler implementations when compared to the plain voltage-sampling. The impact of such filtering effect on the receiver dimensioning is also discussed.

8.2. Author's Contribution to Publications

The author was the main contributor and primary author of all of the attached original papers, except for the paper [P8], in which the author had significant but small contribution. It goes without saying that numerous discussions with the Prof. Valkama have contributed to the resulting research considerably, especially at the starting phase of the research.

It was Prof. Valkama who proposed the topic of phase-noise analysis, estimation and mitigation in OFDM transceivers to the author. The SIR analysis part of the paper [P8] and all the writing in other papers was done by the author. Prof. Valkama naturally had significant contribution in the final appearance of the papers. Also, Mr. V. Lehtinen had contribution on the final appearance of the paper [P9].

In paper [P1], the author found the problems in, and created the techniques to improve the performances of, the existing phase-noise estimation algorithms. For publications [P2], [P3] and [P4], all the signal models and algorithms were developed by the author. However, Prof. Valkama directed the author to the right track by pointing out some key publications and interesting ideas in sampling jitter modelling, thus having enabling contribution to developed algorithms. In publication [P5], the author independently created the new channel estimation technique for the phase-noise mitigation algorithms. A sketch that was basis of the phase noise analysis in [P6] was originally developed by Prof. Valkama and contributed also by Dr. Y. Zou. The analysis was polished and developed further to the form given in the paper by the author. Mr. V. Lehtinen first noticed that in some charge-sampling implementations, the error due to jitter gets shaped. After Prof. Valkama and Mr. V. Lehtinen proposed the topic for the

author, the author created all the signal models and proofs about the filtering effect, which were published in [P9]. The author then also analysed the other charge sampling implementation ways that do not have the filtering effect or just have partial filtering effect present. The original papers [P7] and [P10] are fruits of independent research work of the author.

For all the publications except for the publications [P8], the author also independently implemented all the algorithms and built the corresponding simulators for all the performance analysis of the algorithms, signal models and the error analysis. For the SIR analysis of the publication [P8], the author only implemented and simulated the results that are written in this thesis, not the simulation results that appear in the publication. The SIR analysis in the publication [P8] is, in this thesis, expanded to SINR analysis to match better with analysis in [P6].

Bibliography

[1] A. Abidi, “Evolution of a software-defined radio recever’s RF front-end,” in *Proc. Radio Frequency Integrated Circuits (RFIC) Symposium 2006*, San Francisco, CA, June 2006.

[2] L. Anttila, *Digital Front-End Signal Processing with Widely-Linear Signal Models in Radio Devices*, PhD dissertation, Tampere University of Technology, 2011. 122 p. ISBN 978-952-15-2651-0.

[3] L. Anttila, M. Valkama, and M. Renfors, ”Circularity-based I/Q imbalance compensation in wideband direct-conversion receivers,” *IEEE Transactions on Vehicular Technology*, Vol. 57, No. 3, pp. 2099-2113, July 2008.

[4] L. Anttila, M. Valkama, and M. Renfors, ”Frequency-selective I/Q mismatch calibration of wideband direct-conversion transmitters,” *IEEE Transactions on Circuits and Systems II: Express Briefs*, Vol. 55, No. 4, pp. 359-363, April 2008.

[5] V. J. Arkensteijn, E. A. M. Klumperink, and B. Nauta, “Jitter requirements of the sampling clock in software radio receivers,” *IEEE Transactions on Circuits and Systems-II: Express Briefs*, Vol. 53, No. 2, pp. 90-94, February 2006.

[6] A. Armada and M. Calvo, “Phase noise and sub-carrier spacing effects on the performance of an OFDM communication system,” *IEEE Communications Letters*, Vol. 2, No. 1, pp. 11-13, January 1998.

[7] R. Bagheri *et al.*, “Software-defined radio receiver: dream to reality,” *IEEE Communications Magazine*, Vol. 44, No. 8, pp. 111-118, August 2008.

[8] S. Bittner, A. Frotzscher, G. Fettweis, and E. Deng, “Oscillator phase noise compensation using Kalman tracking,” in *Proc. International Conference on Acoustics, Speech and Signal Processing 2009* (*ICASSP’09*), Taipei, Taiwan, April 2009, pp. 2529-2532.

[9] S. Bittner, W. Rave, and G. Fettweis, “Joint iterative transmitter and receiver phase noise correction using soft information,” in *Proc. IEEE International Conference on Communications 2007* (*ICC’07*), Glasgow, Scotland, June 2007, pp. 2847-2852.

[10] S. Bittner, E. Zimmermann, and G. Fettweis, “Exploiting phase noise properties in the design of MIMO-OFDM receivers,” in *Proc. IEEE Wireless Communications and Networking Conference 2008* (*WCNC’08*), Las Vegas, NV, March 2008, pp. 940-945.

[11] S. Bittner, E. Zimmermann, and G. Fettweis, "Iterative phase noise mitigation in MIMO-OFDM systems with pilot aided channel estimation," in *Proc. Vehicular Technology Conference 2007 Fall* (*VTC'07-Fall*), Baltimore, MD, September 2007, pp. 1087-1091.

[12] J. Bhatti, M. Moeneclaey, "Iterative soft-decision-directed phase noise estimation from a DCT basis expansion," in *Proc. International Symposium on Personal, Indoor and Mobile Radio Communications* (*PIMRC'09*), Tokyo, Japan, September 2009, pp. 3228-3232.

[13] J. Bhatti, N. Noels, and M. Moeneclaey, "Algorithms for iterative phase noise estimation based on a truncated DCT expansion," in *Proc. International Workshop on Signal Processing Advances in Wireless Communications* (*SPAWC'11*), San Francisco, CA, June 2011, pp. 51-55.

[14] J. Bhatti, N. Noels, and M. Moeneclaey, "Phase noise estimation and compensation for OFDM systems: a DCT-based approach," in *Proc. International Symposium on Spread Spectrum Techniques and Applications 2010*, Taichung, Taiwan, October 2010, pp. 93-97.

[15] M. Brownlee, P. K. Hanumolu, K. Mayaram, and U. Moon, " A 0.5-GHz to 2.5-GHz PLL with fully differential supply regulated tuning," *IEEE Journal of Solid-State Circuits*, Vol. 41, No. 12, pp.2720-2728, December 2006.

[16] L. K. Carley and T. Mukherjee, "High-speed low-power integrating CMOS sample-and-hold amplifier architecture," in *Proc. Custom Integrated Circuits Conference*, Santa Clara, CA, May 1995, pp. 543-546.

[17] A. B. Carlson, P. Crilly, and J. Rutledge, *Communication Systems*, McGraw-Hill Schience/Engineering/Math, 4th edition, 864 p., 2001, ISBN 978-0070111271.

[18] R. Casas, S. Biracree, and A. Youtz, "Time domain phase noise correction for OFDM signals," *IEEE Transactions on Broadcasting*, Vol. 48, No. 3 , pp. 230-236, September 2002.

[19] R. Corvaja and A. Armada, "Join channel and phase noise compensation for OFDM in fast-fading multipath applications," *IEEE Transactions on Vehicular Technology*, Vol. 58, No. 2, pp. 636-643, February 2009.

[20] A. Demir, "Computing timing jitter from phase noise spectra for oscillators and phase-locked loops with white and 1/f noise," *IEEE Transactions on Circuits and Systems-I: Regular Papers*, Vol. 53, No. 9, pp. 1869-1884, September 2006.

[21] A. Demir, "Phase noise and timing jitter in oscillators with colored-noise sources," *IEEE Transactions on Circuits and Systems I: Fundamental Theory and Applications*, Vol. 49, No. 12, pp. 1782-1791, December 2002.

[22] A. Demir, "Phase noise in Oscillators: A unifying theory and numerical methods for characterization," *IEEE Transactions on Circuits and Systems-I: Fundamental Theory and Applications*, Vol. 47, No. 5, pp. 655-674, May 2000.

[23] G. Fettweis, M. Löhning, D. Petrovic, M. Windisch, P. Zillmann, and W. Rave, "Dirty-RF: A new paradigm", in *Proc. International Symposium on Personal, Indoor and Mobile Radio Communications 2005* (*PIMRC'05*), Berlin, Germany, September 2005, pp. 2347-2355, Vol. 4.

[24] A. Goldsmith, *Wireless Communication*, Cambridge University Press, 2005, 672 p., ISBN 978-0521837163.

[25] Y. Gong and X. Hong, "A new algorithm for OFDM joint data detection and phase noise cancellation," in *Proc. IEEE International Conference on Communications* (*ICC'08*), Beijing, China, May 2008.

[26] Y. Gong and X. Hong, "OFDM joint data detection and phase noise cancellation based on minimum mean square prediction error," *Elsevier Signal Processing*, Vol. 89, No. 4, pp. 502-509, April 2009.

[27] Y. Gong and X. Hong, "OFDM joint data detection and phase noise cancellation for constant modulus modulations," *IEEE Transactions on Signal Processing*, Vol. 57, No. 7, pp. 2864-2868, July 2009.

[28] J. Heiskala and J. Terry, *OFDM Wireless LANs: A Theoretical and Practical Guide*, Sams Publishing, 2002, 336 p., ISBN 978-0672321573..

[29] Y.-C. Ho, R. B. Staszewski, K. Muhammad, C.-M. Hung, D. Leipold, and K. Maggio, "Charge-domain signal processing of direct RF sampling mixer with discrete-time filter in Bluetooth and GSM receivers," *EURASIP Journal on Wireless Communications and Networking*, Vol. 2006, pp. 1-14, March 2006.

[30] IEEE Communications Society, *A Brief History of Communications*, 2002, ISBN 0-7803-9825-4.

[31] S. Karvonen and J. Kostamovaara, "Charge-domain FIR sampler with programmable filtering coefficients," in *Proc. International Symposium on Circuits and Systems 2005* (*ISCAS'05*), Kobe, Japan, May 2005, pp. 4425-4428, Vol. 5.

[32] S. Karvonen, T. Riley, and J. Kostamovaara, "On the effect of timing jitter in charge sampling," in *Proc. International Symposium on Circuits and Systems 2003* (*ISCAS'03*), Bangkok, Thailand, May 2003, pp. 737-740, Vol. 1.

[33] S. Karvonen, T. Riley, S. Kurtti, and J. Kostamovaara, "A quadrature charge-domain sampler with embedded FIR and IIR filtering functions," *IEEE Journal of Solid-State Circuits*, Vol. 41, No. 2, pp. 507-515, February 2006.

[34] M. Krondorf, S. Bittner, and G. Fettweis, "Numerical performance evaluation for OFDM systems affected by phase noise and channel estimation errors," in *Proc.*

Vehicular Technology Conference Fall 2008 (*VTC'08-Fall*), Calgary, Canada, September 2008.

[35] E. Lee and D. Messerschmitt, *Digital Communication*, 2nd edition 1993, 912 p., ISBN 978-0792393917.

[36] D. D. Lin and T. J. Lim, "The variational inference approach to joint data detection and phase noise estimation in OFDM," *IEEE Transactions on Signal Processing*, Vol. 55, No. 5, pp. 1862-1874, May 2007.

[37] S. Lindfors, A. Pärssinen, and K. Halonen, "A 3-V 230-MHz CMOS decimation subsampler," *IEEE Transactions on Circuits and Systems II: Analog and Digital Signal Processing*, Vol. 50, No. 3, pp. 105-117, March 2003.

[38] P. Mathecken, T. Riihonen, S. Werner, and R. Wichman, "Performance analysis of OFDM with wiener phase noise and frequency selective fading channel," *IEEE Transactions on Communications*, Vol. 59, No. 5, pp. 1321-1331, May 2011.

[39] A. Molisch, *Wireless Communications*, John Wiley & Sons Ltd., 2nd edition, 827 p., 2011, ISBN 978-0470741863.

[40] K. Muhammad *et al.*, "A discrete-time Bluetooth receiver in a 0.13 μm digital CMOS process," in *Proc. International Solid-State Circuits Conference*, San Francisco, CA, February 2004.

[41] K. Muhammad, R. B. Staszewski, and D. Leipold, "Digital RF processing: towards low-cost reconfigurable radios," *IEEE Communications Magazine*, Vol. 43, No. 8, pp. 105-113, August 2005.

[42] P. Mörters and Y. Peres, *Brownian Motion*, Cambridge University Press, 2010, ISBN 978-0521760188.

[43] N. Noels, M. Moeneclaey, F. Simoens, and D. Delaruelle, "A low-complexity iterative phase noise tracker for bit-interleaved coded CPM signal in AWGN," *IEEE Transaction on Signal Processing*, Vol. 59, No. 9, pp. 4271-4285, Semptember 2011.

[44] U. Onunkwo, Y. Li, and A. Swami, "Effect of timing jitter on OFDM-based UWB systems," *IEEE Journal on Selected Areas in Communications*, Vol. 24, No. 4, pp. 787-793, April 2006.

[45] D. Petrovic, W. Rave, and G. Fettweis, "Effect of phase noise on OFDM systems with and without PLL: Characterization and compensation," *IEEE Transactions Communications*, Vol. 55, No. 8, pp. 1607-1616, August 2007.

[46] J. Proakis, *Digital Communications*, McGraw-Hill Science/Engineering/Math, 4th edition 2000, 1024 p., ISBN 978-0072321111.

[47] P. Rabiei, W. Namgoong, and N. Al-Dhahir, "A non-iterative technique for phase noise ICI mitigation in packec-based OFDM systems," *IEEE Transactions on Signal Processing*, Vol. 58, No. 11, pp. 5945-5950, November 2010.

[48] P. Rabiei, W. Namgoong, and N. Al-Dhahir, "Reduced-complexity joint baseband compensation of phase noise and I/Q imbalance for MIMO-OFDM systems," *IEEE Transactions on Wireless Communications*, Vol. 9, No. 11, pp. 3450-3460, November 2010.

[49] B. Razavi, "Design considerations for direct-conversion receivers," *IEEE Transactions on Circuits and Systems – II: Analog and Digital Signal Processing*, Vol. 44, No. 6, pp. 428-435, June 1997.

[50] J. Rinne and M. Renfors, "An equalizations method for orthogonal frequency division multiplexing systems in channels with multipath propagation, frequency offset and phase noise," in *Proc. Global Telecommunications Conference 1996* (*GLOBECOM'96*), London, United Kingdom, November 1996, pp. 1442-1446.

[51] P. Robertson and S. Kaiser, "Analysis of the effects of phase noise in orthogonal frequency division multiplex (OFDM) systems," in *Proc. IEEE International Conference on Communications 1995* (*ICC'95*), Seattle, WA, June 1995, pp. 1652-1657, Vol. 3.

[52] U. Rohde and J. Whitaker, *Communications Receivers: DSP, Software Radios, and Design*, McGraw-Hill Professional, 3rd edition, 2000, 656 p., ISBN 978-0071361217.

[53] R. Rutten, L. J. Breems, and R. H. M. van Veldhoven, "Digital jitter-cancellation for narrowband signals," in *Proc. IEEE International Symposium on Circuits and Systems 2008*, (*ISCAS 2008*), Seattle, WA, May 2008, pp. 1444-1447.

[54] T. Schenk, *RF Impairments in Multiple Antenna OFDM: Influence and Mitigation*, PhD dissertation, Technische Universiteit Eindhoven, 2006. 291 p. ISBN 90-386-1913-8.

[55] T. Schenk, R. van der Hofstad, and E. Fledderus, "Distribution of the ICI term in phase noise impaired OFDM systems," IEEE Transactions on Wireless Communications, Vol. 6, No. 4, pp. 1488-1500, April 2007.

[56] T. Schenk, X.-J. Tao, P. Smulders, and E. Fledderus, "Influence and suppression of phase noise in multi-antenna OFDM," in *Proc. IEEE Vehicular Technology Conference 2004 Fall* (*VTC'04-Fall*), Los Angeles, CA, September 2004, pp. 1443-1447.

[57] A. Shahed hagh ghadam, *Contributions to Analysis and DSP-based Mitigation of Nonlinear Distortion in Radio Transceivers*, PhD dissertation, Tampere University of Technology, 2011. 122 p. ISBN 978-952-15-2650-3.

[58] A. Shahed hagh ghadam, S. Burglechner, A. Gökceoglu, M. Valkama, and A. Springer, "Implementation and performance of DSP-oriented feedforward power amplifier linearizer," *IEEE Transactions on Circuits and Systems I: Regular papers*, Vol. 59, No. 2, 2012.

[59] D. Shen, C.-M. Hwang, B. Lusignan, and B. Wooley, "A 900-MHz RF front-end with integrated discrete-time filtering," *IEEE Journal of Solid-State Circuits*, Vol. 31, No. 12, pp. 1945-1954, December 1996.

[60] M. Shinagawa, Y. Akazawa, and T. Wakimoto, "Jitter analysis of high-speed sampling systems," *IEEE Journal of Solid-State Circuits*, Vol. 25, No. 1, pp. 220-224, February 1990

[61] T. B. Sorensen, P. E. Mogersen, and F. Frederiksen, "Extension of the ITU channel models for wideband (OFDM) systems," in *Proc. IEEE Vehicular Technology Conference Fall 2005* (*VTC'05-Fall*), Dallas, TX, September 2005, pp. 392-396.

[62] V. Syrjälä, M. Valkama, and M. Renfors, "Design considerations for direct RF sampling receiver in GNSS environment," in *Proc. Finnish Wireless Comm. Workshop* (*FINSIG'07*), Oulu, Finland, August 2007.

[63] V. Syrjälä, M. Valkama, and M. Renfors, "Design considerations for direct RF sampling receiver in GNSS environment," in *Proc. Workshop on Positioning, Navigation and Communications 2008* (*WPNC'08*), IEEE, Hannover, Germany, March 2008.

[64] V. Syrjälä, M. Valkama, and M. Renfors, "Efficient jitter model for high-frequency bandpass sampling," in *Proc. Finnish Wireless Comm. Workshop* (*FINSIG'07*), Oulu, Finland, August 2007.

[65] N. N. Tchamov, J. Rinne, V. Syrjälä, M. Valkama, Y. Zou, and M. Renfors, "VCO phase noise trade-offs in PLL design for DVB-T/H receivers," in *Proc. IEEE International Conference on Electronics, Circuits and Systems 2009* (*ICECS'09*), Yasmine Hammamet, Tunisia, December 2009, pp. 527-530.

[66] S.-K. Ting, A. H. Sayed, "Frequency domain compensation of spurious sidebands in A/D circuits," in *Proc. Acoustics, Speech and Signal Processing* (*ICASSP'11*), Prague, Czech Republic, June 2011, pp. 4000-4003.

[67] L. Tomba, "On the effect of Wiener phase noise in OFDM systems," *IEEE Transactions on Communications*, Vol. 46, No. 5, pp. 580-583, May 1998.

[68] D. Tse and P. Viswanath, *Fundamentals of Wireless Communication*, Cambridge University Press, 2005, 586 p., ISBN 978-0521845274.

[69] J. Tubbax, B. Côme, L. Van der Perre, S. Donnay, M. Engels, H. De Man, and M. Moonen, "Compensation of IQ imbalance and phase noise in OFDM systems," *IEEE Transactions on Wireless Communications*, Vol. 4, No. 3, pp. 872-877, May 2005.

[70] M. Valkama, A. Shahed hagh ghadam, L. Anttila, and M. Renfors, "Advanced digital signal processing techniques for compensation of nonlinear distortion in wideband multicarriers radio receivers," *IEEE Transactions on Microwave Theory and Techniques*, Vol. 54, No. 6, Part 1, pp. 2356-2366, June 2006.

[71] H. Wu, S. Yang, J. Ou, and L. Yang, "Phase noise estimation and equalization for OFDM systems based on interpolation of common phase error," *International Journal of Digital Content Technology and its Applications*, Vol. 5, No. 9, September 2011.

[72] S. Wu and Y. Bar-Ness, "A phase noise suppression algorithm for OFDM-based WLANs," *IEEE Communications Letters*, Vol. 6, No. 12, pp. 535-537, December 2002.

[73] S. Wu and Y. Bar-Ness, "OFDM systems in the presence of phase noise: Consequences and solutions," *IEEE Transactions on Communications*, Vol. 52, No. 11, pp. 1988-1997, November 2004.

[74] C.-H. Yih, "BER analysis of OFDM systems impaired by phase noise in frequency-selective Rayleigh fading channels," in *Proc. Global Telecommunications Conference 2008* (*GLOBECOM'08*), New Orleans, LO, December 2008.

[75] Q. Zou, A. Tarighat, and A. H. Sayed, "Compensation of phase noise in OFDM wireless systems," *IEEE Transactions on Signal Processing*, Vol. 55, No. 11, November 2007.

Publications

Publication 1

V. Syrjälä, M. Valkama, N. N. Tchamov, and J. Rinne, "Phase noise modelling and mitigation techniques in OFDM communications systems," in *Proc. Wireless Telecommunications Symposium 2009* (*WTS'09*), IEEE, Prague, Czech Republic, April 2009.

Phase Noise Modelling and Mitigation Techniques in OFDM Communications Systems

Ville Syrjälä, Mikko Valkama, Nikolay N. Tchamov, and Jukka Rinne
Tampere University of Technology
Department of Communications Engineering
Korkeakoulunkatu 1, FI-33720 Tampere, Finland
E-mail: ville.syrjala@tut.fi

***Abstract*—This paper addresses the analysis and mitigation of the signal distortion caused by oscillator phase noise (PN) in OFDM communications systems. Two new PN mitigation techniques are proposed, especially targeted for reducing the intercarrier interference (ICI) effects due to PN. The first proposed method is a fairly simple one, stemming from the idea of linearly interpolating between two consecutive common phase error (CPE) estimates to obtain a linearized estimate of the time-varying phase characteristics. The second technique, in turn, is an extension to the existing state-of-the-art ICI estimation methods. Here the idea is to use an additional interpolation stage to improve the phase estimation performance around the boundaries of two consecutive OFDM symbols. The paper also verifies the performance improvement of these new PN estimation techniques by comparing them to the existing state-of-the-art techniques using extensive computer simulations. To emphasize practicality, the simulations are carried out in 3GPP-LTE downlink –like system context, covering both additive white Gaussian noise (AWGN) and extended ITU-R Vehicular A multipath channel types.**

***Index Terms*—phase noise; OFDM; common phase error; intercarrier interference; LTE**

I. Introduction

ORTHOGONAL Frequency-Division Multiplexing (OFDM) is a multicarrier modulation scheme used in many modern and emerging communications standards, e.g., Digital Video Broadcasting (DVB), wireless local area networks such as IEEE 802.11g, and 3GPP Long Term Evolution (LTE). Compared to traditional single carrier modulation methods, OFDM has its strengths and weaknesses. Stemming from the long symbol duration and thus efficiently implementable guard interval (GI), OFDM is relatively immune against inter-symbol interference (ISI). Furthermore, multicarrier transmission enables efficient use of adaptive modulation and coding schemes, and also provides robustness against frequency-selective fading in terms of fairly simple equalization. On the other hand, OFDM imposes high demands for the quality of the used radio devices, being especially sensitive, e.g., to oscillator non-idealities. These include different synchronization errors as well as random phase fluctuations called phase noise [2], [15], [17].

On radio implementation side, there are currently big demands for smaller and more energy efficient radio transmitters and receivers. Even higher demands for the radios will be set, when many transceivers, or parts of the transceivers, must be operating simultaneously in a single device. This kind of configuration comes into play, e.g., when implementing radio devices for multiple-input multiple-output (MIMO) transmission systems. In general, because of these high demands for the transceivers, it is very important to understand and try to mitigate possible non-idealities in the transmission chain components. This is called dirty-RF signal processing in general [10].

The impact of PN on OFDM systems has been extensively studied, e.g., in [2], [12] and [15]. The distortion due to PN can in general be divided into two components: common phase error (CPE) and intercarrier interference (ICI). While CPE refers to the constant phase rotation experienced by all the subcarriers within one OFDM symbol interval, ICI corresponds to neighbouring subcarriers interfering with each other. The mitigation of CPE alone has generally been widely investigated. A simple method for CPE mitigation has been presented in [12], and the same method has been further improved in [16], also trying to remove some ICI. In addition, various techniques for ICI mitigation have been developed. For example, [11] has presented a very illustrative technique for ICI mitigation stemming from iterative detection principles. The same group has also published some performance improvements to their methods in [4] and [5].

This paper concentrates on enhanced PN modelling and mitigation schemes. In Section II, modelling of free-running and PLL-based oscillators is shortly addressed. Section III concentrates on the analysis of PN effects on OFDM waveforms. Section IV then gives a short review of essential state-of-the-art in PN mitigation including [5], [11], and [16].

This work was supported by the Finnish Funding Agency for Technology and Innovation (Tekes, under the project "Advanced Techniques for RF Impairment Mitigation in Future Wireless Radio Systems"), the Technology Industries of Finland Centennial Foundation, Finnish Foundation for Technology Promotion, EUREKA CELTIC E!3187 B21C-Broadcasting for 21st Century, and TUT Graduate School.

1-4244-2589-1/09/$20.00 ©2009 IEEE.

Section V is the main contribution of this paper, introducing two new PN mitigation schemes. The first one is relatively simple and is based on linear interpolation of the CPE values over adjacent OFDM symbols. The second one concentrates on improving the ICI estimation performance of the methods presented in [11] and [5] by improving the PN estimation accuracy at symbol boundaries using proper interpolation. Section VI then actually analyzes the mitigation performance of the proposed and reference techniques using computer simulations. Finally, Section VII concludes the work.

II. Phase Noise Modelling

In addition to ordinary carrier frequency and phase offsets, the time-varying phase behaviour of the used oscillator(s) is one of the most challenging non-idealities in radio devices. In this paper, we focus on the phase noise aspects, and both free-running and phase-locked loop (PLL) type oscillators are considered. A general signal-level model for a noisy complex (I/Q) oscillator is typically formulated as

$$\alpha_{osc}(t) = e^{j2\pi f_c t} e^{j\phi(t)}, \tag{1}$$

where $\phi(t)$ denotes the phase noise and f_c is the nominal oscillating frequency, i.e. carrier frequency for oscillators in direct conversion receiver. In the following, more detailed characteristics of the phase noise $\phi(t)$ are addressed for different types of oscillators.

A. Free-Running Oscillators

Free-running oscillator model is very simple and illustrative. In the literature [13], the phase noise of a free-running oscillator is typically assumed to follow Brownian motion (also called Wiener Process). Accurately, we can define the PN for a free-running oscillator as

$$\phi(t) = \sqrt{c} B(t), \tag{2}$$

in which $B(t)$ denotes standard Brownian motion and c is the so-called diffusion rate [13]. Standard Brownian motion $B(t)$, in turn, is defined as a random process for which $B(t_2) - B(t_1)$ is Gaussian distributed with zero mean and variance $|t_2 - t_1|$. Thus, we are able to model the PN process with a single parameter c. The process in (2) has a variance that linearly increases with time [9], written here as

$$\sigma_\phi^2(t) = c \times t. \tag{3}$$

Decay of power spectral density (PSD) is a commonly used quantity to define oscillator PN properties. Now, we can map the diffusion rate c to the PSD in order to simplify the parameterization of the model. First of all, one-sided PSD of the oscillator α_{osc} in (1) around the carrier frequency attains the Lorenzian spectrum and is given by

$$S(\Delta f) = \frac{c}{(2\pi\Delta f)^2 + (c/2)^2}, \tag{4}$$

where Δf is the frequency offset from the nominal centre frequency f_c of the oscillator [13]. From (4), the rate of decay at larger offsets is -20 dB/decade, and the 3 dB bandwidth of the PSD is given by

$$\beta = \frac{c}{4\pi}. \tag{5}$$

This 3 dB bandwidth in (5) gives us an easily interpretable reference parameter and is used from now on in free-running oscillator characterizations.

B. Phase-Locked-Loop Oscillators

In practice, phase-locked-loop (PLL) based oscillators are typically used. Here, a PLL phase noise model, which contains both white and flicker noise perturbations to $\phi(t)$, is presented. In general, the PLL PN output is dominated by the reference crystal oscillator (CO) below the loop bandwidth f_{LBW}, and by the voltage controlled oscillator (VCO) above f_{LBW}. Contemporary integrated CMOS VCOs can exhibit significant flicker noise contributions that cannot be neglected [6]. For a free-running VCO with flicker noise, the variance of $\phi(t)$ over time t becomes [8]

$$\sigma^2_{\substack{white+\\flicker}}(t) = (2\pi f_c)^2 \left\{ c_\omega t + c_f \int_0^t \int_0^t R_{Nm}(t_1 - t_2)\, dt_1 dt_2 \right\}, \tag{6}$$

where c_ω and c_f are the constants describing white and flicker noise perturbations. These constants can, in practice, be found through circuit simulator or spot PN-PSD measurements at large offsets, from [8]

$$L(\Delta f) = \frac{f_c^2 \left(c_\omega + c_f S_f(\Delta f) \right)}{\pi^2 f_c^4 \left(c_\omega + c_f S_f(\Delta f) \right)^2 + \Delta f^2}. \tag{7}$$

In (7), $S_f(\Delta f)$ is the flicker noise PSD at offset Δf from the carrier and can be written as [8]

$$S_f(\Delta f) = \frac{1}{|\Delta f|} - \frac{2}{\pi \Delta f} \tan^{-1}\left(\frac{\gamma_c}{2\pi \Delta f} \right), \tag{8}$$

where γ_c specifies the cutoff frequency at which the flicker noise PSD deviates from its nominal $1/\Delta f$ slope.

In the PLL model, the excess phase variance deviates from (3) depending on the PLL implementation and noise type perturbations. In first-order PLL with white noise perturbations only, the variance of $\phi(t)$ saturates at [7]

$$\lim_{t\to\infty}\sigma^2_{\phi,white}(t)=\frac{2\pi f_c^2 c_\omega}{f_{LBW}}. \quad (9)$$

Notice also that, the implemented PLL model flattens the VCO and CO excess phase PSD $S_\Phi(\Delta f)$ to constant levels at small offsets Δf and thus eliminates a singularity at the carrier that is associated with the Brownian motion model [7]. An example generation of the PLL output PN PSD with $f_{LBW}=2$ kHz is shown in Fig. 1. The corresponding PN spot measurements are summarized in Table I.

III. OFDM System Modelling

In a general OFDM system with N subcarriers, the time-domain waveform samples are obtained by N-point inverse fast Fourier transform (IFFT) of the subcarrier data symbols [3]. Thus, at m-th OFDM symbol interval, these samples can be written as

$$x_m(n)=\frac{1}{\sqrt{N}}\sum_{k=0}^{N-1}X_m(k)e^{j2\pi nk/N}, \quad (10)$$

where $X_m(k)$ denotes the k-th subcarrier data symbol during m-th OFDM symbol interval. Every OFDM symbol has also a cyclic prefix (CP), which copies the last G samples of (10) before the first samples, giving the extended OFDM-symbol length of $N+G$ samples. [11]

After the impact of a multipath channel, receiver down-conversion with PN, and removal of the CP, we can write the received samples for m-th OFDM symbol as a vector

$$\mathbf{r}_m=\mathrm{diag}(e^{j\boldsymbol{\phi}_m})(\mathbf{x}_m\otimes\mathbf{h}_m)+\mathbf{n}_m. \quad (11)$$

Here, $\otimes$ is a circular convolution operator, $\mathbf{x}_m$ is the vector of samples of m-th transmitted OFDM symbol, $\mathbf{h}_m$ is the channel impulse response, and $\mathbf{n}_m$ is Additive White Gaussian Noise (AWGN) vector. In addition, $\boldsymbol{\phi}_m$ is a vector that has PN realization samples within m-th OFDM symbol, so $\boldsymbol{\phi}_m=[\,\phi_m(0),\ldots,\phi_m(N\text{-}1)\,]^{\mathrm{T}}$. In this model, it is assumed that transmitter has no PN. This assumption can be made because receiver PN has been shown to dominate the contribution PN has on the total system performance [13]. Also, as mentioned in [11], with small PN bandwidths, the transmitter PN can be effectively referred to RX side.

Next, the received signal vector is demodulated using FFT. The resulting frequency-domain signal vector, following directly from (11), is given by

$$\mathbf{R}_m=\mathbf{J}_m\otimes(\mathbf{X}_m\bullet\mathbf{H}_m)+\boldsymbol{\eta}_m. \quad (12)$$

Here, $\bullet$ is an element-wise multiplication operator, $\mathbf{X}_m$ is the vector of transmitted subcarrier symbols, $\mathbf{H}_m$ is the channel

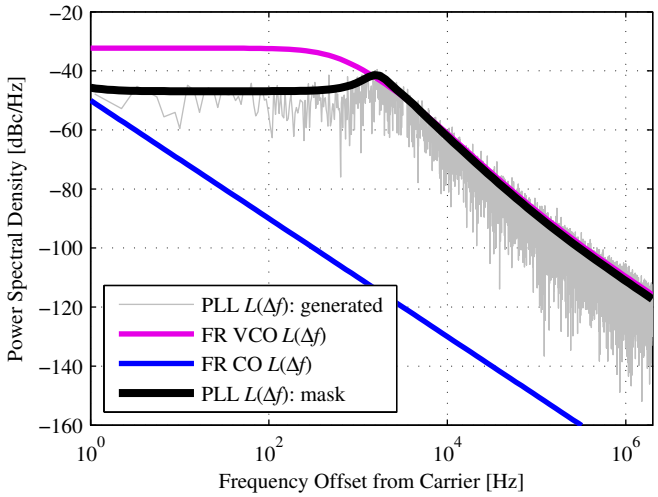

Fig. 1. Example of PLL output phase noise for centre frequency of 1.5915 GHz.

TABLE I
EXAMPLE PLL MODEL PARAMETERS

PN spot reading	Flicker noise perturbation region (-30 dB/decade)	White noise perturbations region (-20 dB/decade)
CO	No flicker noise region	L_{CO}(100 Hz) = -90 dBc/Hz
VCO	L_{VCO}(30 kHz) = -75 dBc/Hz	L_{VCO}(1 MHz) = -110 dBc/Hz

transfer function, $\boldsymbol{\eta}_m$ is the FFT of AWGN, and $\mathbf{J}_m$ is the FFT of $\exp(j\boldsymbol{\phi}_m)$. The $\mathbf{J}_m$ can be written explicitly as

$$J_m(k)=\frac{1}{\sqrt{N}}\sum_{n=0}^{N-1}e^{j\phi_m(n)}e^{-j2\pi nk/N}. \quad (13)$$

Now, it can be noted that the components of (12) can be written essentially in two parts as

$$R_m(k)=X_m(k)H_m(k)J_m(0)+\sum_{l=0,l\neq k}^{N-1}X_m(l)H_m(l)J_m(k-l)+\eta_m(k). \quad (14)$$

This splitting is very important for our analysis purposes, because it divides the PN contribution to two different parts. The first and the second parts of (14) are the CPE corrupted and ICI corrupted parts of the signal, respectively. The CPE means common phase rotation of every subcarrier data inside one OFDM symbol. ICI, on the other hand, is the intercarrier interference that every subcarrier causes to each other due to frequency spreading by PN. [11], [17]

IV. State-of-the-Art Phase Noise Estimation and Mitigation Techniques

This Section gives a short overview of state-of-the-art PN mitigation techniques, originally presented in [5], [11] and [16], for reference. CPE and ICI mitigation schemes are considered separately to emphasize readability.

A. CPE Estimation

As (14) shows, CPE has exactly the same effect on every subcarrier inside one OFDM symbol. Thus, we can estimate the CPE term $J_m(0)$ for an OFDM symbol by using, e.g., pre-known pilot subcarriers (S_P). To focus on CPE, we can modify (14) so that the ICI and AWGN are just combined into one variable $\varepsilon_m(k)$. This results in

$$R_m(k) = X_m(k)H_m(k)J_m(0) + \varepsilon_m(k)\,. \tag{15}$$

When we consider the case $k \in S_P$, we can estimate $J_m(0)$ with, e.g., least squares (LS) estimation, given that also the channel response $H_{\mathrm{m}}(k)$ is known [16]. This estimate can be formulated as

$$\hat{J}(0) = \frac{\sum_{k\in S_P} R_m(k)X_m^*(k)H_m^*(k)}{\sum_{k\in S_P} \left|X_m(k)H_m(k)\right|^2}, \tag{16}$$

where $()^*$ is a complex conjugate operator. In [16], additional means to improve this estimate were also introduced for the cases where the number of pilot subcarriers ($k \in S_P$) is low. In our case though, we are mostly focusing on 3GPP LTE -like system with large number of subcarriers, and thus also many pilot subcarriers per OFDM symbol [1]. Thus, (16) is used as the primary CPE estimation implementation in the forthcoming developments.

B. ICI Estimation

In CPE estimation above, only the first term of $\mathbf{J}_m$ vector is estimated for each OFDM symbol. All the other terms of $\mathbf{J}_m$ represent ICI as (14) illustrates. The $\mathbf{J}_m$ vector has altogether N elements in it. With practical number of subcarriers, it would be computationally very heavy to try to estimate all of these values. Gladly, this is not needed. Stemming from the PN modelling in Section II, phase has typically steeply descending low-pass natured spectrum around the nominal oscillating frequency. Thus the components around the centre frequency are the most important ones in most practical cases. Thus below, we consider only the spectral components near the centre frequency, $J_m(k)$, $k \in \{0, ..., u, N-u, ..., N-1\}$, or with circular indexing $k \in \{-u, ..., u\}$ [11]. Now, if we estimate only ICI terms with $k \in \{-u, ..., u\}$, we can write $R_m(k)$ in (14) more conveniently as

$$R_m(k) = \sum_{l=-u}^{u} X_m(k-l)H_m(k-l)J_m(l) + \zeta_m(k)\,. \tag{17}$$

Here, variable $\zeta_m(k)$ has the AWGN terms and all non-estimated ICI-terms in it. Furthermore, if we only consider a subset of the subcarriers $k \in \{l_1, ..., l_{\mathrm{P}}\}$, $P > 2u+1$, we can write (17) in a matrix form

$$\begin{bmatrix} R_m(l_1) \\ \vdots \\ R_m(l_P) \end{bmatrix} = \begin{bmatrix} A_m(l_1+u) & \cdots & A_m(l_1-u) \\ \vdots & \ddots & \vdots \\ A_m(l_P+u) & \cdots & A_m(l_P-u) \end{bmatrix} \begin{bmatrix} J_m(-u) \\ \vdots \\ J_m(u) \end{bmatrix} + \boldsymbol{\zeta}_m\,, \tag{18}$$

or equivalently as $\mathbf{R}_{m,p} = \mathbf{A}_{m,u}\mathbf{J}_{m,u} + \boldsymbol{\zeta}_{m,u}$, in which $A_m(k) = X_m(k)H_m(k)$. In practice, this subset of subcarriers can be selected so that it consists of subcarriers that are the most reliable after initial detection [11]. Reliability, in turn, can be measured, e.g., with the help of coding [4]. Now assuming that both $X_m(k)$ and $H_m(k)$ are known for the considered subcarriers, estimating $\mathbf{J}_{m,u}$ is easy using, e.g., the pseudo inverse of $\mathbf{A}_{m,u}$ as

$$\hat{\mathbf{J}}_{m,u} = \left(\mathbf{A}_{m,u}^H \mathbf{A}_{m,u}\right)^{-1} \mathbf{A}_{m,u}^H \mathbf{R}_{m,p}\,. \tag{19}$$

The resulting PN spectrum estimate can then be used to deconvolve the effect of the PN out of the system, i.e., ICI can be removed. Notice that instead of the least-squares estimator presented in (19), a more complicated minimum mean-squared error (MMSE) estimator was deployed in [11]. MMSE approach requires quite detailed knowledge of the statistical properties of the phase noise at hand [11]. The LS approach is chosen here for computational simplicity since in 3GPP LTE -like systems with high numbers of subcarriers, the calculation of these statistics is relatively demanding.

As the above method obviously needs knowledge of the data symbols at the considered subcarriers, the idea is to do the processing iteratively [11]. In the first iteration, only the CPE is removed from the received signal and the relevant subcarrier data is detected. These symbol decisions are then used as known symbols in (18)-(19), yielding an estimate of the PN spectral components. After removing the ICI from the received signal block using this estimate, the subcarrier data is detected again, yielding yet more reliable data decisions. This whole procedure is then iterated.

Stemming from the utilized block-wise or truncated Fourier series approach for PN estimation in [11], and also here in (18)-(19), the resulting PN estimation quality at the "tails" (close to symbol boundaries) inside each OFDM symbol is very poor. This will be illustrated graphically in Section V. This problem can be relieved with the edge substitution method presented in [5]. In the edge substitution technique, the edges of PN estimates for each OFDM symbol are replaced by so called periodic extensions. This periodic extension is calculated by observing the PN estimate samples in different order, so that the interesting edge is mapped to the middle parts of the OFDM symbol. After reordering the PN estimate, the estimated PN in the middle parts that correspond to the edge parts of the original PN estimate can be used as a substitution for the edges. This is done separately for both, leading and trailing, edges of the PN estimate within each OFDM symbol. [5]

V. New ICI Estimation and Mitigation Techniques

In this Section, new linear interpolation based ICI estimation technique (LI-CPE) and new linear interpolation based tail-estimation technique (LI-TE) are proposed. Here, instead of other more complex interpolators, linear interpolation is used as the main tool to emphasize computational simplicity. Also, in case of free-running oscillators, linear interpolation has been shown in [18] to be the optimum way to process and estimate time-domain phase noise values, which further justifies its use in LI-TE approach.

In both LI-CPE and LI-TE methods, after obtaining the final estimate for the time-domain phase noise behaviour within the processed OFDM symbol, the actual mitigation of the ICI is done by deconvolving the corresponding received signal block with the FFT of the estimated phase noise waveform.

A. ICI Estimation Using CPE Interpolation (LI-CPE)

The proposed LI-CPE PN estimation technique is based on simple linear interpolation of two consecutive CPE estimates. If we study PN and CPE realizations in Fig. 2, we notice that by linearly interpolating the CPE realization from the middle of each symbol to the middle of the next symbol, our result, on average, is closer to the PN realization than the CPE estimate alone. These interpolated CPE characteristics estimate also the ICI behaviour by trying to reconstruct the phase behaviour inside individual symbols. In addition, the estimation procedure is formulated here so that the CPE of the final interpolated phase matches the original CPE value inside each OFDM symbol. An example of the overall estimated phase as a function of time using the above estimation approach is given in Fig. 2.

One drawback of the above estimation procedure is that it imposes an extra delay of one OFDM symbol compared to plain CPE estimation. Notice also that any existing CPE estimation scheme, such as the one in (16), can be used to obtain the initial CPE estimates used in the interpolation stage.

B. Iterative ICI Estimation Using Tail Interpolation (LI-TE)

The new LI-TE PN estimation technique improves the estimation performance of iterative ICI estimation technique presented in [11]. As already noted in [5], the ICI estimation method does not work perfectly. It has problems especially with the tails of each symbol, because Fourier series approximation does not give good PN estimates in the edges of an OFDM symbol. This is also demonstrated in Fig. 3. The problems can be reduced simply by linearly interpolating the phase over these badly estimated parts of the PN estimate. The linear interpolation seems to perform best when using linear interpolation over about 15 % of the total samples from the end and the beginning of each symbol. Fig. 3 illustrates how the method improves the PN estimate accuracy. Indeed,

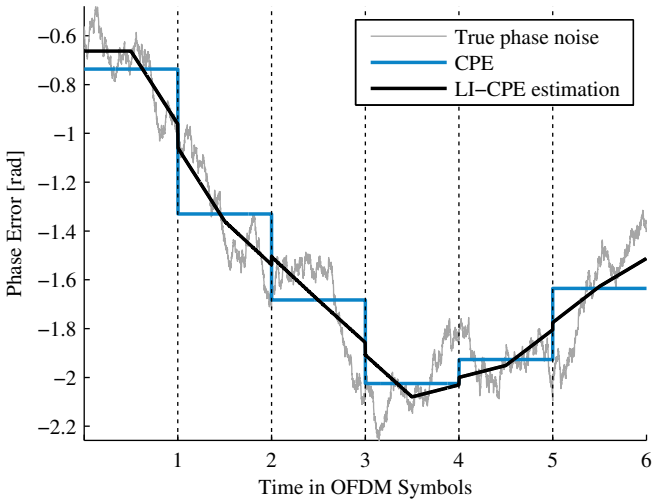

Fig. 2. LI-CPE method demonstrated for a free-running oscillator with 100 Hz spectral width (β) over six OFDM symbols.

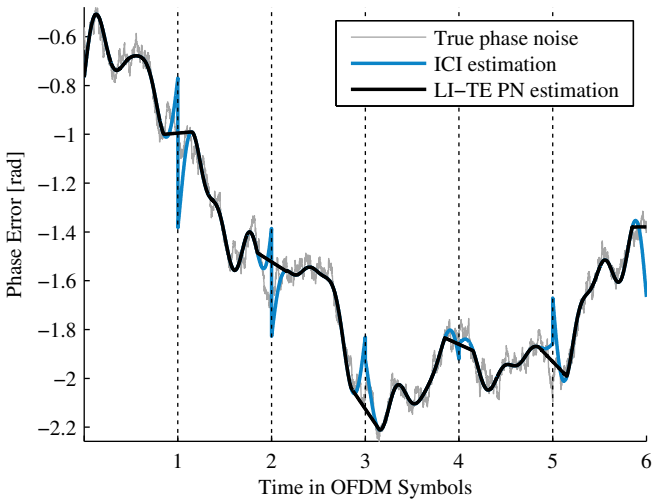

Fig. 3. LI-TE method demonstrated for a free-running oscillator with 100 Hz spectral width (β) over six OFDM symbols. For demonstration purposes, only one iteration in ICI estimation is used.

the earlier ICI estimation method gives corrupted ICI estimates, and the interpolation method improves the quality of the estimate noticeably.

When LI-TE is applied to the iterative method of [11], interpolation can be utilized at each iteration. It should be noted though, that when using only a single iteration, we need estimates of previous and next symbol to do the interpolation, meaning a delay of one OFDM symbol. When using two iterations, we need the second iteration output of the adjacent symbols, thus our delay increases to two symbols and so on. This is not a major problem though since the iterative ICI estimation method gets altogether computationally heavier and heavier as the number of iterations increases, so many iterations are not feasible anyways. In the forthcoming performance evaluations, we use interpolation only over two iterations for simplicity.

VI. Simulations and Performance Analysis

In the simulations, the performances of all the presented PN mitigation techniques are studied and compared. Simulation model is based on 3GPP LTE downlink -like system [1], where 1024 subcarriers with 15 kHz subcarrier spacing are used, 600 of which are carrying 16QAM data. The 600 active subcarriers are selected so that 300 of them are on the both sides of the centre subcarrier. Of these 600 active subcarriers, 18 carry pilot symbols, and are not used for data transmission. The length of the cyclic prefix is 63 samples.

The simulation process is carried out as follows. First, data symbols are generated using 16QAM subcarrier modulation. These are then OFDM-modulated, and send to the channel. As a channel, we use both additive white Gaussian noise (AWGN) channel and extended Vehicular A [14] multipath channel models. Extended Vehicular A is used so that the channel is static for blocks of 12 OFDM symbols after which new channel realization is drawn. After the channel, receiver PN is modelled and applied. Both free-running and PLL-based oscillators are applied in the simulations. The PN effect is then mitigated with presented techniques, and channel is equalized. In the channel equalization, perfect channel knowledge is assumed. After mitigation and equalization, the actual symbol detection is done separately for each subcarrier using the well-known minimum-distance principle.

For ICI estimation, we use 2 iterations and estimate three PN spectral components ($u=3$) around the DC-bin (CPE). For edge substitution technique of [5] and LI-TE technique, we use edge window length of 70 and 155 samples, respectively. These values were confirmed by simulations to be, on average, the best window length values for each technique. The used window length of the tail substitution technique also conforms to the proposed window length in [5]. In LI-TE, in turn, a relatively long interpolation window is used, compared to tail-substitution reference technique, in order to utilize the neighbouring symbol PN estimates as efficiently as possible.

The performances of PN mitigation techniques presented in Sections IV and V are compared to each other. The results for AWGN and extended Vehicular A channels are presented in Fig. 4 and Fig. 5, respectively, for free-running oscillator case. In the simulations, at least fifty-thousand OFDM symbols are transmitted for every (SNR, β) pair. From the AWGN channel simulations in Fig. 4, we can see noticeable performance increase when comparing the performance of LI-TE method over that of the state-of-the-art tail substitution method [5]. Also, the simple LI-CPE method gives a nice performance boost over the basic CPE estimation. From Fig. 5, it can be seen that the performance of the best methods get relatively near to the ideal case, but at the same time the significance of the PN mitigation methods decrease compared to AWGN channel case. This is natural because the relative

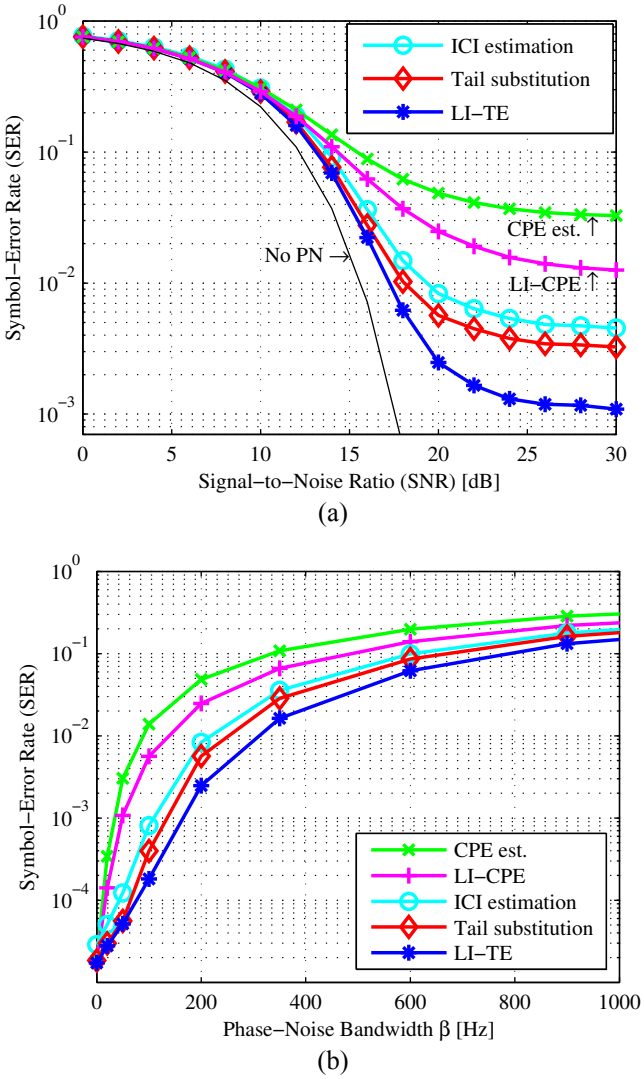

Fig. 4. Simulated SER as a function of (a) SNR, and $\beta=200$ Hz (b) β, and SNR = 20 dB. PN is generated with free-running oscillator and AWGN channel is used.

contribution of the PN gets smaller when the channel becomes more difficult. Still, LI-TE method outperforms the reference methods. The performance of LI-CPE method, on the other hand, seems to get quite near to the performance of the state-of-the-art ICI estimation methods.

When simulating the PLL oscillator case, PN of PLL oscillator is generated using the mask in Fig. 1. The mitigation results for the PLL case are given in Fig. 6. Compared to the free-running case, the relative performance differences between the mitigation techniques remain almost the same. LI-TE still outperforms its rivals. It is noticeable though that the LI-CPE method works especially well in a PLL case where PN has less high frequency components. It gives near the performance of the basic ICI estimation and tail substitution methods in high SNR region also, with considerably lower computational complexity.

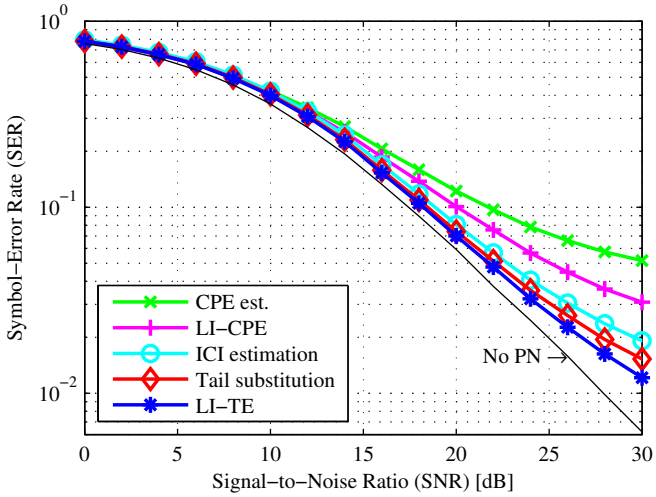

Fig. 5. Simulated SER as a function of SNR. PN is generated with free-running oscillator (β= 200 Hz). Extended ITU-R Vehicular A channel model is used.

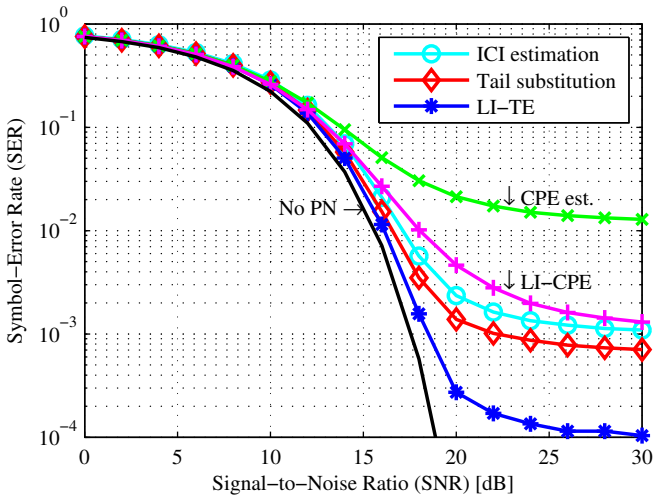

Fig. 6. Simulated SER as a function of SNR. PN is generated with PLL-based oscillator. AWGN channel is used.

VII. Conclusions

Phase noise is a critical impairment in OFDM type multicarrier systems. We introduced two new linear interpolation based techniques to estimate PN. The first technique, LI-CPE, is a simple way to improve the performance of general pilot-based CPE estimate by interpolating the PN estimate over adjacent OFDM symbols. The second technique, LI-TE, improves the performance of the state-of-the-art ICI mitigation techniques by decreasing the PN estimation error in tail parts of each OFDM symbol. Utilizing both free-running and PLL-based oscillators, the mitigation performances of all the techniques were analyzed using simulations. The simulations showed that LI-CPE gave a very good performance increase over general CPE mitigation. LI-TE, on the other hand, noticeably increased the performance of the state-of-the-art ICI mitigation technique. In addition, we noticed that the significance of ICI mitigation is relatively lower under challenging radio propagation environments, compared to plain AWGN. Still, clear performance improvement is achieved in high SNR region.

References

[1] 3GPP Technical Specification, TS 36.211 v8.3.0. Physical Channels and Modulation (release 8), May 2008.

[2] A. Armada, and M. Calvo, "Phase noise and sub-carrier spacing effects on the performance of an OFDM communication system," *IEEE Communications Letters*, Vol. 2, No. 1, pp. 11-13, January 1998.

[3] J. A. C. Bingham, "Multicarrier modulation for data transmission: an idea whose time has come," *IEEE Communications Magazine*, Vol. 28, No. 5, pp. 5-14, May 1990.

[4] S. Bittner, W. Rave, and G. Fettweis, "Joint iterative transmitter and receiver phase noise correction using soft information," in *Proc. IEEE International Conference on Communications 2007 (ICC'07)*, June 2007, pp. 2847-2852.

[5] S. Bittner, E. Zimmermann, and G. Fettweis, "Exploiting phase noise properties in the design of MIMO-OFDM receivers," in *Proc. IEEE Wireless Communications and Networking Conference (WCNC'08)*, March 2008, pp. 940-945.

[6] M. Brownlee, P. K. Hanumolu, K. Mayaram, and U. Moon, "A 0.5-GHz to 2.5-GHz PLL with fully differential supply regulated tuning," *IEEE Journal of Solid-State Circuits*, Vol. 41, No. 12, pp. 2720-2728, December 2006.

[7] A. Demir, "Computing timing jitter from phase noise pectra for oscillators and phase-locked loops with white and 1/f noise," *IEEE Transactions on Circuits and Systems I: Regular Papers*, Vol 53, No. 9, pp. 1869-1884, September 2006.

[8] A. Demir, "Phase noise and timing jitter in oscillators with colored-noise sources," *IEEE Transactions on Circuits and Systems I: Fundamental Theory and Applications*, Vol. 49, No. 12, pp. 1782-1791, December 2002.

[9] A. Demir, A. Mehrotra, and J. Roychowdhury, "Phase noise in oscillators: a unifying theory and numerical methods for characterization," *IEEE Transactions on Circuits and Systems - I: Fundamental Theory and Applications*, Vol. 47, No. 5, pp. 655-674, May 2000.

[10] G. Fettweis,"Dirty RF: A new paradigm", in *Proc. 16th International Symposium on Personal, Indoor and Mobile Radio Communications, 2005*, September 2005, pp. 2347-2355, Vol. 4.

[11] D. Petrovic , W. Rave, and G. Fettweis, "Effects of phase noise on OFDM systems with and without PLL: Characterization and compensation," *IEEE Transactions on Communications*, Vol. 55, No. 8, pp. 1607-1616, August 2007.

[12] P. Robertson, and S. Kaiser, "Analysis of the effects of phase-noise in orthogonal frequency division multiplex (OFDM) systems," in *Proc. IEEE International Conference on Communications*, June 1995, pp. 1652-1657, Vol. 3.

[13] T. Schenk, *RF Impairments in Multiple Antenna OFDM: Influence and Mitigation*, PhD dissertation, Technische Universiteit Eindhoven, 2006. ISBN 90-386-1913-8. 291 p.

[14] T. B. Sorensen, P. E. Mogersen, and F. Frederiksen, "Extension of the ITU channel models for wideband (OFDM) systems," in *Proc. IEEE Veh. Technol. Conf.*, September 2005, pp. 392-396.

[15] L. Tomba, "On the effect of Wiener phase noise in OFDM systems," *IEEE Transactions on Communications*, Vol. 46, No. 5, pp. 580-583, May 1998.

[16] S. Wu, and Y. Bar-Ness, "A phase noise suppression algorithm for OFDM-based WLANs," *IEEE Communications Letters*, Vol. 6, No. 12, pp. 535-537, December 2002.

[17] S. Wu, and Y. Bar-Ness, "OFDM systems in the presence of phase noise: Consequences and solutions," *IEEE Transactions on Communications*, Vol. 52, No. 11, pp. 1988-1997, November 2004.

[18] Q. Zou, A. Tarighat, and A. H. Sayed, "Compensation of phase noise in OFDM wireless systems," *IEEE Translations on Signal Processing*, Vol. 55, No. 11, November 2007.

Publication 2

V. Syrjälä and M. Valkama, "Jitter mitigation in high-frequency bandpass-sampling OFDM radios," in *Proc. IEEE Wireless Communications & Networking Conference 2009* (*IEEE WCNC'09*), Budapest, Hungary, April 2009.

Jitter Mitigation in High-Frequency Bandpass-Sampling OFDM Radios

Ville Syrjälä and Mikko Valkama

Tampere University of Technology
Department of Communications Engineering
Korkeakoulunkatu 1, FI-33720 Tampere, Finland
E-mail: {ville.syrjala, mikko.e.valkama}@tut.fi

***Abstract*—This paper presents a new way to address and mitigate sampling jitter in high-frequency bandpass-sampling OFDM radio receivers. Baseband model for mapping the sampling jitter to certain type of phase noise is first presented, and stemming from this model, state-of-the-art phase noise mitigation techniques are then proposed to remove the jitter-induced signal distortion. Performances of the proposed jitter mitigation techniques are analyzed with extensive computer simulations in high-speed bandpass sampling multicarrier system context. In the link performance simulations, both additive white Gaussian noise (AWGN) and extended ITU-R vehicular A multipath (eVehA) radio channel types are used, combined with realistic sampling clock and jitter modelling.**

***Index Terms*—Bandpass sampling, sampling jitter, phase noise, OFDM, intercarrier interference.**

I. Introduction

In modern communications receivers, maximizing flexibility and re-configurability while minimizing power consumption, size and costs are some of the main design criteria. When signals are sampled directly at radio frequencies (RF), very high flexibility and re-configurability can be achieved. Also, the number of analogue components is generally decreased, compared to many other radio architectures, thus resulting in potentially lower power consumption, size and costs.

Still, many problems remain in direct RF sampling receiver concept [4], [7]. With current technologies, maximum sampling frequencies are limited to a few tens or few hundreds of MHz range. The used carrier-frequencies, on the other hand, are typically in the GHz range, which leads to bandpass sub-sampling concepts [4], [14]. This, in turn, sets relatively high demands for RF band-limitation filtering, prior to sampling, to control harmful aliasing effects. In addition to filtering requirements, also the power consumption of the sampling circuitry itself can be somewhat higher, compared to ordinary low-frequency/baseband sampling approaches. This is because the usable sub-sampling frequencies depend essentially on both the signal bandwidth and centre-frequency, and are typically somewhat higher than the corresponding minimum sampling rates in ordinary low-frequency sampling [14]. Furthermore, as the frequency range of the sampled signals increases, the effects of timing inaccuracies or jitter in the sampling process increase as well. In fact, these timing inaccuracies start to noticeably limit the overall receiver and system performance when sampling signals directly at commonly used carrier frequencies [1], [8]. Thus, there is a clear need to study and mitigate the effects of timing jitter in such high-speed bandpass sampling radios.

The impact of sampling jitter on radio system performance has been recently studied in [5], assuming orthogonal frequency-division multiplexing (OFDM) waveforms. Furthermore, the essential signal-to-noise ratio (SNR) reduction due to jitter has been addressed using system calculation principles, e.g., in [8], [11]. This paper, in turn, shows that with fairly reasonable assumptions on received signal and sampling clock characteristics, jitter noise acts similarly as phase noise in bandpass sampling based receivers. Based on this modelling, this paper then also proposes the use of sophisticated phase noise mitigation schemes for jitter mitigation. As a practical example, OFDM waveforms are assumed also in this paper since they are generally found very sensitive to any phase noise –like phenomena [13], [16].

The organization of the rest of the paper is as follows: In Section II, efficient and accurate jitter model is presented for bandpass sampling receivers. In addition, Section II describes how the model essentially maps sampling jitter to phase noise, and thereon to intercarrier interference (ICI) in case of OFDM. Then, Section III describes state-of-the-art techniques for phase noise mitigation to reduce the jitter effects in direct-sampling OFDM receivers. Section IV, in turn, describes the used simulation model and demonstrates the obtained mitigation performance in realistic 3GPP Long Term Evolution (LTE) –type multicarrier radio system context. Finally, Section V concludes the work.

This work was supported by the Finnish Funding Agency for Technology and Innovation (Tekes, under the project "Advanced Techniques for RF Impairment Mitigation in Future Wireless Radio Systems"), the Academy of Finland, the Technology Industries of Finland Centennial Foundation, Finnish Foundation for Technology Promotion, and TUT Graduate School.

II. Jitter Modelling and OFDM Radios

In this Section, a simple yet efficient model for mapping sampling jitter to phase noise in high-frequency bandpass sampling receivers is presented. In addition, using this modelling, jitter impact on direct-sampling OFDM receivers is studied in detail.

A. Jitter Modelling and Connection to Phase Noise

Stemming from the earlier work in [10], we present a simple jitter model for bandpass sampling based radio receivers. The model exploits the general features of bandpass communications waveforms. In general, an arbitrary received bandpass signal is first written as

$$r(t) = x_I(t)\cos(2\pi f_c t) - x_Q(t)\sin(2\pi f_c t)\,, \tag{1}$$

where x_I and x_Q are the I and Q components of the received signal, respectively, and f_c is the corresponding formal centre-frequency. Now, if the jitter is taken into account, we end up with a signal of the form

$$\begin{aligned} r\{t+\xi(t)\} = {} & x_I\{t+\xi(t)\}\cos\{2\pi f_c[t+\xi(t)]\} \\ & -x_Q\{t+\xi(t)\}\sin\{2\pi f_c[t+\xi(t)]\}, \end{aligned} \tag{2}$$

where $\xi(t)$ models the uncertainty on the time axis due to jitter. Now, assuming that the centre-frequency f_c of the incoming signal $r(t)$ is large compared to the corresponding bandwidth of the signal, the jitter contribution to the I and Q components is much lower compared to the contribution on the high-frequency carrier components. Furthermore, assuming that the jitter values $\xi(t)$ are relatively small compared to the essential time-dynamics of the I and Q components, it follows that $x_I\{t+\xi(t)\} \approx x_I(t)$ and $x_Q\{t+\xi(t)\} \approx x_Q(t)$, and we can essentially approximate (2) as

$$\begin{aligned} r\{t+\xi(t)\} \approx {} & x_I(t)\cos\{2\pi f_c[t+\xi(t)]\} \\ & -x_Q(t)\sin\{2\pi f_c[t+\xi(t)]\}. \end{aligned} \tag{3}$$

Notice that at this stage, no other assumptions have been made yet on the more detailed structure of the modulating I and Q components. Depending on the RF filtering prior to sampling, these can, e.g., contain several radio signals or channels on different carrier-frequencies.

In practice, the above assumption of small jitter values can be seen reasonable with practical processing bandwidths in the order of a few tens of MHz and with jitter RMS values in the tens of ps range. Such relatively small jitter values, in turn, are realistic in many practical sampling circuitries, utilizing some sophisticated (e.g., phase-locked loop, PLL, based) oscillators in generating the sampling instants. For an example spectral characteristics, see Fig. 1. On the other hand, the small jitter approximation does not necessarily hold for free-running type oscillators where the oscillator phase variance, and thereon the variance of the sample instants, increases over time, and thus relatively high jitter values are also possible.

In the actual sampling process, we observe (1) at time instants $t_n = nT_S + \xi_n$, where $\xi_n = \xi(nT_S)$ denotes the time-deviation of the n-th sample instant from the nominal sample grid nT_S, T_S is the time between adjacent samples (in the corresponding ideal sample stream) and sample index $n \in \mathbf{N}$. Thus, based on the approximation in (3), the n-th sample can now be written as

$$\begin{aligned} r_n &= r(nT_S + \xi_n) \\ &\approx x_I(nT_S)\cos[2\pi f_c(nT_S + \xi_n)] \\ &\quad -x_Q(nT_S)\sin[2\pi f_c(nT_S + \xi_n)]. \end{aligned} \tag{4}$$

Stemming from the bandpass sub-sampling principle, the signal is aliased in a controlled manner to an intermediate frequency (IF), i.e., $\cos(2\pi f_c nT_S) = \cos(2\pi f_{\mathrm{IF}} nT_S)$ and $\sin(2\pi f_c nT_S) = \sin(2\pi f_{\mathrm{IF}} nT_S)$ [4], [7], [14]. Now, using simple manipulations, the above signal can also be written as

$$r_n \approx \mathrm{Re}\{[x_I(nT_S) + jx_Q(nT_S)]e^{j2\pi f_{\mathrm{IF}} nT_S} e^{j2\pi f_c \xi_n}\}\,. \tag{5}$$

Thus, the final baseband observation after digital IF-to-baseband conversion is given by

$$\begin{aligned} y_n &\approx [x_I(nT_S) + jx_Q(nT_S)]e^{j2\pi f_c \xi_n} \\ &= x_n e^{j2\pi f_c \xi_n} \\ &= x_n e^{j\phi_n}, \end{aligned} \tag{6}$$

where $x_n = x_I(nT_s) + jx_Q(nT_s)$ and $\phi_n = 2\pi f_c \xi_n$. Based on the above signal model, sampling jitter results in time-varying excess phase fluctuations in the observed low-frequency signal and can thus be essentially modelled as phase noise in high-frequency bandpass sub-sampling receivers.

B. Jitter Impact on Direct-Sampling OFDM Receiver

Next, we focus on interpreting the above signal model (6) from direct-sampling OFDM receiver point of view. We further assume that the RF filtering stage prior to sampling attenuates the neighbouring channel signals. Then, the signal x_n corresponds to the received OFDM waveform samples, and the jitter contribution is modelled into the system according to (6). Denoting the transmit waveform samples by s_n, the received samples are given by $x_n = h_n \star s_n + z_n$ where h_n represents the radio channel impulse response, $\star$ denotes convolution and z_n represent additive noise. Combining then this signal model and the earlier jitter model in (6), the observed signal after receiver FFT within m-th OFDM symbol can be written as

$$\begin{aligned} Y_m(k) &= S_m(k)H_m(k)J_m(0) \\ &\quad + \sum_{n=0}^{N-1} S_m(l)H_m(l)J_m(k-l) + Z_m(k). \end{aligned} \tag{7}$$

Here $S_m(k)$ denotes the transmit symbol at k-th subcarrier during m-th OFDM symbol interval, $H_m(k)$ is the corresponding channel transfer function, $J_m(k)$ is the Fourier transform of the complex exponential of the jitter phase noise values during the m-th OFDM symbol and finally $Z_m(k)$ is the FFT of the AWGN term. In deriving (7), it has been further assumed that the transmit signal contains a cyclic prefix longer than the channel delay spread, being then properly discarded in the receiver prior to FFT. For reference, see e.g. [15] where similar analysis is carried out assuming ordinary oscillator phase noise.

The signal model presented in (7) is important as it divides the jitter contribution to two essential parts, i.e., common phase error (CPE) and intercarrier interference (ICI) parts [15]. CPE is common phase rotation within an OFDM symbol for all the subcarriers, where as ICI is the distortion that neighbouring subcarriers cause to each other due to spectral spread caused by the jitter.

III. Jitter Estimation and Mitigation

Stemming from (6) and (7), jitter mitigation in direct-sampling OFDM radios can be accomplished by estimating and cancelling the CPE and ICI caused by jitter-induced phase noise. In this Section, state-of-the-art phase noise estimation techniques used then for jitter mitigation are shortly presented. In short, CPE and ICI estimation corresponds to estimating the essentially non-zero spectral components $J_m(k)$ of the complex exponential of the phase noise. Since the jitter-induced phase noise changes from OFDM symbol to another, this estimation needs to be carried out for each symbol interval. In general, after estimating the essential phase noise spectral components, the actual mitigation is done by circular deconvolution. This results directly from (7) in which phase noise is seen as circular convolution.

A. CPE Estimation

CPE estimation used in this paper is based on the work in [15]. CPE estimation is conceptually easy because CPE causes each subcarrier symbol within an OFDM symbol duration to be multiplied by the same complex multiplier. We can then use e.g. least squares estimation to estimate the CPE contribution of the phase noise with the help of pilot symbols and channel information [15].

B. ICI Estimation Using CPE Interpolation (LI-CPE)

Plain CPE estimation gives us effectively constant estimate for the phase noise within the duration of an individual OFDM symbol. In effect, this is the average value of the true phase noise within one OFDM symbol, so the CPE estimation gives very simplified phase noise estimate. So-called LI-CPE approach [12] is then a very simple method to improve the phase noise estimation performance by linearly interpolating between the CPE estimates of adjacent OFDM symbols. This is done essentially so that, in time domain, a straight line is "drawn" between the CPE estimates at the middle of adjacent OFDM symbols – from the middle of symbol m-1 to the middle of symbol m and from the middle of symbol m to the middle of symbol m+1. In addition, the first spectral component (DC-bin) of this new phase noise estimate inside one OFDM symbol is replaced by the original CPE estimate, because it is likely to be better than the first spectral component of the linear interpolated one. A graphical illustration is given in Fig. 2. For more details, refer to [12].

C. Iterative ICI Estimation Using Tail Interpolation (LI-TE)

Conceptually, the phase noise spectral components can be solved from (7) if both the channel and the transmit symbols are known. In iterative ICI estimation [3], [6], the idea is then to use initial symbol decisions obtained by cancelling first only the CPE, in solving (7) for $J_m(k)$'s (or at least a subset of essentially non-zero ones). Then ICI is cancelled with this estimated ICI profile and the signal is detected again. Altogether this whole procedure can be then repeated to iteratively improve the quality of both detection and ICI estimation. In LI-TE technique [12], this iterative procedure is the starting point. LI-TE method then further improves the quality of the ICI estimates at the borders of each OFDM symbol. This can be done because the original ICI estimation method gives very poor estimates at the border areas of OFDM symbols [3], [6]. LI-TE uses then linear interpolation to obtain better estimates for the phase noise realization over the unreliable region of the original estimate [12]. The interpolation of LI-TE at the OFDM symbol borders is also visible in the example of Fig. 2.

IV. Performance Simulations

In this Section, OFDM link simulation model is first described and then the obtained simulation results are presented and analyzed.

A. Simulation Model

In performance simulations, we use 3GPP LTE downlink – like system [1] operating at so called "2.6 GHz band" (i.e., at 2500-2690 MHz) as a practical example scenario. First we generate OFDM signal with 1024 subcarriers using 15 kHz subcarrier spacing. 600 of these 1024 subcarriers are active, and for these, 16QAM subcarrier modulation is used. This corresponds to 1024×15 kHz = 15.36 MHz transmitter sampling rate for baseband waveform generation, and the RF waveform bandwidth is roughly 10 MHz. Cyclic prefix of 63 samples is then added to the signal, which corresponds to around 4 μs maximum delay spread for the radio channel. This signal is then put through either (*i*) plain AWGN channel or (*ii*) extended ITU-R Vehicular A multipath (eVehA) [9] channel. In the eVehA channel case, the channel impulse response is assumed to be static for a period of 12 OFDM symbols after which a totally new channel realization is drawn (quasi-static simulation approach). In the receiver model, the initial sampling rate for modelling the bandpass sampling

stage is assumed to be 138.24 MHz which corresponds to 9 times over-sampling factor compared to basic waveform sample rate of 15.36 MHz. In this sampling process, the jitter contribution is modelled according to the low-frequency model (6), using an assumed example RF carrier frequency of 2661.12 MHz, fitting well in the planned LTE downlink band 7 [1]. This assumed example centre-frequency and the used sampling frequency effectively alias the signal to an IF of 2661.12 – 19×138.24 = 34.56 MHz in a controlled manner.

For sampling clock modelling, we use phase-locked loop (PLL) oscillator model presented in [12]. This models the oscillator phase noise characteristics by taking both white and flicker noise contributions into account. The resulting jitter behaviour is in general normalized to different practical RMS-values in the ps range, as will be illustrated in the following sub-section. An example of the spectral characteristics of non-normalized oscillator is depicted in Fig. 1. After this, the detection of symbols is done with help of state-of-the-art phase noise mitigation techniques described in Section III. We use basic CPE estimation scheme, linear interpolation based ICI estimation (LI-CPE), and basic ICI estimation [5] enhanced with linear interpolation based tail-estimation technique (LI-TE). For more details, refer to [5], [12], [15].

B. *Obtained Results*

In the simulations, the obtained jitter mitigation performances using the above phase noise mitigation techniques are evaluated, in terms of detection error rate, and compared against reference cases with (*i*) no jitter (jitter-free sampling) and (*ii*) no jitter removal. For practicality, both the AWGN and eVehA channels are simulated.

First, we visually demonstrate the jitter estimation performance in time domain. An example result is shown in Fig. 2. There, the true jitter realization is plotted in same figure with the corresponding LI-CPE and LI-TE estimation results. As can be seen in the figure, LI-CPE and LI-TE give very high-quality estimates.

The results of simulated receiver symbol-error rate (SER) in AWGN channel case can be seen in Fig. 3 and Fig. 4. Based on Fig. 3, it can be seen that with 15 ps RMS jitter, one can get very nice performance improvement with phase noise mitigation techniques. The non-mitigated signal, in turn, suffers very heavily from the jitter. Even basic CPE mitigation gives relatively good performance improvements. The LI-CPE method further improves the performance of the system, while the LI-TE method removes almost all the jitter distortion in the interesting SNR region. From Fig. 4, very similar conclusions can be made. When SNR is set to an example value of 18 dB, the LI-TE gives almost perfect jitter estimation up to 15-20 ps RMS jitter values. With higher jitter values, the mitigation performance starts to decrease, but still with greatly increased RMS jitter values even in the order 30-50 ps, relatively good detection performance is obtained.

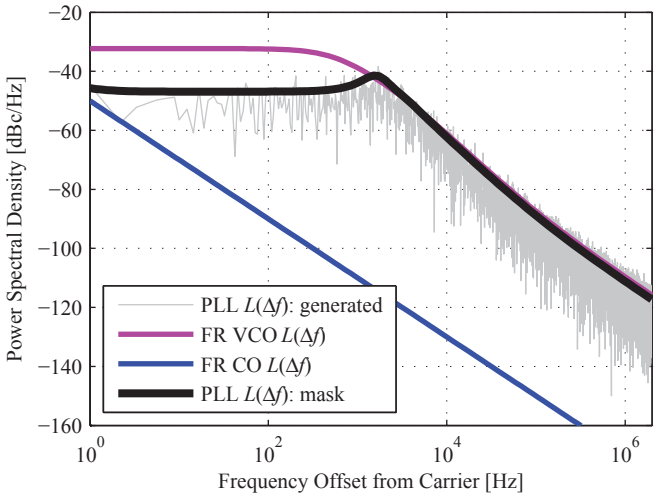

Fig. 1. PLL output phase noise characteristics [12]. Spectra of reference Crystal Oscillator (CO, dominating below 2 kHz) and Voltage Controlled Oscillator (VCO, dominating above 2 kHz) are presented.

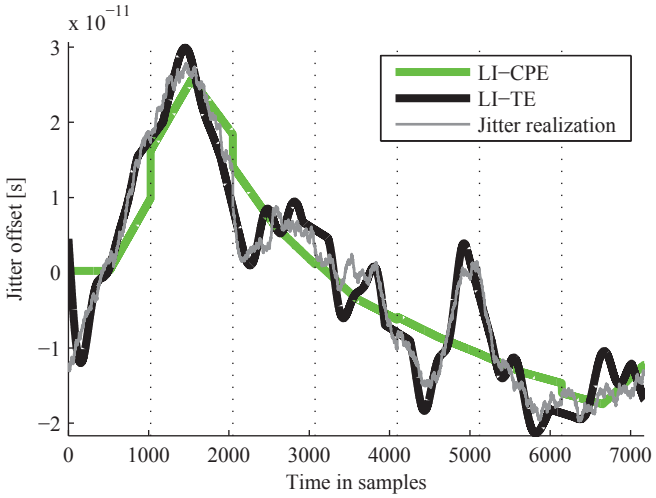

Fig. 2. An example of true jitter realization and the obtained estimates with 20 ps RMS jitter, plotted for a period of 7 OFDM symbols separated by dotted lines. 18 dB received SNR and AWGN channel.

For eVehA channel case, the obtained simulation results can be seen in Fig. 5 and Fig. 6. From these, we can see that when more challenging channel conditions are experienced, the phase noise mitigation techniques still give relatively similar performance as in the AWGN channel case. From Fig. 5, we can see that for an example RMS jitter of 15 ps, LI-TE method mitigates the jitter effects almost perfectly. In addition, LI-CPE method gives also very good performance even in high-SNR region. Furthermore, even the basic CPE mitigation yields considerable performance improvement over the no mitigation case. The Fig. 6 shows further that in the eVehA channel case, the LI-TE method gives almost perfect jitter estimation even up to 20-25 ps RMS jitter range. In addition, the simpler estimation methods also perform relatively well as can be seen in the figure.

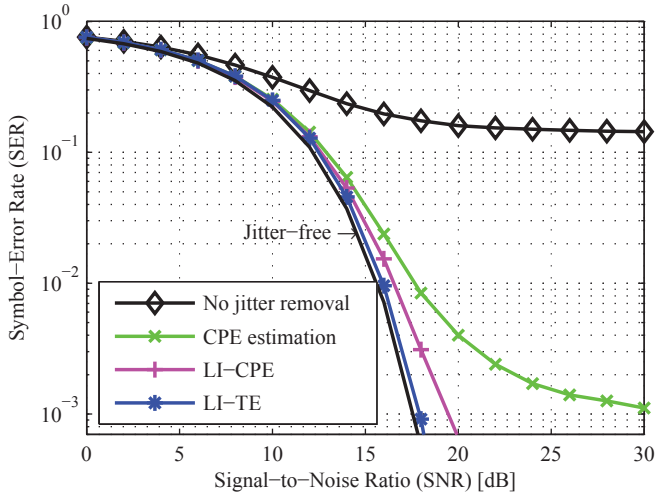

Fig. 3. Simulated SER as a function of SNR in LTE-type OFDM system with direct-sampling receiver. AWGN channel, 15 ps RMS jitter and 16QAM subcarrier modulation are used.

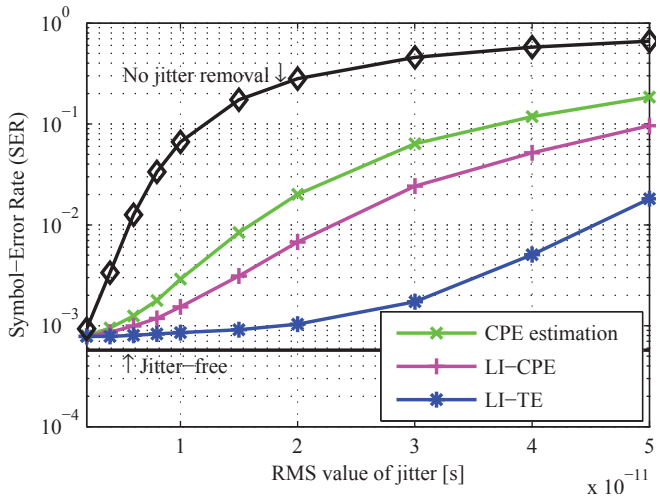

Fig. 4. Simulated SER as a function of RMS jitter with 18 dB received SNR in LTE-type OFDM system with direct-sampling receiver. AWGN channel and 16QAM subcarrier modulation are used.

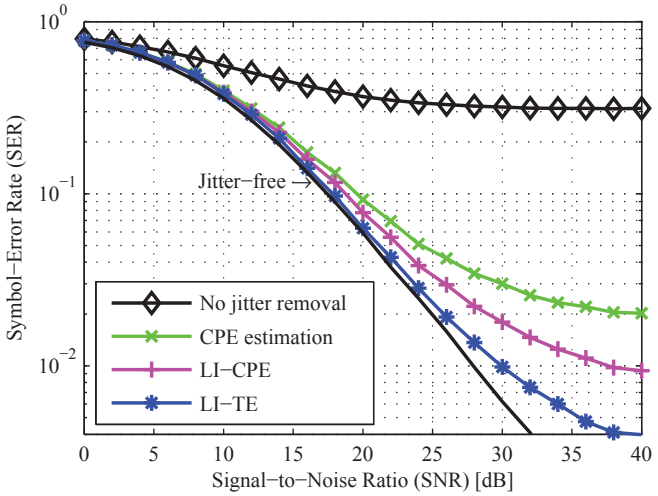

Fig. 5. Simulated SER as a function of SNR in LTE-type OFDM system with direct-sampling receiver. Extended ITU-R Vehicular A multipath channel, 15 ps RMS jitter and 16QAM subcarrier modulation are used.

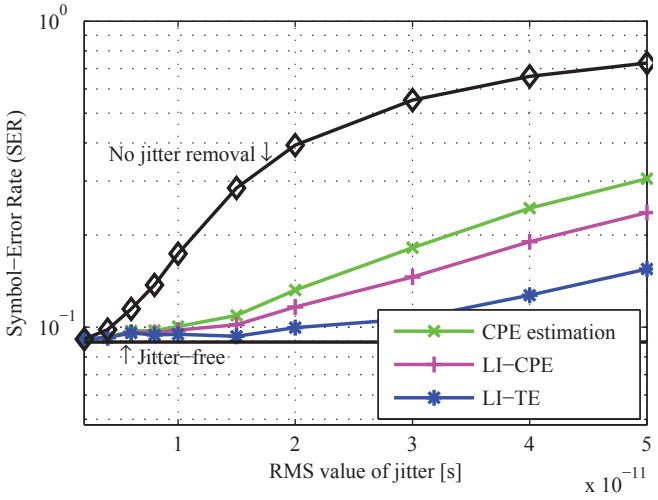

Fig. 6. Simulated SER as a function of RMS jitter with 18 dB received SNR in LTE-type OFDM system with direct-sampling receiver. Extended ITU-R Vehicular A multipath channel and 16QAM subcarrier modulation are used.

V. Conclusions

Sampling jitter causes noticeable performance decrease in high-frequency bandpass-sampling receivers in general. In this paper, we first derived a baseband model, which essentially maps the jitter to certain type phase noise. This allows us to use state-of-the-art phase noise mitigation techniques to reduce the jitter effects in RF sampling receivers. The link simulations showed that, in OFDM systems, using advanced phase noise mitigation techniques, huge performance improvements are generally achieved over the case with no jitter removal, with both AWGN and extended Vehicular A multipath channel types. With the best mitigation method, the so-called LI-TE technique, we got almost perfect jitter mitigation performance with reasonable jitter RMS values in the order of 10 – 20 ps.

References

[1] 3GPP Technical Specification, TS 36.101 v8.2.0. Physical Channels and Modulation (release 8), May 2008.

[2] B. Amin, and A. G. Dempster, "Sampling and jitter considerations for GNSS software receivers," in *Proc. IGNSS Symposium 2006*, July 2006, 15 p.

[3] S. Bittner, E. Zimmermann, and G. Fettweis, "Exploiting phase noise properties in the design of MIMO-OFDM receivers," in *Proc. IEEE Wireless Communications and Networking Conference* (WCNC'08), Las Vegas, NV, March 2008, pp. 940-945.

[4] M. E. Frerking, *Digital Signal Processing in Communication Systems*. International Thomson Publishing Services, 1994, 644 p.

[5] U. Onunkwo, Y. Li, and A. Swami, "Effect of timing jitter on OFDM-based UWB systems,", *IEEE Journal on Selected Areas in Communications*, Vol. 24, No. 4, pp. 787-793, April 2006.

[6] D. Petrovic , W. Rave, and G. Fettweis, "Effects of phase noise on OFDM systems with and without PLL: Characterization and compensation," *IEEE Transactions on Communications*, Vol. 55, No. 8, pp. 1607-1616, August 2007.

[7] B. Razavi, *RF Microelectronics*. Prentice Hall PTR, Upper Saddle River, NJ, USA, 1998, 335 p.

[8] M. Shinagawa, Y. Akazawa, and T. Wakimoto, "Jitter analysis of high-speed sampling systems," *IEEE Journal of Solid State Circuits*, Vol. 25, No. 1, pp. 220-224, February 1990.

[9] T. B. Sorensen, P. E. Mogersen, and F. Frederiksen, "Extension of the ITU channel models for wideband (OFDM) systems," in *Proc. IEEE Vehicular Technology Conference* (VTC-Fall'05), Dallas, TX, September 2005, pp. 392-396.

[10] V. Syrjälä, M. Valkama, and M. Renfors, "Efficient jitter model for high-frequency bandpass sampling," in *Proc. Finnish Signal Processing Symposium* (FINSIG'07), Oulu, Finland, August 2007.

[11] V. Syrjälä, M. Valkama, and M. Renfors, "Design considerations for direct RF sampling receiver in GNSS environment," in *Proc. 5th Workshop on Positioning, Navigation and Communication* (WPNC'08), Hannover, Germany, March 2008, pp.9-13.

[12] V. Syrjälä, M. Valkama, N. N. Tchamov, and J. Rinne, "Phase noise modelling and mitigation techniques in OFDM communications systems," in *Proc. Wireless Telecommunications Symposium 2008* (WTS'09), Prague, Czech Republic, April 2009.

[13] L. Tomba, "On the effect of Wiener phase noise in OFDM systems," *IEEE Transactions on Communications*, Vol. 46, No. 5, pp. 580-583, May 1998.

[14] R. G. Vaughan, N. L. Scott, and D. R. White, "The theory of bandpass sampling," *IEEE Transactions on Signal Processing*, Vol. 39, pp. 1973-1984, Sept. 1991.

[15] S. Wu, and Y. Bar-Ness, "A phase noise suppression algorithm for OFDM-based WLANs," *IEEE Communications Letters*, Vol. 6, No. 12, pp. 535-537, December 2002.

[16] S. Wu, and Y. Bar-Ness, "OFDM systems in the presence of phase noise: Consequences and solutions," *IEEE Transactions on Communications*, Vol. 52, No. 11, pp. 1988-1997, November 2004.

Publication 3

V. Syrjälä and M. Valkama, "Sampling jitter estimation and mitigation in direct RF sub-sampling receiver architecture," in *Proc. Sixth International Symposium on Wireless Communication Systems 2009* (*ISWCS'09*), IEEE, Siena-Tuscany, Italy, September 2009.

Sampling Jitter Estimation and Mitigation in Direct RF Sub-Sampling Receiver Architecture

Ville Syrjälä and Mikko Valkama

Tampere University of Technology
Department of Communications Engineering
P.O. Box 553, FI-33101, Tampere, Finland
ville.syrjala@tut.fi, mikko.e.valkama@tut.fi

***Abstract*—The sampling jitter is particularly problematic in systems where high-frequency signals are sampled. This paper addresses the sampling jitter estimation and cancellation task in the direct RF sub-sampling type radio receivers. The proposed jitter estimation method is based on carefully injecting or superimposing an additional reference signal to the received signal at sampler input. Proper digital signal processing methods are then devised and applied to estimate the sampling jitter realizations from the obtained jittered samples. Using these jitter estimates, combined with proper jitter modelling, the jitter effects can then be efficiently removed from the actual received signal. Careful performance analysis of the overall estimation-cancellation scheme is also carried out using computer simulations with 3GPP LTE type multicarrier signals, assuming also different amounts of RF filtering prior to RF sub-sampling stage.**

***Keywords*—Sampling jitter; phase noise; mitigation; direct RF sampling; bandpass sampling; sub-sampling**

I. INTRODUCTION

Sampling of high-frequency signals, or signals with powerful interference at nearby frequencies, poses relatively high requirements for the timing accuracy of the sampling process [7]. In traditional communications receivers, down-conversion and analogue filtering are used to bring the signal down to lower frequencies and attenuate most of the interference near the interesting frequencies [5]. This results into relatively relaxed requirements for the dynamics and timing accuracy of the sampling circuitry. However, when emphasizing radio flexibility and re-configurability, more and more of the selectivity filtering is moved to digital domain. Similarly from the frequency-translations point of view, applying sampling already to higher-frequency signals is one of the main trends currently. Under these working assumptions, timing inaccuracies in the sampling process, called sampling jitter, become a severe problem. From the future wireless communications point of view, understanding, modelling and mitigation of the sampling jitter is thus a very interesting and important topic.

Sampling of very high-frequency signals with possibly powerful interferers at neighbouring frequencies is culminated in the so-called direct RF sampling (DRFS) receiver architecture. DRFS itself is, as the name implies, a receiver architecture in which the sampling of the incoming signal is done already at the radio frequencies (RF). DRFS minimizes the amount of analogue components in the receiver, thus emphasizing re-configurability and also potentially minimizing size, power consumption and costs of the receiver compared to more traditional radios. However, the DRFS concept still has many practical implementation issues to be solved [5], [11], and it is thus not commonly considered feasible especially for mobile terminal receivers with today's implementation technologies. The most notable problem with the DRFS approach is that it indeed poses very high demands for the quality of the sampling process. With current technologies, the combined requirements of relatively high sampling frequency and high resolution and timing accuracy for the used sampling circuitry result into relatively high power consumption, which in turn is one of the main concerns in mobile terminals. To circumvent this, digital signal processing (DSP) methods can be developed to lower the quality requirements for the sampling process.

In the literature, DSP-based estimation and mitigation of sampling jitter is not too widely researched because in most of today's receiver architectures, sampling takes place at fairly low frequencies. However, as indicated earlier, this might not be the case in near future, since minimizing the amount of analogue parts in receivers becomes more and more interesting. Furthermore, DSP capabilities of the mobile devices are continuously increasing. Recently, in [9], use of phase noise mitigation techniques [12] in mitigation of sampling jitter in bandpass sampling receivers was proposed for orthogonal frequency division multiplexing (OFDM) systems. In addition, the authors of [6] have proposed a technique to remove sampling jitter effects from general narrowband signals with help of a reference tone. In this paper, the idea of carefully designing and injecting a reference tone on top of the received signal at the sampler input signal is further developed. This paper first proposes an efficient technique to estimate the sampling jitter realizations with the help of such reference tone. The estimates of the jitter realizations are then used to mitigate the effects of the sampling jitter from the actual received waveform, without the limitations of narrowband signals and small jitter values as was assumed in [6]. Special emphasis in modelling and algorithm development is put to the DRFS receiver case where only partial selectivity is implemented at RF prior to sampling.

This work was supported by the Finnish Funding Agency for Technology and Innovation (Tekes, under the project "Advanced Techniques for RF Impairment Mitigation in Future Wireless Radio Systems"), the Academy of Finland, the Technology Industries of Finland Centennial Foundation, Finnish Foundation for Technology Promotion, and TUT Graduate School.

The rest of the paper is organized as follows. In Section II, a novel method to estimate sampling jitter realizations is proposed utilizing a carefully injected reference tone. In addition, the Section discusses design considerations and limitations in applying the estimation principle in DRFS receiver context. Section III then proposes methods to use the acquired estimates of the sampling jitter realizations for actual mitigation of the jitter from the received signal. This covers both narrowband signal case and a more general DRFS receiver case. The performance simulations and the corresponding analysis are given in Section IV, whereas Section V finally concludes the work.

II. Estimating the Sampling Jitter Realization from the Sampled Reference Tone

In this Section, an efficient technique to estimate the sampling jitter realizations ($\hat{\zeta}_n$ in Fig. 1) from sampled signal is proposed. This is done by using the idea of injecting a reference tone to the signal prior to the sampling circuitry [6] combined with proper processing of the jittered samples.

A. Sampling Jitter Estimation at Principal Level

First, let $r(t)$ denote the incoming received signal, and the idea is to inject a reference tone, say $A_{ref}\cos(2\pi f_{ref}t)$ on top of it where f_{ref} denotes the reference tone frequency. Here only one sinusoidal reference signal is used, but also other kinds of known signals could in principle be used, if considered beneficial. Now, with suitable reference tone injected, the sampler input signal is of the form

$$x(t) = r(t) + A_{ref}\cos(2\pi f_{ref}t)\,. \tag{1}$$

Therefore, the jittered output of the sampling process is

$$\begin{aligned} x_n &= r(nT_s+\zeta_n) + A_{ref}\cos\left[2\pi f_{ref}(nT_s+\zeta_n)\right] \\ &= r(nT_s+\zeta_n) + \frac{A_{ref}}{2}\left(e^{j2\pi f_{ref}(nT_s+\zeta_n)} + e^{-j2\pi f_{ref}(nT_s+\zeta_n)}\right), \end{aligned} \tag{2}$$

where T_s is the nominal sample interval, n is sample index and ζ_n is the sampling jitter at the n-th sample moment. Now, given that the reference frequency f_{ref} is outside the band of $r(t)$, we can use complex digital mixing and lowpass filtering (LPF) to isolate the jittered reference tone. Thus at the output of the digital mixer (running at f_{ref}) followed by LPF, we have

$$y_n = \mathrm{LPF}\left(x_n \times e^{-j2\pi f_{ref}nT_s}\right) \simeq e^{j2\pi f_{ref}\zeta_n}/2\,. \tag{3}$$

This represents a sampled reference tone where jitter is seen essentially as phase noise. However, as already indicated above, the last equality is only approximately true because, due to jitter, the spectra of all the components in the sampled signal are spread around their original frequency contents. However, with practical sampling clocks, it is expected that there is some correlation between consecutive jitter values [4] and thus most of the energy of the sampled signal components is still located at the original frequencies. Now, based on (3), estimates for the sampling jitter values can be obtained as

$$\hat{\zeta}_n = \arg\{y_n\}/(2\pi f_{ref})\,. \tag{4}$$

Like discussed already shortly above, there are some essential limitations in the estimation process which should be carefully understood. The reference frequency f_{ref} must be selected so that it is possible to sufficiently separate (filter) the reference tone from the actual incoming signal $r(t)$. In practice, the amount of this separation depends on (*i*) the frequency separation between $r(t)$ and f_{ref}, (*ii*) the amount of jitter and (*iii*) the power ratio between $r(t)$ and the reference tone. In the selection of f_{ref}, it should also be kept in mind that jitter has heavier effect on high-frequency signals, and thus the higher the selected reference frequency is, the easier it is to detect the phase behaviour of the isolated reference tone in (3)-(4). It should also be acknowledged that the reference signal itself must be very accurately known, and it is likely that the selection of f_{ref} affects also the generation accuracy of the reference.

Not only the frequency of the reference tone, but also its amplitude is important in the design. On one hand, if the dynamic range in the incoming signal is high, then also high number of bits is needed in the digital domain signal processing. On the other hand, the sampling jitter itself is easier to estimate if the reference tone is strong (compared to $r(t)$), so from the estimation point of view, we would like to use as powerful reference as possible. Thus a proper compromise is needed in dimensioning the reference signal power in practice.

B. Special Considerations for Sampling Jitter Estimation in DRFS Receiver Context

In applying the above jitter estimation principle in bandpass sub-sampling based DRFS receivers, all the above considerations are still valid. However, stemming from the use of sub-sampling, in which aliasing is used in a controlled manner to bring the incoming RF signal closer to baseband, some additional design considerations must also be taken into account. So in general, bandpass sub-sampling can introduce desired and non-desired aliasing. Thus proper combination of preliminary RF-filtering and choice of the sampling frequency is needed so that non-desired aliasing is minimized. In the proposed jitter injection and estimation technique, this must be done such that minimal aliasing happens over the reference tone, as the jitter estimation is quite sensitive to any additional interference. Of course in order to ease the RF-filter design, the aliasing pattern should be taken into account already when selecting the reference tone frequency. Notice that in general, with high sub-sampling ratio (ratio of the incoming RF-signal centre-frequency and the used sampling frequency), there is anyway lots of flexibility in designing the reference frequency.

III. Jitter Mitigation

This Section proposes an efficient way to use obtained jitter estimates in the jitter mitigation. First, for reference purposes, we study the jitter mitigation task in a similar case that was considered in [6]. Then in the second part of this Section, we focus on the jitter mitigation task in general high-frequency bandpass sampling receiver case.

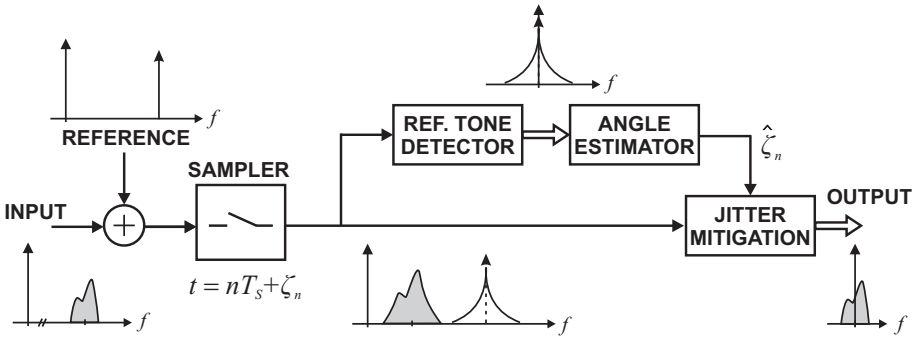

Fig. 1. General illustration of super-imposing a reference tone at sampler input which is then used for digital jitter estimation and cancellation.

A. Case of Narrowband Signal with Nearby Interferer

In [6], the case of narrowband target signal with very powerful interfering adjacent signal was considered. This case is somewhat impractical since huge power differences between the information signal and the neighbouring channel interference were assumed. Furthermore, only very narrowband information and adjacent channel signals were considered, and the jitter values were also assumed very small. Such case is, however, also considered in this Section, as a reference, to demonstrate that the jitter estimation and cancellation methods proposed here outperform the developments of [6] also under similar working conditions assumed in [6].

Thus here we consider a received signal of the form

$$x(t) = A_c \cos\left(2\pi f_c t + \theta_c\right) + A_i \cos\left(2\pi f_i t + \theta_i\right) \tag{5}$$

as the input of the sampler, where $r(t) = A_c \cos\left(2\pi f_c t + \theta_c\right)$ denotes the narrowband target signal, centred at f_c, and $A_i \cos\left(2\pi f_i t + \theta_i\right)$ models the adjacent channel signal at unknown neighbouring frequency f_i. Then, after jittered sampling, we have

$$\begin{aligned} x_n = x(nT_s + \zeta_n) &= A_c \cos\left[2\pi f_c (nT_s + \zeta_n) + \theta_c\right] \\ &+ A_i \cos\left[2\pi f_i (nT_s + \zeta_n) + \theta_i\right] \end{aligned} . \tag{6}$$

For jitter mitigation, this real-valued signal is converted to complex (I/Q) signal by complex frequency translation with desired signal centre-frequency f_c. This yields essentially

$$\begin{aligned} z_n &= \mathrm{LPF}\left(x_n \times e^{-j2\pi f_c n T_s}\right) \\ &\simeq A_c e^{j\theta_c} e^{j2\pi f_c \zeta_n} + A_i e^{j\theta_i} e^{j2\pi (f_i - f_c) n T_s} e^{j2\pi f_i \zeta_n} \end{aligned} . \tag{7}$$

Now to actually mitigate the jitter effect, which is seen here basically as phase noise, this signal is multiplied by the complex exponential $\exp(-j2\pi f_c \hat{\zeta}_n)$ where $\hat{\zeta}_n$ denotes estimated jitter. With ideal jitter estimates, this would yield

$$z_n e^{-j2\pi f_c \zeta_n} = A_c e^{j\theta_c} + A_i e^{j\theta_i} e^{j2\pi (f_i - f_c) n T_s} e^{j2\pi (f_i - f_c)\zeta_n} . \tag{8}$$

Thus the jitter is fully removed from the target signal and also the jitter effect due to neighbouring channel is reduced, being now relative to $\exp(j2\pi(f_i - f_c)\zeta_n)$. Examples will be given in Section IV.

B. Case of Direct RF Sub-Sampling Receiver Architecture

Here we consider a more general case of receiving a bandpass signal $r(t)$ which, depending on the RF filtering, may contain several modulated signals at neighbouring carriers. This signal is first written here as $r(t) = s_I(t)\cos[2\pi f_c t] - s_Q(t)\sin[2\pi f_c t]$ where f_c denotes the formal centre-frequency of the *overall received band* and $s_I(t) + j s_Q(t)$ is the corresponding baseband equivalent. The resulting sample sequence evaluated at sample instants $nT_s + \zeta_n$ is given by $r_n = r(nT_s + \zeta_n) = s_I(nT_s + \zeta_n)\cos[2\pi f_c (nT_s + \zeta_n)] - s_Q(nT_s + \zeta_n)\sin[2\pi f_c (nT_s + \zeta_n)]$. Taking now the sub-sampling principle [3], [5] into account, this equals to

$$\begin{aligned} r_n = {} & s_I(nT_s + \zeta_n)\cos[2\pi f_{IF} n T_s + 2\pi f_c \zeta_n] \\ & - s_Q(nT_s + \zeta_n)\sin[2\pi f_{IF} n T_s + 2\pi f_c \zeta_n] \end{aligned}, \tag{9}$$

where f_{IF} denotes the aliased centre-frequency. Applying then digital I/Q down-conversion from IF to zero frequency yields

$$\begin{aligned} z_n &= \mathrm{LPF}\left(r_n \times e^{-j2\pi f_{IF} n T_s}\right) \\ &= \left[s_I(nT_s + \zeta_n) + j s_Q(nT_s + \zeta_n)\right] e^{j2\pi f_c \zeta_n} \\ &= s(nT_s + \zeta_n) e^{j2\pi f_c \zeta_n} \end{aligned} . \tag{10}$$

Now, if the original RF centre-frequency f_c is much higher than the corresponding signal bandwidth, the jitter contribution on the composite modulating I and Q components is much lower than on the carrier components [10]. Thus we can approximate (10) as

$$\begin{aligned} z_n &\approx [s_I(nT_s) + j s_Q(nT_s)] e^{j2\pi f_c \zeta_n} \\ &= s(nT_s) e^{j2\pi f_c \zeta_n} \end{aligned} . \tag{11}$$

This basically means that the dominant jitter effect on the sub-sampled RF signal can be approximated as phase noise in the composite carriers of the original bandpass signal. [9]

Based on the above, jitter mitigation using $\hat{\zeta}_n$ can be carried out by multiplying the observed complex sample stream z_n with $\exp(-j2\pi f_c \hat{\zeta}_n)$. Assuming perfect jitter estimates, this fully removes the jitter stemming from the original bandpass nature of the sampled signal, i.e. $z_n \times e^{-j2\pi f_c \hat{\zeta}_n} \approx s_I(nT_s + \zeta_n) + j s_Q(nT_s + \zeta_n) \approx s(nT_s)$.

IV. Simulation Environment, Results and Analysis

First, this Section briefly shows the jitter mitigation performance of the proposed technique in case of narrowband signal with nearby interferer, similar to the case studied in [6] by Rutten et al. Then, the used simulation model for the DRFS case is described and the corresponding simulation results are given and analyzed.

A. Case of Narrowband Signal with Nearby Interferer

As an example, we consider a case with narrowband information signal centred at 50 MHz and a powerful sinusoidal interferer at 51 MHz. A reference tone of 20 MHz is injected at sampler input and the sampling frequency is 200 MHz. 20 ps root-mean-square (RMS) jitter is assumed in the sampling (for more detailed statistical properties of the jitter and the sampling clock using phase locked loop, refer to [9] and [12]). Then estimation and mitigation of the jitter is carried out as explained in Sections II and III. The obtained mitigation performance is illustrated in Fig. 2. Clearly very good jitter mitigation is obtained, and also the proposed method outperforms the reference method in [6] by a few dB's.

As already mentioned, this case is as such rather impractical. As can be seen from Fig. 2, the power difference between the interferer and the information signal is originally around 60 dB, but still, the SNR due to jitter is even without mitigation around 50 dB. This is of course due to the fact that 20ps RMS jitter is very small *compared to* used signal frequencies in the order of 50 MHz. The mitigation techniques still anyway improve the SNR by roughly 30 dB, even though the initial SNR would already be sufficient for detection in any practical communication application.

B. Simulation Model for DRFS Receiver Architecture Case

For DRFS architecture case, 3GPP LTE –like system [1] is simulated to keep comparability with the previous work in [9]. OFDM waveform with 1024 subcarriers, of which 600 are active, is deployed with 16QAM subcarrier modulation and 15 kHz subcarrier spacing. Signal is transmitted at 2.6 GHz carrier frequency. After transmitter, this signal travels through either plain additive white Gaussian noise (AWGN) or extended ITU-R Vehicular A multipath [8] channel. When entering the receiver RF sub-sampling stage, both cases with and without neighbouring channel interferers are considered. In the case with adjacent channel interferers, three sinusoidal interferers at 7.495 MHz, 7.5 MHz and 7.505 MHz offset from the desired signal carrier frequency are considered. In addition, bandpass-noise interferer with approximately 4 MHz bandwidth at 9.5 MHz offset from the desired carrier frequency is also added to the other side of the signal as seen in Fig. 3. The interfering signals are considered to be approximately 40 dB above the interesting OFDM signal. Thus the total incoming signal bandwidth is around 19-20 MHz. Stemming from the centre-frequency of 2.6 GHz and the total bandwidth, we use sub-sampling frequency of 16×1024×15 kHz = 245.76 MHz. This aliases the RF signal from 2.6GHz centre-frequency to 11×245.76 MHz – 2600 MHz = 103.36 MHz IF frequency in a controlled manner. At sampler input,

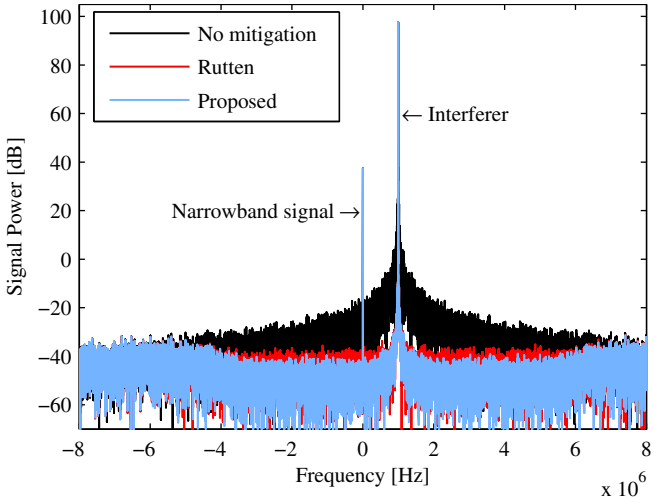

Fig. 2. Down-converted spectrum of signal environment, when 20 ps RMS jitter is applied to narrowband signal and its interferer.

the signal is injected with a reference tone of 36 MHz with approximately the same power level as the interferers. The aliased spectrum after sub-sampling is shown in Fig. 3 for both cases, namely interferer-free case and the case with adjacent channel interferers. After the sampling, the proposed jitter estimation and cancellation method is applied. Then the OFDM waveform is detected and the symbol error-rates (SER) are evaluated as performance indicators.

C. Simulation Results and Analysis

Simulation results for the DRFS receiver case with AWGN channel can be seen in Fig. 4 and Fig. 5. The results show that both techniques improve the receiver performance greatly compared to case without compensation. For interferer-free case, the proposed technique gives practically ideal performance over the whole evaluated SNR and jitter RMS regions. The reference technique from [6] performs nicely for lower than 5 ps jitter RMS. Its performance starts to decrease very fast after the 5 ps point. This is natural, because low-jitter assumption was made in derivation of the reference technique in [6]. In the more challenging case with the neighbouring channel interferers, the proposed technique performs again very well giving near-ideal performance with lower than 10 ps RMS jitter. With jitter RMS over 10 ps, some decrease in performance is seen, as the jitter-spread of the interferers gets higher and higher contaminating also the reference tone band. With the reference technique from [6], the performance is again limited to much lower jitter values.

The corresponding results for extended ITU-R Vehicular A multipath channel case are depicted in Fig. 6. The results are relatively similar to those given for the AWGN channel case. Of course, due to more challenging propagation environment, the detection error rates are generally higher. Thus in general, without mitigation, jitter begins to clearly affect the system performance only at somewhat higher jitter RMS values compared to the AWGN case with similar SNR. Anyway, the proposed technique can again efficiently push down the signal distortion up to 20ps RMS jitter range.

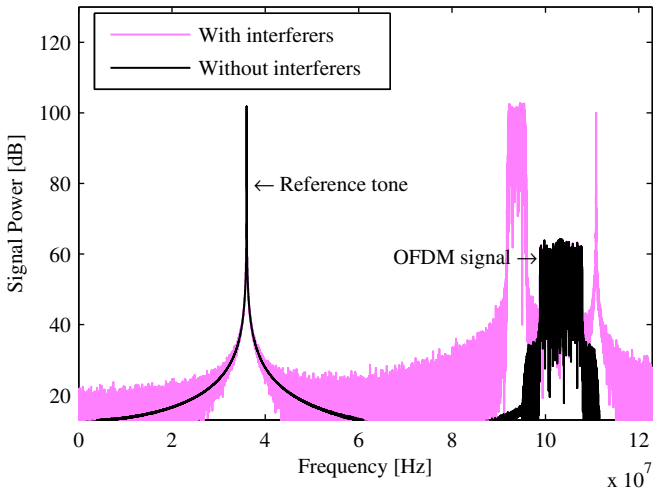

Fig. 3. Spectra of reference tone, OFDM signal (at 2.6 GHz originally) and interferers after aliasing when sampling at 245.76 MHz (20 ps RMS jitter).

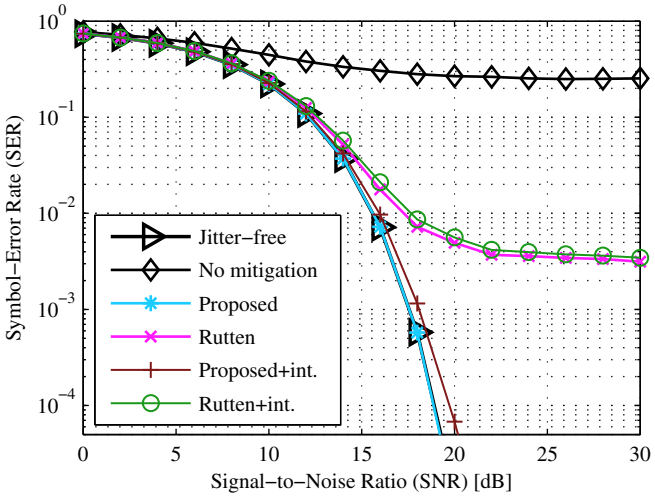

Fig. 5. SER as a function of SNR with fixed RMS jitter of 20 ps in AWGN channel.

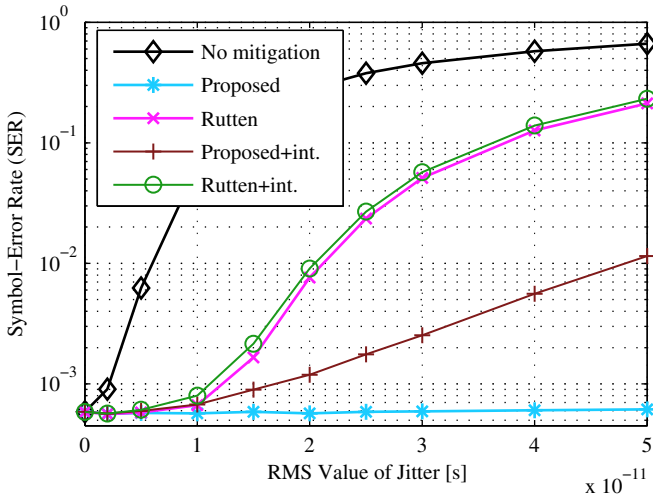

Fig. 4. SER as a function of sampling jitter RMS with fixed SNR of 18 dB in AWGN channel.

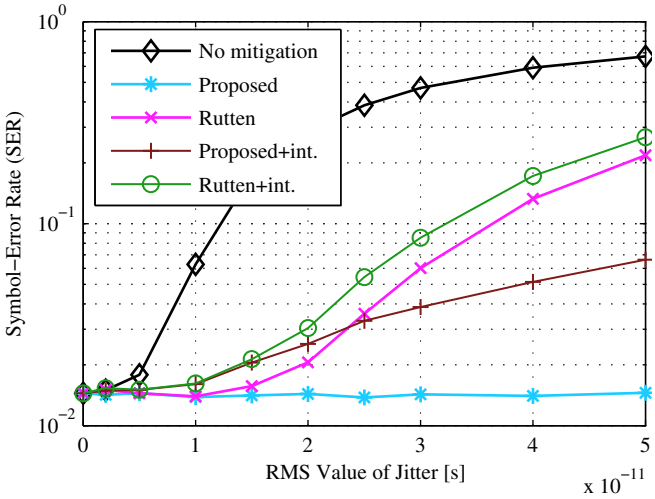

Fig. 6. SER as a function of sampling jitter RMS with fixed SNR of 26 dB in extended ITU-R Vehicular A multipath channel.

V. Conclusions

Sampling jitter is one of the main practical problems in direct RF sub-sampling receiver architecture. We proposed an efficient way to estimate the sampling jitter realization for every taken sample, with the help of an injected reference signal at the sampler input. We also proposed a way to use then these estimates to reduce the effects of the jitter, with special emphasis on DRFS receiver. Based on the performance simulations, the proposed estimation cancellation approach can efficiently mitigate sampling jitter also in the challenging case of strong neighbouring channels entering the sub-sampling radio.

References

[1] 3GPP Technical Specification, TS 36.101 v8.2.0. Release 8, May 2008.

[2] A. Demir, "Computing timing jitter from phase noise spectra for oscillators and phase-locked loops with white and 1/f noise," *IEEE Trans. Circuits and Systems I*, vol. 53, pp. 1869-1884, Sept. 2006.

[3] M.E. Frerking, *Digital Signal Processing in Communication Systems*. New York: Chapman & Hall, 1994.

[4] M. Löhning and G. Fettweis, "The effect of aperture jitter and clock jitter in wideband ADCs," *CSI*, Vol. 29, No. 1, pp. 11-18, January 2007.

[5] B. Razavi, *RF Microelectronics*. Prentice Hall PTR, Upper Saddle River, NJ, USA, 1998, 335 p.

[6] R. Rutten, L.J. Breems, and R.H.M. van Veldhoven, "Digital jitter-cancellation for narrowband signals," in *Proc. IEEE ISCAS 2008*, May 2008, pp. 1444-1447.

[7] M. Shinagawa, Y. Akazawa, and T. Wakimoto, "Jitter analysis of high-speed sampling systems," *IEEE Journal of Solid-State Circuits*, Vol. 25, No. 1, pp. 220-224, February 1990.

[8] T. B. Sorensen, P. E. Mogersen, and F. Frederiksen, "Extension of the ITU channel models for wideband (OFDM) systems," in *Proc. IEEE VTC-Fall 2005*, Dallas, TX, September 2005, pp. 392-396.

[9] V. Syrjälä and M. Valkama, "Jitter mitigation in high-frequency bandpass sampling OFDM radios," in *Proc. IEEE WCNC 2009*, Budapest, Hungary, April 2009.

[10] V. Syrjälä, M. Valkama, and M. Renfors, "Efficient jitter model for high-frequency bandpass sampling," in *Proc. Finnish Signal Processing Symposium (FINSIG'07)*, Oulu, Finland, August 2007.

[11] V. Syrjälä, M. Valkama, and M. Renfors, "Design considerations for direct RF sampling receiver in GNSS environment," in *Proc. 5th Workshop on Positioning, Navigation and Communication (WPNC'08)*, Hannover, Germany, March 2008, pp. 9-13.

[12] V. Syrjälä, M. Valkama, N. N. Tchamov, and J. Rinne, "Phase noise modelling and mitigation techniques in OFDM communications systems," in *Proc. Wireless Telecommunications Symposium 2009, (WTS'09)*, Prague, Czech Republic, April 2009.

Publication 4

V. Syrjälä and M. Valkama, "Sampling jitter cancellation in direct-sampling radio," in *Proc. IEEE Wireless Communications & Networking Conference 2010* (*IEEE WCNC'10*), Sydney, Australia, April 2010.

Sampling Jitter Cancellation in Direct-Sampling Radio

Ville Syrjälä and Mikko Valkama
Department of Communications Engineering
Tampere University of Technology
P.O. Box 553, FI-33101, Tampere, Finland
ville.syrjala@tut.fi, mikko.e.valkama@tut.fi

Abstract—**This paper addresses the sampling jitter estimation and cancellation task in direct RF sub-sampling type radios. The proposed jitter estimation method is based on carefully injecting or superimposing an additional known reference signal to the received signal at the sampler input. Proper digital signal processing methods are then devised and applied to estimate the sampling jitter realizations from the obtained jittered samples. Using these jitter estimates, combined with proper jitter modelling, the jitter effects can then be efficiently removed from the actual received signal. Careful performance analysis of the overall estimation-cancellation scheme is also carried out using computer simulations with 3GPP LTE type multicarrier signals, assuming also different amounts of RF filtering prior to RF sub-sampling stage. In the performance simulations, both additive white Gaussian noise and extended ITU-R Vehicular A multipath radio channel types are considered.**

Keywords-sampling jitter; mitigation; dirty-RF; RF-DSP; direct RF sampling; bandpass sampling; sub-sampling

I. INTRODUCTION

In sampling of high-frequency signals, or signals with powerful neighbouring channels, relatively high requirements are set for the timing accuracy of the sampling process [7], [9], [15], [16]. In traditional radio receivers, relatively low-frequency signals are sampled because of signal down-conversion prior to sampling. In addition, most of the interference near the interesting frequencies is attenuated. These result into relatively relaxed requirements for the dynamics and timing accuracy of the sampling and A/D-conversion circuitry in current receivers. However, when emphasizing radio flexibility and re-configurability, more and more of the selectivity filtering is moved to digital domain [4]-[7]. Similarly from the frequency-translations point of view, applying sampling to higher-frequency signals in the overall receiver signal-processing chain is one of the main trends currently. Under these working assumptions, timing inaccuracies in the sampling process, called sampling jitter, can become a severe problem [2], [4]-[8], [15], [16]. Thus, for the future radio receivers, understanding, modelling and mitigation of the sampling jitter is a very interesting and important topic.

In the so-called direct RF sampling (DRFS) receiver architecture, very high-frequency signals are sampled in conditions with possibly high-power interferers present [6], [7], [13]. DRFS is a receiver architecture in which the sampling of the incoming signal is done already at the radio frequencies (RF). DRFS reduces the amount of analogue components in the receiver, thus emphasizing re-configurability and also potentially minimizing size, power consumption and costs of the receiver compared to more traditional radios. However, the DRFS concept still has many practical implementation issues to be solved [7], [13], and it is thus not commonly considered feasible for mobile terminal receivers with today's implementation technology. The most notable problem with the DRFS approach is that it indeed poses very high demands for the quality of the sampling process. With current technologies, the combined requirements of timing accuracy and relatively high sampling frequency and resolution for the used sampling and A/D-conversion circuitry, result into relatively high power consumption. High power consumption in turn is one of the main concerns in mobile terminals. To circumvent this, digital signal processing (DSP) methods are developed in this paper to lower the quality requirements for the sampling process.

In the literature, DSP-based estimation and mitigation of sampling jitter is not too widely researched yet. This is partially because jitter is inherently a random process varying from sample instant to another and thus its estimation and mitigation at sample level is challenging. Also in most of today's receiver architectures, sampling takes place at fairly low frequencies, and thus jitter is not a major concern. However, as indicated earlier, this might not be the case in near future, since minimizing the amount of analogue parts in receivers while increasing flexibility becomes more and more emphasized. Furthermore, DSP capabilities of the mobile devices are continuously increasing. Recently, in [11], use of phase noise mitigation techniques [14] in mitigation of sampling jitter in bandpass sampling receivers was proposed for orthogonal frequency division multiplexing (OFDM) systems. In addition, the authors of [8] have proposed a technique to remove sampling jitter effects from general narrowband signals with help of a reference tone. In this paper, the idea of carefully designing and injecting a reference tone on top of the received signal at the sampler input is further developed. This paper first proposes an efficient technique to estimate the sampling jitter realizations with the help of such reference tone. The estimates of the jitter realizations are then used online to mitigate the effects of the sampling jitter from the

This work was supported by TUT Graduate School, the Finnish Funding Agency for Technology and Innovation (Tekes), the Academy of Finland and the Technology Industries of Finland Centennial Foundation.

actual received sampled waveform, without the limitations of narrowband signals and small jitter values as was assumed in [8]. Special emphasis in modelling and algorithm development is put to the DRFS receiver case where only partial selectivity is implemented at RF prior to sampling.

After this Section, the paper layout is as follows. Section II proposes the method to estimate sampling jitter values with the help of reference tone. Section III then proposes ways to mitigate the sampling jitter in DRFS system by using the jitter estimates. In Section IV the simulation environment is described and the corresponding simulation results and analysis are given in Section V. Conclusions for the work in this paper is finally given in Section VI.

II. Sampling Jitter Estimation Using a Sampled Reference Tone

In this Section, we propose an efficient technique to estimate the sampling jitter realizations from sampled jittered signal for direct sub-sampling radios. This is done by using the idea of injecting a reference tone to the incoming signal prior to the sampling circuitry [8], combined with proper digital processing of the jittered samples. These jitter estimates are then used with further digital signal processing to cancel the jitter effects from the actual received waveform samples in Section III.

A. Jittered Sub-Sampling Signal Model

First, let $r(t)$ denote the incoming received RF signal, written here as a general bandpass signal of the form

$$\begin{aligned} r(t) &= z_I(t)\cos[2\pi f_c t] - z_Q(t)\sin[2\pi f_c t] \\ &= A_r(t)\cos[2\pi f_c t + \theta_r(t)] \end{aligned}, \qquad (1)$$

where $z(t) = z_I(t) + jz_Q(t) = A_r(t)e^{j\theta_r(t)}$ denotes the composite baseband equivalent of the overall received signal. Notice that depending on the amount of RF filtering, this may contain also several neighbouring channels, in addition to the target signal. Now the idea is to inject a reference tone, say $A_{ref}\cos(2\pi f_{ref}t)$, on top of $r(t)$ where f_{ref} denotes the reference tone frequency. This is illustrated in Fig. 1. Here sinusoidal reference signal is used, but in principle also other kinds of known signals could be used, if considered beneficial. Now, with suitable reference tone injected, the sampled signal is given by

$$\begin{aligned} r_n &= r(nT_s + \zeta_n) + A_{ref}\cos\big[2\pi f_{ref}(nT_s + \zeta_n)\big] \\ &= z_I(nT_s + \zeta_n)\cos\big[2\pi f_c(nT_s + \zeta_n)\big] \\ &\quad - z_Q(nT_s + \zeta_n)\sin\big[2\pi f_c(nT_s + \zeta_n)\big] \\ &\quad + A_{ref}\cos\big[2\pi f_{ref}(nT_s + \zeta_n)\big] \end{aligned}, \qquad (2)$$

where $t_n = nT_s + \zeta_n$ denote the jittered sample instants, $F_s = 1/T_s$ is the nominal sampling frequency, and ζ_n denote jitter. Taking next the sub-sampling principle into account, which aliases the signal into lower frequencies in a controlled manner, this sample stream can also be written as

$$\begin{aligned} r_n &= z_I(nT_s + \zeta_n)\cos\big[2\pi f_{IF} nT_s + 2\pi f_c\zeta_n\big] \\ &\quad - z_Q(nT_s + \zeta_n)\sin\big[2\pi f_{IF} nT_s + 2\pi f_c\zeta_n\big], \\ &\quad + A_{ref}\cos\Big[2\pi f'_{ref} nT_s + 2\pi f_{ref}\zeta_n\Big] \end{aligned} \qquad (3)$$

where f_{IF} and f'_{ref} denote the aliased centre-frequency and (possibly) aliased reference frequency, respectively. Depending on the choice of the reference frequency f_{ref} relative to sampling frequency F_s, $f'_{ref} < f_{ref}$ (controlled aliasing) or $f'_{ref} = f_{ref}$ (no aliasing).

B. Sampling Jitter Estimation

Based on (3), the main effect of jitter is that it causes phase noise to the composite I/Q carriers of the incoming signal as well as to the reference tone. Now, given that the aliased reference frequency f'_{ref} is outside the band of the aliased received signal (at f_{IF}), we can use complex digital mixing and lowpass filtering (LPF) to isolate the jittered reference tone. First we write (3) as

$$\begin{aligned} r_n &= \\ &\mathrm{Re}\{[z_I(nT_s + \zeta_n) + jz_Q(nT_s + \zeta_n)]e^{j2\pi f_{IF} nT_s}e^{j2\pi f_c\zeta_n}\} \\ &+ A_{ref}\,\mathrm{Re}\{e^{j2\pi f'_{ref} nT_s}e^{j2\pi f_{ref}\zeta_n}\} \\ &= \mathrm{Re}\{z(nT_s + \zeta_n)e^{j2\pi f_{IF} nT_s}e^{j2\pi f_c\zeta_n}\} \\ &\quad + A_{ref}\,\mathrm{Re}\{e^{j2\pi f'_{ref} nT_s}e^{j2\pi f_{ref}\zeta_n}\} \end{aligned} . \qquad (4)$$

So at the output of a complex digital mixer running at f'_{ref}, followed by LPF, we have

$$\begin{aligned} y_n &= \mathrm{LPF}\Big(r_n \times e^{-j2\pi f'_{ref} nT_s}\Big) \\ &\simeq e^{j2\pi f_{ref}\zeta_n} \end{aligned}. \qquad (5)$$

This represents a complex exponential where jitter is seen essentially as phase noise. Strictly speaking, the last expression in (5) holds only approximately, because due to jitter, the spectra of all the frequency components in the sampled signal in (4) are spread around their original frequency contents. However, with practical sampling clocks, it is expected that there is some correlation between consecutive jitter values and thus most of the energy of the sampled signal components is still located at the original frequencies. This is, of course, also influenced by the choice of the reference frequency relative to the actual received signal. Finally, based on (5), estimates of the sampling jitter values ζ_n can be obtained as

$$\hat{\zeta}_n = \arg\{y_n\}/(2\pi f_{ref}). \qquad (6)$$

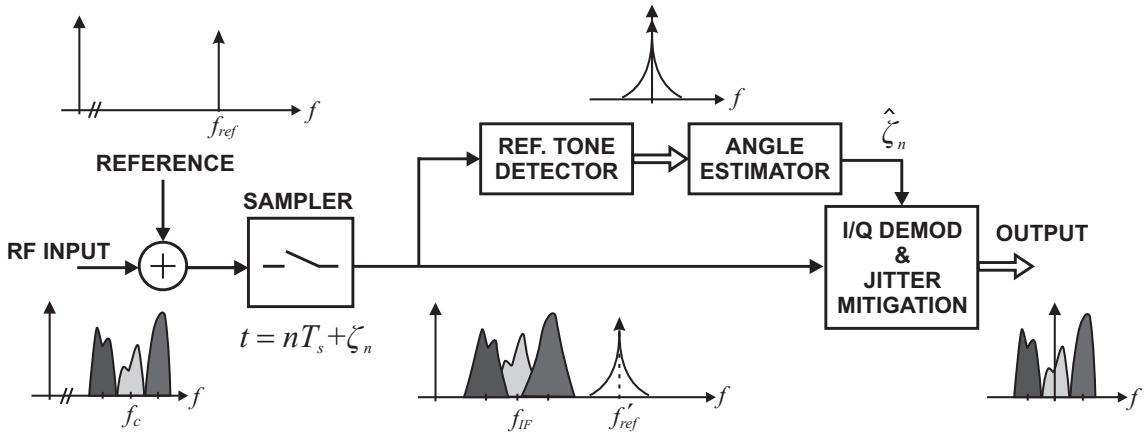

Fig. 1. General illustration of super-imposing a reference tone at sampler input, which is then used for digital jitter estimation and cancellation from the actual received signal in a direct-sampling radio. For illustration purposes, only three received channels are shown, and the target signal is depicted in the lightest grey.

C. Discussion

Like discussed already shortly above, in the estimation process, there are some essential limitations that should be carefully understood. The reference frequency f_{ref} must be selected so that it is possible to sufficiently separate (filter) the reference tone from the actual incoming signal in the jittered sampling. In practice, the amount of this separation depends on (i) the frequency separation between $r(t)$ and f_{ref} (after aliasing), (ii) the amount of jitter and (iii) the power ratio between $r(t)$ and the reference tone. In the selection of f_{ref}, it should also be kept in mind that jitter has heavier effect on high-frequency signals. Thus, the higher the selected reference frequency is, the easier it is, from practical signal processing point of view, to detect the phase behaviour of the isolated reference tone in (5). It should also be acknowledged that the reference signal itself must be very accurately known, and it is likely that the selection of f_{ref} affects also the generation accuracy of the reference. Furthermore, not only the frequency of the reference tone, but also its amplitude is important in the design. On one hand, if the dynamic range in the incoming signal is high, then also high number of bits is needed in the digital domain signal processing. On the other hand, it is easier to estimate the sampling jitter if the reference tone is strong (compared to $r(t)$), so from the estimation point of view, more powerful the reference tone the better. Thus a proper compromise is needed in dimensioning the reference signal power in practice. Concrete examples will be given in Section IV.

III. Sampling Jitter Cancellation

This Section proposes an efficient way to use the obtained jitter estimates $\hat{\zeta}_n$ in (6) for the jitter mitigation of the incoming signal.

A. Basic Cancellation Processing

The cancellation builds upon the received signal modelling in (4). Applying first digital I/Q down-conversion, from IF to zero frequency, and lowpass filtering yields

$$\begin{aligned} z_n &= \mathrm{LPF}\left(r_n \times e^{-j2\pi f_{IF} n T_s} \right) \\ &\simeq [z_I(nT_s + \zeta_n) + j z_Q(nT_s + \zeta_n)] e^{j2\pi f_c \zeta_n} \\ &= z(nT_s + \zeta_n) e^{j2\pi f_c \zeta_n} \end{aligned} . \quad (7)$$

Above, it is assumed that the (jittered) reference tone is essentially suppressed by the LPF. Now, if the original RF centre-frequency f_c is much higher than the corresponding signal bandwidth, the jitter contribution on the composite modulating I and Q components (z_I and z_Q) is much lower than on the carrier components [12]. Thus we can approximate $z_I(nT_s + \zeta_n) \approx z_I(nT_s)$ and $z_Q(nT_s + \zeta_n) \approx z_Q(nT_s)$, and write (7) as

$$\begin{aligned} z_n &\approx [z_I(nT_s) + j z_Q(nT_s)] e^{j2\pi f_c \zeta_n} \\ &= z(nT_s) e^{j2\pi f_c \zeta_n} \end{aligned} . \quad (8)$$

This basically means that the dominant jitter effect on the sub-sampled RF signal can be approximated as phase noise in the composite carriers of the original bandpass signal. Similar conclusion is also drawn in [11].

Based on the above modelling, jitter mitigation (using the jitter estimates $\hat{\zeta}_n$) can be carried out by multiplying the observed complex sample stream z_n with $\exp(-j2\pi f_c \hat{\zeta}_n)$. Assuming perfect jitter estimates ($\hat{\zeta}_n = \zeta_n$), this fully removes the jitter stemming from the original bandpass nature of the sampled signal, i.e.,

$$\begin{aligned} \hat{z}_n &= z_n \times e^{-j2\pi f_c \hat{\zeta}_n} \approx z(nT_s + \zeta_n) \\ &\approx z(nT_s) \end{aligned} . \quad (9)$$

B. Further Interpretations for Multichannel Signals

In the previous Subsection, no explicit assumptions other than $z(nT_s + \zeta_n) \approx z(nT_s)$ were made on the nature of the

incoming signal. Here we build further understanding and interpretations in the case where the overall baseband equivalent signal $z(t)$ of the incoming RF signal contains also neighbouring channels. This is important because jitter is generally most challenging in such scenarios. In an example case of one neighbouring channel on both sides, the overall baseband equivalent is of the form

$$z(t) = z_c(t) + z_{i,1}(t)e^{j2\pi f_{i,1}t} + z_{i,2}(t)e^{j2\pi f_{i,2}t}. \quad (10)$$

Here $z_c(t)$ denotes the complex envelope of the target signal (centred originally at f_c), and $z_{i,1}(t)$ and $z_{i,2}(t)$ denote the complex envelopes of the neighbouring channels located originally at offsets $f_{i,1} > 0$ and $f_{i,2} < 0$ from f_c, respectively. Under these assumptions, the compensated signal in (9) can be written as

$$\begin{aligned} \hat{z}_n &= z_n \times e^{-j2\pi f_c \hat{\zeta}_n} \\ &\approx z(nT_s + \zeta_n) \\ &= z_c(nT_s + \zeta_n) + z_{i,1}(nT_s + \zeta_n)e^{j2\pi f_{i,1} nT_s} e^{j2\pi f_{i,1}\zeta_n} \\ &\quad + z_{i,2}(nT_s + \zeta_n)e^{j2\pi f_{i,2} nT_s} e^{j2\pi f_{i,2}\zeta_n} \end{aligned} . \quad (11)$$

Assuming now that the individual complex envelopes $z_c(t)$, $z_{i,1}(t)$ and $z_{i,2}(t)$ change slowly relative to jitter values (which is always a valid assumption given jitter values in the tens of pico-second range and bandwidths in the order of few or few tens of MHz), we have $z_c(nT_s + \zeta_n) \approx z_c(nT_s)$, $z_{i,1}(nT_s + \zeta_n) \approx z_{i,1}(nT_s)$ and $z_{i,2}(nT_s + \zeta_n) \approx z_{i,2}(nT_s)$. Thus the signal in (11) can be simply written as

$$\begin{aligned} \hat{z}_n &= z_n \times e^{-j2\pi f_c \hat{\zeta}_n} \\ &\approx z_c(nT_s) + z_{i,1}(nT_s)e^{j2\pi f_{i,1} nT_s} e^{j2\pi f_{i,1}\zeta_n} \\ &\quad + z_{i,2}(nT_s)e^{j2\pi f_{i,2} nT_s} e^{j2\pi f_{i,2}\zeta_n} \end{aligned} . \quad (12)$$

Based on (12), the jitter stemming from the target signal is fully removed and also the jitter effects due to neighbouring channels are heavily reduced. The remaining jitter noise in the compensated signal in (12) stemming from the neighbouring channels is now relative to $\exp(j2\pi f_i \zeta_n)$ which is vanishingly small with practical jitter values ζ_n and neighbouring channel frequency offsets f_i.

IV. Simulation Environment

This Section demonstrates the applicability and performance of the proposed jitter estimation and cancellation technique. For reference, also the technique described in [8] by Rutten et al. is implemented. As an example radio system, 3GPP LTE -like system [1] is used. Thus OFDM waveform with 1024 subcarriers, of which 600 are active, is deployed with 16QAM subcarrier modulation and 15 kHz subcarrier spacing. Used RF centre-frequency is 2.6 GHz. After transmitter, the transmit waveform travels through either plain additive white Gaussian noise (AWGN) or extended ITU-R Vehicular A multipath [10] channel. Cases without and with neighbouring channels are simulated.

As a model of the sampling clock, and thereon of the jitter spectrum, the phase locked loop (PLL) based oscillator described in [11] and [14] is deployed. Similar oscillators are also described, e.g., in [2]. In the neighbouring channel studies, three sinusoidal interferers at 7.495 MHz, 7.5 MHz and 7.505 MHz offset (above) from the desired signal carrier frequency together with a bandpass-noise type interferer with approximately 4 MHz bandwidth at 9.5 MHz offset (below) from the desired signal carrier frequency are considered, as illustrated in Fig. 2. Thus the total incoming signal bandwidth is around 19-20 MHz. Stemming from the target centre-frequency of 2.6 GHz and the total bandwidth, we use a sub-sampling frequency of F_s = 16×1024×15 kHz = 245.76 MHz. This aliases the RF signal from 2.6 GHz centre-frequency to 11×245.76 MHz – 2600 MHz = 103.36 MHz IF frequency in a controlled manner. At the sampler input, the received signal is injected with a reference tone of 36 MHz. An example of aliased spectrum after sub-sampling is shown in Fig. 2 for interferer-free case and the case with adjacent channel interferers. After sub-sampling, the proposed jitter estimation and cancellation methods are applied as described in Sections II and III. Then, the digital selectivity filtering is applied and the OFDM waveform is detected and the symbol-error rates (SER) are evaluated as performance indicators.

Two kinds of reference power allocation schemes are assumed in the simulations. In both schemes the adjacent channel signals are considered to be 0 to 40 dB above the interesting OFDM signal. For the first scheme, the reference tone is constantly 40 dB above the interesting OFDM signal. In the second scheme, the reference tone power is allocated so that it has the same power level as the interferers. The latter case might be more practical one, as in such scheme the reference tone does not increase the dynamic requirements of the A/D-circuitry. In practice, the reference tone power can be allocated in connection with the automatic gain control mechanism of the A/D-circuitry, where the power of the signals at the sampler input is calculated anyway.

V. Simulation Results and Analysis

Simulation results with AWGN channel can be seen in Fig. 3. In the results, power levels of the interferers and the reference tone are 40 dB above the interesting signal. The results show that both the proposed technique as well as the reference technique from [8] improve the performance (reduce jitter noise) greatly compared to case without compensation. For interferer-free case, the proposed technique gives practically ideal performance over the whole evaluated SNR region with fixed 20 ps RMS jitter. However, small decrease in performance is visible in the more challenging case with the neighbouring channels included (+int. curves in the figures).

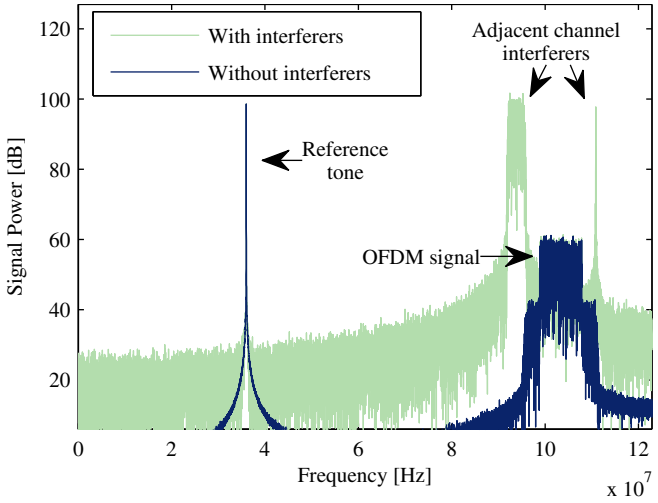

Fig. 2. Example spectra of the reference tone, the OFDM signal and the interferers after aliasing by sub-sampling at 245.76 MHz with 20 ps RMS jitter. The original RF signal centre-frequency is 2.6 GHz while the reference tone frequency is 36 MHz.

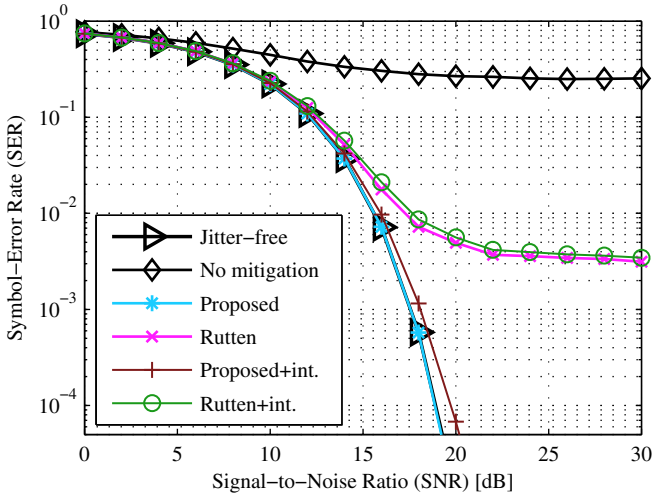

Fig. 3. SER given as a function of received SNR with fixed RMS jitter of 20 ps in AWGN channel.

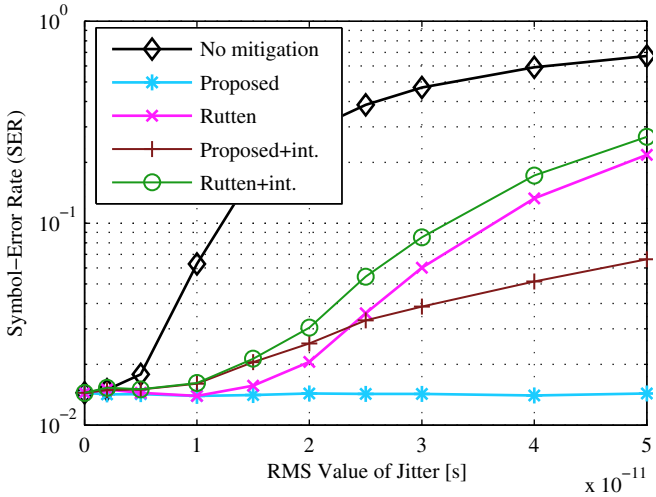

Fig. 4. SER given as a function of sampling jitter RMS with fixed received SNR of 26 dB in extended ITU-R Vehicular A multipath channel.

The results for extended ITU-R Vehicular A multipath channel case are depicted in Fig. 4 for an example fixed received SNR of 26 dB over wide jitter RMS region. Here as well as above, the power of the interferers and the reference tone are 40 dB above the level of useful signal. The reference technique from [8] performs nicely for lower than 15 ps jitter RMS. Its performance starts to decrease very fast after the 15 ps point. This is natural, because a low-jitter assumption was made in derivation of the reference technique in [8] (in AWGN case, already 5 to 10 ps RMS jitter started to affect the performance of the reference technique heavily.) With the neighbouring channels included, the proposed technique performs again very well giving near-ideal performance with lower than 10 ps RMS jitter. With jitter RMS over 10 ps, some decrease in performance is seen, as the jitter noise due to interferers gets higher and higher contaminating also the reference tone band. With the reference technique from [8], the performance is again limited to lower jitter values. Anyway, the proposed technique can again efficiently push down the signal distortion up to 20 ps RMS jitter range.

In Fig. 5, Fig. 6 and Fig. 7, the results are given as a function of the power level of the adjacent channel interferers. This is very interesting because in DRFS receiver, the selectivity is one of the main design concerns. In Fig. 5 the interference and the reference tone power levels are the same. There we see that when the reference tone level is lowered to the level of the OFDM signal, there is significant performance drop. Still, the proposed technique manages to give clear performance increase compared to the case without mitigation. From interference free cases, we see that when the reference tone is less than 10 dB over the useful signal, the spread of the OFDM signal lowers reference tone detection quality. When comparing the results in Fig. 5 to the results in Fig. 6, we see that the spread of the interferers has undesired effect also on the detection of the reference tone. Fig. 6 also shows that when using the reference tone fixed at 40 dB above the useful signal, the performances of the mitigation techniques are very good until the power of the adjacent channel interferers gets high enough to deteriorate the quality of the reference tone due to spreading. Similar conclusion can be made for the case of extended Vehicular A multipath channel, as depicted in Fig. 7. Multipath channel does not change the relative results too much, because most of the errors in the simulations are caused by the sampling process in the receiver.

VI. Conclusions

In direct RF sub-sampling radios, sampling jitter is one of the main practical issues from the practical implementation point of view. This paper proposes digital signal processing methods to estimate the sampling jitter realization sample-by-sample basis. The estimation is done by injecting a reference

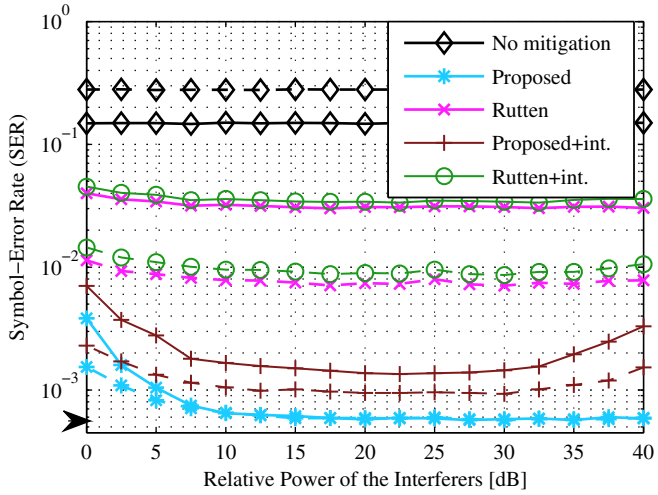

Fig. 5. SER given as a function of relative power of the interferers in AWGN channel with received SNR of 18 dB. The reference tone power is the same as the power of the interferers. RMS jitter is 20 ps (dashed) / 50 ps (solid). The arrow on SER axis shows the jitter-free performance.

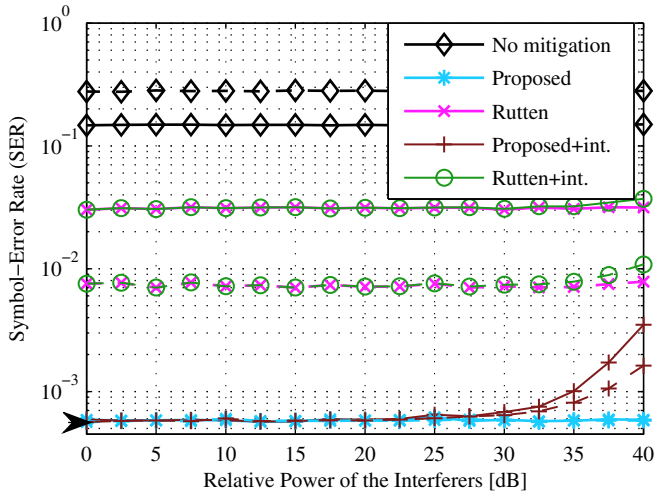

Fig. 6. SER given as a function of relative power of the interferers in AWGN channel with received SNR of 18 dB. The reference tone power is 40 dB above the useful signal power. RMS jitter is 20 ps (dashed) / 50 ps (solid). The arrow on SER axis shows the jitter-free performance.

tone to the sampler input and applying signal processing to that signal after the sampling. Furthermore, an efficient digital signal processing structure, that utilizes these jitter estimates to reduce the jitter effects from the actual received signal, was also proposed with special emphasis on DRFS receiver. Based on the performance simulations, the proposed estimation-cancellation approach can efficiently mitigate sampling jitter also in the challenging case of strong neighbouring channels entering the sub-sampling radio. Simulations showed that the performance of the technique is very good compared to the performance of state-of-the-art technique. One of the most interesting parameters in the proposed technique is the reference tone power, as it affects the dynamic range requirements in the sampling and also dictates the mitigation performance of the proposed technique.

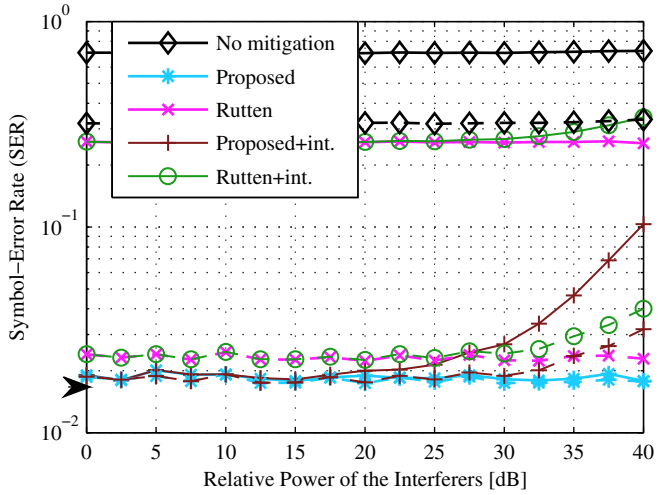

Fig. 7. SER given as a function of relative power of the interferers in extended ITU-R Vehicular A multipath channel with SNR of 26 dB. The reference tone power is 40 dB above the useful signal power. RMS jitter is 20 ps (dashed) / 50 ps (solid). The arrow on SER axis shows the jitter-free performance.

REFERENCES

[1] 3GPP Technical Specification, TS 36.101 v8.2.0. Physical Channels and Modulation (release 8), May 2008.

[2] Analog Devices, "Converting oscillator phase noise to time jitter," MT-008 Tutorial, Rev.A, Oct. 2008, Available online at http://www.analog.com/

[3] A. Demir, "Computing timing jitter from phase noise spectra for oscillators and phase-locked loops with white and 1/f noise," *IEEE Trans. Circuits and Systems I*, vol. 53, pp. 1869-1884, Sept. 2006.

[4] M.E. Frerking, *Digital Signal Processing in Communication Systems*. New York: Chapman & Hall, 1994.

[5] M. Löhning and G. Fettweis, "The effect of aperture jitter and clock jitter in wideband ADCs," *CSI*, Vol. 29, No. 1, pp. 11-18, January 2007.

[6] P.-I. Mak, S.-P U, and R. P. Martins, "Transceiver architecture selection: Review, State-of-the-Art Survey and Case Study", *IEEE Circuits and Systems Mag.*, vol. 7, 2nd quarter 2007, pp. 6-25.

[7] B. Razavi, *RF Microelectronics*. Prentice Hall PTR, Upper Saddle River, NJ, USA, 1998, 335 p.

[8] R. Rutten, L.J. Breems, and R.H.M. van Veldhoven, "Digital jitter-cancellation for narrowband signals," in *Proc. IEEE ISCAS 2008*, May 2008, pp. 1444-1447.

[9] M. Shinagawa, Y. Akazawa, T. Wakimoto, "Jitter analysis of high-speed sampling systems," *IEEE Journal of Solid-State Circuits*, Vol. 25, No. 1, pp. 220-224, February 1990.

[10] T. B. Sorensen, P. E. Mogersen, and F. Frederiksen, "Extension of the ITU channel models for wideband (OFDM) systems," in *Proc. IEEE VTC-Fall 2005*, Dallas, TX, September 2005, pp. 392-396.

[11] V. Syrjälä, M. Valkama, "Jitter mitigation in high-frequency bandpass sampling OFDM radios," in *Proc. IEEE WCNC 2009*, Budapest, Hungary, April 2009.

[12] V. Syrjälä, M. Valkama, and M. Renfors, "Efficient jitter model for high-frequency bandpass sampling," in *Proc. Finnish Signal Processing Symposium (FINSIG'07)*, Oulu, Finland, August 2007.

[13] V. Syrjälä, M. Valkama, and M. Renfors, "Design considerations for direct RF sampling receiver in GNSS environment," in *Proc. 5th Workshop on Positioning, Navigation and Communication (WPNC'08)*, Hannover, Germany, March 2008, pp. 9-13.

[14] V. Syrjälä, M. Valkama, N. N. Tchamov, and J. Rinne, "Phase noise modelling and mitigation techniques in OFDM communications systems," in *Proc. Wireless Telecommunications Symposium 2009, (WTS'09)*, Prague, Czech Republic, April 2009.

[15] R. H. Walden, "Analog-to-digital converter survey and analysis," *IEEE J. Selected Areas in Communications*, vol. 17, no. 4, pp. 539-550, April 1999.

[16] J. A. Wepman, "Analog-to-digital converters and their applications in radio receivers," *IEEE Commun. Mag.*, vol. 33, pp. 39-45, May 1995.

Publication 5

V. Syrjälä and M. Valkama, "Analysis and mitigation of phase noise and sampling jitter in OFDM radio receivers," *International Journal of Microwave and Wireless Technologies*, Vol. 2, No.2, pp. 193-202, April 2010.

International Journal of Microwave and Wireless Technologies, page 1 of 10.
doi:10.1017/S1759078710000309

Analysis and mitigation of phase noise and sampling jitter in OFDM radio receivers

VILLE SYRJÄLÄ AND MIKKO VALKAMA

This article addresses the analysis and digital signal processing (DSP)-based mitigation of phase noise and sampling clock jitter in orthogonal frequency division multiplexing (OFDM) radios. In the phase noise studies, the basic direct-conversion receiver architecture case is assumed with noisy downconverting oscillator. In the sampling jitter case, on the other hand, the so-called direct-radio-frequency-sampling receiver architecture is deployed utilizing bandpass sub-sampling principle. The basis for the DSP-based impairment mitigation techniques is first formed using analytical receiver modeling with incoming OFDM waveform, where the effects of both oscillator phase noise and sampling clock jitter are mapped to certain type subcarrier cross-talk and distortion compared to ideal receiver case. Then iterative detection principles and interpolation techniques are developed to essentially estimate and cancel the subcarrier distortion. Also some related practical aspects, like channel estimation, are addressed. The performance of the proposed mitigation techniques is analyzed and verified with extensive computer simulations. In the simulations, realistic phase-locked-loop-based oscillator models are used for phase noise and sampling clock jitter. In addition, different received signal conditions like plain additive white Gaussian noise channel and extended ITU-R Vehicular A multipath channel are considered for practical purposes. Altogether the obtained results indicate that the effects of oscillator and sampling clock instabilities can be efficiently reduced using the developed signal processing techniques.

Keywords: Direct-conversion receiver, RF sub-sampling receiver, Phase noise, Sampling jitter, OFDM, Intercarrier interference, Mitigation, Cancelation

Received 23 October 2009; Revised 15 February 2010

I. INTRODUCTION

In recent years, raw processing power of mobile radios has been greatly increasing. This has allowed implementation of various computationally intensive digital signal processing (DSP) stages in radios, e.g., for data detection and decoding purposes to improve the overall receiver and link performance [1]. In addition, by using the available DSP power, some nonidealities of the used radio frequency (RF) electronics can be reduced, enabling the use of cheaper, smaller, and less power consuming analog radio components [1]. Good examples are, e.g., power amplifier linearization, I/Q imbalance compensation, reduction of mixer nonlinearities, just to name a few [1]. Due to the above-mentioned rapid advances in digital implementation techniques, the available processing power has risen while also lowering the costs, size, and power consumption of the usable processing units at the same time. On the analog/RF electronics side, on the other hand, the main trend is the miniaturization of the integrated circuitry.

Oscillator is one of the most fundamental analog components used in almost every radio. On the implementation side, the random fluctuations of the instantaneous phase and frequency of the generated oscillator signal are called phase noise, which can cause many problems in novel and future communications systems and the corresponding radio devices [2–5]. In the earlier systems and their device implementations, stemming typically from the single carrier modulation principle combined with the use of superheterodyne or direct-conversion radio architectures, phase noise was hardly a problem. Nowadays, however, the effects of phase noise can be much more severe, since the used waveforms are getting more complex (and thus sensitive to any additional distortion), and also because less receiver selectivity is typically implemented at RF, compared to earlier device implementations. Most emerging radio systems are based on multicarrier modulation, mainly orthogonal frequency division multiplexing (OFDM) or some of its variants. OFDM-type waveforms have generally a fair amount of advantages over the more traditional single carrier signals [6], but there is also price to pay since multicarrier systems are found relatively vulnerable to radio component non-idealities, such as phase noise [2]. This is one of the main themes of this article. Phase noise effect on OFDM waveforms, in terms of in-band distortion, is generally twofold [2]. First of all, it causes rotation of symbol constellation called common phase error (CPE). This effect is very similar to the phase noise effect on single carrier systems, and is thus fairly easily canceled. However, the second effect, namely inter-carrier interference (ICI), is the spread of the subcarriers on top of each other. This is a very complex process by nature and its cancelation is not a simple task anymore [7], because the effect is varying from subcarrier to another.

As already mentioned, traditionally superheterodyne and direct-conversion receiver architectures have been widely used in mobile receivers. However, in order to reduce the size, cost, and power consumption of the receiver while increasing flexibility and re-configurability, the so-called direct-RF-sampling

Department of Communications Engineering, Tampere University of Technology, Tampere, Finland.
Corresponding author:
V. Syrjälä
Email: ville.syrjala@tut.fi

(DRFS) receiver principle has received much attention in the research community (see, e.g., [8] and the references therein). In theory, the idea is simply to sample the incoming radio signal as near to the antenna as possible, using bandpass sampling principle [9, 10]. This, however, is not as simple as it sounds, as it causes very tight requirements for the sampling process, especially if the RF filtering is implemented in any realistic manner. Stemming from the high-frequency nature of the incoming signal, with high rate of change on the time axis, one of the biggest obstacles is the needed timing accuracy in the sampling process [11]. In practice, these sampling instants are determined by the sampling clock. As any oscillating type signals, also the clock signals are inherently noisy, thus causing inaccuracies in the sampling instants called sampling jitter [12].

This article focuses on the understanding and DSP-based reduction of phase noise and sampling jitter in OFDM receivers. In the literature, phase noise mitigation in OFDM systems has already been quite widely studied, e.g., in [7, 13–18]. In [7, 13, 14], the current state-of-the-art techniques are proposed, utilizing iterative detection principles. Sampling jitter mitigation, in turn, has also received some attention in the recent literature, e.g., in [19–21]. Especially for DRFS receivers, in [19, 20], the state-of-the-art techniques for sampling jitter cancelation are given for OFDM systems and for general communications systems, respectively. In this article, DSP methods to cancel phase noise-like phenomena in OFDM systems are further developed and studied. General ICI cancelation methods utilizing iterative detection and interpolation at multicarrier symbol boundaries are developed for reducing the phase noise effects in direct-conversion receivers. Also practical aspects, like channel estimation, are addressed. In addition, we show that it is possible to use the developed phase noise mitigation methods also for sampling jitter cancelation in DRFS type receivers, because the phase noise and sampling jitter phenomena are eventually quite similar. This is shown analytically and further verified using simulations. Comprehensive performance simulations are also generally used to assess the performance of the developed methods, using 3GPP-LTE-like system as a practical example.

Layout of the rest of the paper is as follows. Section II gives OFDM system modeling under the influence of phase noise in direct-conversion receivers. In addition, sampling jitter is studied in DRFS receiver and the phase noise-like effect of the sampling jitter is established. In Section III, the used PLL-based oscillator model is shortly described. Then, Section IV introduces the phase noise mitigation techniques with detailed descriptions of the needed signal processing. Section V depicts the simulation environment used to evaluate the performance of the studied techniques, and gives and analyzes the obtained simulation results. The work is concluded in Section VI.

II. PHASE NOISE AND SAMPLING JITTER IN OFDM RECEIVERS

In this section, the system modeling for phase noise in direct-conversion receiver and sampling jitter modeling for DRFS receivers are given.

A) Phase noise in direct-conversion receiver

OFDM symbols that consist of N subcarriers can be constructed using inverse discrete Fourier transform of length N on vector of same length loaded with complex subcarrier symbols. The corresponding time-domain samples of an individual OFDM symbol can thus be formulated as

$$x_m(n) = \frac{1}{\sqrt{N}} \sum_{k=0}^{N-1} X_m(k) e^{j2\pi nk/N}, \tag{1}$$

where $X_m(k)$ denotes the kth subcarrier data symbol in mth OFDM symbol. In practice, OFDM systems usually implement also a so-called cyclic prefix, which is basically copying the last samples of each OFDM symbol before the first samples. The resulting OFDM symbol is then transmitted using I/Q modulation at desired center frequency. On the receiver side, after traveling through the noisy multipath channel, the signal is I/Q downconverted, filtered, and sampled. Assuming the phase noise process of the downconverting oscillator is denoted by $\phi(t)$, and that the cyclic prefix is longer than the channel delay spread, the received samples corresponding to (1), written in vector form, are given by

$$\mathbf{y}_m = \mathrm{diag}(e^{j\boldsymbol{\Phi}_m})(\mathbf{h}_m \otimes \mathbf{x}_m) + \mathbf{n}_m. \tag{2}$$

Here, $\otimes$ is a circular convolution operator, $\mathbf{x}_m$ is the vector of samples of mth transmitted OFDM symbol in (1), $\mathbf{h}_m$ is the channel impulse response vector, and $\mathbf{n}_m$ is additive white Gaussian noise (AWGN) vector, all at mth OFDM symbol duration. In addition, ϕ_m contains the samples of the phase noise realization within mth OFDM symbol, so $\phi_m = [\phi_m(0), \ldots, \phi_m(N-1)]^{\mathrm{T}}$.

After reception of the signal, OFDM-demodulation is done by using discrete Fourier transform giving frequency domain version of (2) as

$$\begin{aligned} \mathbf{Y}_m &= \mathbf{J}_m^{pn} \otimes (\mathbf{H}_m \bullet \mathbf{X}_m) + \boldsymbol{\eta}_m \\ &= \mathbf{J}_m^{pn} \otimes \mathbf{S}_m + \boldsymbol{\eta}_m, \end{aligned} \tag{3}$$

where $\bullet$ is an element-wise multiplication operator, $\mathbf{X}_m$ is the vector of transmitted subcarrier symbols, $\mathbf{H}_m$ is the channel transfer function, η_m is the discrete Fourier transform (DFT) of AWGN, $\mathbf{S}_m = \mathbf{H}_m \bullet \mathbf{X}_m$, and finally $\mathbf{J}_m^{pn}$ is the DFT of the phase noise exponential $\exp(j\phi_m)$, again all at mth OFDM symbol duration. This vector $\mathbf{J}_m^{pn}$ is referred to as the ICI profile in the following, and its elements can also be written explicitly as

$$J_m^{pn}(k) = \frac{1}{\sqrt{N}} \sum_{n=0}^{N-1} e^{j\phi_m(n)} e^{-j2\pi nk/N}. \tag{4}$$

As mentioned previously, phase noise impact on OFDM system can be divided into two fundamentally different effects, CPE and ICI. These effects can now be quantified by writing the observation at subcarrier k (i.e., kth element of vector $\mathbf{Y}_m$ given in (3)) as

$$\begin{aligned} Y_m(k) = {} & J_m^{pn}(0) H_m(k) X_m(k) \\ & + \sum_{l=0, l\neq k}^{N-1} H_m(l) X_m(l) J_m^{pn}(k-l) + \eta_m(k). \end{aligned} \tag{5}$$

In (5), the received subcarrier signal is divided into two parts, in first of which $J_m^{pn}(0)$ multiplies the interesting signal

(transmit symbol after channel response). This multiplication is the already mentioned CPE effect of the phase noise. The ICI effect of phase noise, in which the OFDM subcarriers are spread over top of each other, is seen as the second term on the right-hand side of (5).

B) Sampling jitter in direct-RF-sampling receiver

Since in the DRFS receiver, the sampling takes place already at high frequencies, also the modeling needs to reflect the bandpass nature of the actual RF signals. For generality, let us consider a general I/Q modulated bandpass waveform of the form

$$r(t) = s_I(t)\cos(2\pi f_c t) - s_Q(t)\sin(2\pi f_c t). \tag{6}$$

Here $s_I(t)$ and $s_Q(t)$ denote the I- and Q-components of the received signal, respectively, and f_c is the corresponding formal center frequency. Notice that the exact structure of the I- and Q-components depend on the assumed RF filtering, i.e., they can model either a single communication waveform (desired signal) or more generally contain also the neighboring channels. Now, if sampling is directly applied to the above general bandpass signal with a jittered sampling clock, the corresponding jittered samples read

$$\begin{aligned} r_n &= r(nT_s + \zeta_n) \\ &= s_I(nT_s + \zeta_n)\cos[2\pi f_c(nT_s + \zeta_n)] \\ &\quad - s_Q(nT_s + \zeta_n)\sin\big[2\pi f_c(nT_s + \zeta_n)\big]. \end{aligned} \tag{7}$$

Here the jittered sample instants are denoted by $t_n = nT_s + \zeta_n$, where ζ_n models the uncertainty of the nth sample instant and T_s is the nominal sampling interval. In this presentation, it is obvious that the jitter implicitly affects both the samples of low-frequency useful signal components (s_I and s_Q), and the high-frequency carrier components (sine and cosine waves). In any realistic received signal scenario, however, the frequency range of the carrier components is in the order of 100–1000 times higher compared to the modulating I and Q components. This means that the sampling jitter has much more significant effect on the carrier components of the signal than on the useful (modulating) part of the signal. Thus for any realistic jitter level, we can basically approximate (7) by

$$\begin{aligned} r_n &= r(nT_s + \zeta_n) \\ &\approx s_I(nT_s)\cos\big[2\pi f_c(nT_s + \zeta_n)\big] \\ &\quad - s_Q(nT_s)\sin\big[2\pi f_c(nT_s + \zeta_n)\big]. \end{aligned} \tag{8}$$

Note that because an arbitrary bandpass signal was assumed in the above derivations, the result in (8) can be deployed in modeling sampling jitter in any realistic bandpass system, independently of the exact communication waveforms used.

Next, we deploy the basic modeling result in (8) and develop it further for DRFS receiver purposes by assuming that the sub-sampling principle [10] is utilized in the receiver implementation. In effect, this means that aliasing is used in a controlled manner to downconvert the received signal to lower frequencies within the sampling process. In such case, $F_s = 1/T_s << f_c$ and (8) can be rewritten as

$$\begin{aligned} r_n &\approx s_I(nT_s)\cos[2\pi f_{IF} nT_s + 2\pi f_c\zeta_n] \\ &\quad - s_Q(nT_s)\sin[2\pi f_{IF} nT_s + 2\pi f_c\zeta_n] \\ &= \mathrm{Re}\{[s_I(nT_s) + js_Q(nT_s)]e^{j2\pi f_{IF} nT_s}e^{j2\pi f_c\zeta_n}\}. \end{aligned} \tag{9}$$

Here, f_{IF} denotes the new aliased center frequency due to sub-sampling. Now, because we are already in digital domain, we can use complex digital mixing from IF to baseband, followed by lowpass filtering, which essentially yields

$$\begin{aligned} y_n &\approx [s_I(nT_s) + js_Q(nT_s)]e^{j2\pi f_c\zeta_n} \\ &= s_n e^{j2\pi f_c\zeta_n} \\ &= s_n e^{j\theta_n}, \end{aligned} \tag{10}$$

where $s_n = s_I(nT_s) + js_Q(nT_s)$ and $\theta_n = 2\pi f_c\zeta_n$. This basically means that we can approximate the sampling jitter effect in DRFS receiver for general bandpass signal just as a multiplication by a complex exponential, just like the phase noise is modeled in general. Here, instead of the phase noise term ϕ induced by the downconversion stage in the earlier direct-conversion receiver case, we simply have a sampling jitter-dependent phase noise term $\theta_n = 2\pi f_c\zeta_n$ as the argument of the multiplying complex exponential. Thus based on the earlier developments in Section II.A, if OFDM waveforms are again assumed, sampling jitter in DRFS receiver will essentially again result in CPE and ICI-type distortions. Thus using similar notations as in Section II.A, the subcarrier observations at mth OFDM symbol duration can be written as

$$\begin{aligned} \mathbf{Y}_m &= \mathbf{J}_m^{jit} \otimes (\mathbf{H}_m \bullet \mathbf{X}_m) + \boldsymbol{\eta}_m \\ &= \mathbf{J}_m^{jit} \otimes \mathbf{S}_m + \boldsymbol{\eta}_m. \end{aligned} \tag{11}$$

Here $\mathbf{J}_m^{jit}$ denotes the DFT of the jitter-induced phase noise exponential within the mth OFDM symbol duration. This observation will be utilized in the actual ICI mitigation developments in Section IV.

III. OSCILLATOR MODELING

In this section, the used oscillator phase noise modeling is shortly addressed. In general, phase noise modeling stems from physical circuit-level analysis or empirical studies. One of the most simple models widely applied in the literature is the so-called free-running oscillator (FRO) model where the oscillator excess phase (phase noise) is assumed to follow the Brownian motion (Wiener process). This basically means that the phase error process is changing from sample to sample by an amount dictated by some variance parameter which, in turn, depends on the 3 dB bandwidth of the oscillator [3]. Effectively, the sampled phase noise process can thus be modeled as a cumulative sum of Gaussian distributed white noise variables whose variance is given by the quality of the oscillator. In this paper, however, more realistic phase-locked-loop (PLL)-based oscillators are considered to emphasize practicality. For simplicity, the same PLL model is used as a basis for both downconversion phase noise, in case of direct-conversion RX,

and sampling clock jitter, in case of DRFS receiver. In the modeling of the sampling jitter, the phase noise realization is normalized to have currently interesting jitter root-mean-square (RMS) value.

The exact PLL modeling in this paper is based on the one developed by the authors in [22]. In [22] the formulae for deriving the overall oscillator spectrum are derived and explained in detail, and are thus ignored here for simplicity. In the model, oscillator properties can be tuned through inputting phase noise spot measurement values of voltage-controlled and reference oscillators (VCO and RO) used inside the PLL. These spot measurement values characterize the phase noise power-spectral density of the VCO and RO used in the corresponding PLL implementation.

The deployed PLL model derives the actual phase noise samples (elements of vector ϕ_m) in three steps: (i) complex Gaussian white noise is generated and Fourier transformed to frequency domain, (ii) frequency-domain noise is shaped by the phase noise mask derived according to the derived specifications in [22], and (iii) the shaped frequency domain noise is transferred back to time domain using inverse Fourier transform giving the phase noise vector ϕ_m. The actual phase noise mask of the PLL-based oscillator used in this paper is depicted in Fig. 1. The same phase noise model was also used in [13]. The exact spot measurement values used are as follows. For VCO, $1/f$-noise-dominated region measurement at 30 kHz offset from the oscillation frequency is -75 dBc/Hz and the thermal-noise-dominated region measurement at 1 MHz offset is -110 dBc/Hz. For reference oscillator, we assume that no meaningful flicker noise is present and that the thermal-noise region measurement at 100 Hz offset is -90 dBc/Hz. Note that these used PLL specs are of course simply one specific example but anyway represent realistic and practical PLL design.

IV. PHASE NOISE AND SAMPLING JITTER MITIGATION

In this section, the actual digital mitigation techniques to reduce the effects of phase noise and sampling jitter are developed, stemming from the previous receiver modeling in Section II. Here we mostly focus on the ICI cancelation because the CPE part is fairly well managed in the literature. These CPE mitigation techniques typically assume ICI to be just additional noise and, e.g., least-squares (or zero forcing) principle is used to estimate the CPE [17] using pilots. CPE mitigation is then done just by inverse rotation of the constellation.

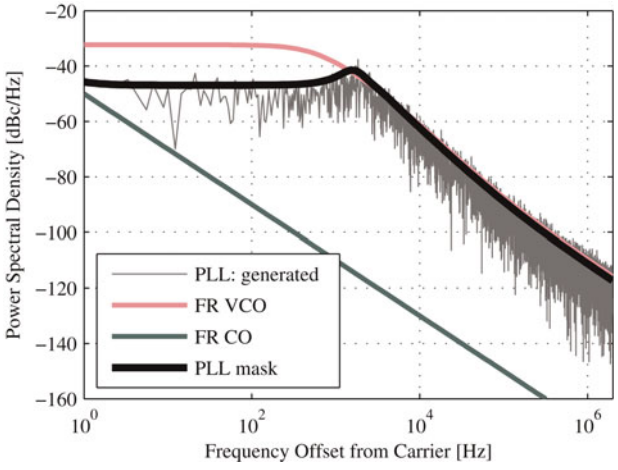

Fig. 1. Example phase noise mask and its underlying components depicted with actual generated PLL-oscillator spectrum centered at 2 GHz.

In the following, we focus on the ICI estimation and cancelation. Notice that given the ICI profile ($\mathbf{J}_m$), the actual mitigation can be done by deploying circular deconvolution between the estimated ICI profile and the observed subcarrier samples $\mathbf{Y}_m$, as (3) and (11) imply. This results in the estimate of $\mathbf{S}_m = \mathbf{H}_m \cdot \mathbf{X}_m$, and can be written as

$$\hat{\mathbf{S}}_m = (\mathbf{P}\hat{\mathbf{J}}_m^*) \otimes \mathbf{Y}_m, \tag{12}$$

where $\hat{\mathbf{J}}_m$ denotes the ICI profile estimate, $\mathbf{P}$ is a permutation matrix that reverses the order of elements in the vector that it multiplies, and $(\cdot)^*$ denotes complex conjugation. Note that due to the structural similarity of the effect of phase noise and sampling jitter in direct-conversion and DRFS receivers, respectively, we do not differentiate those two in the mitigation processing descriptions below, but simply refer to both of them as phase noise. Also the simplified notation $\mathbf{J}_m$ is used for the ICI profile, instead of $\mathbf{J}_m^{pn}$ and $\mathbf{J}_m^{jit}$. In below, we first describe in Section IV.A state-of-the-art reference technique developed in [7]. Then the proposed technique is introduced in Section IV.B, discussed by the authors preliminary in [13]. Section IV.C then discusses the practical channel estimation aspects for the proposed technique.

A) ICI estimation technique of Petrovic *et al.*

To our knowledge, the best available technique for ICI estimation in the literature is the method proposed in [7] by Petrovic *et al.*, to which in this paper we simply refer as Petrovic's technique. In this approach, the idea is to estimate the most dominant frequency bins of the ICI profile. This is motivated by the typically observed steep slopes of the oscillator spectrum around the nominal oscillating frequency. This reduces the computational complexity of the estimation task in a considerable manner, yet not compromising the performance, compared to trying to estimate all the components of the ICI profile. The actual estimation is done by using initial subcarrier symbol decisions (with CPE mitigation only) as reference. To be more specific, given that we want to estimate the center frequency bin of $\mathbf{J}_m$ along with the u adjacent frequency bins on both sides, the system model given in (3) can be first reformulated into form

$$\begin{bmatrix} Y_m(l_1) \\ \vdots \\ Y_m(l_P) \end{bmatrix} = \begin{bmatrix} S_m(l_1+u) & \cdots & S_m(l_1-u) \\ \vdots & \ddots & \vdots \\ S_m(l_P+u) & \cdots & S_m(l_P-u) \end{bmatrix} \times \begin{bmatrix} J_m(-u) \\ \vdots \\ J_m(u) \end{bmatrix} + \begin{bmatrix} \eta_m(l_1) \\ \vdots \\ \eta_m(l_P) \end{bmatrix} \tag{13}$$

$$\Leftrightarrow$$

$$\mathbf{Y}_{m,p} = \mathbf{M}_{m,u}\mathbf{J}_{m,u} + \boldsymbol{\eta}_{m,p},$$

where $l_1, \ldots, l_P$ refer to used subcarriers in the estimation task. This model is obtained by simply picking the $l_1, \ldots, l_P$ rows from the model in (3) and writing the truncated circular

convolution as a matrix–vector product. Now, the elements $S_m(l) = H_m(l)X_m(k)$ of the matrix $\mathbf{M}_{m,u}$ above are first obtained using initial data detection (after CPE mitigation) combined with channel state information. Then, the ICI profile is estimated using, e.g., least-squares technique as

$$\hat{\mathbf{J}}_{m,u} = \left(\mathbf{M}_{m,u}^H \mathbf{M}_{m,u}\right)^{-1} \mathbf{M}_{m,u}^H \mathbf{Y}_{m,p}. \quad (14)$$

Then we do the ICI mitigation, as given in (12), detect the data again and input the resulting detected subcarrier symbols to the ICI estimation algorithm again. This iterative estimation-mitigation technique is then run for a few iterations until no clear improvements in detection results are achieved. For more detailed information, refer to [7].

By the same research group, a way to further improve the above Petrovic's technique was proposed in [14] by Bittner *et al.* In [14], it was noted that the estimation method of [7] gives very poor phase noise estimation performance near the boundaries of OFDM symbols due to the truncated Fourier series approach used. This is why they introduced a technique to "shift" the phase noise effects so that the reliability of the tail parts of the estimates can be improved. For more details on this technique refer to [14]. This improved technique will be used as the main reference in performance evaluations in Section V.

B) Proposed linear interpolation – tail estimation (LI-TE) ICI-estimation technique

Also in [13], the poor estimation performance in the tail parts of the phase noise estimates given by the Petrovic's technique was noticed. In addition, it was noted that the continuous nature of the phase error in time domain can be exploited in the phase noise estimation process quite efficiently. This results in the so-called LI-TE technique which is described in details in the following.

The proposed LI-TE estimation technique builds on the earlier iterative ICI profile estimation scheme and improves the estimation performance of individual iterations by using interpolation over the phase noise estimates at OFDM symbol boundaries in which the initial phase noise estimates are poor. The whole procedure including the initial ICI detection done by Petrovic's technique is depicted in Tables 1 and 2 for the case of two iterations. Thus if the phase noise mitigation is started at the mth OFDM symbol, the initialization of the algorithm described in Table 1 is first deployed, and is then followed by the actual mitigation loop given in Table 2. For simplicity, the formulation is here given for two iterations but it is trivial to extend the algorithms to more than two iterations. Stemming from the interpolation principle, it should

Table 1. ICI estimation algorithm (LI-TE) – initialization.

Step	Action
1	CPE estimation and mitigation, and symbol detection for OFDM symbols m and $m+1$*
2	ICI estimation (14) for OFDM symbols m and $m+1$
3	Linear interpolation at symbol boundary between OFDM symbols m and $m+1$ (LI-TE)
4	Remove estimated phase noise and detect the OFDM symbol m

*Indicates the step where channel estimation is needed.

Table 2. ICI estimation algorithm (LI-TE) – mitigation loop.

Step	Action
1	CPE estimation and mitigation, and symbol detection for OFDM symbol $m+2$*
2	ICI estimation (14) for OFDM symbol $m+2$
3	Linear interpolation at symbol boundary between OFDM symbols $m+1$ and $m+2$ (LI-TE)
4	Remove estimated phase noise and detect the OFDM symbol $m+1$
5	ICI estimation (14) for OFDM symbols m and $m+1$
6	Linear interpolation at symbol boundary between OFDM symbols m and $m+1$ (LI-TE)
7	Remove estimated phase noise and detect the OFDM symbol m
8	Set $m = m+1$ and move to step 1

be acknowledged that the overall estimation–cancelation processing is subject to delay in the final detection. With two iterations, the delay is also two OFDM symbols. In general, adding one further iteration increases also the delay by one symbol.

Next, we consider the implementation of the interpolation stage. First let the interpolation window length for both sides of each OFDM symbol be denoted by L (samples). Then in the individual interpolation stage, the estimated ICI profile is transferred back to time-domain phase noise vector ϕ_m with simple IFFT and taking the angle of the complex exponential as

$$\hat{\boldsymbol{\phi}}_m = \arg\left\{\mathrm{IFFT}\left[\hat{\mathbf{J}}_{m,u}\right]\right\}. \quad (15)$$

Then, assuming that simple linear interpolation is used, the processing of the phase noise estimates at the boundary between OFDM symbols m and $m+1$ can be mathematically formulated as

$$\begin{aligned}\tilde{\boldsymbol{\phi}}_m(N-L+n) &= \hat{\boldsymbol{\phi}}_m(N-L) \\ &\quad + n\frac{\hat{\boldsymbol{\phi}}_{m+1}(L) - \hat{\boldsymbol{\phi}}_m(N-L)}{2L}, \\ \tilde{\boldsymbol{\phi}}_{m+1}(n) &= \hat{\boldsymbol{\phi}}_m(N-L) \\ &\quad + (L+n)\frac{\hat{\boldsymbol{\phi}}_{m+1}(L) - \hat{\boldsymbol{\phi}}_m(N-L)}{2L},\end{aligned} \quad (16)$$

where $\hat{\boldsymbol{\phi}}_m(n)$ refers to the nth sample of the initially estimated phase noise, at OFDM symbol m, whereas $\tilde{\boldsymbol{\phi}}_m(n)$ refers to the corresponding interpolated quantity. Note that the original time domain received signal contains also the cyclic prefix in the boundary area, but the cyclic prefix length is typically relatively small compared to the OFDM symbol length and phase error dynamics. This basically means that we can still consider the phase noise a continuous process, and thus interpolation over the badly estimated boundary regions will indeed improve the performance, as will be demonstrated below and in more details in Section V.

An example estimation result obtained with the proposed technique is depicted in Fig. 2. As demonstrated in Fig. 2, the use of interpolation does indeed greatly improve the quality of the phase noise estimates near OFDM symbol

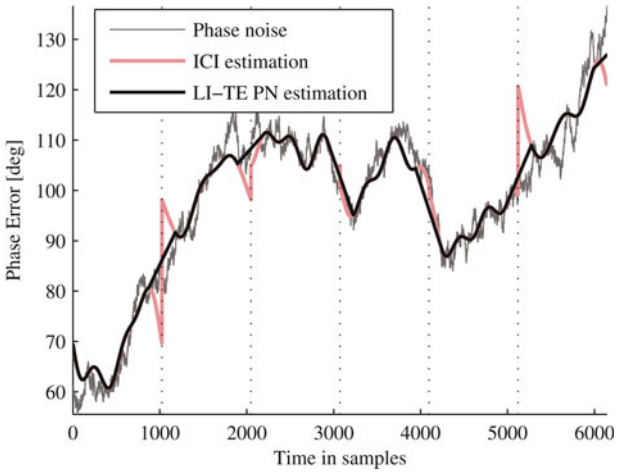

Fig. 2. LI-TE ICI-estimation technique interpolates over the peaking phase noise estimates of Petrovic's technique near the OFDM symbol boundaries. FRO is used with 100 Hz 3 dB bandwidth as an example. Estimation is done under 18 dB received signal conditions.

boundaries. Petrovic's basic ICI estimation technique causes bad peaking of the estimates near the boundaries, which is nicely smoothened by the interpolation stage. More detailed and quantitative performance assessments will be carried out in Section V.

C) Channel estimation aspects

If we do not have channel knowledge in the receiver by default, as is usually the case, we must also consider the channel estimation task in practice. In the iterative ICI estimation setup, already the initial detection needs (estimated) channel knowledge of some kind. Also when building and solving the linear model in (13) and (14), channel knowledge is required in constructing the matrix $\mathbf{M}_{m,u}$. Typically, pilot subcarriers are deployed for channel estimation in practical multicarrier systems. This is also assumed to be the case in the following.

One specific issue, due to the interpolation approach in ICI cancelation, is that the proposed LI-TE technique requires that the effective phase noise process is continuous at symbol boundaries. Now if the combined effect of CPE and multipath channel is estimated and equalized using pilot subcarriers, independently from one multicarrier symbol to another, this is actually not the case because the CPE can easily vary from multicarrier symbol to another. Thus, after equalizing the joint effect of channel and CPE, the continuous nature of the phase noise in the overall system is essentially lost.

However, the effect of CPE can actually be separated from the channel if a quasi-static channel is assumed. In such cases, the channel is assumed changing very slowly being thus virtually static for a period of say K OFDM symbols. This can then be exploited in channel estimation, when we want to recover (separate) the CPE information from the actual radio channel. In the channel estimation stage, pilot subcarriers are first used to estimate the combined response. For example, the zero forcing principle can be used, written as

$$\hat{\mathbf{H}}_{m,pilots} = \mathbf{Y}_{m,pilots} \bullet / \mathbf{P}_m, \tag{17}$$

where $\bullet/$ is point-by-point division operator, $\mathbf{P}_m$ is vector of pilot subcarriers in mth OFDM symbol, and *pilots* sub-index refers to subcarrier symbol indices that carry the pilot data. Now if we assume a quasi-static system, this and the channel estimates for the $K-1$ OFDM symbols around the current symbol should be the same if there were no CPE in the system. So we can now easily estimate the relative CPEs (relative to one of the multicarrier symbols, say mth) by simply dividing the corresponding channel estimates by the channel estimate of the reference symbol, meaning

$$\hat{\mathbf{J}}^{\circ}_{l,rel} = \hat{\mathbf{H}}_{l,pilots} \bullet / \hat{\mathbf{H}}_{m,pilots}. \tag{18}$$

Now, for each of the OFDM symbols within the processing window of K symbols, we have multiple relative CPE estimates in the vectors $\hat{\mathbf{J}}^{\circ}_{l,rel}$. By recognizing that CPE is, by definition, identical for all the subcarriers within single OFDM symbol, we can filter these multiple estimates to a more reliable estimate by, e.g., taking the mean value as

$$\hat{J}_{l,rel}(0) = \overline{\hat{\mathbf{J}}^{\circ}_{l,rel}}. \tag{19}$$

In above, $\overline{\mathbf{x}}$ refers to sample mean of the elements of $\mathbf{x}$. The CPE can then be separated from the estimated channel by dividing the channel estimate vectors for each OFDM symbol by the corresponding CPE estimate in (19). Now, also the quasi-static assumption can be further deployed in actual channel estimation, because the remaining channel estimates do not have CPE (and should thus be constant at any given subcarrier from multicarrier symbol to another). Improved channel estimates can thus be achieved, e.g., simply by taking the mean of the channel estimates over the processing window. Finally, the channel estimates for active subcarriers are obtained using interpolation as in any typical multicarrier receiver. Note that length of the above processing window K is in practice limited by the assumed mobility of the receiver.

In the overall phase noise mitigation setup described in Tables 1 and 2, the channel estimation and the corresponding CPE recovery are carried out in steps marked with (*), namely before CPE is estimated and mitigated.

V. SIMULATION ENVIRONMENT AND OBTAINED RESULTS

In this section, the performances of the previously described phase noise mitigation techniques are studied, for both the case of phase noise mitigation in traditional direct-conversion receiver and the case of sampling jitter mitigation in DRFS receiver. Also the effects of channel estimation procedure are addressed.

A) Simulation parameters

In the simulations, 3GPP-LTE downlink-like [23] system is assumed for practicality, utilizing OFDM with 1024 subcarriers and 15 kHz subcarrier spacing, combined with cyclic prefix of length 63 samples. Of the 1024 subcarriers, 600 are active, 300 on the both sides of the zero-subcarrier. All the other subcarriers are empty (zeroed). 16QAM subcarrier modulation is assumed here for active subcarriers. Concerning the pilot allocation, 18 of the active subcarriers carry pilot data in the basic simulations where perfect

channel knowledge is first assumed. Then, in the simulations where also the channel response is estimated (in addition to ICI profile), every ninth subcarrier carries the pilot data to facilitate reasonable estimation performance.

The simulations are carried out as follows. First, 16QAM subcarrier data are generated and OFDM modulated, and the resulting OFDM signal is sent to the channel. Channel is either AWGN channel or extended ITU-R Vehicular A multipath [24] channel. The channel response is assumed constant for single simulation realization which always contains a packet of 12 OFDM symbols. In a new realization, also new channel response is drawn, and altogether a minimum of 5000 independent channel realizations are always simulated for a given SNR or jitter RMS point. After the channel, receiver phase noise or sampling jitter is applied, according to which case we study. The phase noise and sampling jitter are based on PLL-oscillator phase noise model discussed in Section III. After the impairment has been applied, impairment mitigation and detection are carried out, as explained in Section IV.

In all the iterative techniques, only two iterations are used for implementation simplicity. In ICI estimation, three frequency bins of the ICI profile on both sides of the DC-bin are estimated. For Bittner's technique, shifting window length is 70 samples of length and for LI-TE the interpolation window length L is 155 samples. The window lengths were chosen based on comparative performance simulations.

B) Phase noise mitigation performance in direct-conversion receiver case

In Figs 3 and 4, the performances of the presented mitigation techniques in phase noise corrupted OFDM direct-conversion receiver are given. Figure 3 depicts the performance in AWGN channel case. As can be seen, the ICI estimation techniques offer huge performance increase compared to if only CPE is mitigated. Furthermore, the LI-TE technique improves the performance quite noticeably over the Petrovic's and Bittner's techniques. From Fig. 4 one can see that as the channel gets more demanding, the overall system performance decreases heavily. This pushes the relative performance differences between the mitigation techniques close to each other, but at the same time, the mitigation curves are pushed closer and closer to the ideal performance curve. This happens naturally because the phase noise contribution to the system performance is a little smaller whereas the contribution of the channel gets more dominating. With more demanding oscillator models, the differences would naturally be higher.

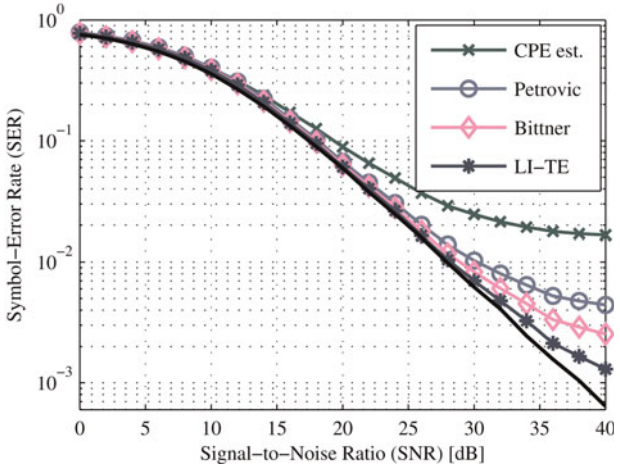

Fig. 4. SER given as a function of SNR with PLL-based oscillator phase noise in extended ITU-R Vehicular A multipath channel.

Overall, the phase noise mitigation techniques work very well in the application they are intended for. The performances of all the ICI cancelation techniques are quite impressive, but the proposed LI-TE method is still showing clearly the best performance.

C) Sampling jitter mitigation performance in direct-RF-sampling receiver case

In Figs 5 and 6, the performances of phase noise mitigation techniques are depicted for sampling jitter mitigation in DRFS receiver with communications over AWGN channel. In the first study, the RMS jitter is fixed to 20 ps, and as shown in Fig. 5, all the mitigation techniques give very nice performance. While LI-TE gives a little better performance than the other techniques, all the ICI mitigation techniques

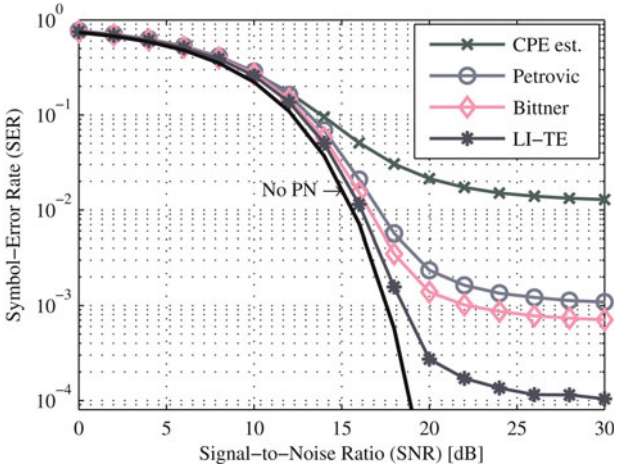

Fig. 3. SER given as a function of SNR with PLL-based oscillator phase noise in AWGN channel conditions.

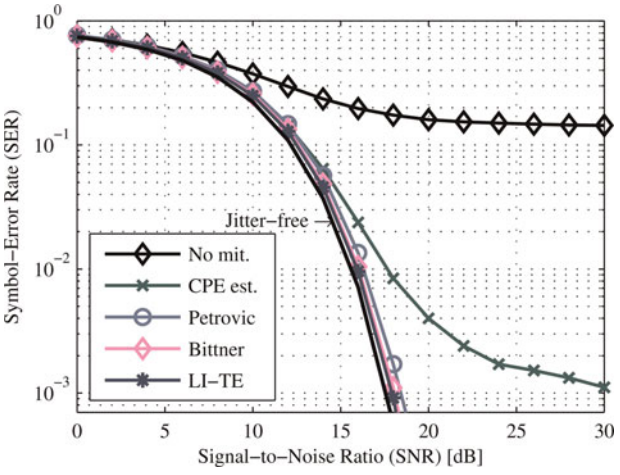

Fig. 5. SER given as a function of SNR with PLL-oscillator shaped sampling jitter fixed at 20 ps RMS. AWGN channel is used.

give almost ideal performance. Next the studied RMS jitter range is widened up to 50 ps. Then, as Fig. 6 indicates, only LI-TE technique gives good performance over the whole studied region while the performance of other methods start to deteriorate fast when the RMS jitter is increased. Notice also that with RMS jitter values less than 15 ps, all the ICI mitigation techniques give almost the same performance and the performances of the techniques are pretty close to the no phase noise case.

From Figs 7 and 8 we can draw similar conclusions for the case with extended ITU-R Vehicular A multipath channel, as we did in the AWGN case. The total system performance is lowered quite noticeably, but the relative differences between the mitigation techniques stay unchanged. It is noticeable though that in AWGN case the SER got so low that the high-SNR region was not visible for the ICI mitigation techniques in the figures. However, with more challenging channel conditions, one can see that differences between the techniques start to get bigger and bigger as the SNR rises. In addition one can see that as the SNR gets very high, the performances of the mitigation techniques start to stabilize to some flooring levels, as was also observed in the earlier phase noise mitigation studies. However, this does not happen with practical SNR values from mobile communications point of view, at least for extended Vehicular A multipath channel.

D) Phase noise mitigation performance in direct-conversion receiver without perfect channel knowledge

Finally, we study the mitigation performance in cases where no prior knowledge of the channel state (response) is available, which is usually the case in practice. For simplicity, we focus on the direct-conversion receiver case. Figure 9 demonstrates the obtained performances under ITU-R Vehicular A multipath channel with two different channel estimation ideologies. The first one is conventional one-shot estimation using pilot subcarriers, which is carried out separately for each multicarrier symbol and interpolated inside each multicarrier symbol for the responses at active data carriers. This obviously suffers from the ICI due to phase noise. The second scheme is the one described in Section IV.C where the assumed quasi-static nature of the channel response is taken advantage of. As Fig. 9 shows, the more advanced channel estimation scheme gives very good performance boost over the conventional channel estimations case with all the simulated techniques. With conventional channel estimation, the LI-TE technique does not work as planned because the technique needs the phase noise to act as a continuous process over the period longer than on OFDM symbol, as was discussed earlier. When the proposed channel estimation is applied, the LI-TE technique outperforms the Bittner's and Petrovic's techniques. In general, the performances stay somewhat behind the case with perfect channel knowledge which is unavoidable with any reasonable channel estimation scheme.

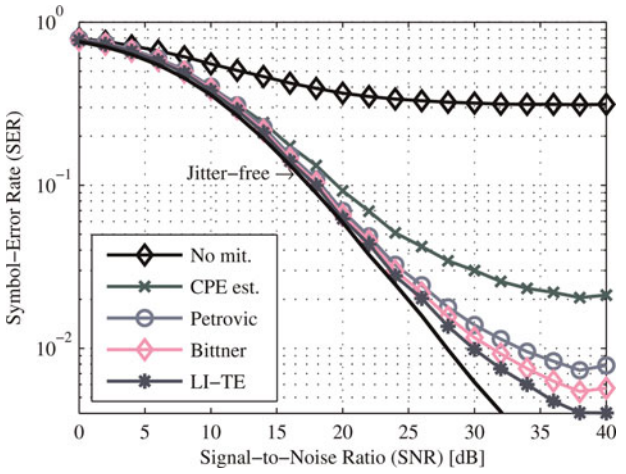

Fig. 7. SER given as a function of SNR with PLL-oscillator shaped sampling jitter fixed at 20 ps RMS. Extended ITU-R Vehicular A multipath channel is used.

VI. CONCLUSIONS

Oscillator impairments such as phase noise and sampling jitter can easily degrade the performance of OFDM system in a considerable manner. In this paper, we presented state-of-the-art mitigation techniques for reducing the effects of oscillator impairments on the receiver side. Two

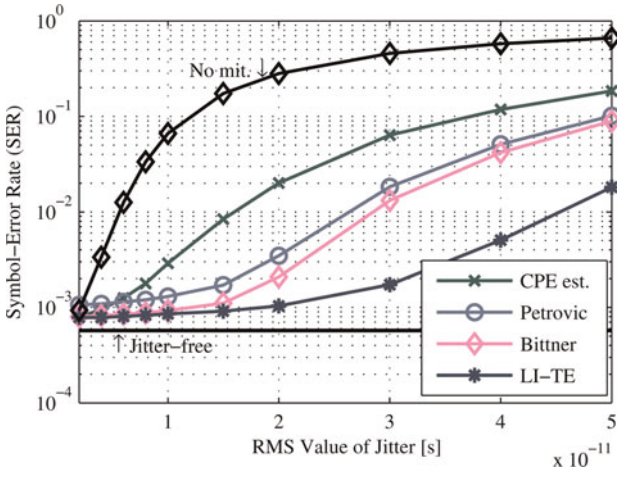

Fig. 6. SER given as a function of RMS jitter. Jitter is shaped by PLL-oscillator. AWGN channel conditions are used with fixed received SNR of 18 dB.

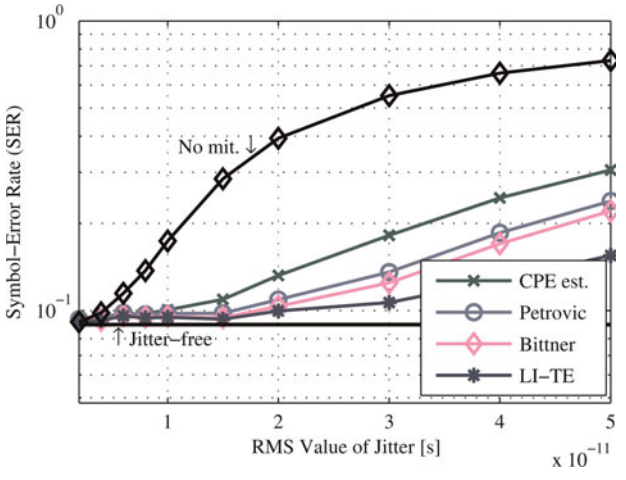

Fig. 8. SER given as a function of RMS jitter. Jitter is shaped by PLL-oscillator. Extended ITU-R Vehicular A multipath channel conditions are used with fixed received SNR of 18 dB.

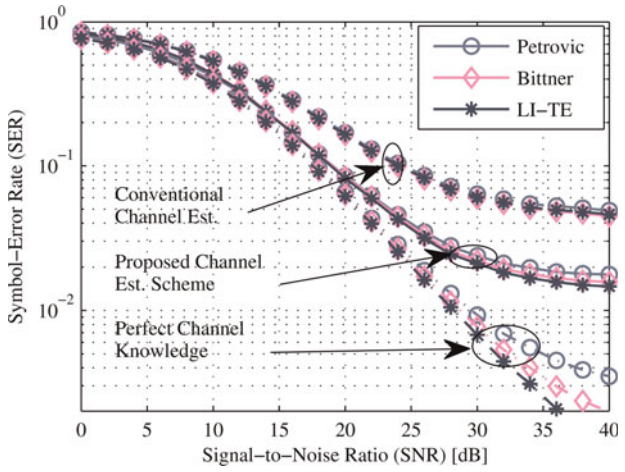

Fig. 9. SER given as a function of SNR with PLL-based oscillator phase noise in extended ITU-R Vehicular A multipath channel. Different levels of prior channel information are studied.

receiver topologies, namely the direct-conversion receiver architecture as well as the DRFS receiver architecture, were considered in more details and analyzed from the phase noise and sampling jitter points of view. Stemming from the modeling, the waveform distortion in both receiver architectures results in certain cross-talk between the OFDM subcarriers. Then generic cross-talk cancelation techniques were presented for mitigation of both sampling jitter as well as phase noise in the considered receiver architectures. It was further demonstrated with the help of simulations that the considered mitigation techniques perform very well under practical phase noise and sampling jitter conditions. Also the channel state information and estimation aspects were addressed. Overall, with practical PLL-based oscillators and practical RMS jitter values, the proposed LI-TE ICI estimation cancelation technique was shown to perform best reducing the signal distortion due to considered oscillator nonidealities in a considerable manner.

ACKNOWLEDGEMENTS

This work was supported by the Finnish Funding Agency for Technology and Innovation (Tekes), the Academy of Finland, the Technology Industries of Finland Centennial Foundation and TUT Graduate School, HPY Research Foundation.

REFERENCES

[1] Fettweis, G.: Dirty RF: A new paradigm, in Proc. 16th Int. Symp. on Personal, Indoor and Mobile Radio Communications 2005, vol. **4**, September 2005, 2347–2355.

[2] Robertson, P. and Kaiser, S.: Analysis of the effects of phase-noise in orthogonal frequency division multiplex (OFDM) systems, in Proc. IEEE Int. Conf. on Communications, vol. **3**, June 1995, 1652–1657.

[3] Schenk, T.: RF Impairments in Multiple Antenna OFDM: Influence and Mitigation, Ph.D. Dissertation, Technische Universiteit Eindhoven, 2006, ISBN 90–386-1913-8, 291pp.

[4] Armada, A.; Calvo, M.: Phase noise and sub-carrier spacing effects on the performance of an OFDM communication system. IEEE Commun. Lett., **2** (1) (1998), 11–13.

[5] Tomba, L.: On the effect of Wiener phase noise in OFDM systems. IEEE Trans. Commun., **46** (5) (1998), 580–583.

[6] Bingham, J.A.C.: Multicarrier modulation for data transmission: an idea whose time has come. IEEE Commun. Mag., **28** (5) (1990), 5–14.

[7] Petrovic, D.; Rave, W.; Fettweis, G.: Effects of phase noise on OFDM systems with and without PLL: characterization and compensation. IEEE Trans. Commun., **55** (8) (2007), 1607–1616.

[8] Razavi, B.: RF Microelectronics, Prentice Hall PTR, Upper Saddle River, NJ, USA, 1998, 335pp.

[9] Frerking, M.E.: Digital Signal Processing in Communication Systems, International Thomson Publishing Services, 1994, 644pp.

[10] Vaughan, R.G.; Scott, N.L.; White, D.R.: The theory of bandpass sampling. IEEE Trans. Signal Process., **39** (1991), 1973–1984.

[11] Amin, B.; Dempster, A.G.: Sampling and jitter considerations for GNSS software receivers, in Proc. IGNSS Symp. 2006, July 2006, 15pp.

[12] Shinagawa, M.; Akazawa, Y.; Wakimoto, T.: Jitter analysis of high-speed sampling systems. IEEE J. Solid State Circuits, **25** (1) (1990), 220–224.

[13] Syrjälä, V.; Valkama, M.; Tchamov, N.N.; Rinne, J.: Phase noise modelling and mitigation techniques in OFDM communications systems, in Proc. Wireless Telecommunications Symp. 2008, Prague, Czech Republic, April 2009.

[14] Bittner, S.; Zimmermann, E.; Fettweis, G.: Exploiting phase noise properties in the design of MIMO-OFDM receivers, in Proc. IEEE Wireless Communications and Networking Conf. 2008, Las Vegas, NV, March 2008, 940–945.

[15] Bittner, S.; Rave, W.; Fettweis, G.: Joint iterative transmitter and receiver phase noise correction using soft information, in Proc. IEEE Int. Conf. on Communications 2007, June 2007, 2847–2852.

[16] Zou, Q.; Tarighat, A.; Sayed, A.H.: Compensation of phase noise in OFDM wireless systems. IEEE Transactions on Signal Processing, **55** (11) (2007), 5407–5424.

[17] Wu, S.; Bar-Ness, Y.: A phase noise suppression algorithm for OFDM-based WLANs. IEEE Commun. Lett., **6** (12) (2002), 535–537.

[18] Wu, S.; Bar-Ness, Y.: OFDM systems in the presence of phase noise: Consequences and solutions. IEEE Trans. Commun., **52** (11) (2004), 1988–1997.

[19] Syrjälä, V.; Valkama, M.: Jitter mitigation in high-frequency bandpass sampling OFDM radios, in Proc. IEEE Wireless Communications and Networking Conf. 2009, Budapest, Hungary, April 2009.

[20] Syrjälä, V.; Valkama, M.: Sampling jitter estimation and mitigation in direct RF sub-sampling receiver architecture, in Proc. Sixth Int. Symp. on Wireless Communication Systems 2009, Siena-Tuscany, Italy, September 2009.

[21] Rutten, R.; Breems, L.J.; van Veldhoven, R.H.M.: Digital jitter-cancellation for narrowband signals, in Proc. IEEE Int. Symp. on Circuits and Systems 2008, May 2008, 1444–1447.

[22] Tchamov, N.N.; Rinne, J.; Syrjälä, V.; Valkama, M.; Zou, Y.; Renfors, M.: VCO phase noise trade-offs in PLL design for DVB-T/H receivers, in Proc. IEEE Int. Conf. on Electronics Circuits and Systems 2009, December 2009.

[23] 3GPP Technical Specification, TS 36.211 v8.3.0, Physical Channels and Modulation (release 8), May 2008.

[24] Sorensen, T.B.; Mogersen, P.E.; Frederiksen, F.: Extension of the ITU channel models for wideband (OFDM) systems, in Proc. IEEE Vehicular Technology Conf., Fall-2005, Dallas, TX, September 2005, 392–396.

Ville Syrjälä was born in Lapua, Finland, on August 23, 1982. He received the M.Sc. degree (with honours) in communications engineering (CS/EE) from Tampere University of Technology (TUT), Finland, in 2007. Currently, he is working as a researcher with the Department of Communications Engineering at TUT, Finland. His general research interests are in communications signal processing and signal processing algorithms for flexible radios.

Mikko Valkama was born in Pirkkala, Finland, on November 27, 1975. He received the M.Sc. and Ph.D. degrees (both with honours) in electrical engineering (EE) from Tampere University of Technology (TUT), Finland, in 2000 and 2001, respectively. In 2002 he received the Best Ph.D. Thesis – award by the Finnish Academy of Science and Letters for his dissertation entitled "Advanced I/Q signal processing for wideband receivers: Models and algorithms." In 2003, he was working as a visiting researcher with the Communications Systems and Signal Processing Institute at SDSU, San Diego, CA. Currently, he is a Full Professor at the Department of Communications Engineering at TUT, Finland. He has been involved in organizing conferences, like the IEEE SPAWC'07 (Publications Chair) held in Helsinki, Finland. His general research interests include communications signal processing, estimation and detection techniques, signal processing algorithms for software defined flexible radios, digital transmission techniques such as different variants of multicarrier modulation methods and OFDM, and radio resource management for *ad hoc* and mobile networks.

Publication 6

V. Syrjälä, M. Valkama, Y. Zou, N. N. Tchamov, and J. Rinne, "On OFDM link performance under receiver phase noise with arbitrary spectral shape," in *Proc. IEEE Wireless Communications & Networking Conference 2011* (*IEEE WCNC'11*), Cancun, Quintana-Roo, Mexico, March 2011.

On OFDM Link Performance under Receiver Phase Noise with Arbitrary Spectral Shape

Ville Syrjälä, Mikko Valkama, Yaning Zou, Nikolay N. Tchamov, and Jukka Rinne

***Abstract*—This article addresses the signal distortion caused by receiver phase noise (PN) on OFDM waveforms in direct-conversion radio receivers. A closed-form solution for the observed signal-to-interference-plus-noise ratio (SINR) is derived, describing the level of intercarrier interference (ICI) stemming from PN. Compared to existing literature, the analysis is valid for arbitrary oscillator spectral shape, the only assumption being that reasonably small phase noise values are observed. The analysis results can be used to derive practical circuit-level oscillator design criteria in terms of the allowable PN spectral density. The applicability and validity of the derived analysis are verified with extensive computer simulations.**

***Index Terms*—Inter-carrier interference, OFDM, performance analysis, phase noise**

I. Introduction

COMMUNICATIONS systems using orthogonal frequency division multiplexing (OFDM) are highly vulnerable to non-idealities of radio device components [1]. Performance-wise one of the most remarkable of these non-idealities is oscillator phase noise [2], [3]. Phase noise spreads the spectral content of the used subcarriers destroying the orthogonality between them. This causes inter-carrier interference (ICI) in addition to well known effect of symbol constellation rotation called common phase error (CPE) [2]. Due to the relatively complex nature of the phase noise induced waveform distortion, and its dependency on the used oscillator characteristics, a closed-form tool describing the level of ICI as a function of the used oscillator spectral density is developed in this article. Such tool can be used already in the design process of the oscillator, e.g., to find out the properties of oscillators that are the most significant from the applied waveform point of view.

The effects of phase noise on the performance of OFDM communications systems are widely studied in the literature, e.g., in [4], [5] and [6]. However, the oscillator models in the reported studies are typically fixed or restricted to highly-simplified models, such as the free-running oscillator (FRO) [3]. In this paper, the effective signal-to-interference-plus-noise ratio (SINR) is analyzed for OFDM systems under the influence of phase noise caused ICI. The phase noise process in this study is based on arbitrary phase noise spectral mask, thus making the model generally applicable for practical oscillators. Only an assumption of an oscillator with reasonably small phase noise values is made without restricting the spectral shape of the phase noise to any predefined criteria. To authors' knowledge, analysis without any restrictions to the spectral shape of the oscillator cannot be found in existing literature.

The rest of this article is organized as follows: Section II gives a compact subcarrier-wise OFDM link model including the radio channel and receiver phase noise. This forms the basis for the SINR analysis. Then, Section III formulates and carries out the actual SINR analysis in detail, while Section IV verifies the derived expressions with the help of link computer simulations. Finally, the work is concluded in Section V.

II. OFDM Link Model

In OFDM systems, the phase noise effects can be divided in two distinct parts [2]. The first effect is called CPE that is the common complex multiplicative effect the phase noise has on all subcarrier symbols within one OFDM symbol. The second effect is called ICI, which is the loss of orthogonality due to frequency spread of the subcarriers on top of each other. The CPE is easily cancelled out in the receiver with help of pilot subcarriers [3]. ICI, however, has more complicated effect on the OFDM systems, thus making its mitigation much more burdensome [3], [7]. This is why the ICI is much more interesting also from the performance analysis point-of-view. Therefore, in this work, we assume that the CPE is known, namely part of the useful signal, while the actual interference is coming from the neighbouring subcarriers. Furthermore, to simplify the analysis, we assume that the interference from adjacent RF bands is negligible, meaning that we focus on the in-band effects only.

Next, to form the basis for SINR analysis, a link model is shortly established taking into account a noisy multipath channel and receiver phase noise. In effect, the observation at subcarrier k can be written as

This work was supported by TUT Graduate School, Finnish Foundation for Technology Promotion, HPY Research Foundation, the Finnish Funding Agency for Technology and Innovation (Tekes, under the project "Advanced Techniques for RF Impairment Mitigation in Future Wireless Radio Systems"), the Technology Industries of Finland Centennial Foundation and EUREKA CELTIC E!3187 B21C-Broadcasting for 21st Century.

Authors are with Department of Communications Engineering, Tampere University of Technology, P.O. Box 553, 33101 Tampere, Finland. (email: {ville.syrjala, mikko.e.valkama, yaning.zou, nikolay.n.tchamov, jukka.rinne}@tut.fi).

$$R_k(m) = X_k(m)H_k(m)J_0(m) + \sum_{l=0,l\neq k}^{N-1} X_l(m)H_l(m)J_{k-l}(m) + Z_k(m). \quad (1)$$

Here, $R_k(m)$ is the received signal, $X_k(m)$ is the transmitted subcarrier symbol, $H_k(m)$ is the channel transfer function, $J_k(m)$ is the frequency-domain phase-noise complex exponential and $Z_k(m)$ is additive white Gaussian noise, all at m th OFDM symbol and k th subcarrier. Furthermore, N is the IDFT/DFT length used in the OFDM modulation/demodulation. The frequency domain phase-noise complex exponential is given by

$$J_k(m) = \sum_{n=0}^{N-1} e^{j\varphi_n(m)} e^{-j2\pi nk/N}, \quad (2)$$

where $\varphi_n(m) = \varphi(m(T_S + T_{CP}) + nT_S/N)$ denotes the actual phase noise value at n th sample within the studied m th OFDM symbol. Here, T_S and T_{CP} indicate the OFDM symbol length and cyclic prefix length, respectively. In (1), the first term of the right hand side is the CPE corrupted term, and the additive sum term is directly the phase noise incurred ICI. Namely, the DC-bin of the phase noise exponential $J_0(m)$ is the complex multiplication caused by the CPE, and all the other terms of $J_k(m)$ summed up denote the effect of the ICI. Since we already concluded that the only relevant effect of the phase noise for this study is caused by the ICI (not by CPE), the SINR due to phase noise can be easily derived from (1). We let the power of the first term of the right hand side to be the useful power of the signal and assume the power of the ICI and noise term to be the interference power. Thus, the SINR is defined as

$$\gamma_k = \frac{E\left[\left|X_k(m)H_k(m)J_0(m)\right|^2\right]}{E\left[\left|\sum_{l=0,l\neq k}^{N-1} X_l(m)H_l(m)J_{k-l}(m) + Z_k(m)\right|^2\right]}. \quad (3)$$

Next, we make natural assumptions that $X_k(m)$, $H_k(m)$, $J_k(m)$ and $Z_k(m)$ are mutually statistically independent, stationary, and that $\forall k: X_k(m)$ are independent of each other and zero mean. Therefore, we can write the SINR equation (3) as

$$\gamma_k = \frac{E\left[\left|X_k(m)\right|^2\right]E\left[\left|H_k(m)\right|^2\right]E\left[\left|J_0(m)\right|^2\right]}{\sum_{l=0,l\neq k}^{N-1} E\left[\left|X_l(m)\right|^2\right]E\left[\left|H_l(m)\right|^2\right]E\left[\left|J_{k-l}(m)\right|^2\right] + \sigma_z^2}, \quad (4)$$

where $\sigma_z^2 = E\left[\left|Z_k(m)\right|^2\right]$ denotes the average power of the additive white Gaussian noise term $Z_k(m)$. Now, we make two other reasonable assumptions that mean of the average transmit symbol powers and average channel power responses are subcarrier independent. Namely,

$$\forall k: E\left[\left|X_k(m)\right|^2\right] = \sigma_x^2, \quad (5)$$

$$\forall k: E\left[\left|H_k(m)\right|^2\right] = \sigma_h^2. \quad (6)$$

Now, stemming from assumptions (5) and (6), we can write

$$\gamma_k = \frac{\sigma_x^2\sigma_h^2 E\left[\left|J_0(m)\right|^2\right]}{\sigma_x^2\sigma_h^2\sum_{k=1}^{N-1} E\left[\left|J_k(m)\right|^2\right] + \sigma_z^2}. \quad (7)$$

Equation (7) can be further simplified to form

$$\gamma_k = \frac{E\left[\left|J_0(m)\right|^2\right]}{\sum_{k=1}^{N-1} E\left[\left|J_k(m)\right|^2\right] + \frac{\sigma_z^2}{\sigma_x^2\sigma_h^2}}. \quad (8)$$

Now by denoting the received signal-to-noise ratio (SNR) without phase noise by $\rho = \sigma_x^2\sigma_h^2/\sigma_z^2$, we can write

$$\gamma_k = \frac{E\left[\left|J_0(m)\right|^2\right]}{\sum_{k=1}^{N-1} E\left[\left|J_k(m)\right|^2\right] + \frac{1}{\rho}}. \quad (9)$$

Here, $J_k(m)$ is simply DFT of complex exponential by definition. Since sum of squared absolute values of N complex exponentials is naturally N, we know according to Parseval's theorem, that

$$\sum_{k=0}^{N-1}\left|J_k(m)\right|^2 = N^2. \quad (10)$$

Now, from the linearity of the expectation operator, it directly stems that

$$\sum_{k=0}^{N-1} E\left[\left|J_k(m)\right|^2\right] = N^2. \quad (11)$$

Thus by combining (9) and (11), we can finally write the SINR as

$$\gamma_k = \gamma = \frac{E\left[\left|J_0(m)\right|^2\right]}{N^2 - E\left[\left|J_0(m)\right|^2\right] + \frac{1}{\rho}}. \quad (12)$$

As (12) shows, the achievable average SINR is independent of the subcarrier index k, even though ICI is also present, and depends only on the received SNR and the second-order statistics of the CPE. Thus to complete the analysis, the average power of the CPE, $E\left[\left|J_0(m)\right|^2\right]$, needs to be

addressed. This will be done in closed-form as a function of the used oscillator spectral shape in the following sections.

III. Oscillator Modelling

Usually in studies like this, free-running or otherwise constrained oscillator model is used. In this paper, however, we use a so-called frequency-masking approach to model the oscillator phase noise. In this model, white noise is first transformed to frequency domain using discrete Fourier transform (DFT), filtered with arbitrary phase-noise frequency-mask and then transformed back to time-domain with inverse DFT [8]. This allows easy modelling of arbitrary oscillators used in OFDM systems, where the used DFT length can be conveniently selected, e.g., as the number of used subcarriers *N*. Practical shapes for the masks can be derived, e.g., with help of point single-sideband (SSB) phase-noise laboratory measurements of the oscillators [9].

Now based on (12), we must derive the average power of $J_0(m)$ for arbitrary oscillator defined by phase-noise frequency-mask. The mask is here defined with subcarrier-specific scaling variables λ_k, $k = 0...N-1$. Then, if we assume that the values of the phase noise $\varphi_n(m)$ are relatively small, $\varphi_n(m) << 1$ rad, as they are in any practical oscillator, we can first make an approximation $e^{j\varphi_n(m)} \approx 1 + j\varphi_n(m)$. The scaled version of this, keeping unit variance, can be written as

$$e^{j\varphi_n(m)} \approx \frac{1 + j\varphi_n(m)}{\sqrt{1+\sigma_\varphi^2}}. \tag{13}$$

Here, σ_φ^2 is the average power of the phase noise $\varphi_n(m)$, derived in the Appendix as a function of the spectral mask.

The first frequency bin of the process $e^{j\varphi_n(m)}$ is the multiplicative effect of the CPE, the average power of which we are interested in. Now, stemming directly from (2), $J_0(m)$ can be written as

$$J_0(m) = \sum_{n=0}^{N-1} e^{j\varphi_n(m)}, \tag{14}$$

Uniting the approximation (13) and the equation (14), we can write

$$J_0(m) \approx \frac{N + j\sum_{n=0}^{N-1}\varphi_n(m)}{\sqrt{1+\sigma_\varphi^2}} = \frac{N + j\Phi_0(m)}{\sqrt{1+\sigma_\varphi^2}}, \tag{15}$$

where $\Phi_0(m)$ is the DC-bin of DFT of the $\varphi_n(m)$. Then, as shown in the Appendix, the average power of $J_0(m)$ can be written as

$$\mathrm{E}\left[\left|J_0(m)\right|^2\right] \approx \frac{N^2 + \sigma_w^2\lambda_0^2}{1+\sigma_\varphi^2} = \frac{N^2 + \sigma_w^2\lambda_0^2}{1 + \frac{\sigma_w^2}{N^2}\sum_{k=0}^{N-1}\lambda_k^2}. \tag{16}$$

The expression in (16) describes the average power of the CPE as a function of some elementary variables. By combining (12) and (16), and by applying some simple manipulations, we end up in the following form for the SINR given by

$$\gamma \approx \frac{N^2 + \sigma_w^2\lambda_0^2}{\sigma_w^2\sum_{k=1}^{N-1}\lambda_k^2 + \frac{\sigma_w^2}{\rho N^2}\sum_{k=0}^{N-1}\lambda_k^2 + \frac{1}{\rho}}. \tag{17}$$

The variable γ can then be used to evaluate the SINR for arbitrary phase noise mask defined by λ_k, $k = 0...N-1$. This form is already usable. However, quantities $\psi_k^2 = \sigma_w^2\lambda_k^2$ are easier to connect to actual oscillator spectral measurements, as they are the energies of the phase noise around the k th subcarrier, as depicted in Fig. 1. These energies can be approximated by the common dBc/Hz measurement values of the oscillator phase noise spectrum at the centre of the k th subcarrier multiplied by the subcarrier spacing $1/T_S$, i.e.,

$$\psi_k^2 = \sigma_w^2\lambda_k^2 \approx \mathrm{PSD}_\varphi\left(k\frac{1}{T_S}\right)\frac{1}{T_S}. \tag{18}$$

Here, PSD_φ is the power spectral density function of the phase noise, that is also depicted in Fig. 1. Now, by using ψ_k^2 in (17), the SINR can be rewritten as a direct function of the spectral measurements as

$$\gamma \approx \frac{N^2 + \psi_0^2}{\sum_{k=1}^{N-1}\psi_k^2 + \frac{1}{\rho N^2}\sum_{k=0}^{N-1}\psi_k^2 + \frac{1}{\rho}} \tag{19}$$

Finally, by nullifying the additive noise contribution ($1/\rho = 0$), we are able to achieve alternative very simple form

$$\gamma \approx \frac{N^2 + \psi_0^2}{\sum_{k=1}^{N-1}\psi_k^2}. \tag{20}$$

This form can be used in calculation of SIR due to oscillator effects alone in noise-free OFDM-system, forming and upper-

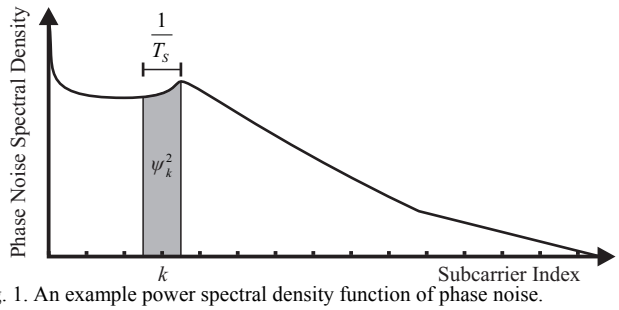

Fig. 1. An example power spectral density function of phase noise.

bound for SIR, which might also be interesting for some oscillator designers.

IV. Verification of the Model and Simulation Analysis

In this Section, the tenability of the above model is verified by comparing the SINR given by the analytical formula (17) to the SINR given by simulations. In addition, the simulation results are shortly analyzed. In this study, we use phase-locked-loop (PLL) based oscillator as an example. We use PLL oscillator because the idea is well-known and the phase-noise frequency-mask can be easily connected to real world oscillator measurements, e.g., by using formulae given in [9]. As mentioned, however, the SINR expression in (17) is applicable to any phase noise spectral shape, so the usage is by no means restricted to the special case of PLL-oscillator.

In simulations, 1000 realizations of OFDM symbols, with 1024 subcarriers with 15 kHz subcarrier spacing and 63 sample cyclic prefix, are generated with 16QAM subcarrier modulation. They are then transmitted through independent realizations of extended ITU-R Vehicular A multipath-channel. Additive white Gaussian noise and receiver phase noise are then modelled to the system as well as OFDM demodulation. From these modelled signal components, then, average powers of useful signal and ICI are numerically calculated, and SINR is then evaluated using these powers, and compared against the analytical results.

In these experiments, SIR and SINR are studied as functions of phase-noise spot measurements L_F and L_W. A principal illustration is given in Fig. 2. These parameters characterize phase-noise power-spectral-density of the free-running voltage-controlled oscillator that is integrated in the PLL. L_F corresponds to the 1/f-noise-dominated region measurement at 10 kHz offset from the oscillation frequency, whereas L_W corresponds to the thermal-noise-dominated region measurement at 1 MHz offset. Here we assume that the spot thermal-noise region measurement for the reference oscillator used in PLL is −160 dBc/Hz at 1 MHz offset, and assume that no significant flicker noise levels are present. Refer to [7] and [9] for more details on the oscillator modelling. Notice that the studies of this paper are applicable for any realistic oscillator model. This oscillator design parameterization above is used here only to reflect a practical example scenario for simulations.

For easier interpretation and visualization, we first consider the case where channel noise is set to zero, i.e., $1/\rho = 0$. Fig. 3 gives the contour plot of the SIR-performance in the simulations. Fig. 4 then shows the difference in simulated SIR-performance and the analytical SIR-performance as formulated in (17). As Fig. 4 depicts, over the studied values of parameters L_W and L_F, the simulated and theoretical performances are very near to each other. Maximum performance difference in the studied parameter region is about 1.6 dB. This is excellent accuracy especially because we are having nearly 0 dB SIR in the worst case region as shown in Fig. 3. In regions, where SIR is over 10 dB, the theoretical results match the simulated ones almost perfectly. As one can remember, the theoretical analysis developments were stemming from the small phase noise (practical oscillator) assumption, so the small performance difference in 0-10 dB SIR range is understandable as the oscillator gets very noisy and the small phase noise assumption, $\varphi_n(m) << 1$ rad, is violated.

According to SINR results in Fig. 5, when additive channel noise is also considered present in the system, the formula (17) still gives accurate results. Fig. 5 shows the simulated performance versus theoretical performance in fixed PLL-oscillator with example parameters $L_F = -82$ dBc/Hz and $L_W = -120$ dBc/Hz, the spectrum of which can be seen in Fig. 2. According to simulations, with these parameters the PLL-oscillator causes SIR of 40 dB in case without additive noise as shown in Fig. 3. In Fig. 5, we can see the expected 40 dB

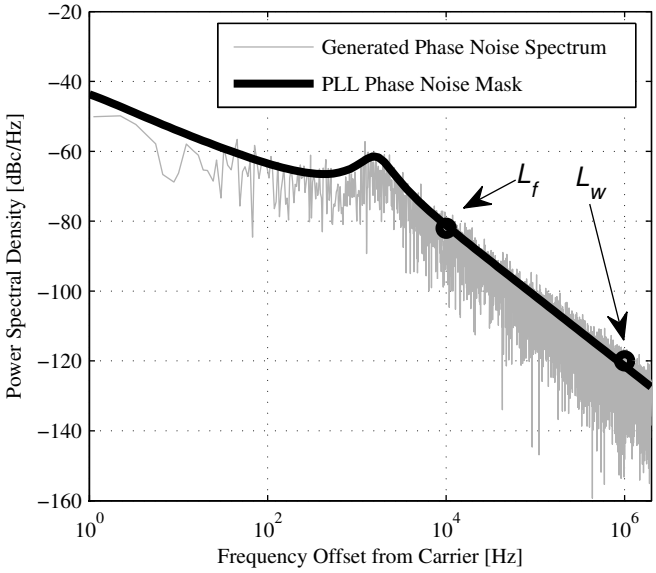

Fig. 2. Example spectrum of the oscillator phase noise generated with parameters $L_F = -82$ dBc/Hz and $L_W = -120$ dBc/Hz.

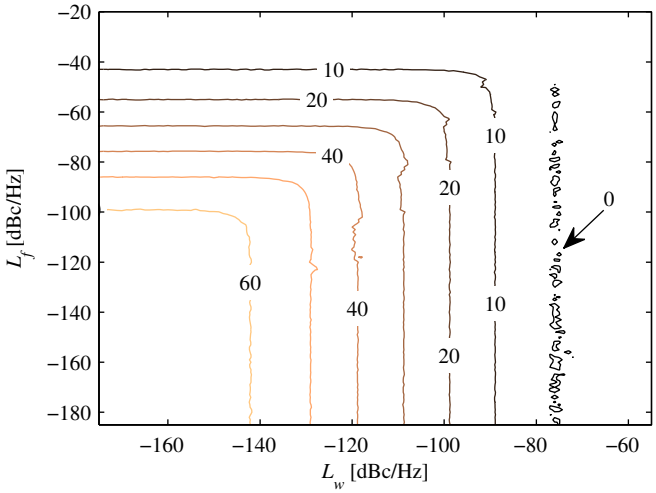

Fig. 3 Contour plot for the value of SIR (in dB) as a function of L_F and L_W, given by the simulations. No additive channel noise.

upper performance boundary and the 37 dB SINR when the received SNR is 40 dB. In that operating point, ICI and channel noise are equally strong implying thus 3 dB penalty compared to no phase noise (ideal receiver) case.

Already from Fig. 3, one can see that there is indeed margin to play when designing the down-converting oscillator for OFDM receiver under the assumed PLL topology. One can see that with fixed L_F one can play with L_W quite much without practically affecting the SIR, and vice versa. The derived formula is thus quite interesting from receiver design point-of-view, meaning that one can trade higher phase noise spectral densities at certain frequencies without essentially affecting the receiver detection performance. This was actually observed empirically already in [9] and is now analytically justified.

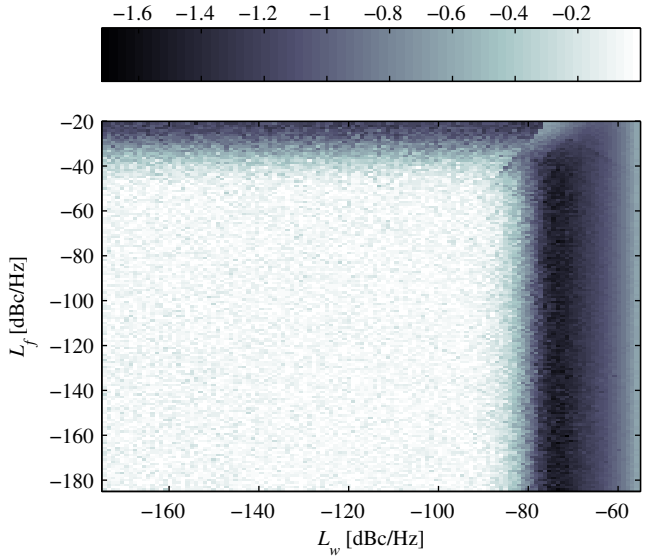

Fig. 4. SIR error given for PLL-type example oscillator as a function of L_F and L_W. Absolute value of the difference between the theoretical SIR given by (20) and simulated SIR is depicted. Error is given in dB scale. No additive channel noise.

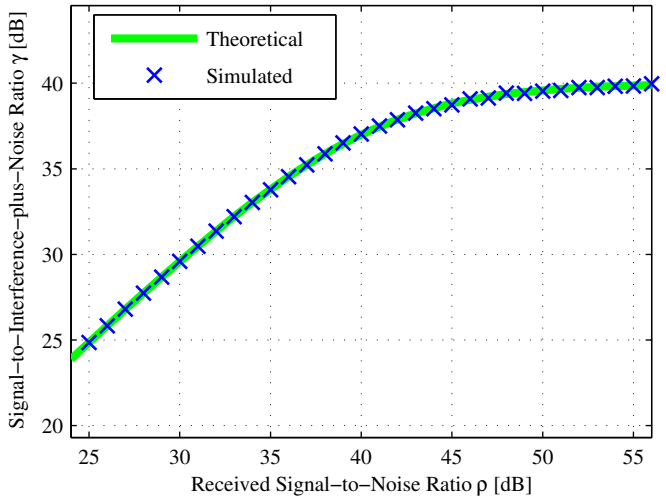

Fig. 5. Theoretical and simulated SINR as a function of SNR compared in case with additive noise present. Fixed oscillator with parameters $L_F = -82$ dBc/Hz and $L_W = -120$ dBc/Hz.

V. Conclusion

Phase noise is one of the main impairments in OFDM radio receivers. In this paper, a simple and efficient analytical tool was derived for oscillators with arbitrary spectral shape to calculate average subcarrier-level SINR due to ICI stemming from down-converting oscillator phase-noise. The tool derivation is based on using a sampled phase-noise frequency-mask to characterize the phase noise spectral density. Also, OFDM system was simulated in order to verify the accuracy of the tool. Simulation results verified that the performance given by the tool corresponds accurately to the performance given by the simulations. In practice, the analysis results can be used to derive RF design requirements for the receiver oscillator module in terms of the allowable phase noise spectral density at given frequencies.

Appendix: Derivation of Phase Noise Variance

Here we derive the variance of the phase noise generated by an arbitrary frequency-domain phase-noise mask vector $\boldsymbol{\lambda} = [\lambda_0, \lambda_1, \ldots, \lambda_{N-1}]^T$. Initially, in phase noise vector generation, we only have white noise vector $\mathbf{u}$ with covariance $\sigma_u^2\mathbf{I}$. After transforming this to frequency-domain with DFT matrix $\mathbf{A}$, we have still white noise, since the covariance of $\mathbf{w} = \mathbf{A}\mathbf{u}$ is of the form

$$\mathrm{E}\left[\mathbf{w}\mathbf{w}^H\right] = \mathbf{A}\mathrm{E}\left[\mathbf{u}\mathbf{u}^H\right]\mathbf{A}^H = \mathbf{A}\sigma_u^2\mathbf{I}\mathbf{A}^H = N\sigma_u^2\mathbf{I} = \sigma_w^2\mathbf{I}. \quad (21)$$

Then, we apply the frequency-domain phase-noise mask to this frequency-domain white noise. This results into signal $\mathbf{q} = \boldsymbol{\Lambda}_M\mathbf{w}$, where $\boldsymbol{\Lambda}_M$ is a diagonal matrix corresponding to elements of the phase noise mask $\lambda_k, k = 0 \ldots N-1$. The corresponding covariance matrix is then given by $\sigma_w^2\boldsymbol{\Lambda}_M^2$ as is easy to show. Finally, after inverse DFT we end up having the phase noise vector $\boldsymbol{\varphi} = \mathbf{B}\mathbf{q}$, where $\mathbf{B}$ is the inverse-DFT matrix. The covariance matrix for phase noise vector $\boldsymbol{\varphi}$ is then given by

$$\begin{aligned}\mathrm{E}\left[\boldsymbol{\varphi}\boldsymbol{\varphi}^H\right] &= \mathbf{B}\mathrm{E}\left[\mathbf{q}\mathbf{q}^H\right]\mathbf{B}^H = \sigma_w^2\mathbf{B}\boldsymbol{\Lambda}_M^2\mathbf{B}^H \\ &= \sigma_w^2\sum_{k=0}^{N-1}\lambda_k\mathbf{b}_k\mathbf{b}_k^H \quad ,\end{aligned} \quad (22)$$

where $\mathbf{b}_k$ is the k th column of the inverse DFT matrix $\mathbf{B}$. From (22), we can see that the variance of the l th sample of the phase noise vector $\boldsymbol{\varphi}$ can be written as

$$\begin{aligned}\sigma_\varphi^2(l) &= \mathbf{e}_l^T\mathrm{E}\left[\boldsymbol{\varphi}\boldsymbol{\varphi}^H\right]\mathbf{e}_l = \sigma_w^2\sum_{k=0}^{N-1}\lambda_k^2\left|\mathbf{b}_k(l)\right|^2 \\ &= \frac{\sigma_w^2}{N^2}\sum_{k=0}^{N-1}\lambda_k^2 = \sigma_\varphi^2 \quad ,\end{aligned} \quad (23)$$

where $\mathbf{e}_l$ is the l th unit vector (column vector of all zeros except for l th element which equals one) and N is the length of vectors $\boldsymbol{\varphi}$, $\mathbf{b}_k$ and $\mathbf{e}_l$. We can see that variance given by (23) is actually not dependent on the sample index l, and depends essentially only on the mask values.

REFERENCES

[1] G. Fettweis, "Dirty-RF: A new paradigm", in *Proc. 16th International Symposium on Personal, Indoor and Mobile Radio Communications, 2005 (PIMRC'05)*, Berlin, Germany, September 2005, pp. 2347-2355, Vol. 4.

[2] P. Robertson, and S. Kaiser, "Analysis of the effects of phase-noise in orthogonal frequency division multiplex (OFDM) systems," in *Proc. IEEE International Conference on Communications (ICC'95)*, Seattle, WA, June 1995, pp. 1652-1657, Vol. 3.

[3] D. Petrovic, W. Rave, and G. Fettweis, "Effects of phase noise on OFDM systems with and without PLL: Characterization and compensation," *IEEE Transactions on Communications*, Vol. 55, No. 8, pp. 1607-1616, August 2007.

[4] C.-H. Yih, "BER analysis of OFDM systems impaired by phase noise in frequency-selective Rayleigh fading channels," in *Proc. Global Telecommunications Conference 2008 (GLOBECOM'08)*, New Orleans, LO, December 2008.

[5] M. Krondorf, S. Bittner, and G. Fettweis, "Numerical performance evaluation for OFDM systems affected by phase noise and channel estimation errors," in *Proc. Vehicular Technology Conference 2008 (VTC'08-Fall)*, Calgary, Canada, September 2008.

[6] T. Schenk, *RF Impairments in Multiple Antenna OFDM: Influence and Mitigation*, PhD dissertation, Technische Universiteit Eindhoven, 2006. ISBN 90-386-1913-8. 291 p.

[7] V. Syrjälä, M. Valkama, N. N. Tchamov, and J. Rinne, "Phase noise modelling and mitigation techniques in OFDM communications systems," in *Proc. Wireless Telecommunications Symposium 2009 (WTS'09)*, Prague, Czech Republic, April 2009.

[8] Y. Ferdi, A. Taleb-Ahmed, and M. R. Lakehal, "Efficient generation of 1/f^beta noise using signal modelling techniques," IEEE Transactions on Circuits and Systems—I: Regular Papers, Vol. 55, No. 6, pp. 1704-1710, July 2008.

[9] N. N. Tchamov, J. Rinne, V. Syrjälä, M. Valkama, Y. Zou, and M. Renfors, "VCO phase noise trade-offs in PLL design for DVB-T/H receivers," in *Proc. IEEE International Conference on Electronics, Circuits and Systems (ICECS'09)*, Yasmine Hammamet, Tunisia, December 2009.

Publication 7

V. Syrjälä and M. Valkama, "Receiver DSP for OFDM systems impaired by transmitter and receiver phase noise," in *Proc. IEEE International Conference on Communications 2011* (*IEEE ICC'11*), Kyoto, Japan, June 2011.

Receiver DSP for OFDM Systems Impaired by Transmitter and Receiver Phase Noise

Ville Syrjälä and Mikko Valkama

***Abstract*—This paper proposes a time-domain digital signal processing method for estimating and mitigating transmitter and receiver oscillator phase-noise effects in OFDM radio systems on the receiver side of the link. The idea is based on re-constructing time-domain OFDM signal at the receiver from initially detected symbols and using this as a reference in phase noise estimation. The knowledge of heavily low-pass nature of realistic phase noise processes is then utilized in the estimation process to improve the estimation quality. The algorithm can also be used iteratively, inside individual OFDM symbols, to further improve the accuracy of the obtained phase noise estimate. Performance analysis shows that the proposed algorithm outperforms existing state-of-the-art phase noise mitigation techniques, under both additive white Gaussian noise and extended ITU-R Vehicular A multipath channels.**

***Index Terms*—OFDM; phase noise; ICI; mitigation; digital signal processing; dirty-RF**

I. Introduction

In recent years, there have been great advances in digital signal processor implementation techniques. This has enabled significant increases in signal processing capabilities of small devices, such as mobile phones, without the increase in size, cost and power consumption. The increased computational power allows moving the complexity of the transceiver units from the analogue component side to the digital signal processing (DSP) side. Actually used analogue components in transceivers can thus be small, cheap and low-power. Even though having more complex signal processing algorithms to handle, overall costs, sizes and power consumptions of transceivers can be significantly lowered [1].

Orthogonal frequency domain multiplexing (OFDM) is a multicarrier modulation technique used in many current and future communications systems (such as DVB-T, WiMAX, 3G LTE, etc.). Even though it has many advantages, OFDM is very prone to transceiver RF-impairments [2]. One of the most harmful of these impairments is phase noise. In addition to well-known rotating effect, called common phase error (CPE), phase noise also causes subcarriers to lose their orthogonality by spectrally spreading subcarriers on top of each other [3]. The spread is called intercarrier interference (ICI) and its effect changes from subcarrier to another making the compensation difficult [3], [4]. It is thus very important to develop new signal processing algorithms to mitigate the phase noise effects in OFDM systems.

By today, the phase noise impaired OFDM systems have already received quite extensive attention in the literature. Phase noise effects on OFDM systems have been studied, e.g., in [3] and [5]. Deeper pen-and-paper analysis of the phase noise effects was carried out, e.g., in [6]. Mitigation of the CPE part of the phase noise has been considered already in [3], and in [7] mitigation performance of such CPE mitigation technique was improved. Furthermore, in [7] they also proposed a simplistic ICI mitigation algorithm. More advanced ICI mitigation technique was then proposed in [4] and some improvements for this method in [8] and [9]. In [10] and [11], the authors of this paper proposed further modifications for the technique proposed in [4] to improve its performance.

In this paper, a novel DSP algorithm is proposed for phase noise mitigation and its performance is compared to the performances of the state-of-the-art techniques from the literature. The technique works on time domain signal in an iterative manner. The technique does not need any prior information about the phase noise process, making it easily implementable and versatile. Only assumption that needs to be made is that the phase noise process is heavily low-pass natured. This is true for all practical oscillators.

The rest of the paper is structured as follows. In Section II, OFDM transmission chain and phase noise are modelled. Section III then gives the proposed phase noise mitigation algorithm and practical considerations related to its implementation. After this, the performance of the proposed algorithm is compared to the state-of-the-art phase noise mitigation techniques in Section IV. At length, the work is concluded in Section V.

II. System Modelling

This Section gives the overall OFDM transmission chain and oscillator phase noise modelling as a basis for the algorithm development.

This work was supported by TUT Graduate School, HPY Research Foundation, the Finnish Funding Agency for Technology and Innovation (Tekes, under the project "Advanced Techniques for RF Impairment Mitigation in Future Wireless Radio Systems") and the Technology Industries of Finland Centennial Foundation.

The authors are with Department of Communications Engineering, Tampere University of Technology, P.O. Box 553, 33101 Tampere, Finland (email: {ville.syrjala, mikko.e.valkama}@tut.fi).

A. OFDM Transmission Chain Model

In OFDM symbol generation, first modulated symbols $X_k(m)$ are grouped in blocks of N subcarrier symbols $k = 0,1,\ldots,N-1$, where m th block refers to the m th OFDM symbol. These blocks are then inverse discrete Fourier transformed (IDFT) giving sampled OFDM symbols, where n th sample is

$$x_n(m) = \frac{1}{\sqrt{N}} \sum_{k=0}^{N-1} X_k(m) e^{j2\pi kn/N} . \quad (1)$$

Here, sampling indices are $n = 0,1,\ldots,N-1$. So, the resulting OFDM symbol is N samples long giving it length of NT_s seconds and subcarrier spacing of $f_s = 1/(NT_s)$, where T_s is the sampling interval. Furthermore, to exploit the advantage of having relatively long symbol durations, a cyclic prefix is added to the OFDM symbols before transmission. Namely, we transmit G last samples of each OFDM symbol prior the actual symbol samples. This effectively makes the sent blocks partially circular making the stream immune to inter-symbol interference if the maximum delay spread of the transmission channel is shorter than the duration of the cyclic prefix GT_s. Then, the overall OFDM symbol length is $(G+N)T_s$. [12]

In this work, we assume that the maximum channel delay spread is less than the length of the cyclic prefix. So in the receiver, after the signal has gone through the ideal up-conversion, the transmission channel, the ideal down-conversion and the removal of the cyclic prefix, we can write the received signal as

$$\mathbf{r}^{(m)} = \left(\mathbf{h}^{(m)} * \mathbf{x}^{(m)}\right) + \mathbf{z}^{(m)} . \quad (2)$$

Here, operator $*$ denotes circular convolution between the elements of the operated vectors. $\mathbf{h}^{(m)}$ is a $(D \times 1)$ channel impulse response vector $(D < G)$ and vector $\mathbf{x}^{(m)} = \left[x_0(m), x_1(m), \ldots, x_{N-1}(m)\right]^T$. Vector $\mathbf{z}^{(m)}$ denotes additive white Gaussian noise. Now, when transmitter and receiver oscillator phase noises are assumed present, (2) can be written as

$$\mathbf{r}^{(m)} = \mathrm{diag}\left(e^{j\boldsymbol{\varphi}_R^{(m)}}\right)\left(\mathbf{h}^{(m)} * \left(\mathrm{diag}\left(e^{j\boldsymbol{\varphi}_T^{(m)}}\right)\mathbf{x}^{(m)}\right)\right) + \mathbf{z}^{(m)} , \quad (3)$$

where $\mathrm{diag}(\,)$ is a function which creates a diagonal matrix that has the input vector in its diagonal. The vectors of the sampled transmitter and receiver phase noise realizations during the m th OFDM symbol are $\boldsymbol{\varphi}_T^{(m)}$ and $\boldsymbol{\varphi}_R^{(m)}$, respectively. For n th sample of m th OFDM symbol, they are defined as $\boldsymbol{\varphi}_X^{(m)} = \left[\varphi_{0,X}(m), \varphi_{1,X}(m), \ldots, \varphi_{N-1,X}(m)\right]^T$, $X \in \{T, R\}$, where $\varphi_{n,T}(m)$ and $\varphi_{n,R}(m)$ are the transmitter and receiver phase noise samples, respectively. Since reasonable channel delay spread is assumed, the channel coherence bandwidth is reasonably high. Therefore, since phase noise process is typically a steep low-pass process [2], [4], (3) can be approximated as

$$\begin{aligned} \mathbf{r}^{(m)} &\approx \mathbf{h}^{(m)} * \left[\mathrm{diag}\left(e^{j\boldsymbol{\varphi}_R^{(m)}}\right)\mathrm{diag}\left(e^{j\boldsymbol{\varphi}_T^{(m)}}\right)\mathbf{x}^{(m)}\right] + \mathbf{z}^{(m)} \\ &= \mathbf{h}^{(m)} * \left[\mathrm{diag}\left(e^{j\left[\boldsymbol{\varphi}_R^{(m)} + \boldsymbol{\varphi}_T^{(m)}\right]}\right)\mathbf{x}^{(m)}\right] + \mathbf{z}^{(m)} \\ &= \mathbf{h}^{(m)} * \left[\mathrm{diag}\left(e^{j\boldsymbol{\varphi}^{(m)}}\right)\mathbf{x}^{(m)}\right] + \mathbf{z}^{(m)} \end{aligned} . \quad (4)$$

Here, $\boldsymbol{\varphi}^{(m)} = \boldsymbol{\varphi}_T^{(m)} + \boldsymbol{\varphi}_R^{(m)}$ denotes the total effective phase noise. Thus, stemming from the approximation made in (4), we are able to model the receiver phase noise similarly as the transmitter phase noise. The phase noises can be effectively summed together and the sum viewed as transmitter phase noise. Modelling both phase noises as transmitter phase noise is beneficial in algorithm derivation later on. Now, by using a circular convolution matrix [12] for the convolution in (4), we can write the final link model as

$$\mathbf{r}^{(m)} \approx \mathbf{H}^{(m)} \mathrm{diag}\left(e^{j\boldsymbol{\varphi}^{(m)}}\right)\mathbf{x}^{(m)} + \mathbf{z}^{(m)} , \quad (5)$$

where $\mathbf{H}^{(m)}$ is $(N \times N)$ channel circular convolution matrix.

B. Phase Noise Model

In the phase noise modelling, we are interested in how phase noise behaves as a function of sample index. In this Subsection, let us simply denote an arbitrary sampled phase noise process as $\phi_n = \phi(nT_s)$. In the literature, the phase noise is usually assumed to follow the well-known free-running oscillator model [2], [3]. The model assumes that there is no phase lock, so the next phase realization depends only on the previous realization and on the quality of the oscillator. This is perceived as a Brownian motion process, where the variance determines the oscillator quality. The phase can be written as

$$\phi_n = \sqrt{\frac{\beta}{4\pi}} B(nT_s) , \quad (6)$$

where $B(\,)$ is the standard Brownian motion function, namely $B(t_1) - B(t_2) \sim \mathcal{N}(0, |t_2 - t_1|)$, and β is one-sided 3-dB bandwidth of the phase noise process. Equation (6) can be also written as

$$\phi_n = \sqrt{\frac{\beta T_s}{4\pi}} B_n , \quad (7)$$

where the B_n is merely a process of cumulatively summed realizations of standard normal distributed $\mathcal{N}(0,1)$ random variable. So eventually, we can characterize the whole phase noise process with just a one parameter β. In general, this kind of free-running oscillator gives very demanding conditions for phase noise mitigation task [10]. For this reason, even though phase locked loop (PLL) type oscillators are more commonly deployed in practice, the free-running oscillator case is assumed in the forthcoming performance simulations.

III. The Phase Noise Mitigation Algorithm

The first part of this Section gives the basic idea and formulation of the proposed algorithm. The second part gives a method to further improve the performance of the algorithm. The last part of the Section gives some practical issues that must be considered when using the proposed algorithm.

A. Proposed Algorithm

The whole algorithm from the sampled down-converted waveform to detected symbols is depicted in Fig. 1.

The derivation of the proposed phase noise mitigation algorithm begins from the received signal waveform (5). After channel equalization and CPE mitigation, (5) reaches a form

$$\begin{aligned}\mathbf{y}^{(m)} &\approx \mathrm{diag}\left(e^{-\hat{\varphi}_{CPE}^{(m)}}\right)\left(\hat{\mathbf{H}}^{(m)}\right)^{-1}\left[\mathbf{H}^{(m)}\,\mathrm{diag}\left(e^{j\boldsymbol{\varphi}^{(m)}}\right)\mathbf{x}^{(m)}+\mathbf{z}^{(m)}\right]\\ &\approx \mathrm{diag}\left(e^{j\left(\boldsymbol{\varphi}^{(m)}-\hat{\varphi}_{CPE}^{(m)}\right)}\right)\mathbf{x}^{(m)}+\mathrm{diag}\left(e^{-\hat{\varphi}_{CPE}^{(m)}}\right)\left(\hat{\mathbf{H}}^{(m)}\right)^{-1}\mathbf{z}^{(m)}\\ &= \mathrm{diag}\left(e^{j\left(\boldsymbol{\varphi}^{(m)}-\hat{\varphi}_{CPE}^{(m)}\right)}\right)\mathbf{x}^{(m)}+\left(\hat{\mathbf{H}}_{CPE}^{(m)}\right)^{-1}\mathbf{z}^{(m)}\end{aligned} \quad . (8)$$

Here, $\hat{\varphi}_{CPE}^{(m)}$ is the estimated CPE and $\hat{\mathbf{H}}^{(m)}$ is the estimated channel circular convolution matrix during the mth OFDM symbol. $\hat{\mathbf{H}}_{CPE}^{(m)}$ has also the CPE rotation combined with the channel. Now, after discrete Fourier transform (DFT) and symbol detection, we get the initial symbol estimates. Already at this stage, when only the channel and CPE are compensated, the symbol estimates $\hat{X}_k(m), k=0,\ldots N-1$ are relatively reliable with reasonable phase noise levels [3], [10]. Therefore, with the reliability assumption, we can use these symbol decisions in the phase noise estimation process. When we take the symbol estimates, and turn them back into OFDM time-domain waveform with IDFT, we get the estimate of the transmitted waveform $\hat{\mathbf{x}}^{(m)}$. Now, by point-by-point dividing $\mathbf{y}^{(m)}$ in (8) with $\hat{\mathbf{x}}^{(m)}$, we get the estimate for the phase-noise complex exponential

$$\begin{aligned}\boldsymbol{\vartheta}^{(m)} &\approx \left[\mathrm{diag}\left(e^{j\left(\boldsymbol{\varphi}^{(m)}-\hat{\varphi}_{CPE}^{(m)}\right)}\right)\mathbf{x}^{(m)}+\left(\hat{\mathbf{H}}_{CPE}^{(m)}\right)^{-1}\mathbf{z}^{(m)}\right]\mathrm{diag}^{-1}\left(\hat{\mathbf{x}}^{(m)}\right)\\ &\approx e^{j\left(\boldsymbol{\varphi}^{(m)}-\hat{\varphi}_{CPE}^{(m)}\right)}+\left(\hat{\mathbf{H}}_{CPE}^{(m)}\right)^{-1}\mathbf{z}^{(m)}\,\mathrm{diag}^{-1}\left(\hat{\mathbf{x}}^{(m)}\right)\end{aligned} \quad . (9)$$

In some rare realizations $\hat{\mathbf{x}}^{(m)}$ has zero-elements in it. Those elements must be set to non-zero value prior to division to prevent the division by zero. In this study, we use high value $a\,(a\to\infty)$ to replace zeros, because it minimizes the potential error in the resulting phase noise estimate.

Since $\boldsymbol{\varphi}^{(m)}-\hat{\varphi}_{CPE}^{(m)}$ has heavily decreasing low-pass spectrum, it has almost all of its power at very low frequencies. Thus by taking argument (denoted by arg-function) and filtering the signal with a highly selective low-pass filter (denoted by LPF-function), we obtain phase noise estimate of the form

$$\hat{\boldsymbol{\varphi}}_{est}^{(m)} = \mathrm{LPF}\left\{\arg\left(\boldsymbol{\vartheta}^{(m)}\right)\right\} \approx \arg\left\{\mathrm{LPF}\left(\boldsymbol{\vartheta}^{(m)}\right)\right\} \approx \boldsymbol{\varphi}^{(m)}-\hat{\varphi}_{CPE}^{(m)} . \quad (10)$$

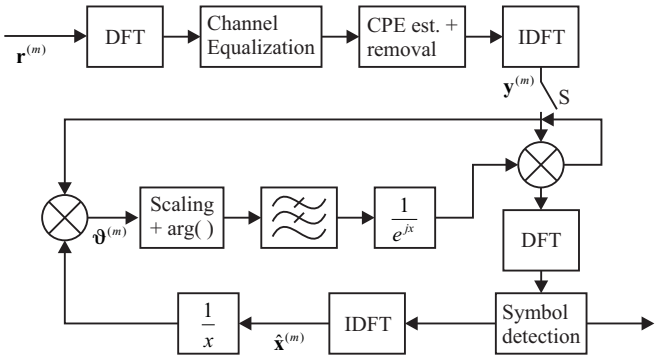

Fig. 1. The overall algorithm described in a block diagram to ease up the implementation. The vectors written in the diagram correspond to vectors with the same names in the equations. Variables x in block markings denote the input signal for the corresponding block. Switch S is connected only for the first iteration.

Due to the fact that phase noise process and its complex exponential are both heavily low-frequency processes, there is actually no correct order to do argument and low-pass filtering tasks in (10). According to simulations, taking the argument before low-pass filtering works better in phase noise dominated systems, whereas the other order of the operations works better in additive noise dominated systems. For simplicity, from now on we consider only the case where argument operator precedes the low-pass filter.

In the first iteration, with above phase noise estimate, the actual mitigation is done by dividing the time-domain waveform $\mathbf{y}^{(m)}$ by the complex exponential of the estimated phase noise. Then, symbols are detected. In later iterations, mitigated signal, namely $\mathbf{y}^{(m)}$ after the phase noise compensation, is fed back to the algorithm input instead of using $\mathbf{y}^{(m)}$ directly, as shown in Fig. 1. The remaining phase noise is then estimated and mitigated, and symbols are detected again.

B. Performance Improvements with Scaling

It is well known that OFDM signal has a very high peak-to-average power ratio (PAPR). Because of this, when we calculate the needed time-domain OFDM signal estimate $\hat{\mathbf{x}}^{(m)}$ for the algorithm, which we use as a point-by-point denominator in (9), the errors in very low amplitude parts of $\hat{\mathbf{x}}^{(m)}$ cause relatively high errors in the corresponding result vector $\boldsymbol{\vartheta}^{(m)}$. The low amplitude samples are also more prone to errors due to AWGN. It is thus beneficial to scale the signal in some part of the estimation process so that the samples more prone to cause errors are given less weight. The scaling can be done, e.g., before the low-pass filtering in (10). This is a good stage of the estimation process for the scaling because the convolving filtering operation would spread the potential error to adjacent samples. Furthermore, even though not marked in (10), the output signal from the low-pass filter is somewhat scaled since a practical highly-selective low-pass filter drains the power of the low-pass natured signal of interest. So at the same time with this scaling, the proposed scaling operation can be also be done.

There are many ways to do the scaling. The optimal scaling

depends on the used system parameters. In this paper, we assume simple scaling with squared absolute values of the elements of $\hat{\mathbf{x}}^{(m)}$ divided by the mean power of the time-domain OFDM symbol. The latter can be easily calculated when the used OFDM system configuration is known. In addition, the filter dependent constant scaling is also taken into account at the same time. So the more practical form of (10) is then

$$\mathrm{LPF}\left\{\mathrm{diag}\left(\mathbf{q}\right)\arg\left(\mathfrak{I}^{(m)}\right)\right\} \approx \boldsymbol{\varphi}^{(m)} - \hat{\varphi}_{CPE}^{(m)} = \hat{\boldsymbol{\varphi}}_{est,q}^{(m)}, \qquad (11)$$

where $\mathbf{q}$ is the scaling vector optimized to correspond to the used filter and the used OFDM configuration. In the simulations later on in the paper, an example for $\mathbf{q}$ is given for the used filter and system parameters considered in this paper.

C. Further Thoughts on the Algorithm

The properties of the used low-pass filter have big impact on the obtained estimation performance. The filter must be optimized while keeping several things in mind. Basically to get the best possible performance, highly selective filter should be used. However, this means that a high-order filter must be used, which increases computational complexity of the overall algorithm and also increases the length of the transients on both ends of the filtered signal. There are many ways to design a highly selective filter with low computational complexity, but the transient problem cannot be averted but by lowering the selectivity of the filter. Anyway, as shown by the simulations later on this paper, very good performance is achievable, even though the transient problem remains.

One of the strengths of this algorithm is that we do not need any prior information about the phase noise in the estimation. Only an assumption of realistic phase noise process has to be made, namely the phase noise process must be heavily low-pass natured. This assumption holds for the free-running oscillator [2] but it also holds for more practical oscillators, such as oscillators using phase-locked loop (PLL) [13].

IV. Performance Simulations and Analysis

In this Section, the performance simulations are carried out and analyzed for OFDM direct-conversion link corrupted by phase noise on the transmitter and the receiver. First, the simulation parameters are given and then the performances of state-of-the-art phase noise mitigation techniques are compared to the performance of the proposed algorithm.

A. Simulation Parameters and Flow

Here, 3GPP Long Term Evolution (LTE) downlink –like OFDM communications link is simulated [14]. We use OFDM system with 1024 subcarriers and 15 kHz subcarrier spacing. Of these 1024 subcarriers, 600 are active 16QAM modulated, 300 on both sides of the centre subcarrier. Other subcarriers are zero-subcarriers. The used cyclic prefix length is 63 samples and 18 of the active subcarriers carry pilot data.

The flow of the simulations is as follows. First, 16QAM modulated symbols are generated. They are then OFDM modulated as described in (1). After this, the cyclic prefix is added, transmitter phase noise is modelled and the resulting signal is send through the communications channel. The channel is either an additive white Gaussian noise (AWGN) channel or an extended ITU-R Vehicular A (VEHA) multipath channel [15] depending on the studied case. In the VEHA case, the channel realizations are independent of each other. After going through the channel, the signal is impaired by the receiver phase noise, cyclic prefix is then removed and the resulting signal is OFDM demodulated. The transmitter and receiver phase noises are independent processes but for easier presentation of the results, they have the same 3 dB bandwidth (β) values. Actual β values reported in the figures below, are the sums of the individual transmitter and receiver β values, namely the total link phase noise.

In the actual impairment mitigation at the receiver, the channel is assumed to be known and it is compensated after the OFDM demodulation. After this, the CPE is estimated and mitigated with very simple least squares and pilot based approach described in [7] and [10]. Now, the phase noise mitigation algorithms to mitigate the ICI part of the phase noise are implemented. We use algorithms proposed in [4] (Petrovic), [9] (Bittner) and [10] (LI-TE) in addition to the proposed technique. Finally, the enhanced signals are detected and symbol-error rates (SER) are computed.

Parameters for the reference phase noise algorithms are the same that were used in [10], namely empirically optimized. For the proposed algorithm, parameters are as follows. For the low-pass filter, we use a selective filter of order 200 for the AWGN case and a filter of order 350 for the VEHA case. Both are designed using the well-known Remez algorithm. This is not the best way to design the filter, but the actual design and optimization are not on the scope of this paper and are left for another study. Prior to low-pass filter, we use a scaling vector

$$\mathbf{q} = \frac{\sqrt{2}\left|\hat{\mathbf{x}}^{(m)}\right|^2}{N_a / N}, \qquad (12)$$

where N_a is the number of active subcarriers and N is the total number of subcarriers, namely N_a / N is the expected signal power of $\hat{\mathbf{x}}^{(m)}$. $\left|\hat{\mathbf{x}}^{(m)}\right|^2$ is a vector of squared absolute values of elements of $\hat{\mathbf{x}}^{(m)}$. This scaling assumes that the channel response is normalized to unity, which in practice can be achieved, e.g., with receiver power control. This scaling is good because it gives exponentially less stress on very low-amplitude signal values of the $\hat{\mathbf{x}}^{(m)}$, so the most noisy components of the phase noise estimate are given less weight, as explained earlier.

B. Simulation Results and Performance Analysis

1) Performance of the proposed algorithm

The simulation results for the additive white Gaussian noise channel case for all the studied mitigation techniques are depicted in Fig. 2 and Fig. 3. For Petrovic [4], Bittner [9], LI-TE [10] and the proposed technique, three iterations are used. As depicted in the Fig. 2, the proposed technique clearly

outperforms the competition over the whole studied phase noise 3-dB bandwidth region from 0 to 1500 Hz with a fixed SNR of 18 dB. The same conclusions can be made from Fig. 3, in case of fixed β of 350 Hz over the received SNR region from 0 to 30 dB. The proposed technique actually gives almost ideal performance up until 17 dB of received SNR, and then starts to floor. However, the floor is significantly lower than the floor of the reference techniques.

In the more challenging case of extended ITU-R Vehicular A multipath channel, the performance differences change a little as can be seen from Fig. 4 and Fig. 5. As Fig. 4 shows, when system performance is capped by low effective SNR and not by the high phase noise, namely when the phase noise level in the system is very small, the proposed technique cannot reach the performance of the LI-TE. However, the performance differences in such cases are hardly visible, and after β of 200 Hz, the scales are turned for the advantage of the proposed technique. After β of 350 Hz, the proposed technique already outperforms the reference techniques clearly up until the end of the studied region at 1500 Hz. With higher SNR values the proposed technique performs much better also with very low phase noise 3-dB bandwidths as the additive noise is not the dominating noise source in the system. The AWGN case gave a good example of this. From Fig. 5, we can see that when we have fixed β of 350 Hz, the proposed technique outperforms the competitors already after received SNR of 10 dB, and gives very nice performance up until the end of the studied region at 40 dB of received SNR.

Overall, the proposed technique performs very well, and only suffers from very bad noise conditions. In such cases the performance differences are however almost unnoticeable between the studied techniques. Furthermore, in very low-SNR conditions, all the techniques almost achieve the no phase noise performance limit, so the phase noise is indeed dominated by the additive noise.

2) Iterative performance of the proposed algorithm

Fig. 6 and Fig. 7 demonstrate how the proposed technique scales up with the increased number of iterations. The scaling of the proposed technique is compared to the best performing reference technique, LI-TE. As depicted in Fig. 6, already two iterations of the proposed technique outperform five iterations of LI-TE technique. Furthermore, the scalability of the proposed technique stays high even with higher number of iterations. There is a clear performance gain in higher β region when comparing the five and eight iterations cases. The same conclusions can be drawn from Fig. 7, where fixed β of 350 Hz is used and simulations are run over the SNR region.

V. Conclusions

OFDM transceivers suffer heavily from phase noise. We proposed a new phase noise mitigation algorithm to address this problem taking into account both the transmitter and receiver phase noise sources. In the proposed algorithm, time-domain estimation of the phase noise is done by exploiting the steep low-pass natured spectrum of the phase noise process in

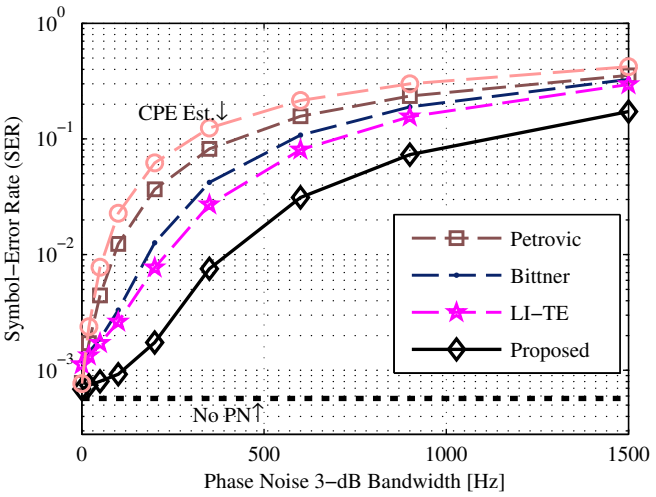

Fig. 2. Simulated SER as a function of β. AWGN channel is used with fixed received SNR of 18 dB.

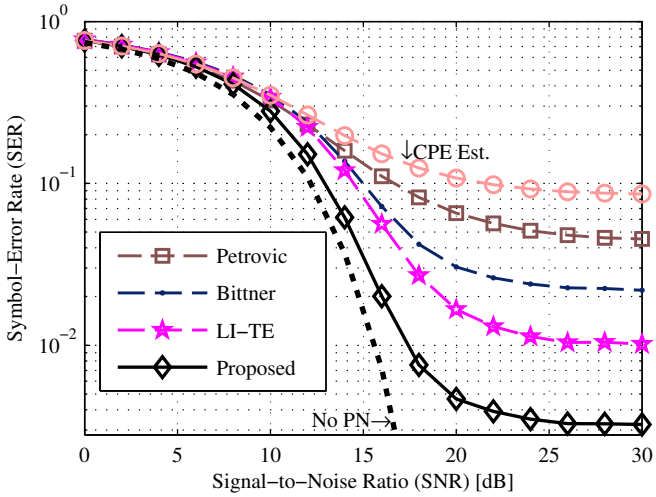

Fig. 3. Simulated SER as a function of received SNR in AWGN channel. Fixed β of 350 Hz is used.

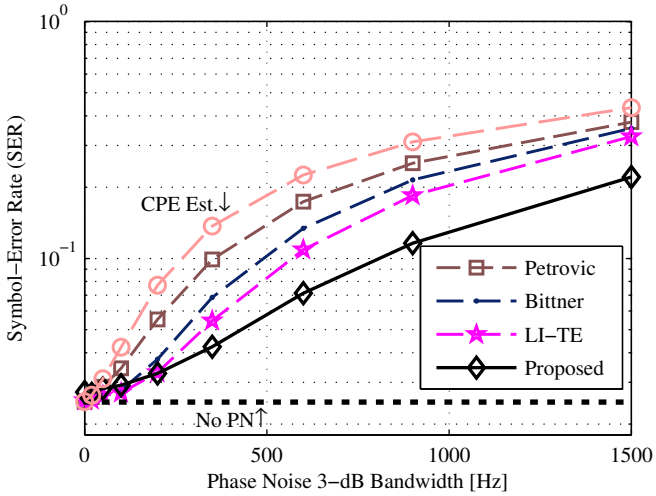

Fig. 4. Simulated SER as a function of β. Extended ITU-R Vehicular A multipath channel is used with fixed received SNR of 24 dB.

iterative manner using also the initial symbol decisions. This allowed accurate estimation of the phase noise without any prior knowledge of the statistics of the phase noise process. The performance of the algorithm was compared to the performances of the state-of-the-art phase noise mitigation techniques from the literature. The performance of the proposed algorithm was very good. It outperformed the reference methods in additive white Gaussian noise channel case as well as in extended ITU-R Vehicular A multipath channel case.

REFERENCES

[1] G. Fettweis, "Dirty-RF: A new paradigm", in *Proc. 16th International Symposium on Personal, Indoor and Mobile Radio Communications 2005 (PIMRC'05)*, Berlin, Germany, September 2005, pp. 2347-2355, Vol. 4.

[2] T. Schenk, *RF Impairments in Multiple Antenna OFDM: Influence and Mitigation*, PhD dissertation, Technische Universiteit Eindhoven, 2006, 291 p. ISBN 90-386-1913-8

[3] P. Robertson, and S. Kaiser, "Analysis of the effects of phase-noise in orthogonal frequency division multiplex (OFDM) systems," in *Proc. IEEE International Conference on Communications 1995 (ICC'95), Seattle, WA*, June 1995, pp. 1652-1657, Vol. 3.

[4] D. Petrovic , W. Rave, and G. Fettweis, "Effects of phase noise on OFDM systems with and without PLL: characterization and compensation," *IEEE Transactions on Communications*, Vol. 55, No. 8, pp. 1607-1616, August 2007.

[5] L. Tomba, "On the effect of Wiener phase noise in OFDM systems," *IEEE Transactions on Communications*, Vol. 46, No. 5, pp. 580-583, May 1998.

[6] M. Krondorf, S. Bittner, and G. Fettweis, "Numerical performance evaluation for OFDM systems affected by phase noise and channel estimation errors," in *Proc. Vehicular Technology Conference 2008 (VTC'08-Fall)*, Calgary, Canada, September 2008.

[7] S. Wu, and Y. Bar-Ness, "OFDM systems in the presence of phase noise: consequences and solutions," *IEEE Transactions on Communications*, Vol. 52, No. 11, pp. 1988-1997, November 2004.

[8] S. Bittner, W. Rave, and G. Fettweis, "Joint iterative transmitter and receiver phase noise correction using soft information," in *Proc. IEEE International Conference on Communications 2007 (ICC'07)*, Glasgow, Scotland, June 2007, pp. 2847-2852

[9] S. Bittner, E. Zimmermann, and G. Fettweis, "Exploiting phase noise properties in the design of MIMO-OFDM receivers," in *Proc. IEEE Wireless Communications and Networking Conference 2008 (WCNC'08)*, Las Vegas, NV, March 2008, pp. 940-945.

[10] V. Syrjälä, M. Valkama, N. N. Tchamov, and J. Rinne, "Phase noise modelling and mitigation techniques in OFDM communications systems," in *Proc. Wireless Telecommunications Symposium 2009 (WTS'09)*, Prague, Czech Republic, April 2009.

[11] V. Syrjälä and M. Valkama, "Analysis and mitigation of phase noise and sampling jitter in OFDM radio receivers," *International Journal of Microwave and Wireless Technologies*, Vol. 2, No. 2, pp. 193-202, April 2010.

[12] A. Goldsmith, *Wireless Communication*, Cambridge University Press, 2005, 672 p. ISBN 978-0521837163.

[13] N. N. Tchamov, J. Rinne, V. Syrjälä, M. Valkama, Y. Zou, and M. Renfors, "VCO phase noise trade-offs in PLL design for DVB-T/H receivers," in *Proc. IEEE International Conference on Electronics, Circuits and Systems 2009 (ICECS'09)*, Yasmine Hammamet, Tunisia, December 2009.

[14] *E-UTRA; LTE physical layer; General description*, 3GPP TS 36.201 V9.1.0 (2010-03) Technical Specification.

[15] T. B. Sorensen, P. E. Mogersen, and F. Frederiksen, "Extension of the ITU channel models for wideband (OFDM) systems," in Proc. IEEE Vehicular Technology Conference 2005 (VTC'05-Fall), Dallas, TX, September 2005, pp. 392-396.

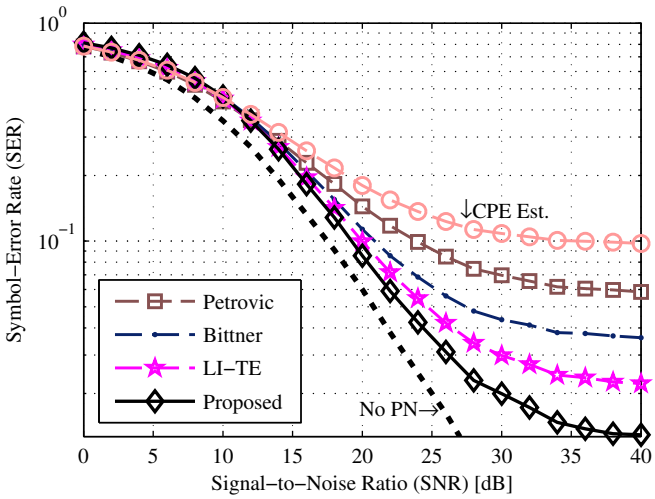

Fig. 5. Simulated SER as a function of SNR in extended ITU-R Vehicular A multipath channel. Fixed β of 350 Hz is used.

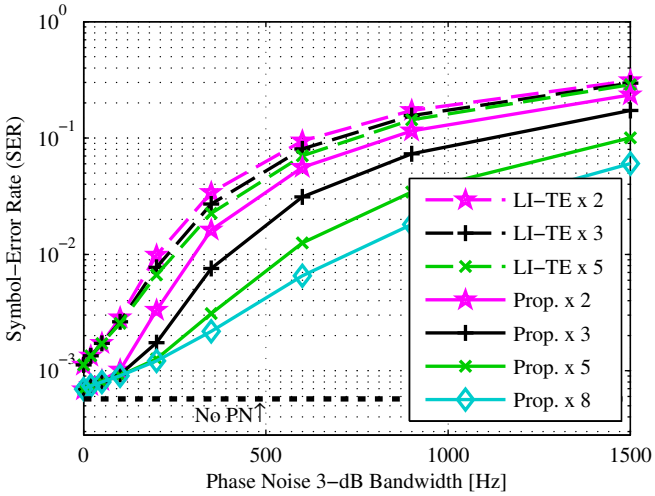

Fig. 6. Simulated SER as a function of β for different levels of iteration for the proposed technique and the best performing reference technique. AWGN channel with fixed received SNR of 18 dB is used.

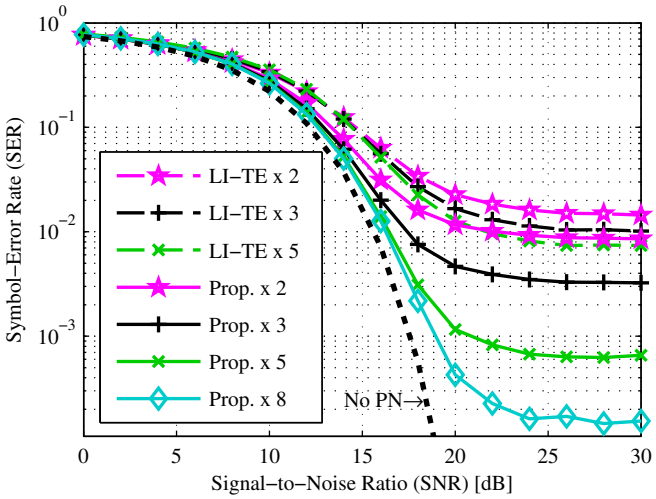

Fig. 7. Simulated SER as a function of received SNR for different levels of iteration for the proposed technique and the best performing reference technique. Fixed β of 350 Hz is used.

Publication 8

N. N. Tchamov, V. Syrjälä, J. Rinne, M. Valkama, Y. Zou, and M. Renfors, "System- and circuit-level optimization of PLL designs for DVB-T/H receivers", ***Analog Integrated Circuits and Signal Processing Journal*****, January 2012, 10.1007/s10470-011-9823-2.**

Analog Integr Circ Sig Process
DOI 10.1007/s10470-011-9823-2

System- and circuit-level optimization of PLL designs for DVB-T/H receivers

Nikolay N. Tchamov · Ville Syrjälä · Jukka Rinne · Mikko Valkama · Yaning Zou · Markku Renfors

Received: 8 January 2011 / Revised: 2 November 2011 / Accepted: 16 December 2011

Abstract This article proposes a framework for the optimization of voltage-controlled oscillator (VCO) designs in frequency synthesizers for digital video broadcasting – terrestrial/handheld (DVB-T/H) receivers. Linear time-invariant phase-domain model of a charge-pump phase-locked loop (PLL) is devised and includes both flicker (1/*f*) and thermal noise contributions from the loop oscillators. By modeling the entire receiver, it is shown that there are combinations of flicker and thermal noise contributions that result in a constant sum of inter-carrier interference (ICI) and adjacent channel interference, and constant symbol error rate as well. Consequently, optimization of the VCO phase noise spectrum is defined while maintaining the standard-specified symbol-error rate. Link-level performance evaluation is carried out to validate the stipulated trade-off. The effect of ICI mitigation schemes is discussed. Circuit-level VCO design approaches utilizing the derived trade-off are finally presented. The proposed optimization procedure is generic and is also applicable to other systems based on Orthogonal Frequency-Division Multiplexing.

Keywords Phase noise · DVB-T · DVB-H · PLL · VCO · Inter-carrier interference · Adjacent channel interference

1 Introduction

Digital video broadcasting – terrestrial/handheld (DVB-T/H) [1, 2] systems rely on orthogonal frequency-division multiplexing (OFDM) transmission to provide efficient means for high data rates in severe multipath environments. Cyclic prefix (CP) extends the OFDM symbol duration and ensures no inter-symbol interference (ISI) in multipath channels. Adversely, the frequency-synthesizer-related carrier frequency offset and phase noise (PN) give rise to common phase error (CPE) and inter-carrier interference (ICI) [3] that can significantly impair the terminal and link performance. Additionally, in the presence of adjacent channel signals [2, 4, 5], PN also causes the energy of the adjacent channels to leak on top of the desired signal band, thus creating increased in-band interference levels.

Design guidelines for optimal voltage-controlled oscillator (VCO) implementations in phase-locked loops (PLL) are critical for the minimization of ICI, CPE, and meeting the stringent requirements for adjacent channel interference (ACI) as specified in the Mobile DVB-T/H Selectivity Test Patterns S1 and S2 [2, 4, 5]. Given these constraints, both optimal RF circuit design techniques and baseband mitigation of phase-noise-induced impairments play an important role in ensuring a robust integrated design optimizing both cost and power consumption. More importantly, the joint optimization of RF circuit performance and baseband signal processing with respect to power consumption can achieve conforming and affordable devices [6–9].

From integration point of view, DVB-T/H terminals are desirably integrated in deep sub-micron CMOS processes, allowing for low cost and the co-existence of RF and baseband modules. Adversely, inexpensive CMOS PLL implementations are characterized by low-quality passive components and significant levels of intrinsic flicker noise from the active CMOS devices [10, 11]. Flicker noise contributions to PLL PN are often visible above the PLL bandwidth and deteriorate the system performance [12].

N. N. Tchamov (✉) · V. Syrjälä · J. Rinne · M. Valkama · Y. Zou · M. Renfors
Department of Communications Engineering, Tampere University of Technology, Tampere, Finland
e-mail: nikolay.n.tchamov@tut.fi

Published online: 14 January 2012

In order to derive practical guidelines for PLL design in CMOS and to complement OFDM charge-pump PLL (CHPLL) studies in the presence of thermal (white) noise [13], this paper uses a linear time-invariant (LTI) phase-domain PLL model [14], to include also the flicker (1/*f*) noise sources in the loop [15, 16]. In this work we propose to use system-level performance evaluation for obtaining a beneficial trade-off entailing the balance of flicker and thermal noise from the VCO of the CHPLL. System symbol error rate (SER) is evaluated in the presence of ACI, when the mobile and portable DVB-T/H radio access interface specification (MBRAI) PN mask [2, 4, 5] is utilized. This mask specifies the largest allowable PN levels as a function of frequency offset from the carrier and, accordingly, provides the lowest allowable SER for the system. Sets of compliance masks for VCO PN are then derived to abide by the MBRAI-conforming SER, while not necessarily obeying the MBRAI mask at all offsets. The obtained PN mask sets provide a trade-off between flicker and thermal noise specifications. This trade-off is also further demonstrated through analytical closed-form signal-to-interference-ratio analysis quantifying the total amount of PN distortion in the presence of adjacent channels for arbitrary PN spectral shape. Thus, in contrast to existing studies, e.g., [17], we do not assume flat PN power spectral density (PSD) across adjacent system channels, which is known to result in sub-carrier-independent interference due to ACI. Utilizing practical CHPLL PN PSDs, an additional degree of freedom is provided for the optimization of receiver-side frequency synthesizers. Link performance evaluation of the CHPLL with flicker noise in the DVB-T/H systems context validates the stipulated trade-off.

The paper is organized as follows. Sect. 2 of this paper discusses the utilized PN models for free-running (FR) oscillators and CHPLLs. Sect. 3 describes the system-level PN aspects, analyzes ACI in closed-form, and discusses several baseband methods for CPE and ICI mitigation that facilitate trade-offs in VCO design. In Sect. 4, the VCO trade-off between flicker and thermal noise components is addressed in detail from system-level performance point of view. Practical circuit design techniques for employing the trade-off are discussed in Sect. 5.

2 CHPLL noise modelling

We begin by summarizing the state-of-the-art in the modeling of FR oscillator PN with thermal and flicker [15, 16] noise perturbations. Then, the CHPLL model [14] utilized in this paper, including flicker noise is also described and compared to other existing models.

2.1 FR oscillators: thermal and 1/*f*-noise

The baseband equivalent of a FR oscillator can be defined as $A_{\mathrm{osc,bb}}(t) = e^{j\phi(t)}$, where $\phi(t)$ is the oscillator excess phase. The excess phase PSD, $S_\Phi(f)$, is approximately equal to the single-sideband (SSB) ratio of the oscillator, $L(f)$, specified in dBc/Hz, for frequency offsets much larger than the Lorentzian corner frequency $\Delta f_{3\mathrm{dB}}$ of the PN process [15]:

$$L(f) = 10\log_{10}\left(\frac{f_c^2(c_w + c_{fl}S_{fl}(f))}{\pi^2 f_c^4 (c_w + c_{fl}S_{fl}(f))^2 + f^2}\right). \tag{1}$$

Here f_c is the carrier frequency, the frequency-independent coefficients c_w and c_{fl} scale thermal (white) and flicker noise contributions, respectively. Flicker noise is described as a stationary process with PSD $S_{fl}(f)$ of the form [15]:

$$S_{fl}(f) \quad = \frac{1}{|f|} - \frac{4}{2\pi f} tan^{-1}\left(\frac{\gamma_c}{2\pi f}\right), \tag{2}$$

where γ_c is the 'deviation frequency' from the flicker PSD 1/*f* slope. Coefficients c_w, c_{fl}, and γ_c are sufficient to describe a complete oscillator PSD in the presence of thermal and flicker noise.

We then derive the first two coefficients from two single-point SSB measurements $L(f_w)$ and $L(f_{fl})$ at offsets much larger than the Lorentzian corner $\Delta f_{3\mathrm{dB}}$ [15] and in the well defined regions of -20 and -30 dB/dec slopes, respectively as:

$$c_{fl} = \frac{f_w - f_{fl}}{f_w f_{fl}}\left[\left(\frac{f_{fl}^2}{f_c^2}\right)10^{\frac{L(f_{fl})}{10}} - \left(\frac{f_w^2}{f_c^2}\right)10^{\frac{L(f_w)}{10}}\right], \tag{3}$$

$$c_w = \frac{1}{f_{fl} - f_w}\left[\left(\frac{f_{fl}^3}{f_c^2}\right)10^{\frac{L(f_{fl})}{10}} - \left(\frac{f_w^3}{f_c^2}\right)10^{\frac{L(f_w)}{10}}\right]. \tag{4}$$

The use of spot SSB ratio measurements provides directly usable circuit-design specifications, whereas PN bandwidth $\Delta f_{3\mathrm{dB}}$ [13, 15] is not readily available in circuit simulators. To complete the description of the entire VCO PSD, knowledge of the 'deviation' frequency has to be obtained as well. Without the use of a circuit simulator, this is possible by solving for $\int_{-\infty}^{+\infty} 10^{L(f)/10} df = 1$. With Eq. 1, a closed-form solution of the integral is not possible, thus numerical methods have to be used.

In the presence of thermal noise perturbations only, the excess phase variance of the FR oscillator [15] is linearly increasing with time *t*:

$$\sigma_\phi^2(t) = (2\pi f_c)^2 c_w t \tag{5}$$

which in the next sub-section will be shown to saturate when the VCO is enclosed in the PLL loop.

2.2 CHPLL PN model in the presence of thermal and flicker noise – LTI phase-domain approach

A PLL loop compares the phases of the VCO and the reference oscillator (RO) and minimizes their difference. A schematic representation and the LTI phase-domain model of a 3rd-order CHPLL are shown in Fig. 1 along with the noise sources from the loop components.

In Fig. 1, LF is the loop filter with a transfer function:

$$H_{\mathrm{LF}}(f) = \frac{1 + j2\pi f R C_s}{j2\pi f\left(C_{\mathrm{s}} + C_{\mathrm{p}} + j2\pi f R C_{\mathrm{p}} C_{\mathrm{s}}\right)}, \tag{6}$$

where $1/M$ and $1/D$ represent the integer frequency dividers for the RO and VCO, respectively, CHP is the charge-pump with transfer function $H_{\mathrm{CP}}(f) = I_{\mathrm{p}}/(2\pi)$, and $\phi_{\mathrm{buffering}}$ is the noise of the PLL output buffering. The noise transfer functions are derived following [14, 16], and an example plot for the transfer functions for the RO phase and VCO phase is given in Fig. 2. We note that the VCO phase undergoes a high-pass, while the RO phase undergoes and low-pass and amplified response, as shown in Fig. 2, to the PLL output:

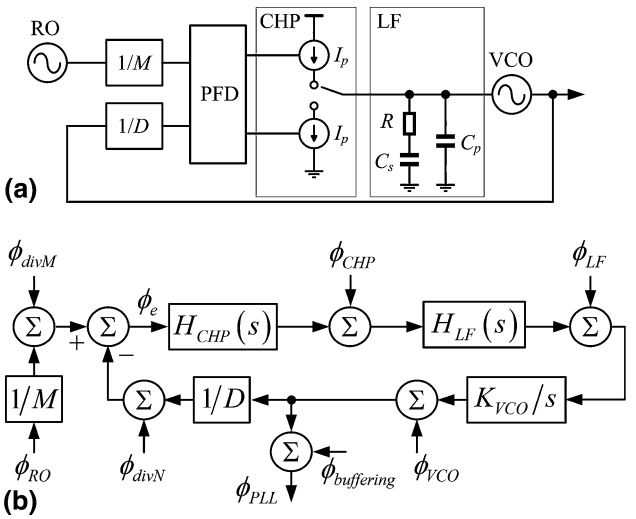

Fig. 1 CHPLL – schematic (**a**), LTI phase-domain model (**b**)

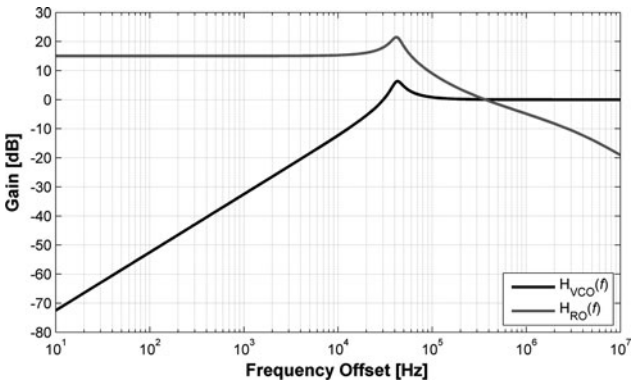

Fig. 2 Example loop transfer functions for the VCO and RO excess phase

$$H_{\mathrm{VCO}}(f) = \frac{\Phi_{\mathrm{PLL}}(f)}{\Phi_{\mathrm{VCO}}(f)} = \frac{j2\pi f D}{j2\pi f D + I_{\mathrm{p}} K_{\mathrm{VCO}} H_{\mathrm{LF}}(f)}, \tag{7}$$

$$H_{\mathrm{RO}}(f) = \frac{\Phi_{\mathrm{PLL}}(f)}{\Phi_{\mathrm{RO}}(f)} = \frac{D I_{\mathrm{p}} K_{\mathrm{VCO}} H_{\mathrm{LF}}(f)}{M\left(j2\pi f D + I_{\mathrm{p}} K_{\mathrm{VCO}} H_{\mathrm{LF}}(f)\right)}. \tag{8}$$

As the proposed work aims at analyzing the PN effects of the RO and VCO alone, we assume these and the output buffering as the only noisy components in the model. In accordance to the LTI phase domain model, the CHPLL output PSD is then given as:

$$\begin{aligned} S_{\Phi,\mathrm{out}}(f) &= |H_{\mathrm{VCO}}(f)|^2 S_{\Phi,\mathrm{VCO}}(f) \\ &+ |H_{\mathrm{RO}}(f)|^2 S_{\Phi,\mathrm{RO}}(f) + S_{\Phi,\mathrm{buffering}}(f) \end{aligned} \tag{9}$$

where $S_{\Phi,\ \mathrm{VCO}}(f)$ and $S_{\Phi,\ \mathrm{RO}}(f)$ are obtained through Eq. 1. The variance of the excess phase at the output of the CHPLL [16] as a function of accumulation time T, as attributed to the VCO and RO separately is given by:

$$\sigma^2_{\phi,\mathrm{VCO}}(T) = \int_{-\infty}^{+\infty} \frac{|H_{\mathrm{VCO}}(f)|^2 \sin(\pi f T)^2 4\pi^2 k_{\mathrm{VCO}} c_{\mathrm{w,VCO}}}{(\pi f)^2} df, \tag{10}$$

$$\sigma^2_{\phi,\mathrm{RO}}(T) = \int_{-\infty}^{+\infty} \frac{|H_{\mathrm{RO}}(f)|^2 \sin(\pi f T)^2 4\pi^2 k_{\mathrm{RO}} c_{\mathrm{w,RO}}}{(\pi f)^2} df. \tag{11}$$

The variance of the excess phase at the output of the CHPLL from Eqs. 10–11 saturates after one PLL loop time constant [16], unlike the FR oscillator phase variance in Eq. 5. In Fig. 3 we show two cases – one for flicker noise being dominant and one for thermal noise being dominant.

Other methods for CHPLL modeling were also taken into consideration. The work in [13] utilizes a stochastic differential equation model of a CHPLL [18] for a performance study of OFDM systems in the presence of PN, which unlike the approach used in this article, can take into account noise folding in the loop. While being more accurate, it has been established that it does not accommodate the effects of flicker noise and thus is unsuitable for the purposes of our study.

2.3 Example CHPLL design for DVB-T/H performance evaluation

The LTI phase-domain CHPLL model above is next utilized to implement an example CHPLL design for evaluation of the effect of flicker noise in the VCO on the link performance of a DVB-T/H receiver. In this paper we roughly follow the CHPLL designs targeting DVB

receivers in [4, 5, 19] and set the PLL bandwidth to approximately 30 kHz. The CHPLL parameters used in our work are $R = 2\ \text{k}\Omega$, $C_\text{s} = 400$ pF, $C_\text{p} = 20$ pF, $f_\text{c} = 806$ MHz, $M = 1$, $D = 32$, and $I_\text{p} = 79\ \mu\text{A}$. Stability was verified through the linearized sampled analysis presented in [14]. We assume flat noise PSD for the VCO buffer and divider-by-D.

A sample plot of a CHPLL PSD with a divider-by-D, VCO buffering and thermal-noise-only RO and VCO contributions can be found in Fig. 4. The point SSB measurements for the RO and the VCO are $L_\text{RO}(1\ \text{MHz}) = -160$ dBc/Hz and $L_{VCO}(1\ \text{MHz}) = -130$ dBc/Hz, respectively; the noise

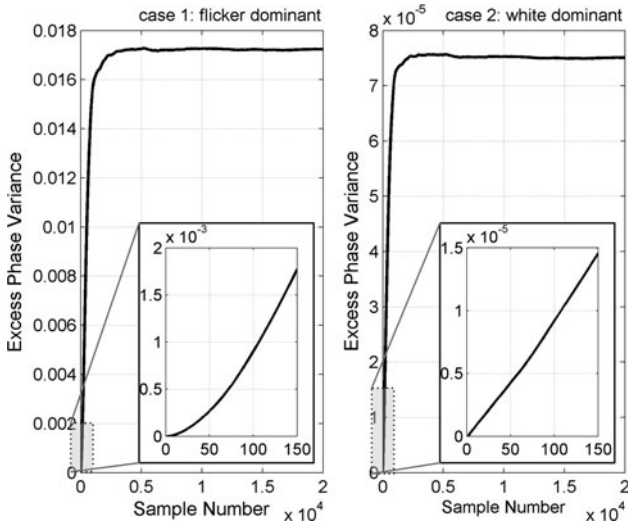

Fig. 3 CHPLL variance versus time for a given PLL design: (*left*) VCO flicker noise is dominant over thermal noise, (*right*)—VCO thermal noise dominant over flicker noise

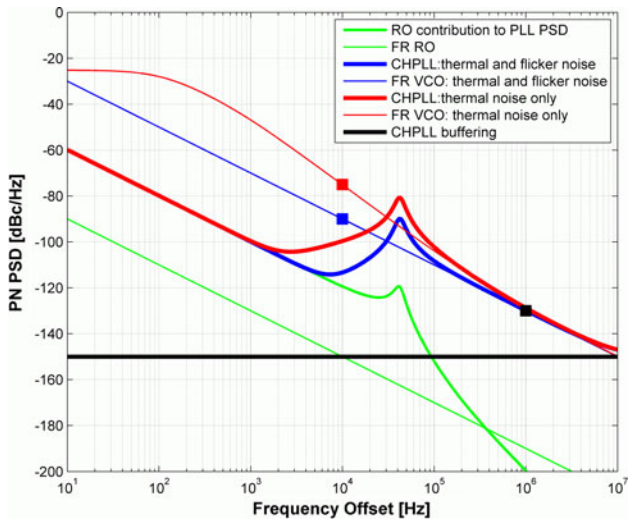

Fig. 4 CHPLL PSD with and without flicker noise, markers specify the varied values of $L_\text{VCO}(10\ \text{kHz})$ and $L_\text{VCO}(1\ \text{MHz})$

PSD of the VCO buffering and divide-by-D circuit are at levels -150 and -155 dBc/Hz, respectively. The PSDs of the FR RO and VCO are also shown for reference.

Next, we add flicker noise contributions expected within the VCO implementations in CMOS. Utilizing $L_\text{VCO}(10\ \text{kHz}) = -75$ dBc/Hz in Eqs. 3 and 4, we plot the CHPLL PSD in Fig. 4 to underline the significant augmentation of the PSD after adding flicker noise. The plots suggest that neglecting VCO flicker noise [13] would yield inadequate expectations for OFDM system performance in a realistic CMOS design. The measurement results in [4] also display a near -30 dB/dec slope outside the PLL bandwidth, thus signifying the strong presence of flicker noise in the VCO.

2.4 Implementation of the proposed CHPLL model

Implementation of the CHPLL model and subsequent DVB-T/H receiver performance evaluation are carried out in the Matlab [20] environment. In the simulations, the proposed PLL model is implemented through the generation of the PLL excess phase $\phi(n)$. White Gaussian noise is multiplied in frequency domain by the CHPLL PSD mask in Fig. 3, and is then transformed into time domain excess phase series. For this to be valid, we thus assume $S_\Phi(f) \cong L(f)$. The assumption is considered valid for frequencies much larger than the respective oscillators' bandwidths Δf_3dB [15, 16]. To justify this constraint, we will separately look into the RO and VCO contributions to the output PLL PSD. The RO is usually of high quality (small $c_\text{w,RO}$) which translates to a very small bandwidth $\Delta f_\text{3dB} = \pi f_\text{w}^2 10^{L(f_\text{w})/10} = 314\ \mu\text{Hz}$. This very small bandwidth justifies $S_\Phi(f) \cong L(f)$ in the case of the RO. The VCO contributions, on the other hand, are visible at the PLL output at frequency offsets higher than the PLL bandwidth. With PLL_BW in the order of 30 kHz, taking VCOs of $L(f_\text{w}) = -140\ldots-110$ dBc/Hz at $f_\text{w} = 10$ MHz, we obtain corner frequencies $\Delta f_\text{3dB,VCO}$ of 1.98 and 314.16 Hz, respectively. Thus, the generation method satisfies $S_\Phi(f) \cong L(f)$ since $\Delta f_\text{3dB,VCO} << PLL_\text{BW}$.

3 DVB-T/H system modelling and receiver-side methods for CPE and ICI mitigation

3.1 System overview

The testbench for the proposed CHPLL model is based on the DVB-T/H systems specifications [1, 2]. The raw SER at the de-mapper is observed. The block diagram of the implemented system is shown in Fig. 5. The employed CHPLL is shown in the shaded part of Fig. 5. Two interfering adjacent channels are added, with levels 37 dB higher than the desired one, emulating the MBRAI S1 Selectivity

Pattern [2, 4, 5]. In the system, $S \in \{2048, 4096, 8192\}$ orthogonal sub-carriers span the system bandwidth $W = 8$ MHz, with sub-carrier spacing $W/S \in \{4464, 2232, 1116\}$ Hz, respectively. CP extends cyclically the OFDM symbol and thus makes it possible to avoid ISI. Zero data carriers form two frequency guard bands for reducing ACI. In the experiments, the static DVB-T F_1 channel [1] is used.

Assuming no frequency and timing offsets, the received samples within the mth OFDM symbol duration are:

$$r_{\mathrm{n}}(m) = [x_{\mathrm{n}}(m) \otimes h_{\mathrm{n}}(m) + \eta_{\mathrm{n}}(m) + \xi_{\mathrm{n}}(m)]e^{j\phi_{\mathrm{n}}(m)} \tag{12}$$

where $\otimes$ denotes circular convolution, $x_{\mathrm{n}}(m)$, $h_{\mathrm{n}}(m)$, $\xi_{\mathrm{n}}(m)$, $\eta_{\mathrm{n}}(m)$, and $\phi_{\mathrm{n}}(m)$ are the transmitted signal, the channel impulse response, additive white Gaussian noise (AWGN), ACI, and excess phase (PN). AWGN has been added after observing the signal power in the whole desired band, thus all sub-carriers are not having the same signal-to-noise ratio (SNR) due to the selectivity of the F_1 channel.

In the following, we observe a bandwidth of 3 W to account for 2 channels adjacent to the desired channel, with sub-carrier indices as follows: $-N/2$ to α for the left adjacent channel, α to β for the desired, and the right-adjacent from β to $N/2-1$. Then the received signal within the band of interest after receiver filtering, CP removal, and FFT, in frequency-domain at the kth sub-carrier and mth OFDM symbol interval is then:

$$\left.\begin{aligned} R_{\mathrm{k}}(m) = {} & X_{\mathrm{k}}(m)H_{\mathrm{k}}(m)J_0(m) \\ & + \sum_{\mathrm{l}=\alpha,\, \mathrm{l}\neq \mathrm{k}}^{\beta} X_{\mathrm{l}}(m)H_{\mathrm{l}}(m)J_{\mathrm{k}-\mathrm{l}}(m) \\ & + \tau_{\mathrm{k}}(m) \\ & + \sum_{\mathrm{l}=-\mathrm{N}/2}^{\alpha-1} X_{\mathrm{l}}(m)H_{\mathrm{l}}(m)J_{\mathrm{k}-\mathrm{l}}(m) \\ & + \sum_{\mathrm{l}=\beta+1}^{\mathrm{N}/2-1} X_{\mathrm{l}}(m)H_{\mathrm{l}}(m)J_{\mathrm{k}-\mathrm{l}}(m) \end{aligned}\right\} \quad for\ k \in [\alpha, \beta]\,, \tag{13}$$

where the FFT coefficient of the PN process $e^{j\varphi(\mathrm{n})}$ in the mth OFDM symbol are:

$$J_{\mathrm{k}}(m) = \sum_{n=-\mathrm{N}/2}^{\mathrm{N}/2-1} e^{j\phi_n(m)} e^{-j\frac{2\pi}{N}\mathrm{nk}}. \tag{14}$$

The first term in Eq. 13 represents the transmitted data scaled by the complex channel response sampled at sub-carrier k and by the CPE term $J_0(m)$ of the mth OFDM symbol. The second term in Eq. 13 denotes the ICI degradation [3, 8, 13] due to the sub-carriers within the desired band. The third term represents the transformed AWGN. The fourth and fifth terms account for the interference coming from the two adjacent channels.

3.2 ACI analysis

The addition of ACI in the simulation environment is illustrated in Fig. 6. Two interfering adjacent channels are placed on both sides of the desired channel, at distances of one channel bandwidth F_{ch}. Upon down-conversion in the receiver, CHPLL PN is responsible for the leakage of the adjacent channels in the band of the desired channel. The MBRAI specification calls for a flat PN PSD over the adjacent channels, as shown in Fig. 7. The CHPLL PSD may not be necessarily flat immediate outside our desired channel, as suggested in Fig. 4. In such a scenario the signal-to-interference ratio (SIR), not including AWGN $\xi_{\mathrm{n}}(m)$, will be dependent on the sub-carrier index. In the following, we proceed to show both analytically and experimentally that a set of CHPLL PSDs can result in identical amounts of ICI and ACI across the desired channel bandwidth. Based on the sets of these PSDs, we will consequently derive the VCO design trade-off between flicker and thermal noise.

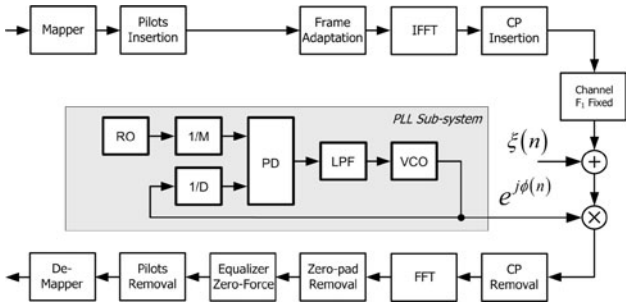

Fig. 5 System testbench for DVB-T/H systems with CHPLL

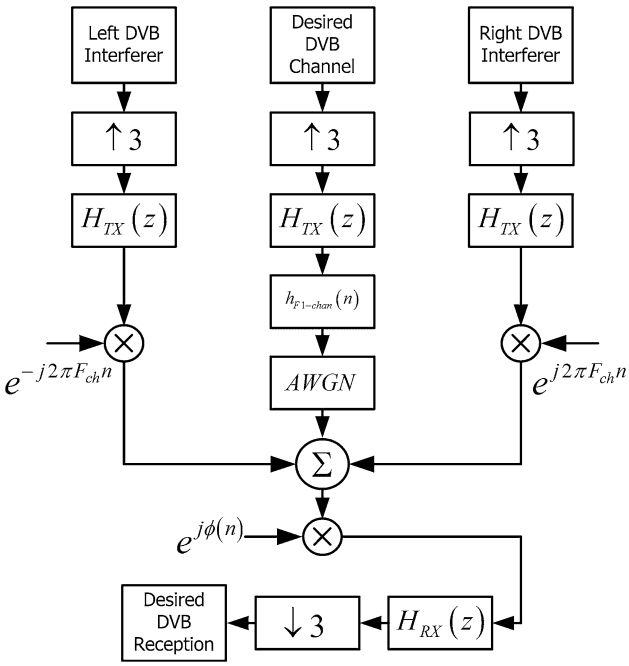

Fig. 6 System testbench with ACI

Utilizing the approach of SIR analysis due to ICI under PN in [21], we next include ACI in the model. To obtain a simplified scenario expression of the effect of ACI, we define the SIR across the desired band consisting of sub-carriers $k \in [\alpha, \beta]$ as in Eq. 15:

$$\gamma_k = \frac{E\left[|X_k(m)|^2\right] E\left[|H_k(m)|^2\right] E\left[|J_0(m)|^2\right]}{P_{ICI,k} + P_{ACI,k}} \tag{15}$$

where we have two terms:

$$\begin{aligned} P_{ICI,k} &= \sum_{l=\alpha, l\neq k}^{\beta} E\left[|X_l(m)|^2\right] E\left[|H_l(m)|^2\right] E\left[|J_{k-l}(m)|^2\right], \\ P_{ACI,k} &= \sum_{l=-N/2}^{\alpha-1} E\left[|X_l(m)|^2\right] E\left[|H_l(m)|^2\right] E\left[|J_{k-l}(m)|^2\right] + \\ &\quad \sum_{l=\beta+1}^{N/2-1} E\left[|X_l(m)|^2\right] E\left[|H_l(m)|^2\right] E\left[|J_{k-l}(m)|^2\right], \end{aligned} \tag{16}$$

accounting for the interference due to in-band ICI and for the interference from the adjacent channels, respectively. We note that in accordance to our simulation setup in Fig. 6, in Eq. 16 no additive noise is modelled for the adjacent channel interferers. Next, we assume that the adjacent channels are of fixed power σ^2_{adj}, and that the power of the desired channel transmitted subcarrier symbols are fixed at σ^2_{cur} as:

$$\begin{aligned} k \in [\alpha, \beta]: &\quad E\left[|X_k(m)|^2\right] = \sigma^2_{cur}, \\ k \in [-N/2, N/2-1] \backslash [\alpha, \beta]: &\quad E\left[|X_k(m)|^2\right] = \sigma^2_{adj}. \end{aligned} \tag{17}$$

Therefore, by following the derivations in [21], the SIR for the subcarrier k, when the average power of that subcarrier is σ^2_{cur}, can be written as:

$$\gamma_k = \frac{E\left[|J_0(m)|^2\right]}{\frac{\sigma^2_{cur}}{\sigma^2_{cur}} \sum_{l=\alpha, l\neq k}^{\beta} E\left[|J_{k-l}(m)|^2\right] + \frac{\sigma^2_{adj}}{\sigma^2_{cur}} \sum_{l=-N/2, k\notin[\alpha,\beta]}^{N/2-1} E\left[|J_{k-l}(m)|^2\right]}. \tag{18}$$

Now by simplifying the indexing of the PN dependent terms, we can write:

$$\gamma_k = \frac{E\left[|J_0(m)|^2\right]}{\sum_{l=k-\beta, l\neq k}^{k-\alpha} E\left[|J_l(m)|^2\right] + \frac{\sigma^2_{adj}}{\sigma^2_{cur}} \sum_{l=k-\alpha+1}^{k-\beta-1+N} E\left[|J_l(m)|^2\right]}. \tag{19}$$

Now the unknowns in Eq. 19 are $E\left[|J_0(m)|^2\right]$ and $E\left[|J_l(m)|^2\right]$. Following the PN expression in [21] we utilize the sub-carrier dependent scaling variables λ_k:

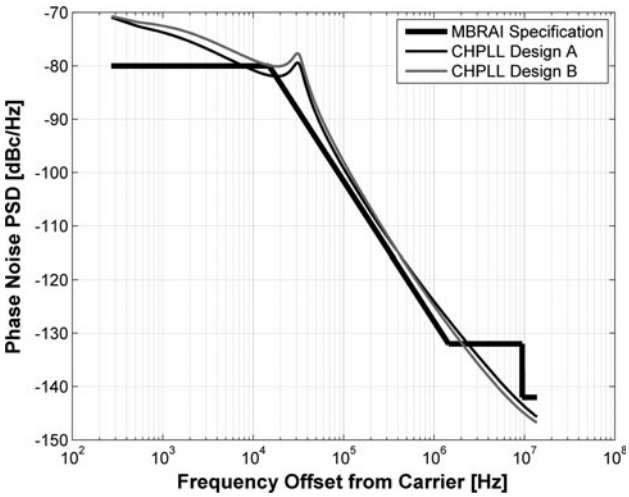

Fig. 7 CHPLL PSD comparison: MBRAI versus designs A and B

$$\begin{aligned} k = 0: &\quad \mathrm{E}\left[|J_0(m)|^2\right] \approx \frac{N^2 + \sigma^2_w \lambda^2_0}{1 + \frac{\sigma^2_w}{N^2} \sum_{k=0}^{N-1} \lambda^2_k} \\ k \neq 0: &\quad \mathrm{E}\left[|J_k(m)|^2\right] \approx \frac{\sigma^2_w \lambda^2_k}{1 + \sigma^2_\varphi} = \frac{\sigma^2_w \lambda^2_k}{1 + \frac{\sigma^2_w}{N^2} \sum_{k=0}^{N-1} \lambda^2_k}. \end{aligned} \tag{20}$$

Therefore, by using Eq. 20 we can write Eq. 19 as:

$$\gamma_k = \frac{N^2 + \sigma^2_w \lambda^2_0}{\sum_{l=k-\beta, l\neq 0}^{k-\alpha} \sigma^2_w \lambda^2_l + \frac{\sigma^2_{adj}}{\sigma^2_{cur}} \sum_{l=k-\alpha+1}^{k-\beta-1+N} \sigma^2_w \lambda^2_l}. \tag{21}$$

Finally, by using PN spectral mask values defined in [21] as $\psi^2_k = \sigma^2_w \lambda^2_k$, we have the final form for the SIR:

$$\gamma_k = \frac{N^2 + \psi^2_0}{\sum_{l=k-\beta, l\neq 0}^{k-\alpha} \psi^2_l + \frac{\sigma^2_{adj}}{\sigma^2_{cur}} \sum_{l=k-\alpha+1}^{k-\beta-1+N} \psi^2_l}. \tag{22}$$

The above derivation provides an analytical basis for an intuitive observation: several PLL PSDs, of distinct spectral mask values ψ_k can results in identical SIR and thereon receiver performance due to ICI and ACI. We also notice that unlike in [21] without adjacent channels, the SIR is now a quantity that depends on the subcarrier index k. This is logical result, because the ACI has higher effect on the symbols near the boundary of the interesting signal band. In Fig. 8 we experimentally show the SIR in the 8K DVB-T/H mode for the cases when ACI is present and absent. Clearly, as shown analytically with a realistic CHPLL and ACI present, the SIR is dependent on the sub-carrier index.

As this work aims at optimizing VCO performance within the PLL loop, we next investigate in Figs. 9 and 10 the average SIR after sweeping the values for $L(f_w)$ and

$L(f_{\mathrm{fl}})$ at $f_{\mathrm{w}} = 1$ MHz, and $f_{\mathrm{fl}} = 10$ kHz, which represent low-offset flicker noise contributions and large-offset thermal noise contributions respectively.

The results show a strong dependence on both flicker and thermal noise from the VCO in the CHPLL. As stipulated, there exist combinations of $L(f_{\mathrm{w}})$ and $L(f_{\mathrm{fl}})$ resulting in the exact same SIR. Stemming from this observation, the assumption is made that for a given SIR, these different VCO designs could also result in equivalent SER performance. Then exact matching to the MBRAI PSD mask in Fig. 7 is not a hard requirement, rather the target system SER metric is. We show in the next section that this assumption holds. Below we proceed to outline several methods in the receiver baseband that are commonly used and vital for the mitigation of the effects of CPE and ICI.

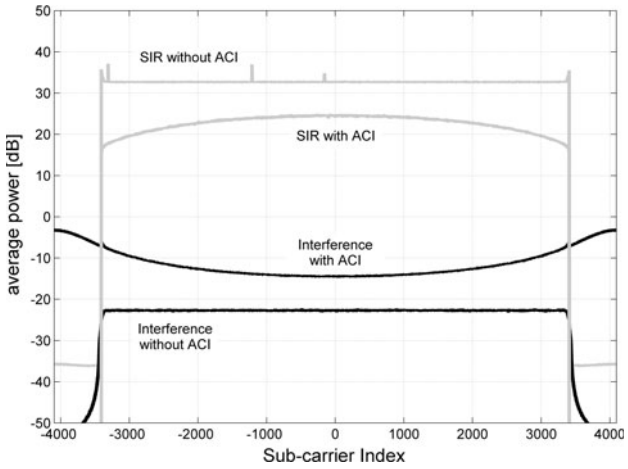

Fig. 8 8K-mode SIR with and without the presence of ACI

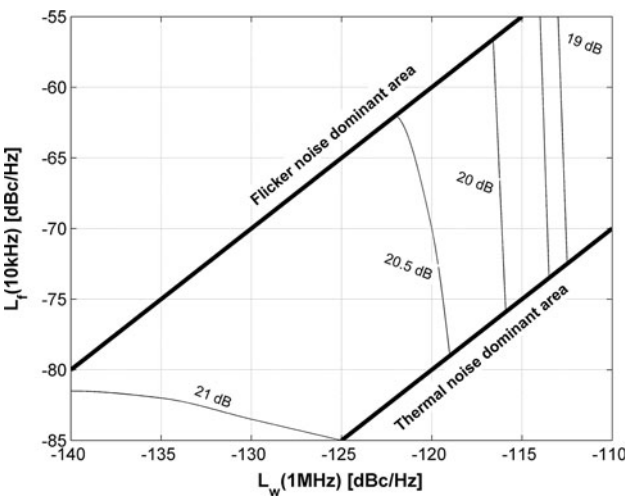

Fig. 9 Constant SIR curves with ACI, VCO thermal and flicker noise varied

3.3 Estimation and compensation of CPE, ICI, and channel

Proper receiver functioning is impossible if none of the effects of PN are mitigated, with at least CPE correction being implied in standardization and conformance documents [1, 2]. Below we summarize several algorithms for CPE and ICI mitigation that are implemented in the simulation system in order to show how much the SER can be improved in the baseband domain. This improvement will then be used to define the VCO design trade-off in the next section.

The scattered and continual pilots of the DVB standards are commonly used to estimate the effect of the channel and PN in each symbol [3, 8, 13]. Commonly, CPE and channel correction is performed using linear interpolation between pilots in each OFDM symbol. After compensation for the joint effect, ICI, ACI and AWGN are the remaining degradation. Allocation of the implemented CPE and ICI mitigation methods within the receiver is summarized in Fig. 11.

We note that the degree of SER improvement from utilization of ICI mitigation can be significantly limited by large levels of ACI as compared to ICI. This is exemplified in Fig. 12, where the ACI-to-ICI ratio is given for varied VCO flicker and thermal noise contributions. It can be noted that for very low levels of $L(f_{\mathrm{w}})$ and $L(f_{\mathrm{fl}})$, while ICI is at a minimum, the thermal noise floor from the buffering stage, Eq. 9, is introducing significantly larger amounts of ACI, thus limiting the applicability of ICI mitigation techniques. Contrary, for increased PN values, the ICI becomes more comparable to ACI and the use of ICI mitigation techniques becomes a necessity, especially given the lower SER values expected.

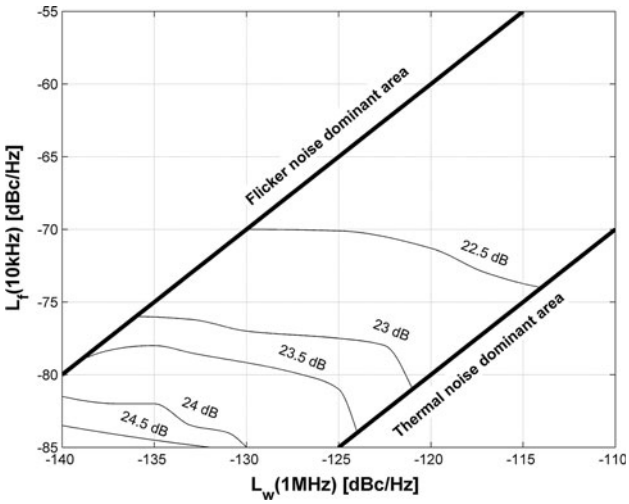

Fig. 10 Constant SIR curves without ACI, VCO thermal and flicker noise varied

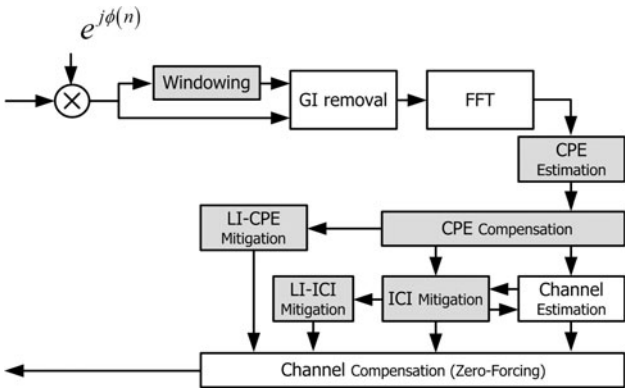

Fig. 11 Receiver blocks for CPE and ICI mitigation (*shaded*)

The estimation of ICI components J_k from Eq. 14 is performed relying on knowledge of the channel transfer function and symbol decisions after CPE compensation [13]. An advanced development of this method, linear-interpolation ICI (LI-ICI), is presented in [8] and implemented in this work. Linear interpolation of the reconstructed PN waveform around the OFDM symbol boundaries, improves the phase waveform restoration and further decreases the SER. Joint channel and ICI estimation has been addressed in [22] and in the case of LI-ICI in [23], but have not been implemented in this work. The methods rely on the LS algorithm [8], to solve for $2u + 1$ dominant ICI components as described by Eqs. 23–24:

$$\begin{bmatrix} R_{l_1}(m) \\ \vdots \\ R_{l_P}(m) \end{bmatrix} = \begin{bmatrix} A_{l_1+u}(m) & \dots & A_{l_1-u}(m) \\ \vdots & \ddots & \vdots \\ A_{l_P+u}(m) & \dots & A_{l_P-u}(m) \end{bmatrix} \begin{bmatrix} J_{-u}(m) \\ \vdots \\ J_{+u}(m) \end{bmatrix} + \boldsymbol{\chi}_m$$
$$\Leftrightarrow \quad \mathbf{R}_{m,u} = \mathbf{A}_{m,u}\mathbf{J}_{m,u} + \boldsymbol{\chi}_m \tag{23}$$

where $R_{l_k}(m)$ is the received signal at subcarrier l_k and symbol m, the term $\boldsymbol{\chi}$ accumulates AWGN, ACI, and the omitted ICI components larger than u at subcarrier indexes $\{l_1 \dots l_P\}$, and $A_{l_k}(m) = H_{l_k}(m)X_{l_k}(m)$. Solving for totally $2u + 1$ ICI components, u on each side of the CPE term, is performed as:

$$\hat{\mathbf{J}}_{m,u} = \left(\mathbf{A}^H_{m,u}\mathbf{A}_{m,u}\right)^{-1}\mathbf{A}^H_{m,u}\mathbf{R}^H_{m,u}. \tag{24}$$

Additionally, linear interpolation of the CPE (LI-CPE) estimates [8] has been considered. In Fig. 13, we show example results for the PN waveform reconstruction for three consecutive symbols using the methods described above. In the example, the benefit of using ICI component estimation is evident. In the LI-ICI method, 6% of the symbol duration on each boundary of the symbol is interpolated, using $u = 3$ for 4 iterations.

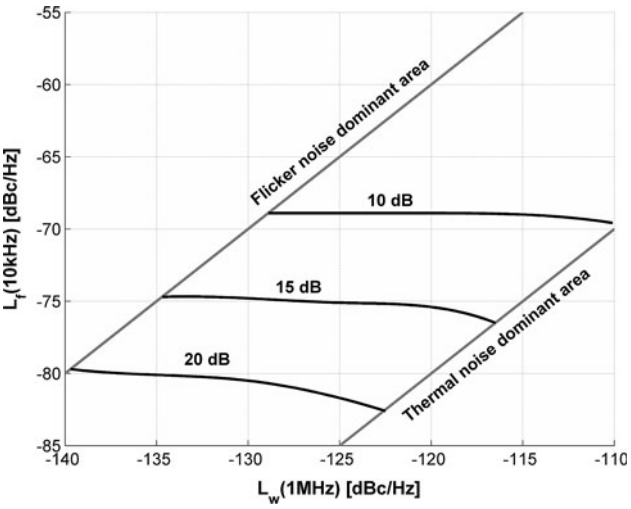

Fig. 12 ACI-to-ICI ratio with varied $L(f_w)$ and $L(f_{fl})$

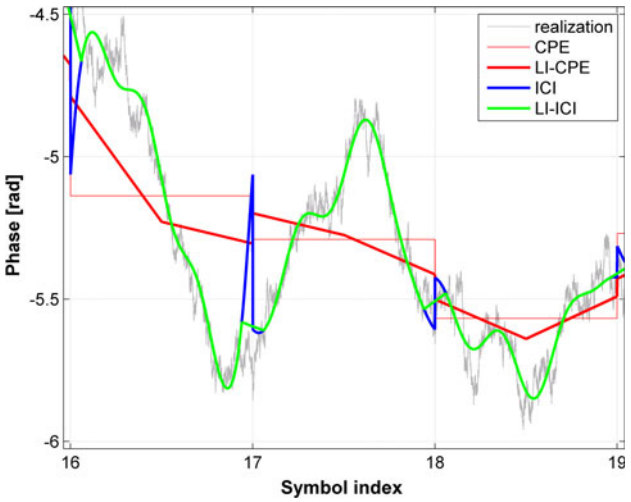

Fig. 13 Example performance of LI-CPE, ICI, and LI-ICI mitigation methods

The windowing [24] method has also been considered. While originally intended for ICI mitigation stemming from channel variations, it has been shown to provide reasonable gains for mitigation of ICI due to PN [25]. The window is specified as:

$$w(n) = \begin{cases} 0 & for \quad -N_g \le n < -N_g + K \\ 0.5 & for \quad -N_g + K \le n \le -1 \\ 1.0 & for \quad 0 \le n < N - N_g + K \\ 0.5 & for \quad N - N_g + K \le n \le N - 1 \end{cases} \tag{25}$$

where K is the channel multipath spread in samples and N_g is the CP duration in samples. The method provides good results for small channel spreads and the largest available N_g, but at the expense of decreased capacity.

4 VCO design trade-off

In the following we show that the MBRAI PN mask [2, 4] may be re-defined to suit practical CHPLL designs while still achieving the system target raw SER. This allows for a trade-off between thermal and flicker noise contributions from the VCO and also provides a degree of freedom in the circuit design stage of DVB-T/H receiver implementation. The trade-off is validated through link performance evaluation of the DVB-T/H systems.

4.1 ACI and in-band integral PN requirements

The MBRAI PN mask [2, 4] specifies the maximum allowed PN density across neighboring channels. It is defined as flat across channels at offsets 1.45 and 9.45 MHz from the outermost data sub-carrier of the desired channel, as shown in Fig. 7. As visible from the sample CHPLL in Fig. 4 and measured results in [4], PN is generally not flat across adjacent channels. As a result, the in-band SIR degradation is frequency-selective, as shown in the analysis in the Sect. 3.2. In such situation the MBRAI mask in Fig. 7 is the advisory goal, but not an absolute limit for the CHPLL PSD. The mask may thus be modified, upon ensuring that modifications comply with the raw SER measurements of the system when the MBRAI mask is substituted for simulation reference. As a second standard requirement, the integral of the in-band PN from 1 kHz to 3.8 MHz is specified to be at −33 dBc or lower [2, 4].

4.2 VCO design trade-off confirmation: flicker versus thermal noise

To empirically show that the MBRAI PN mask may be re-defined, we start by introducing two specific CHPLL designs, called A and B, with VCO parameters as marked in Fig. 7. In Fig. 14 we show that the two masks result in raw SER, with 8K mode and 16-QAM, better than the raw SER when the MBRAI PN profile is used within the test system. We note that the two designs may exceed at points the MBRAI PN mask requirement. Also, design A is of larger in-band integral PN than the −33 dBc. Thus, we consider the MBRAI PN mask SER results as the reference for the derivation of the VCO trade-off.

4.3 VCO design spaces

We next extend the simulations to provide the VCO trade-off curves for equal SER in Fig. 15, when $L(f_w)$ and $L(f_{fl})$ are varied. The simulations employ CPE correction using the pilot sub-carriers and channel compensation through linear interpolation between the pilots. These techniques are specified in [1, 2] and will be used to obtain the required SER of the system. The two MBRAI PN requirements are shown for reference. Also we plot the −33, −32, and −31 dBc of in-band integrated PN from the MBRAI mask resulting from different combinations of L(100 kHz) and L(1 MHz).

Two examples of equal SER are shown for SNRs of 18 and 26 dB, equivalent to SER of $10\ e^{-1.3}$ and $10\ e^{-2.1}$ simulated from the MBRAI PN specification. The obtainable VCO trade-off is observed between the end points of each SNR curve on the flicker and thermal noise dominance boundaries. It is in the order of 10 dB increase of thermal noise contributions at 1 MHz offset for a 10 dB decrease of flicker contributions at 100 kHz offset. This number is the ultimate trade-off that can be achieved, and it is expected that reasonable designs would not be fully dominated by flicker noise.

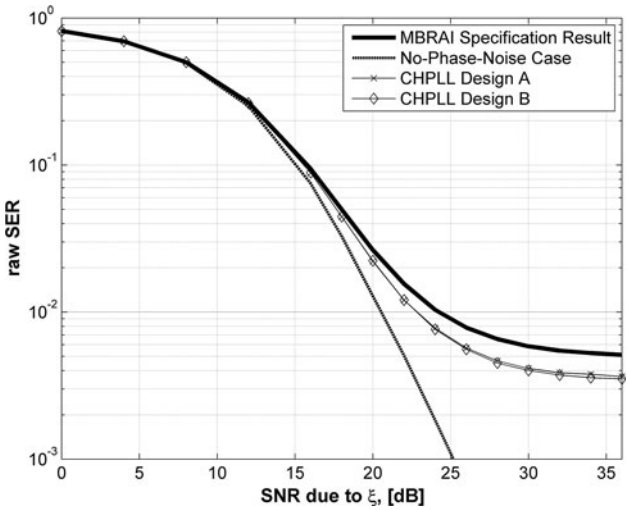

Fig. 14 8K-mode, 16-QAM simulation of SER versus SNR from AWGN with MBRAI interferers

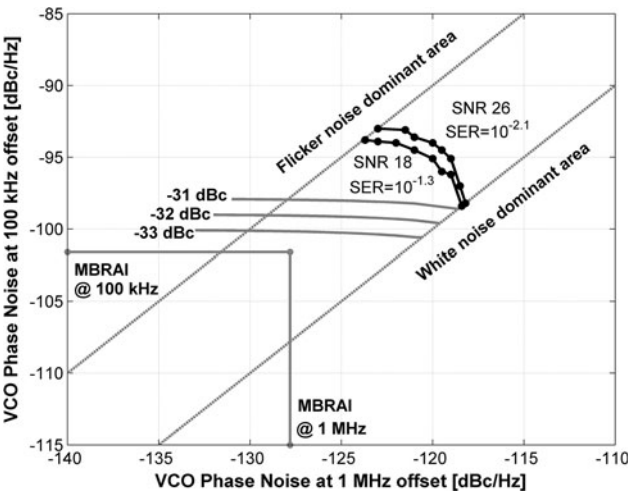

Fig. 15 Equal SER for 8K-mode, 16-QAM, MBRAI interference

The trade-off presents a significant benefit for circuit design, since flicker noise suppression can be achieved more easily in terms of implementation complexity than improvement of the passive components' quality factors. In the following, we utilize the CPE and ICI mitigation approaches summarized in Sect. 3 to obtain the augmented trade-off margins and relaxed specification for $L(1\text{ MHz})$ after the application of baseband processing. In Figs. 16, 17, 18, 19 and 20 we summarize the results for SNR = 18 dB at the boundary cases of dominant flicker noise at 10 kHz offset and dominant thermal noise at 1 MHz offset as visible from Fig. 15. The figures also show the performance when no ACI is present as a reference. The trade-off is visible at the intersection points with the MBRAI performance when CPE and channel are compensated through linear interpolation between pilot subcarriers. The results show that for all cases approximately 5 dB of 1 MHz offset

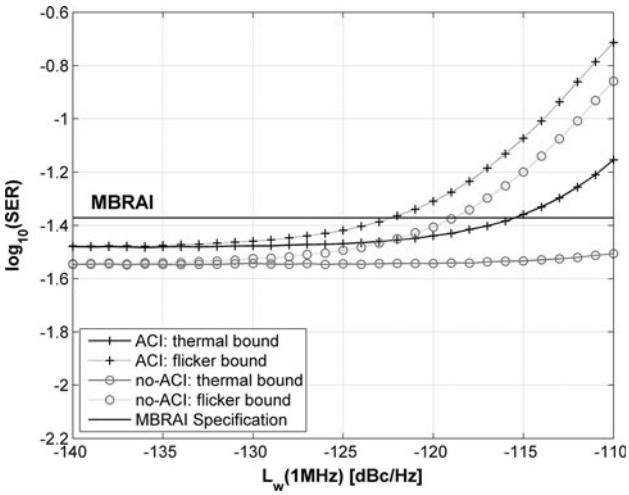

Fig. 18 SER: Windowing method, SNR = 18 dB, CP = 1/32

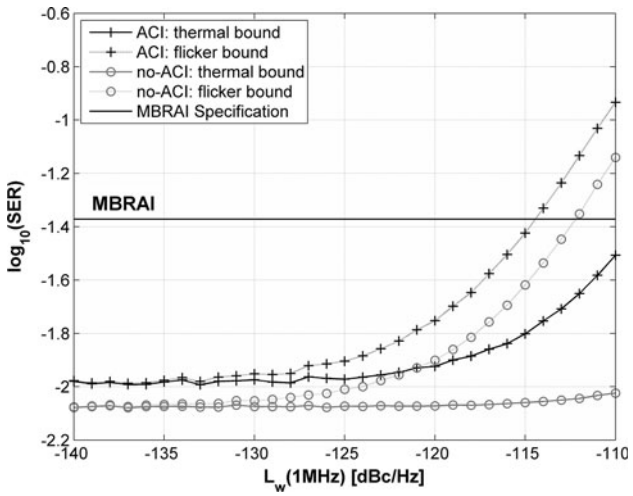

Fig. 16 SER: ideal CPE, channel knowledge, SNR = 18 dB

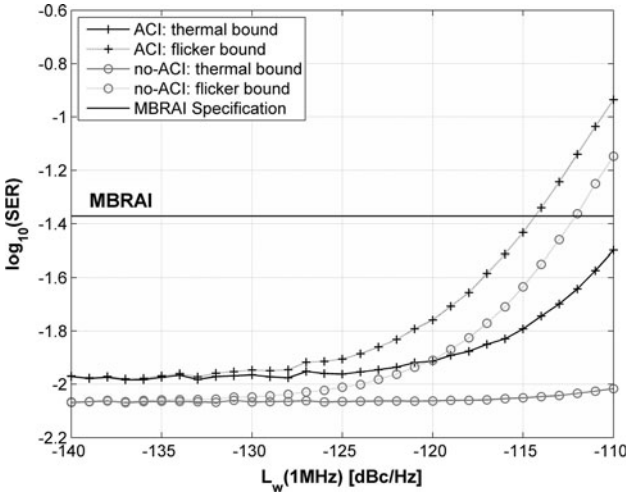

Fig. 19 SER: ICI method with $u = 3$, SNR = 18 dB, CP = 1/32

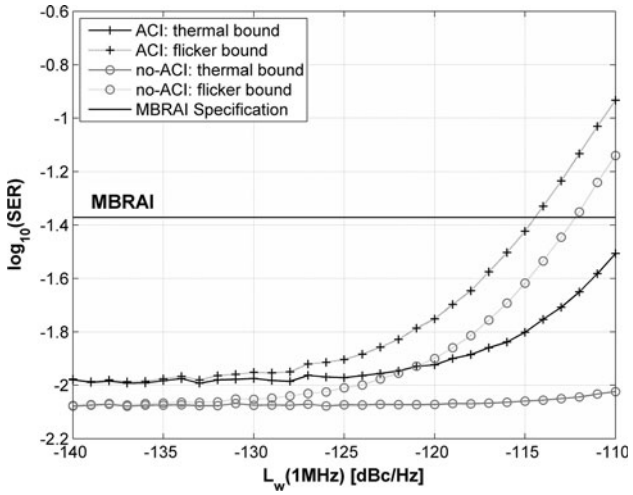

Fig. 17 SER: LI-CPE method, channel knowledge, SNR = 18 dB

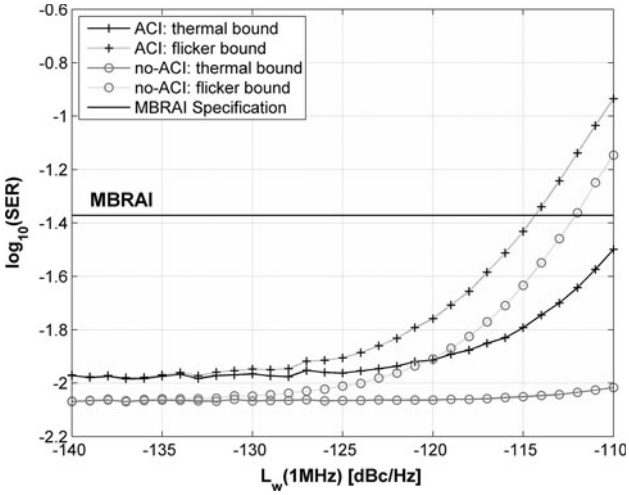

Fig. 20 SER: LI-ICI method with $u = 3$, SNR = 18 dB, CP = 1/32

PN can be increased for a 20 dB decrease of flicker noise components around 10 kHz offset. Secondly, the maximum $L(1\ \text{MHz})$ level that results in conforming CHPLL design is increased by the application of more sophisticated techniques such as ICI and LI-ICI.

We note that in this example CHPLL design with wide bandwidth the contamination by ICI is dominated by ACI, as the case with ideal CPE removal and ideal channel knowledge is very comparable to the more sophisticated methods for ICI cancellation [8, 13]. This is attributed to the fact that the excess phase variance is very small and the restored phase waveform is very similar to the CPE estimate. Of all employed techniques, the Windowing technique provides the worst results. On the other hand, ICI methods have been shown to provide very significant gains in the case of FR oscillators and CHPLL with a narrower bandwidth [8, 13]. Thus, the effect of smaller CHPLL bandwidths is next discussed.

4.4 Effect of CHPLL bandwidth

We next explore the effect of a narrower CHPLL bandwidth on the SER and resulting VCO trade-off. After decreasing the CHPLL bandwidth by factor of approximately 10, the resulting SER for the ideal CPE knowledge and most complex LI-ICI method are shown in Figs. 21 and 22.

The LI-ICI can clearly provide very good performance gains for low-bandwidth CHPLL as the ICI components estimated are of significant magnitude. As seen in the figures, the LI-ICI relaxes the specification for the required $L(f_w)$ and $L(f_{fl})$ of the VCO for achieving the MBRAI performance.

In conclusion, in both narrow-band and wide-band CHPLL designs there exists a trade-off between flicker and thermal noise contributions from the VCO. The trade-off allows for increased large-offset PN by decreasing low-offset PN. This is possible by redefining the receiver PN mask requirement in accordance to SER requirements. In the shown examples, the trade-off has allowed for increase of $L(1\ \text{MHz})$ PN by at least 5 dB for a 10 dB decrease in $L(100\ \text{kHz})$.

4.5 Summary of achievable trade-off margins

Below, in Table 1, we summarize the main findings of the carried system-level simulations when using the two CHPLL designs. As summarized previously, the CPE and ICI mitigation techniques are of distinct performance with lower PLL bandwidths, allowing to trade 20 dB increase in 1 MHz offset PN for 20 dB decrease at 10 kHz. On the contrary, with large PLL bandwidths and smaller VCO contribution to the CHPLL PSD, the trade-off is practically constant across CPE and ICI mitigation algorithms and yields only 5 dB increase in 1 MHz offset for complete flicker noise suppression by 20 dB at 10 kHz offset.

Also, the use of sophisticated ICI mitigation techniques provides more relaxed specifications for large-offset phase noise at 1 MHz.

5 Trade-off implementation: circuit techniques

The goal of this section is twofold. Firstly, we discuss several circuit design techniques that can be benefited by the derived trade-off. Secondly, two circuit topologies are

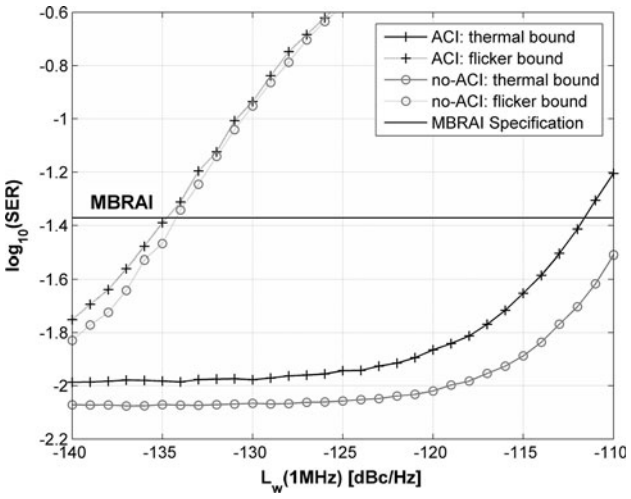

Fig. 21 SER: ideal CPE compensation and channel knowledge, SNR = 18 dB, CP = 1/32, CHPLL bandwidth decreased by factor of 10

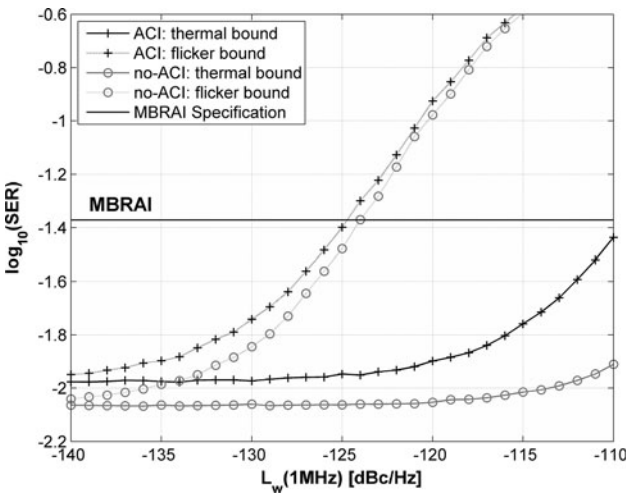

Fig. 22 SER: LI-ICI method with $u = 3$, SNR = 18 dB, CP = 1/32, CHPLL bandwidth decreased by factor of 10

Table 1 Maximum VCO Trade-off with *ACI* Amount of allowed $L(1\text{ MHz})$ increase versus $L(10\text{ kHz}) = 20$ dB decrease; Worst-case $L(1\text{ MHz})$ PN requirement

	Narrowband PLL	Wideband PLL
Ideal CPE	Margin <20 dB	Margin <5 dB
	$L_{MAX}(1\text{ MHz}) = -112$ dBc/Hz	$L_{MAX}(1\text{ MHz}) = -107$ dBc/Hz
LI-CPE	Margin <20 dB	Margin <5 dB
	$L_{MAX}(1\text{ MHz}) = -112$ dBc/Hz	$L_{MAX}(1\text{ MHz}) = -107$ dBc/Hz
Windowing	Margin <20 dB	Margin <4 dB
	$L_{MAX}(1\text{ MHz}) = -116$ dBc/Hz	$L_{MAX}(1\text{ MHz}) = -116$ dBc/Hz
ICI	Margin <20 dB	Margin <5 dB
	$L_{MAX}(1\text{ MHz}) = -108$ dBc/Hz	$L_{MAX}(1\text{ MHz}) = -106$ dBc/Hz
LI-ICI	Margin <20 dB	Margin <5 dB
	$L_{MAX}(1\text{ MHz}) = -108$ dBc/Hz	$L_{MAX}(1\text{ MHz}) = -106$ dBc/Hz

selected and used in example designs for the suppression of flicker noise up-conversion for use with the trade-off.

5.1 Overview of some circuit techniques suited for use with the derived VCO trade-off

Trade-off between flicker and thermal noise perturbations can be achieved in a fixed oscillator topology in two principal ways. Firstly, regulating the large-offset PN through the passive components' quality factor Q, as $L(f_w) \sim 1/Q$, or by optimization of the oscillator loaded quality factor [26]. Secondly, the levels of flicker noise, affecting $L(f_{fl})$, can be regulated by either decreasing the intrinsic flicker noise of CMOS transistors before up-conversion [27] or minimizing the conversion. Possible optimization of CMOS device noise can be derived from the function of device channel width W_{chan} and length L_{chan}:

$$\overline{i^2_{total}} = \overline{i^2_{thermal}} + \overline{i^2_{flicker}} = \frac{4kT\mu_{eff}}{L^2}|Q_N| + \frac{K_f}{f}\cdot\frac{g_m^2}{W_{chan}L_{chan}C_{ox}^2} \quad (26)$$

where k, μ_{eff}, T, Q_N, K_f, g_m, C_{ox} are the Boltzmann constant, electron effective mobility, absolute temperature, inversion layer charge, transconductance, process constant, and oxide thickness. In Eq. 26, $g_m = (2\mu_{eff}\ C_{ox}I_D W_{chan}/L_{chan})^{1/2}$, where I_D is the CMOS transistor drain node current.

As an alternative to fixed topologies, various topological augmentations to basic VCO architectures have been proposed to suppress the up-conversion of flicker noise [26, 28–32]. These techniques are potentially more suited for the implementation of the derived trade-off since they can achieve a more thorough suppression of flicker noise and thus utilize the full margin as derived in the previous section. In the following, we implement practical designs of two topologies [28, 31] minimizing flicker noise up-conversion.

5.2 Example of flicker noise suppression in a current-biased VCO

The work in [28] modifies the basic differential LC oscillator from Fig. 23b with a source-node decoupling, Fig. 23b, to optimally suppress flicker noise up-conversion. Flicker noise from the differential pair and bias transistor is modeled as noise voltage sources, as shown in Fig. 24, in one half of the oscillation cycle. Flicker noise will up-convert around the carrier frequency through a variety of up-conversion mechanisms [28]. Flicker noise from bias transistor M_{11} up-converts through AM–PM process in both varactor and differential pair device capacitances, and

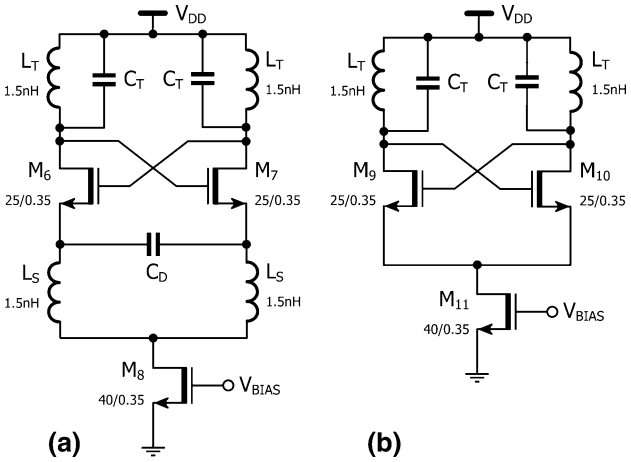

Fig. 23 Circuits – **a** current-biased circuit [28], **b** basic LC oscillator with identical MOS devices, tank and bias

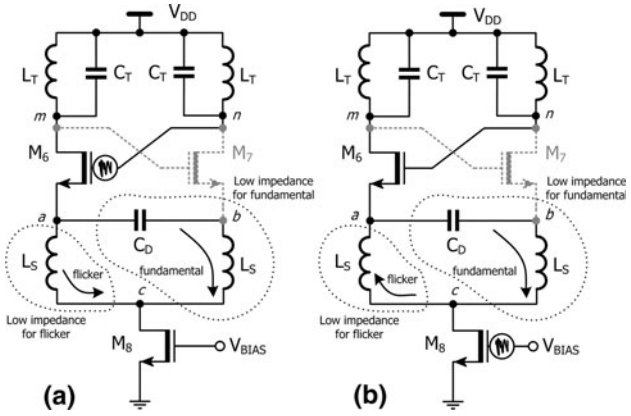

Fig. 24 Current-biased circuit half-period model with M_6 on (*solid lines*) and M_7 off (shown in *dashed lines*): **a** effect of differential pair flicker noise, **b** effect of bias transistor flicker noise

through modulation of the harmonic content of the differential current. Flicker noise from differential pair M_9–M_{10} up-converts through modulation of the duty-cycle and harmonic content of the differential current and also through the introduction of a noisy current in the tail capacitance across M_{11}.

To provide noiseless switching of M_7 to on-state for the next half-period, its gate-source voltage V_{mb} should be free of flicker noise. Its gate terminal *m* is connected to the LC tank, tuned at the oscillation frequency f_O, and thus, is free of flicker noise. However, its source terminal *b* is susceptible to flicker noise contamination. Thus, the flicker noise current component should be diverted away from the *abc*-branch in order not to contaminate the source node of M_7. At the same time the fundamental frequency current component should see a low-impedance path in the *abc*-branch to facilitate the current steering through the relaxation capacitor C_D. Diverting flicker noise current components from the differential pair and bias transistor away from the *abc*-branch and into the *ac*-branch requires:

$$Z_{a-c}(f) = j2\pi f L_S \rightarrow 0 \quad for \quad f < f_{1/f-\text{corner frequency}} \tag{27}$$

Supplying low impedance path for the fundamental frequency current through the *abc*-branch necessitates:

$$Z_{a-b-c}(f) = j\frac{(2\pi f)^2 L_S C_D - 1}{2\pi f L_S} = 0 \tag{28}$$

at the oscillation frequency $f = f_O$. From (28), the optimal value of C_D at f_O becomes:

$$C_{D,\text{optimal}}(f_O) = \frac{1}{L_S(2\pi f_O)^2}. \tag{29}$$

With (29) satisfied, the duty cycle of the differential current and its harmonic content are unaffected by flicker noise and thus the mechanisms of flicker noise up-conversion from are suppressed.

Naturally, this is an approximation model of the exact processes of differential pair switching. To obtain a realistic design for mitigation of flicker noise up-conversion, we next quantitatively evaluate the architecture through Cadence [33]. SpectreRF simulations in a 0.35 μm CMOS process. The circuit is designed to operate at fixed 4.81 GHz, to correspond to DVB channel 37 at UHF after division-by-8. The choice of this frequency was prompted by the 1.5 nH tank inductance quality factor peaking around 5 GHz at approximate value of 7. Metal–Insulator–Metal (MIM) tank capacitances of 660 fF were chosen for a good quality factor over polysilicon-capacitances in this fixed-frequency design for demonstrating the concept. Parasitic capacitances at each drain and source node are found to be approximately 100 fF, extracted parasitic simulations were not carried out. The circuit draws 6.2 mA from a 2 V voltage supply.

According to the expression for optimal suppression, we expect flicker noise suppression to occur at approximately 700 fF. Sweeping for the decoupling capacitance C_D we obtain the flicker noise contributions from the differential pair and current sink in Fig. 25 and the curves for PN at 10 kHz, 1 MHz in Fig. 26. The actual optimum for flicker noise suppression is at 720 fF which corresponds well to (29) after taking the parasitic capacitances into account. We also show in Fig. 27 a PN comparison of the circuits in Fig. 23 under identical component values and operation conditions when 720 fF decoupling has been employed in the proposed circuit – flicker noise suppression is significant without deterioration of large-offset PN. We next proceed to a final example of flicker noise suppression in a voltage-biased VCO.

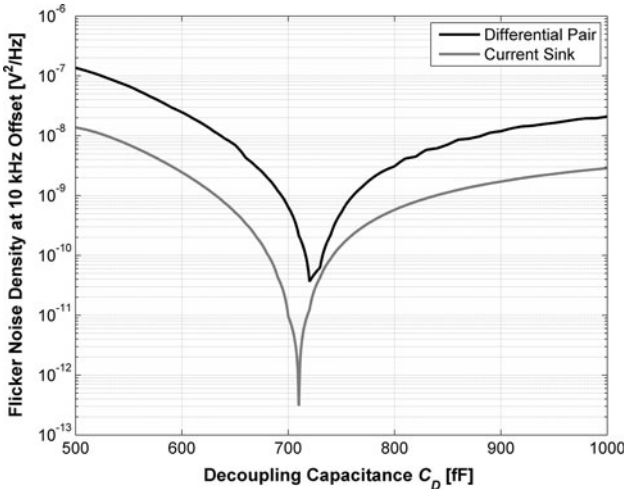

Fig. 25 Flicker noise from the circuit in [28]: differential pair and current sink contributions at 10 kHz offset versus Decoupling capacitance C_D

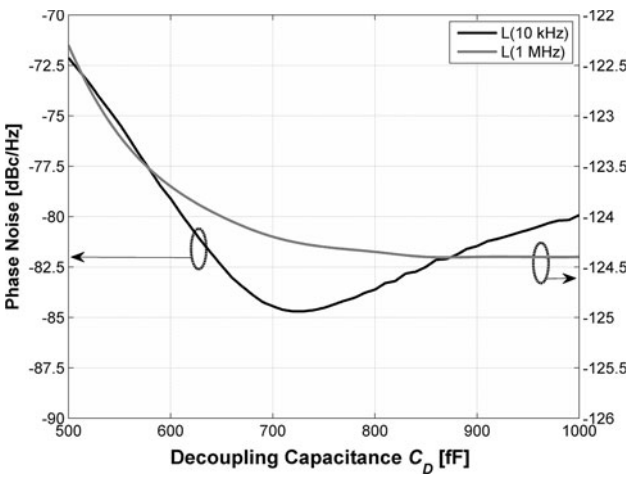

Fig. 26 Circuit results for the circuit in Fig. 23a: *L*(10 kHz) and *L*(1 MHz) versus decoupling capacitance C_D

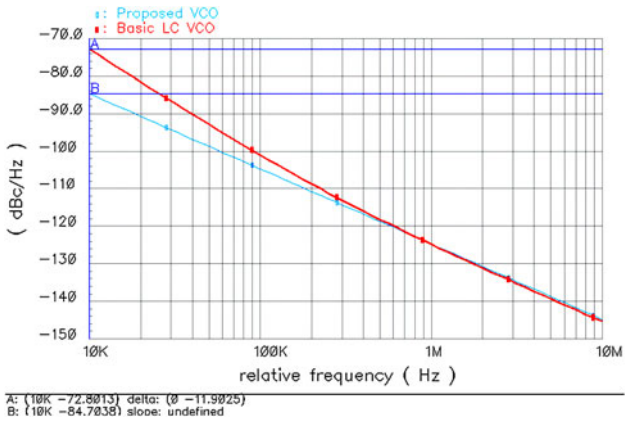

Fig. 27 Phase noise comparison of circuits in Fig. 23 with identical L_T-C_T resonator tanks, differential pair, bias transistors, and bias conditions

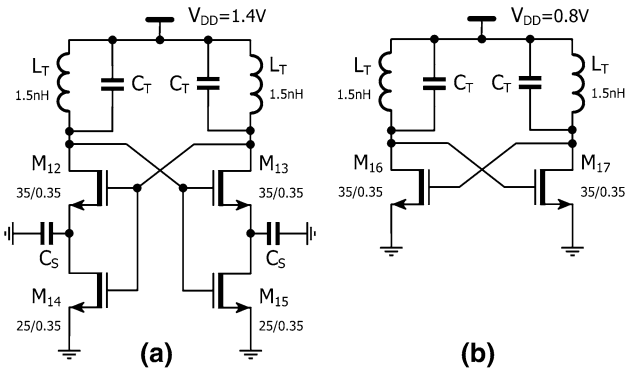

Fig. 28 Circuits – **a** voltage-biased circuit in [31], **b** basic LC oscillator with identical MOS devices, LC tank, and current consumption

5.3 Example of flicker noise suppression in a voltage-biased VCO

The work in [31] employs a dual-g_m architecture, as shown in Fig. 28. The lower transistor pair M_{14}–M_{15} exhibits a very low g_m and in accordance to Eq. 26 mitigates the up-conversion of flicker noise. In Fig. 29 we have shown the PN comparison of the circuits in Fig. 28 under identical component values and identical supply currents. In our test of the concept, complete flicker noise suppression was not achieved as no extensive optimization was carried out. Nonetheless, clear improvement is visible for the approach in [31]. The two circuits draw 1.2 mA from a 1.1 and 0.9 V voltage supplies, respectively.

5.4 Concluding remarks on VCO topology choices

The combination of approaches for varying both $L(f_w)$ and $L(f_{fl})$ depends on both circuit topology, process parameters and design cost. Evaluation of the sources of thermal and flicker noise, affecting $L(f_w)$ and $L(f_{fl})$, respectively, is

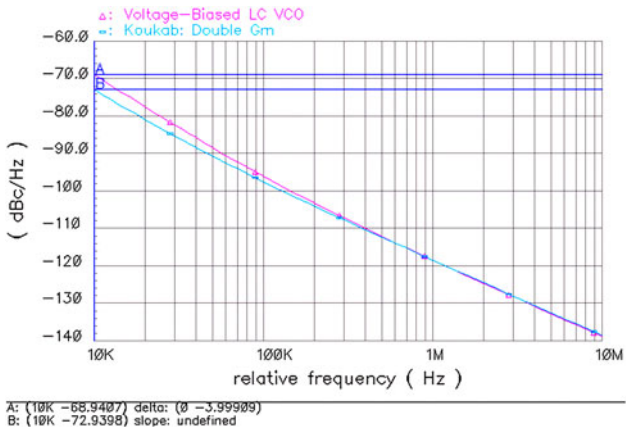

Fig. 29 Phase noise comparison of circuit in [31] and voltage-biased LC oscillator with identical L_T-C_T resonator tanks, differential pair, bias transistors, and bias conditions

possible through the use of circuit simulators, such as Cadence [33], that provide a noise summary of the generated circuit.

The trade-off, entailing an increased offset PN $L(f_w)$ for a decrease in $L(f_{fl})$, allows for the use of less expensive integrated passive components [26], thus possibly decreasing production costs. Also it can decrease design efforts in circuit design optimization efforts [26, 27] that aim at increasing the LC tank loaded quality factor. Additionally, increased $L(f_w)$ while maintaining high-quality components can be achieved by lowering VCO power consumption, which can allow for dynamic power allocation to the PLL block.

6 Conclusion

CHPLL PN modeling and performance study was carried out in the DVB-T/H system context. The derived design spaces of equal raw SER in DVB-T/H terminals provide a trade-off in VCO performance with respect to flicker and thermal noise, allowing for optimized VCO design cost and effort. ICI mitigation techniques play an important role in relaxing receiver frequency synthesizer specifications. The proposed optimization approach was demonstrated for two separate CHPLL designs and can be naturally extended to other designs. Circuit design techniques for the implementation of the proposed trade-off were discussed and implemented.

Acknowledgments This work was supported by the Finnish Funding Agency for Technology and Innovation (TEKES) under the project "Enabling Methods for Dynamic Spectrum Access and Cognitive Radio", the Technology Industries of Finland Centennial Foundation, the Academy of Finland under Projects 129077, "Hybrid Analog-Digital Signal Processing for Communications Transceivers", 251138 "Digitally-Enhanced RF for Cognitive Radio Devices", Austrian Competence Center in Mechatronics (ACCM), EUREKA CELTIC E!3187 B21C-Broadcasting for 21st Century, TUT Graduate School,

Jenny and Antti Wihuri Foundation, Ulla Tuominen Foundation, and HPY Research Foundation.

References

1. ETSI. (1997). Digital video broadcasting (DVB): Framing structure, channel coding and modulation for digital terrestrial television. *Technical Report EN, 300*, 744.
2. EICTA. (2007). Mobile and Portable DVB-T/H Radio Access—Part2: Interface Conformance Testing, MBRAI 2.0.
3. Armada, A. G. (2001). Understanding the effects of phase noise in orthogonal frequency division multiplexing (OFDM). *IEEE Transactions on Broadcasting, 47*(2), 153–159.
4. Antoine, P., et al. (2005). A direct-conversion receiver for DVB-H. *IEEE Journal of Solid-State Circuits, 40*(12), 2536–2546.
5. Amiot, S., et al. (2007). A low power DVB-T/H Zero-IF tuner IC design in 0.25 μm BiCMOS technology for mobile TV reception. *IEEE Transactions on Broadcasting, 53*(1), 434–440.
6. Debaillie, B., Van Wesemael, P., Vandersteen, G., & Craninckx, J. (2009). Calibration of direct-conversion transceivers. *IEEE Journal of Selected Topics in Signal Processing, 3*(3), 488–498.
7. Tubbax, J., et al. (2005). Compensation of IQ imbalance and phase noise in OFDM systems. *IEEE Transactions on Wireless Communications, 4*(3), 872–877.
8. Syrjälä, V., Valkama, M., Tchamov, N. N., & Rinne, J. (2009). Phase noise modelling and mitigation techniques in OFDM communications systems. Wireless Telecommunications Symposium, 1–7. doi:10.1109/WTS.2009.5068965.
9. Lim, K., et al. (2011). A 2x2 MIMO tri-band dual-mode direct-conversion CMOS transceiver for worldwide WiMAX/WLAN applications. *IEEE Journal of Solid-State Circuits, 46*(7), 1648–1658.
10. Sanchez-Lopez, C., & Tlelo-Cuautle, E. (2004). Symbolic noise analysis in analog integrated circuits. *International Symposium on Circuits and Systems, 5*, 245–248.
11. Chang, J., Abidi, A. A., & Viswanathan, C. R. (1994). Flicker noise in CMOS transistors from subthreshold to strong inversion at various temperatures. *IEEE Transactions on Electron Devices, 41*(11), 1965–1971.
12. Klumperink, E. A. M., Gierkink, S. L. J., van der Wel, A. P., & Nauta, B. (2000). Reducing MOSFET 1/f noise and power consumption by switched biasing. *IEEE Journal of Solid-State Circuits, 35*(7), 994–1001.
13. Petrovic, D., Rave, W., & Fettweis, G. (2007). Effects of phase noise on OFDM systems with and without PLL: characterization and compensation. *IEEE Transactions on Communications, 55*(8), 1607–1616.
14. Gardner, F. (1980). Charge-pump phase-lock loops. *IEEE Transactions on Communications, 28*(11), 1849–1858.
15. Demir, A. (2002). Phase noise and timing jitter in oscillators with colored-noise sources. *IEEE Transactions on Circuits and Systems I: Fundamental Theory and Applications, 49*(12), 1782–1791.
16. Demir, A. (2006). Computing timing jitter from phase noise spectra for oscillators and phase-locked loops with white and 1/f noise. *IEEE Transactions on Circuits and Systems I: Regular Papers, 53*(9), 1869–1884.
17. Fu, Z., & Apsel, A. (2010). A tool for power and phase noise optimization in frequency synthesizers. *Analog Integrated Circuits and Signal Processing, 64*(2), 91–101.
18. Mehrotra, A. (2002). Noise analysis of phase-locked loops. *IEEE Transactions on Circuits and Systems I: Fundamental Theory and Applications, 49*(9), 1309–1316.
19. Khemchandani, S. L., et al. (2010). RF and mixed signal circuits for a DVB-H receiver. *Analog Integrated Circuits and Signal Processing, 65*(1), 1–14.
20. The MathWorks, Inc., Natick, Massachusetts 01760 USA.
21. Syrjälä, V., Valkama, M., Zou, Y., Tchamov, N.N., & Rinne, J. (2011). On OFDM link performance under receiver phase noise with arbitrary spectral shape. IEEE Wireless Communications and Networking Conference, 1948–1953. doi:10.1109/WCNC.2011.5779457.
22. Corvaja, R., & Armada, A. G. (2009). Joint channel and phase noise compensation for ofdm in fast-fading multipath applications. *IEEE Transactions on Vehicular Technology, 58*(2), 636–643.
23. Syrjälä, V., & Valkama, M. (2010). Analysis and mitigation of phase noise and sampling jitter in OFDM radio receivers. International Journal of Microwave and Wireless Technologies, 2(2). doi:10.1017/S1759078710000309.
24. Faulkner, M., Wilhelmsson, L. R., & Svensson, J. (2006). Low-Complex ICI Cancellation for Improving Doppler Performance in OFDM Systems. IEEE Vehicular Technology Conference, 1–5. doi:10.1109/VTCF.2006.181.
25. Tchamov, N. N., Hazmi, A., Rinne, J., Valkama, M., & Renfors, M. (2010). Performance comparison of DVB-T and DVB-T2 in the presence of phase noise. 15th International OFDM-Workshop.
26. Hegazi, E., Sjoland, H., & Abidi, A. A. (2001). A filtering technique to lower LC oscillator phase noise. *IEEE Journal of Solid-State Circuits, 36*(12), 1921–1930.
27. Jerng, A., & Sodini, C. G. (2005). The impact of device type and sizing on phase noise mechanisms. *IEEE Journal of Solid-State Circuits, 40*(2), 360–369.
28. Tchamov, N. N., & Tchamov, N. T. (2007). Technique for flicker noise up-conversion suppression in differential LC oscillators. *IEEE Transactions on Circuits and Systems II: Express Briefs, 54*(11), 959–963.
29. Levantino, S., Bonfanti, A., Romanò, L., Samori, C., & Lacaita, A. L. (2005). Differentially-tuned vco with reduced tuning sensitivity and flicker noise up-conversion. *Analog Integrated Circuits and Signal Processing, 42*(1), 21–29.
30. Shanan, H. N., & Kennedy, M. P. (2004). A technique to reduce flicker noise up-conversion in CMOS LC voltage-controlled oscillators. Solid-State Circuits Conference, 123–126. doi:10.1109/ESSCIR.2004.1356633.
31. Koukab, A. (2010). LC-VCO design with dual-Gm, boosted for RF oscillation and attenuated for LF noise. *IEEE Microwave and Wireless Components Letters, 20*(12), 675–677.
32. Levantino, S., Zanuso, M., Samori, C., & Lacaita, A. (2010). Suppression of flicker noise upconversion in a 65 nm CMOS VCO in the 3.0-to-3.6 GHz band. IEEE International Solid-State Circuits Conference Digest of Technical Papers 50–51. doi:10.1109/ISSCC.2010.5434054.
33. Cadence Design Systems, Inc., San Jose, CA, USA.

Nikolay N. Tchamov was born in Sofia, Bulgaria, on July 14, 1978. He received the M.Sc. Degree in communications engineering (CS/EE) from Tampere University of Technology (TUT), Finland, in 2006. Currently, he is working as a researcher with the Department of Communications Engineering at TUT, Finland. His general research interests are in integrated RF circuit design and baseband methods for mitigation of RF impairments.

Ville Syrjälä was born in Lapua, Finland, in 1982. He received the M.Sc. Degree (with honours) in communications engineering (CS/EE) from Tampere University of Technology (TUT), Finland, in 2007. Currently, he is working as a researcher with the Department of Communications Engineering at TUT, Finland. His general research interests are in communications signal processing and signal processing algorithms for flexible radios.

Jukka Rinne received the Master of Science (MSc) and Licentiate of Technology (Lic. Tech.) degrees from Tampere University of Technology, Finland. He is currently working as a researcher at Department of Communications Engineering of Tampere University of Technology. He has been working with Digital Video Broadcasting (DVB) systems, consisting of work with system specification, verification and validation including receiver algorithm development. In general his research interests include multicarrier systems, channel modeling, and digital signal processing algorithms for telecommunication applications.

Mikko Valkama was born in Pirkkala, Finland, on November 27, 1975. He received the M.Sc. and Ph.D. Degrees (both with honours) in electrical engineering (EE) from Tampere University of Technology (TUT), Finland, in 2000 and 2001, respectively. In 2002 he received the Best PhD. Thesis - award by the Finnish Academy of Science and Letters for his dissertation entitled "Advanced I/Q signal processing for wideband receivers: Models and algorithms". In 2003, he was working as a visiting researcher with the Communications Systems and Signal Processing Institute at SDSU, San Diego, CA. Currently, he is a Full Professor at the Department of Communications Engineering at TUT, Finland. He has been involved in organizing conferences, like the IEEE SPAWC'07 (Publications Chair) held in Helsinki, Finland. He has published more than 100 scientific articles in international referee journals and conference proceedings. His general research interests include communications signal processing, estimation and detection techniques, signal processing algorithms for software defined and cognitive radios, different sampling methods including compressive sampling, digital transmission techniques such as different variants of multicarrier modulation methods and OFDM, and radio resource management for ad-hoc and mobile networks.

Yaning Zou was born in Chengdu, China, on September 21, 1980. She received the Bachelor Degree in communications engineering from University of Electronic Science and Technology of China (UESTC), Chengdu, China, in 2002, and the M.Sc. Degree and PhD. Degree in electrical engineering from Tampere University of Technology (TUT), Tampere, Finland, in 2005 and 2009 respectively. In 2008, she was a Visiting Researcher with the Danube Integrated Circuits Engineering (DICE) GmbH, Linz, Austria, and the Institute for Communications and Information Engineering, Johannes-Kepler University, Linz, Austria. Currently, she is working as a postdoctoral research fellow with the Department of communications engineering at TUT. Her general research interests are in wireless communication system design, as well as digital signal processing-based RF impairment calibration techniques for building high performance yet cost-efficient software defined and cognitive radios.

Markku Renfors received the Doctor of Technology Degree from Tampere University of Technology (TUT) in 1982. Since 1992 he has been a professor at the Department of Communications Engineering of TUT. He was the Head of the Department from 1992-2010. Dr. Renfors is a Fellow of IEEE and recipient of the 1987 IEEE Circuits and Systems Society's Guillemin-Cauer Award (together with Tapio Saramäki). His main research areas include multicarrier transmission techniques and signal processing algorithms for flexible communications receivers and transmitters, with special focus on filter bank applications and spectrum sensing in cognitive radio.

Publication 9

V. Syrjälä, V. Lehtinen, and M. Valkama, "Sampling jitter in charge sampling radio," in *Proc. IEEE Wireless Communications & Networking Conference 2012 Workshops* (*IEEE WCNCW'12*), Paris, France, April 2012.

Sampling Jitter in Charge Sampling Radio

Ville Syrjälä, Vesa Lehtinen and Mikko Valkama

***Abstract*—This article addresses some implementation challenges in the potentially very energy-efficient charge-sampling radios. Alternative ways to implement charge sampler in charge sampling radio are considered, and the impacts and spectral shape characteristics of the sampling jitter induced signal distortion are analytically studied in these cases. The analysis shows that the spectrum of the distortion caused by the sampling jitter in a charge sampling receiver is not necessary flat, which in turn has direct impacts on the receiver design and dimensioning. The validity of the analytical results is verified with computer simulations. In simulations, both white Gaussian noise -type clock jitter and clock jitter generated by a phase-locked-loop oscillator are considered.**

***Index Terms*—Charge sampling; sampling jitter**

I. Introduction

CHARGE sampling, or charge-domain sampling, is a sampling technique that is based on integrating the signal current derived from the signal voltage, instead of sampling the signal voltage directly [1]. The approach potentially allows building energy-efficient sampling circuits that work at very high frequencies [1], [2], [3], [4]. In such circuits, sampling jitter still remains as one of the implementation problems.

Sampling jitter effects on charge sampled signal have been studied, e.g., in [5]. They derived a formula for signal-to-noise ratio (SNR) due to sampling jitter with assumption that the sampling jitter instants are mutually independent and uncorrelated white Gaussian noise. However, to our best knowledge, frequency domain behaviour of sampling jitter error in charge sampler (CS) has not been studied in existing literature. In this paper, we study the spectrum of the noise caused by the sampling jitter in CS. We show that the noise spectrum is not necessarily white, and in certain cases power spectrum has a strongly frequency-dependent shape. This is an important finding because the SNR is only deteriorated by noise within the band of interest, as out-of-band noise will be filtered out or at least attenuated.

The structure of the rest of the paper is as follows. In the second section, general charge sampling radio and general model for charge sampled bandpass-signal are derived. In the third section, the effect of the sampling jitter is analyzed in different charge-sampling receiver implementation cases. The analytical results and discussion in the third section are verified with simulations in the fourth section. In fifth section, charge-sampling receiver design-considerations are shortly given based on the spectral shape of the sampling-jitter error. Finally the sixth section concludes the work.

Notation in this paper is as follows. Sampling interval T_s is the time between the discrete samples at the sampler output and T_i is the integration time within the sampling interval during which the sample is integrated in the CS. Sampling rate is the inverse of the sampling interval.

The work was supported by TUT graduate school, Jenny and Antti Wihuri Foundation, HPY Research Foundation, Ulla Tuominen Foundation, the Academy of Finland, and the Finnish Funding Agency for Technology and Innovation.

The authors are with Department of Communications Engineering, Tampere University of Technology, P.O. Box 553, 33101 Tampere, Finland (email: {ville.syrjala, vesa.lehtinen, mikko.e.valkama}@tut.fi).

II. Charge Sampling Radio

This section gives general description of a charge sampling radio and a signal model for general IQ-modulated signal received by such radio.

A. General Description of Charge Sampling Radio

Charge sampling radios are proposed for direct RF sampling receiver architecture, e.g., in [2] and [3]. Principle structure of such direct RF sampling radio using charge sampling is illustrated in Fig. 1. In the structure, the signal is charge sampled after amplification and then processed further in sample domain. Unlike more traditional voltage sampler, CS does heavily shape the spectrum of the sampled signal. The frequency response of CS (magnitude response illustrated in Fig. 2 is $H(\omega) = c\,\mathrm{sinc}(T_i\omega/2)$, where ω is the angular frequency, T_i is the length of the integration interval used in CS, c is a constant that depends on the sampling circuit, and $\mathrm{sinc}(\cdot)$ is the unnormalized sinc function [1]. In order to tackle the signal corruption at the output of a CS, either 1) the incoming signal should be very narrowband with respect to the integration interval or 2) proper digital equalization should be done after the CS.

B. Model for Charge Sampled IQ-Signal

General operation of CS is illustrated in upper parts of Fig. 3 and Fig. 4. In model of Fig. 3, it is assumed that the previous integration interval always ends at the same time that the next integration interval begins. Fig. 4 on the other hand gives a more general CS model. In the more general model, integration window length is not necessary equal to the sampling interval. In Fig. 4, the same notation is used as in the following analysis.

Let us consider a general IQ-modulated continuous bandpass-signal

$$r(t) = x_I(t)\cos(\omega_c t) - x_Q(t)\sin(\omega_c t). \quad (1)$$

Here, ω_c is the carrier frequency, and $x_I(t)$ and $x_Q(t)$ are the I and Q components of the baseband message signal, respectively. When the bandpass signal is sampled with an ideal CS, (1) achieves the form

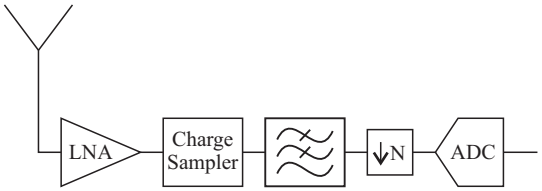

Fig. 1. Principal structure of charge sampling radio, consisting of low-noise amplifier, CS, lowpass filter, downsampler and analogue-to-digital converter.

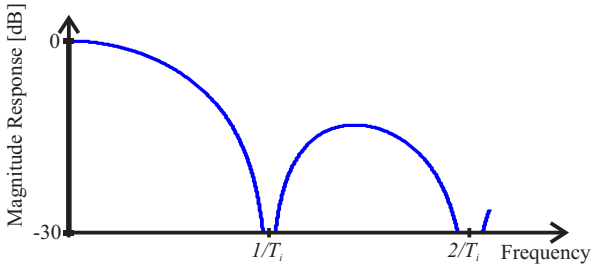

Fig. 2. Normalized (max. 0 dB) magnitude response of a charge sampler. T_i denotes the integration interval of the sampler.

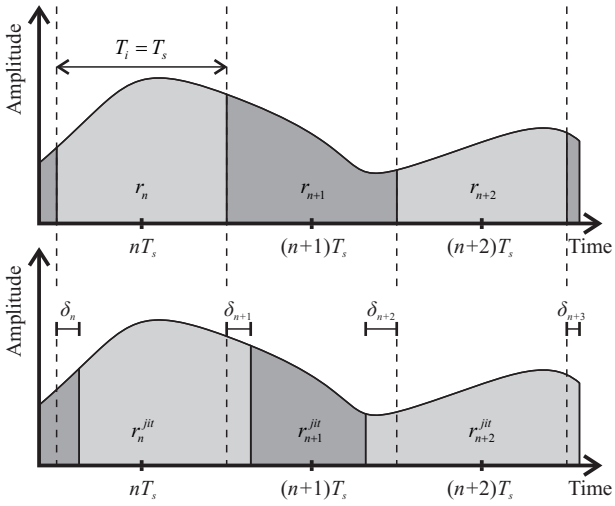

Fig. 3. An example demonstration of charge sampling in case 1. Here, next integration intervals starts when previous ends. Upper figure is without sampling jitter and lower figure is with sampling jitter. Dashed lines mark the ideal integration boundaries.

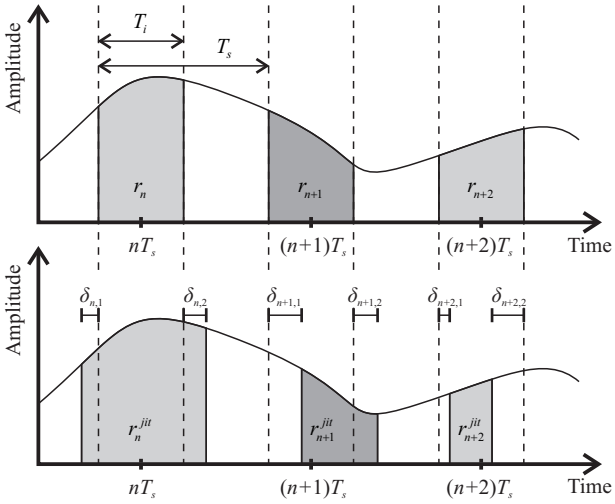

Fig. 4. A general demonstration of the charge sampling in case 2. There is a gap between the end of the previous and start of the next integration intervals. Upper figure is without sampling jitter and lower figure is with sampling jitter. Dashed lines mark the ideal integration boundaries.

$$r_n = \int_{nT_s - T_i/2}^{nT_s + T_i/2} \left[x_I(t)\cos(\omega_c t) - x_Q(t)\sin(\omega_c t) \right] dt = \int_{t - T_i/2}^{t + T_i/2} \left[x_I(\tilde{t})\cos(\omega_c \tilde{t}) - x_Q(\tilde{t})\sin(\omega_c \tilde{t}) \right] d\tilde{t} \Big|_{t = nT_s}, \quad (2)$$

where T_s is the sampling interval. From now on for the sake of compactness we mark $t_{n,1} = nT_s - T_i/2$ and $t_{n,2} = nT_s + T_i/2$. The samples correspond to those of the voltage sampler, but with the discussed filtering response. The response is also visible in (2), as the boxcar filtering in time domain corresponds to the sinc pulse in frequency domain.

III. Sampling Jitter in Charge Sampling Radio

Given a conventional voltage sampler, sampling jitter modelling is usually a simple task [6]. The clock signal that controls the sampler can simply be considered to be generated, e.g., by a phase-locked loop (PLL) oscillator or similar. The phase noise of such oscillator then gives directly a relatively good basis to model the statistics of the sampling jitter. However, modelling the jitter process in CS is not such a simple task. This section concentrates on the analysis, modelling and the effects of the sampling jitter in CS.

A. Charge Sampled Signal Corrupted by Sampling Jitter

Now, let us consider CS that is impaired by sampling jitter. The jitter only affects the integration intervals in (2), thus giving a signal model

$$r_n^{jit} = \int_{nT_s - T_i/2 + \delta_{n,1}}^{nT_s + T_i/2 + \delta_{n,2}} \left[x_I(t)\cos(\omega_c t) - x_Q(t)\sin(\omega_c t) \right] dt . \quad (3)$$

Here, $\delta_{n,1}$ and $\delta_{n,2}$ are the sampling jitters at the beginning and at the end of the nth integration period, respectively. Now, by using partial integration and denoting $t_{n,1}^{jit} = nT_s - T_i/2 + \delta_{n,1}$ and $t_{n,2}^{jit} = nT_s + T_i/2 + \delta_{n,2}$, we can separate (3) in two parts as

$$r_n^{jit} = \frac{1}{\omega_c}\left[x_I(t_{n,2}^{jit})\sin(\omega_c t_{n,2}^{jit}) + x_Q(t_{n,2}^{jit})\cos(\omega_c t_{n,2}^{jit}) - x_I(t_{n,1}^{jit})\sin(\omega_c t_{n,1}^{jit}) - x_Q(t_{n,1}^{jit})\cos(\omega_c t_{n,1}^{jit}) \right] - \frac{1}{\omega_c}\int_{t_{n,1}^{jit}}^{t_{n,2}^{jit}} \left[\frac{dx_I(t)}{dt}\sin(\omega_c t) + \frac{dx_Q(t)}{dt}\cos(\omega_c t) \right] dt . \quad (4)$$

Here, notation dy/dt refers to derivative of y with respect to t. Now, when using the partial integration again in the integral in (4), the result would once again be divided by ω_c. Because we consider direct RF sampling system, we are sampling relatively narrowband signal at a very high carrier frequency ω_c (around 10^{10} radians/s). From this it stems that when ω_c indeed divides the integral in (4), it makes the integral term diminishingly low-valued compared to the value of first term of (4). Thus we can approximate (4) as

$$r_n^{jit} \approx \frac{1}{\omega_c}\left[x_I(t_{n,2}^{jit})\sin(\omega_c t_{n,2}^{jit}) + x_Q(t_{n,2}^{jit})\cos(\omega_c t_{n,2}^{jit}) - x_I(t_{n,1}^{jit})\sin(\omega_c t_{n,1}^{jit}) - x_Q(t_{n,1}^{jit})\cos(\omega_c t_{n,1}^{jit}) \right]. \quad (5)$$

Now, since the I and Q components of the baseband signal are always multiplied with the corresponding high-frequency carrier components (sine and cosine waves), the time error caused by the sampling jitter to the I and Q components is very small compared to the time error caused to high-frequency carrier components [7]. We can thus further approximate (5) as

$$r_n^{jit} \approx \frac{1}{\omega_c}\Big[x_I(t_{n,2})\sin(\omega_c t_{n,2}^{jit}) + x_Q(t_{n,2})\cos(\omega_c t_{n,2}^{jit}) - x_I(t_{n,1})\sin(\omega_c t_{n,1}^{jit}) - x_Q(t_{n,1})\cos(\omega_c t_{n,1}^{jit})\Big]. \quad (6)$$

We also know that the jitter terms $\delta_{n,1}$ and $\delta_{n,2}$ in general are relatively small values, so we can use the well-known small phase approximation for the sine and cosine terms and get

$$\begin{aligned} r_n^{jit} \approx \frac{1}{\omega_c}\Big\{ & x_I(t_{n,2})\Big[\sin(\omega_c t_{n,2}) + \omega_c\delta_{n,2}\cos(\omega_c t_{n,2})\Big] \\ & + x_Q(t_{n,2})\Big[\cos(\omega_c t_{n,2}) - \omega_c\delta_{n,2}\sin(\omega_c t_{n,2})\Big] \\ & - x_I(t_{n,1})\Big[\sin(\omega_c t_{n,1}) + \omega_c\delta_{n,1}\cos(\omega_c t_{n,1})\Big] \\ & - x_Q(t_{n,1})\Big[\cos(\omega_c t_{n,1}) - \omega_c\delta_{n,1}\sin(\omega_c t_{n,1})\Big]\Big\}. \end{aligned} \quad (7)$$

This approximately gives the model for a signal sampled with CS impaired by the sampling jitter.

B. Sampling-Jitter Error in Charge Sampled Signal

Above we have derived a model for the sampling jitter impaired charge sampled signal in (7). With the same approximation used to obtain (5), the signal without sampling jitter can be written as

$$r_n \approx \frac{1}{\omega_c}\Big[x_I(t_{n,2})\sin(\omega_c t_{n,2}) + x_Q(t_{n,2})\cos(\omega_c t_{n,2}) - x_I(t_{n,1})\sin(\omega_c t_{n,1}) - x_Q(t_{n,1})\cos(\omega_c t_{n,1})\Big]. \quad (8)$$

It is thus trivial to derive the model for the actual error or distortion caused by the sampling jitter. As can be seen, (7) and (8) are already simplified to forms from which their difference is easily calculated. This difference is the error signal caused by the sampling jitter and can be written as

$$\begin{aligned} e_n^{jit} &= r_n^{jit} - r_n \\ &\approx \frac{1}{\omega_c}\Big\{\omega_c\delta_{n,2}\Big[x_I(t_{n,2})\cos(\omega_c t_{n,2}) - x_Q(t_{n,2})\sin(\omega_c t_{n,2})\Big] \\ &\quad - \omega_c\delta_{n,1}\Big[x_I(t_{n,1})\cos(\omega_c t_{n,1}) - x_Q(t_{n,1})\sin(\omega_c t_{n,1})\Big]\Big\} \\ &= \delta_{n,2}r(t_{n,2}) - \delta_{n,1}r(t_{n,1}). \end{aligned} \quad (9)$$

We can see that the noise caused by the sampling jitter is simply sum of two terms, $\delta_{n,2}r(t_{n,2})$ and $-\delta_{n,1}r(t_{n,1})$. Both of the terms are product of the sampling jitter and the IQ signal. The only difference between the two terms is timing. What the actual sampling jitter caused noise is like, especially in frequency domain, depends on the relationship between the sampling jitter and the IQ signal at the different moments in time ($t_{n,1}$ and $t_{n,2}$).

C. How to Model the Timing Jitter in Charge Sampler

The sampling jitter modelling depends on the hardware implementation of the sampler and the sampling clock. This is because in a CS the sampling jitter effect on a sample does not depend only on a time error caused by a simple timing offset in the time when the sample is taken. This is the case in voltage sampler, but in a CS, as Fig. 3, Fig. 4 and (9) illustrate, the error depends on the time error in the beginning and in the end of the integration period. One implementation approach assumes that timing jitter merely moves the boundary in which the previous integration ends and the next one starts. This assumption is made in the case in Fig. 3. In this case a sample window ends and the next window starts at the same instant, hence they share the same time offset. This corresponds to the case of jitter-free switches fed by a clock contaminated by jitter. A more general model is depicted in Fig. 4. There sampling jitter values $\delta_{n,1}$ and $\delta_{n,2}$ for $\forall n$ may either depend on each other, may not depend on each other, or only some of them may depend on each other, depending on the implementation of the CS. So the main question in sampling jitter modelling is how the sampling jitter terms in (9) depend on each other, and what kind of an effect does that have on the error caused by the sampling jitter.

D. Effect of the Sampling Jitter on Charge Sampler

Here sampling jitter effect is studied in two interesting cases.

1) Case 1

Case 1 is depicted in Fig. 3. In case 1 the next integration period start at the same time as the previous ends. This means that in (9) $\delta_{n,2} = \delta_{n+1,1} \triangleq \delta_{n+1}$ and $r(t_{n,2}) = r(t_{n+1,1}) \triangleq r(t_{n+1})$, as can be seen by comparing Fig. 3 and Fig. 4. Also, $r(t_n) = r(nT_s - T_s/2)$. Therefore, based on (9), the jitter can be written in the form

$$e_n^{jit} \approx \delta_{n+1}r(t_{n+1}) - \delta_n r(t_n). \quad (10)$$

This is equivalent to filtering signal $\delta_n r(t_n)$ with digital filter $H(z) = 1 - z^{-1}$. This means that the sampling jitter is directly the filtered product of the voltage sampled IQ-signal $r(t_n)$ and the sampling jitter process δ_n.

2) Case 2

The case 2 is the one depicted in Fig. 4. Here, $\delta_{n,1}$, $\delta_{n,2}$ and $\delta_{n+1,1}$ are not mutually pair-wise fixed to be equal to each other. The error term due to jitter is directly the one derived in (9), namely sum of terms $\delta_{n,2}r(t_{n,2})$ and $-\delta_{n,1}r(t_{n,1})$. If the sampling jitter process is assumed to be white Gaussian noise (WGN), then there is no filtering effect, and the resulting sampling-jitter noise is white. To show this explicitly, the correlation of the sampling-jitter-induced noise samples e_n^{jit} and e_k^{jit} for $k \neq n$ must be zero. From approximation in (9), we can conclude, that this is indeed the case in case 2 when sampling jitter process is assumed to be WGN. However, if all the sampling jitter terms $\delta_{n,1}$ and $\delta_{n,2}$ for $\forall n$ come from the same correlated process, e.g., the sampling jitter sequence is generated by PLL, there might be some filtering effect. This happens when $\delta_{n,2} \approx \delta_{n+1,1}$ and $r(t_{n,2}) \approx r(t_{n+1,1})$, namely when we are very close to the case 1, i.e. when T_i is near to T_s. In such case, the strength of the filtering effect depends on how close T_i actually is to T_s.

In case 2 it should be noted that if the integration interval length T_i is made narrower, also the charge integrated by the CS is relatively small. At the same time the power of the sampling-jitter noise, however, is not affected by the shorter integration period, resulting in relatively low SNR. Of course, not integrating all the time gives savings in used energy.

IV. Simulations and Simulation Analysis

In this section, we verify that simulations confirm the analytical results. This is verified by simple spectrum comparisons. In simulations a baseband equivalent OFDM signal with 12 MHz bandwidth is first created at sampling frequency 15.36 MHz. The signal is then 2^{18} times oversampled and IQ mixed around carrier frequency f_c of 867.5 MHz. These parameter values are selected for the sake of example. After the signal creation, the CS with jitter is modelled. We model a CS working at sampling frequency of 3932.16 MHz, so we are oversampling the baseband waveform by 2^8 times. This allows us to use the remaining 2^{10} times oversampling, to model the sampling jitter. Furthermore, we use linear interpolation to make the simulation of the sampling jitter even more accurate. The used PLL-type sampling-jitter sequence is generated with the PLL-type oscillator model used, e.g., in [8].

Simulation results are given in Figures 5 to 9. In these, term semianalytical refers to calculating sampling-jitter error using (9) and inputting the same waveforms to it as used in the simulations. The magnitude response of $H(z)=1-z^{-1}$ filter curve is also given in the figures where considered relevant.

Fig. 5 depicts the case 1 with 20-ps root-mean-square (RMS) WGN-type sampling jitter. As expected, the simulations confirm the analytical results. The sampling jitter caused error indeed has the shape of $H(z)=1-z^{-1}$ discrete time filter. In case of PLL-type sampling jitter in Fig. 6, we can see the same shaping effect. In Fig. 7, the case with PLL-type sampling jitter for which $\delta_{n,1}$ and $\delta_{n,2}$ come from the separate PLLs is depicted (this corresponds to case 2 with $T_i = T_s$). When comparing the results of Fig. 6 to results of Fig. 7, we can indeed see that the former results have the clear filtering effects present, whereas the latter results do not have any filtering effect at all. In Fig. 7, we only see the resulting spectrum when the information signal is multiplied with the sampling jitter sequence.

Now, for the case 2 results change a little. For WGN-type sampling jitter, there is no noise shaping at all. The sampling jitter caused noise is thus WGN as well. Fig. 8 and Fig. 9 depict the case with PLL-type noise in case when sampling jitter is generated with a single PLL, for $2T_i = T_s$ and $4T_i = T_s$, respectively. In this case, $\delta_{n,1}$ and $\delta_{n,2}$ correlate with each other. We can see that, as expected, in $2T_i = T_s$ case there is still minor filtering effect visible, but as integration interval gets narrower and narrower (e.g. $4T_i = T_s$), the filtering effect ceases to exist due to lack of correlation either between $\delta_{n,2}$ and $\delta_{n+1,1}$ or between $r(t_{n,2})$ and $r(t_{n+1,1})$.

V. Impact on Receiver Design

The spectral shape of the sampling jitter in the sampling clock signal that controls a CS has been ignored in most of the earlier studies in the literature. Such is the case, e.g., in our case 2 with the white Gaussian noise like jitter model, when the sampling jitter at the end of the previous integration period and at the beginning the current integration period are not dependent on each other. However, when CS is implemented so that the sampling jitter at the end of the previous integration period equals to, or is heavily depends on, the sampling jitter at the beginning of the next integration period, the error caused by the sampling jitter is not white anymore. This must be taken into account in the receiver design as is demonstrated in Fig. 10.

Fig. 10 demonstrates the signal and the jitter-noise shaping in case 1 when WGN shaped sampling jitter is assumed. The figure tells how the signal or sampling-jitter noise is shaped

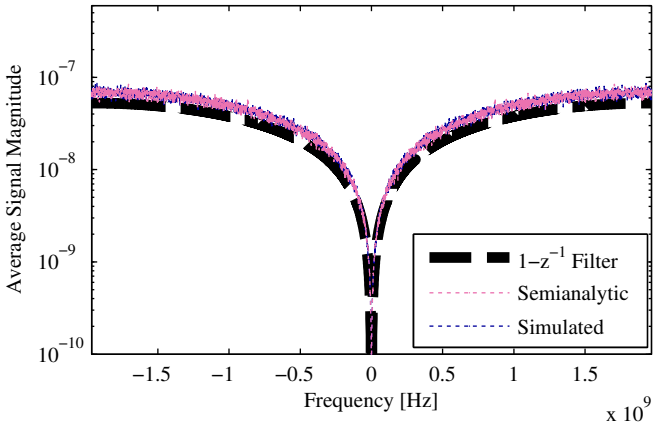

Fig. 5. Error spectrum caused by sampling jitter, when jitter is white Gaussian noise. 20-ps RMS jitter, case 1 (with $T_i = T_s$).

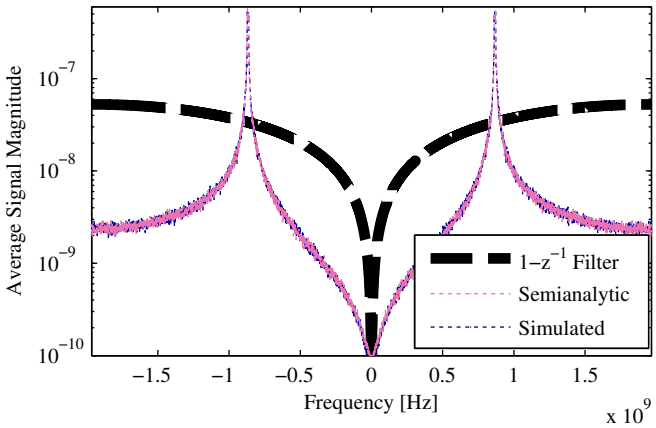

Fig. 6. Error spectrum caused by sampling jitter when jitter is generated by PLL oscillator. 20-ps RMS jitter, case 1 (with $T_i = T_s$).

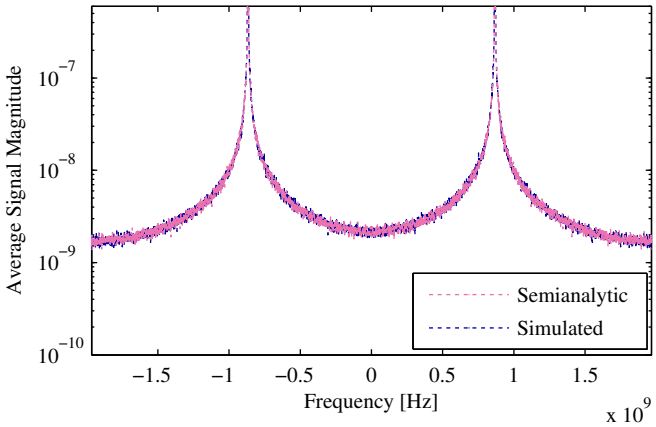

Fig. 7. Error spectrum caused by sampling jitter when jitter is generated by PLL oscillator, but sampling jitters at the beginnings and the ends of the integration intervals are independent of each other. 20-ps RMS jitter, case 2 (with $T_i = T_s$).

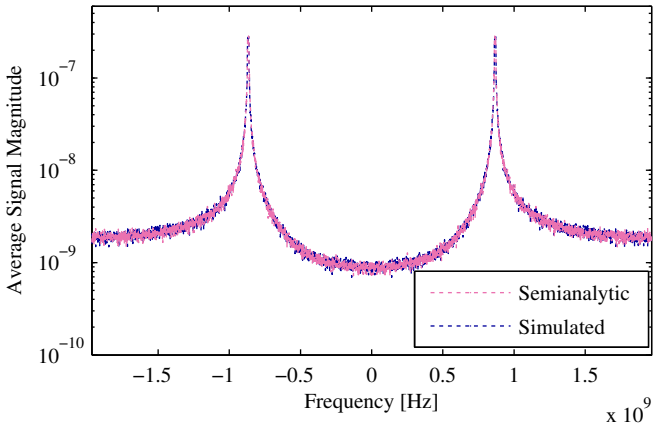

Fig. 8. Error spectrum caused by sampling jitter when jitter is generated by PLL oscillator. 20-ps RMS jitter, case 2 (with $2T_i = T_s$).

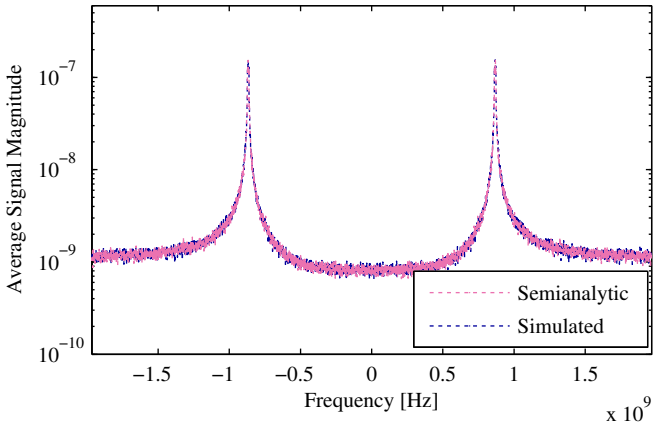

Fig. 9. Error spectrum caused by sampling jitter when jitter is generated by PLL oscillator. 20-ps RMS jitter, case 2 (with $4T_i = T_s$).

when the useful signal is at a certain carrier (or centre) frequency (horizontal axis). Signal response curve gives the basic signal response without sampling jitter, jitter noise response curve is the response that was derived for the sampling jitter in this work, signal-to-jitter-noise density gain curve is the gain in signal-to-jitter-noise ratio compared to traditional voltage sampling scheme, and finally signal-to-noise density ratio curve has also the additive thermal noise in addition to sampling jitter.

In case 1, the receiver designer can exploit the sampling jitter spectrum by adjusting the relationship between carrier frequency f_c and sampling rate F_s so that the information signal is in a region where sampling jitter is attenuated and the useful signal is not. This only happens when very high oversampling is used as Fig. 10 suggests. The same can be done for case 2 when the filtering effect is present, namely in case when the sampling jitter is generated with a single PLL process and when T_i and T_s are relatively close to each other. In other cases, the spectrum of the sampling jitter behaves similarly as in the voltage sampling.

For example, in [9] bandpass CS is used to sample a radio signal with centre frequency f_c at sampling rate $F_s = 2f_c$. Unfortunately, Fig. 10 shows that the jitter noise shaping observed in case 1 boosts the jitter noise at these frequencies. On the other hand, the jitter-noise notches coincide with the signal notches, the only exception being the jitter-noise notch at the zero frequency, where the advantages can be achieved, with a cost of high sampling frequencies of course.

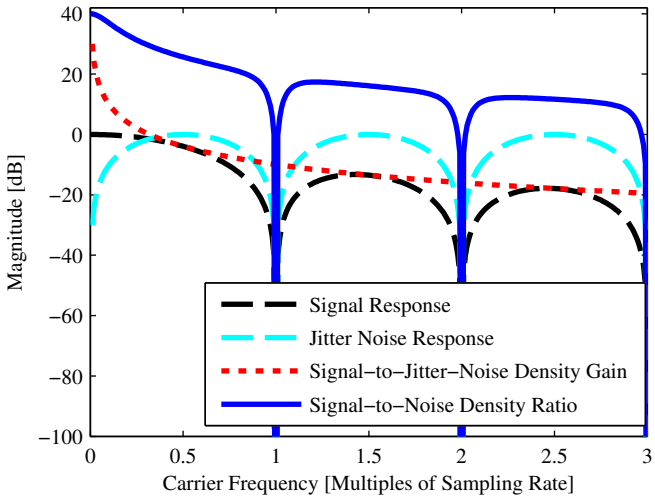

Fig. 10. Signal and noise shaping of case 1 CS. Horizontal axis is the carrier (or centre) frequency of the relatively narrowband signal waveform. For the signal-to-noise density ratio curve, 40-dB SNR due to thermal noise is assumed. Unshaped jitter noise power is 30 dB under the signal power.

VI. Conclusion

As in all systems that sample high-frequency signals, sampling jitter is also an interesting phenomenon in charge sampling radio. We studied the spectral shape of the sampling-jitter induced noise in various charge sampler implementation scenarios. In certain implementations, the charge sampler shapes the spectrum of sampling jitter generated noise in a way that differs from the way the spectrum of the useful signal is shaped. This difference can and should be exploited directly in receiver design, to optimize the receiver chain SNR.

References

[1] L. R. Carley and T. Mukherjee, "High-speed low-power integrating CMOS sample-and-hold amplifier architecture," in *Proc. Custom Integrated Circuits Conference*, Santa Clara, CA, May 1995, pp. 543-546.

[2] J. Yuan, "A charge sampling mixer with embedded filter function for wireless applications," in *Proc. International Conference on Microwave and Millimeter Wave Technology*, Beijing, China, September 2000, pp. 315-318.

[3] K. Muhammad *et al.*, "A discrete-time Bluetooth receiver in a 0.13µm digital CMOS process," in *Proc. International Solid-State Circuits Conference*, San Francisco, CA, February 2004.

[4] R. Bagheri *et al.*, "Software-defined radio receiver: dream to reality," IEEE Communications Magazine, Vol. 44, No. 8, pp. 111-118, August 2006.

[5] S. Karvonen, Thomas Riley, and J. Kostamovaara, "On the effects of timing jitter in charge sampling," in *Proc. Internation Symposium on Circuits and Systems*, Bangkok, Thailand, May 2003, pp. I-737-740.

[6] M. Shinagawa, Y. Akazawa, and T. Wakimoto, "Jitter analysis of high-speed sampling systems," *IEEE Journal of Solid-State Circuits*, Vol. 25, No. 1, pp. 220-224, February 1990.

[7] V. Syrjälä, M. Valkama, and M. Renfors, "Design considerations for direct RF sampling receiver in GNSS environment," in *Proc. Finnish Wireless Comm. Workshop*, Oulu, Finland, August 2007, pp. 9-13.

[8] N. N. Tchamov, V. Syrjälä, J. Rinne, M. Valkama, Y. Zou, and M. Renfors, "System- and circuit-level optimization of PLL designs for DVB-T/H receivers", *Analog Integrated Circuits and Signal Processing Journal*, January 2012, 10.1007/s10470-011-9823-2.

[9] Y-C Ho *et al.*, "Charge-domain signal processing of direct RF sampling mixer with discrete-time filter in Bluetooth and GSM receivers," *EURASIP Journal on Wireless Communications and Networking*, Vol. 2006, pp. 1-14, March 2006.

Publication 10

V. Syrjälä and M. Valkama, "Iterative receiver signal processing for joint mitigation of transmitter and receiver phase noise in OFDM-based cognitive radio link," in *Proc. International ICST Conference on Cognitive Radio Oriented Wireless Networks* (*CROWNCOM'12*), Stockholm, Sweden, June 2012.

Iterative Receiver Signal Processing for Joint Mitigation of Transmitter and Receiver Phase Noise in OFDM-Based Cognitive Radio Link

Ville Syrjälä and Mikko Valkama
Department of Communications Engineering
Tampere University of Technology
P.O. Box 553, 33101 Tampere, Finland
ville.syrjala@tut.fi and mikko.e.valkama@tut.fi

***Abstract*—Ordinary radio devices targeted to operate only at specific regulated parts of the radio spectrum (e.g. GSM bands) typically build on dedicated specific-purpose radio hardware optimized for the given radio system characteristics and pre-allocated center-frequency. In opportunistic spectrum access and cognitive radio, such approach is not always feasible since the device is assumed to be operating over a very wide range of radio frequencies (RF), ultimately from 100MHz to several GHz. This has been recently acknowledged in the literature and implies that severe implementation imperfections can take place in the RF modules of the devices. One such imperfection is oscillator phase noise which can seriously limit the performance of a cognitive radio transceiver. In this article, we study the impact and DSP-based mitigation of oscillator phase noise in OFDM-based cognitive radio link. The paper proposes an iterative receiver-side DSP algorithm for joint transmitter and receiver phase noise mitigation. In the algorithm, the received signal is first detected, and the detection results combined with channel state estimate are used to form an estimate of the time-varying phase noise process. This phase noise estimate is then used to suppress the phase noise effects from the original received signal after which the signal is detected again. After this, the algorithm can be used iteratively. Simulation results show that the proposed algorithm gives significant performance improvement over the existing phase noise mitigation algorithms especially in demanding received signal conditions.**

***Index Terms*—Cognitive radio, OFDM, phase noise, mitigation, digital signal processing, Dirty-RF**

I. Introduction

ORHOGONAL frequency division multiplexing (OFDM) is a widely-applied way to convey information in spectrally efficient manner in digital radio communications. It is also the basis in many emerging cognitive radio developments, offering possibilities to utilize multiple, and possibly scattered, frequency slices for secondary radio communications through properly assigned subcarrier allocations [1]. However, OFDM as such is also very sensitive to many transceiver/RF implementation imperfections, like I/Q imbalance, phase noise and transmitter nonlinearities [2], [3]. Such RF imperfection aspects are emphasized even more in dynamic spectrum access and cognitive radio (CR) where the used radios, when understood at large scale, should operate over extremely wide bandwidths, covering several decades of spectrum (0.01…10 GHz) as a whole, and be able to sense and communicate under extreme dynamic range conditions in the order of 50-100 dB. This has been recently acknowledged by the leading researchers in the field, e.g., in [4].

In this article, we focus particularly on oscillator phase noise and its effects in OFDM-based radio communications and cognitive radio. In the state-of-the-art literature, the phase noise mitigation in OFDM systems has already been widely studied. Advanced phase noise mitigation techniques were already discussed, e.g., in [5], [6], [7], [8], [9], [10] and [11]. To the authors' best knowledge, even though being computationally demanding, the phase noise mitigation technique in [11] is currently the best performing technique available. This paper proposes significant improvements to the compensation structure. The compensation structure proposed in this paper is built to improve the performance mainly when a challenging communications channel is present, whereas the previous algorithm was built originally from the no-channel perspective. Also, the algorithm in [11] did not exploit the cyclic prefix. However, in the proposed algorithm, the structure is changed so that the cyclic prefix can be exploited in the phase noise estimation process. As illustrated in this article, the proposed method clearly outperforms all the existing state-of-the-art methods, including the method in [11].

This paper is structured as follows. The Section II gives shortly the phase noise and OFDM link models. The actual phase noise mitigation algorithm is presented in Section III. In Section IV, the performance of the proposed phase noise mitigation algorithm is compared to that of the state-of-the-art

This work was supported by Tampere University of Technology graduate school, Jenny and Antti Wihuri Foundation, Ulla Tuominen Foundation, HPY Research Foundation, Academy of Finland (under the project "Digitally-Enhanced RF for Cognitive Radio Devices"), the Finnish Funding Agency for Technology and Innovation (Tekes; under the projects "Enabling Methods for Dynamic Spectrum Access and Cognitive Radio" and "Reconfigurable Antenna-based Enhancement of Dynamic Spectrum Access"), the Austrian Competence Center in Mechatronics (ACCM, Austria).

techniques, and finally Section V concludes the work.

II. Phase Noise and OFDM Link Modelling

This section shortly describes the used phase noise model. It also gives OFDM link model used in the simulations and in the derivation of the proposed phase noise mitigation algorithm.

A. Phase Noise Model

The phase noise model used in this paper is very simple free-running oscillator (FRO) model very often used in the literature [12]. Previous studies have shown that the FRO model is very demanding for phase noise mitigation algorithms [6], [9], [10], [11]. It is thus sufficient for the performance evaluation of such algorithms. If the studied algorithms are capable of mitigating the phase noise of the wandering nature, they are able to mitigate, e.g., phase-locked-loop (PLL) type phase-noise with ease. Therefore, in this paper, the results with PLL oscillator are omitted, and only the more challenging case of FRO is considered for the sake of compactness.

Sampled FRO phase noise sequence is easily generated by cumulatively summing white Gaussian noise samples of certain variance [12]. This kind of a process is called Wiener process or Brownian motion and the l th sample of such process can be written with the help of the standard Brownian motion as

$$\phi_l = \sqrt{c}\, B(lT_s), \tag{1}$$

where $B(\cdot)$ denotes the standard Brownian motion, c is the variance of the cumulatively summed white Gaussian noise, namely diffusion rate, and T_s is the sampling interval. For the standard Brownian motion, it is known that the spectrum has the well-known Lorentzian shape [12]. From this fact we are able to derive the one-sided 3-dB bandwidth of the process in (1) as

$$\beta = \frac{c}{4\pi}, \tag{2}$$

and thus the whole process can be written with the help of β as

$$\phi_l = \sqrt{4\pi\beta}\, B(lT_s) = \sqrt{4\pi\beta T_s}\, B(l). \tag{3}$$

Here, since $l \in \mathbb{N}$, process $B(l)$ is a cumulative sum of standard normal distributed noise. The whole process is characterized with a single parameter β (in addition of the sampling interval naturally.)

B. OFDM Link Model under Phase Noise

OFDM symbol is generated by inverse discrete Fourier transforming block of N modulated symbols. The n th sample of the m th OFDM symbol in the resulting OFDM signal with N subcarriers can then be written as

$$x_n(m) = \frac{1}{\sqrt{N}} \sum_{k=0}^{N-1} X_k(m)\, e^{j2\pi kn/N}, \tag{4}$$

where $X_k(m)$ for $k = 0, 1, \ldots, N-1$ are the subcarrier modulated symbols. In practice, also cyclic prefix is used in OFDM signal. This is simply done by sending G last samples of each OFDM symbol before the actual symbol is sent. When the signal with cyclic prefix goes through a channel whose maximum delay spread is shorter than the cyclic prefix, the m th OFDM symbol at the receiver after cyclic prefix removal can be written in vector form as

$$\mathbf{r}_m = (\mathbf{h}_m * \mathbf{x}_m) + \mathbf{z}_m = \mathbf{H}_m \mathbf{x}_m + \mathbf{z}_m, \tag{5}$$

where $\mathbf{r}_m$ is the $N \times 1$ vector of the received samples, and $*$ is circular convolution operator. $\mathbf{h}_m$ is $D \times 1$ channel impulse response vector, $\mathbf{x}_m$ is $N \times 1$ vector having OFDM symbol samples given in (4) as its elements, $\mathbf{z}_m$ is vector of additive white Gaussian noise and $\mathbf{H}_m$ is $N \times N$ circulant convolution matrix [13]. This is the model for the OFDM link without any phase noise.

After also phase noise of the upconverting oscillator in the transmitter and the downconverting oscillator in the receiver are taken into account, the received signal can be written as

$$\mathbf{r}_m \approx \mathrm{diag}\left(e^{j\boldsymbol{\phi}_{R,m}}\right) \mathbf{H}_m\, \mathrm{diag}\left(e^{j\boldsymbol{\phi}_{T,m}}\right) \mathbf{x}_m + \mathbf{z}_m. \tag{6}$$

Here $\mathrm{diag}(\cdot)$ transforms the input vector to a diagonal matrix, and $\boldsymbol{\phi}_{T,m}$ and $\boldsymbol{\phi}_{R,m}$ are $N \times 1$ vectors of sampled transmitter and receiver phase noises, respectively. The above equation is only an approximation, because the cyclic prefix and the corresponding end part of the OFDM symbol are multiplied with different phase-noise complex-exponentials. Therefore, the cyclic prefix does not precisely work as intended. Then since we also know that $\mathbf{H}_m$ is (by definition) circulant matrix, we are able to rewrite (6) as

$$\mathbf{r}_m \approx \mathrm{diag}\left(e^{j\boldsymbol{\phi}_{R,m}}\right) \mathrm{diag}\left(e^{j\boldsymbol{\phi}_{T,m}}\right) \mathbf{H}_m \mathbf{x}_m + \mathbf{z}_m. \tag{7}$$

In this form, we effectively mapped the transmitter phase noise as receiver phase noise, and by writing $\boldsymbol{\phi}_m = \boldsymbol{\phi}_{R,m} + \boldsymbol{\phi}_{T,m}$, we can further simplify (7) into form

$$\mathbf{r}_m \approx \mathrm{diag}\left(e^{j\boldsymbol{\phi}_m}\right) \mathbf{H}_m \mathbf{x}_m + \mathbf{z}_m. \tag{8}$$

From the above model, if taken to frequency domain through FFT (as done e.g. in [6]), it is clear that phase noise causes intercarrier interference (ICI). This is further emphasized if some of the subcarriers, like the neighbouring channel subcarriers, are more powerful than those that our receiver is interested in. This is exactly the scenario in cognitive radio where the available spectral chunks are surrounded in frequency domain by strong primary user signals. This very simple form is used as a basis to derive the phase noise mitigation algorithm. The performance of the derived algorithm is in the end used as justification of the used approximations.

III. Proposed Phase Noise Mitigation Algorithm

From the received signal, first the cyclic prefix is removed, and then the signal is OFDM demodulated by discrete Fourier

transform. After this, the channel is estimated and equalized, and common phase error (CPE) [5], [6] is estimated and removed. Finally, the symbols are detected. At this point, the receiver has done everything that conventional OFDM receiver with CPE mitigation block does to obtain symbol decisions. These operations are also depicted in the overall structure of the algorithm in Fig. 1.

After conventional symbol detection with CPE mitigation, the proposed structure reconstructs the sent time-domain waveform by doing inverse discrete Fourier transform and cyclic prefix addition. This is followed by channel modelling, which is done based on the channel estimate. The signal at this point is an approximate of the received waveform without phase noise, $\hat{\mathbf{r}}_{m,noPN}^{(CP)}$. Now, when we multiply the received waveform $\mathbf{r}_m^{(CP)}$ by the complex conjugate of this phase-noise free estimate of the received waveform, the result is a very crude estimate of the phase noise complex exponential, but with some non-constant amplitude. The resulting signal can be written as

$$\begin{aligned}\boldsymbol{\varphi}_m &\approx \mathrm{diag}\left(\hat{\mathbf{H}}_m^*\hat{\mathbf{x}}_m^*\right)\left[\mathrm{diag}\left(e^{j\boldsymbol{\phi}_m}\right)\mathbf{H}_m\mathbf{x}_m+\mathbf{z}_m\right]\\ &\approx \mathrm{diag}\left(\hat{\mathbf{H}}_m^*\hat{\mathbf{x}}_m^*\right)\mathrm{diag}\left(e^{j\boldsymbol{\phi}_m}\right)\mathbf{H}_m\mathbf{x}_m+\mathrm{diag}\left(\hat{\mathbf{H}}_m^*\hat{\mathbf{x}}_m^*\right)\mathbf{z}_m \qquad (9)\\ &\approx \mathrm{diag}\left(\left|\hat{\mathbf{H}}_{m,CP\mathrm{E}}\hat{\mathbf{x}}_m\right|^2\right)e^{j(\boldsymbol{\phi}_m)}+\mathrm{diag}\left(\hat{\mathbf{H}}_m^*\hat{\mathbf{x}}_m^*\right)\mathbf{z}_m\,.\end{aligned}$$

Here, $\hat{\mathbf{x}}_m$ and $\hat{\mathbf{H}}_m$ are the estimates of the sent symbols and the channel convolution matrix, respectively. Superscript $*$ denotes the complex conjugate. As seen from (9), the estimate is very crude as it still has the additive noise component present. Furthermore, each of the sample estimates are multiplied by the corresponding approximate power of the received signal samples without noise.

To greatly improve the estimate of the phase noise complex exponential in (9), the estimate is low-pass filtered. This is a very natural way to improve the estimate since we know that phase noise and its complex exponential are both steep low-pass processes. Therefore also the used filter must be relatively selective low-pass filter. The filter should be designed so that is passes through only few of the centre-most spectral components of the phase noise complex exponential and so that it attenuates the other components heavily because of the noise in them [6], [11]. Prior to the low-pass filtering it is good to scale the signal so that the most reliable sample estimates get more weighted in the filtering process. Fortunately, the scaling has already been done. The sample estimates of the phase noise complex exponential in (9) have indeed already been multiplied by the corresponding approximate powers of the received signal samples without noise, since it is built-in in the multiplication of a signal with its complex conjugate (in [11] the scaling was separately applied, since division operator was used instead of complex conjugate multiplication). This scaling gives more weight to samples that are estimated to have more power at the receiver input, so they are most likely least corrupted by the noise. After the very selective low-pass filter (the filter must be very selective since in (9) the additive noise contributed term dominates the phase-noise complex-exponential everywhere else except at very low frequencies), the estimate of the complex exponential is then given by

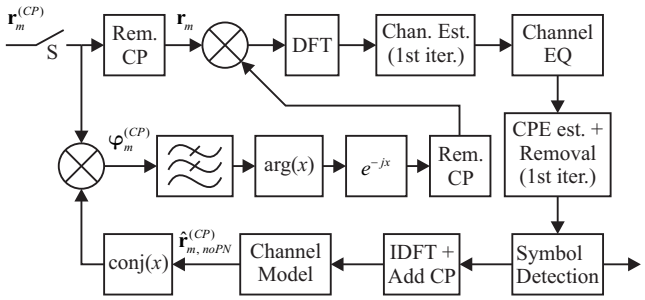

Fig. 1. The proposed phase noise mitigation algorithm. The switch S remains open until the iterations have been completed, and closes to receive next incoming OFDM symbol. Symbol x always denotes the block input. Blocks $\arg(x)$ and $\mathrm{conj}(x)$ take an argument and a complex conjugate of the input samples, respectively.

$$\mathrm{LPF}\left\{\boldsymbol{\varphi}_m\right\} \approx e^{j\boldsymbol{\phi}_m}\,. \qquad (10)$$

Even though this is an estimate of the complex exponential, the absolute values of the samples are not unity as they should be. This is why we also take the argument of (10), and then the inverse complex exponential of the result as depicted in Fig. 1. Finally, the received signal without cyclic prefix is multiplied with the inverse complex exponential (from which the cyclic prefix part is also removed) to get rid of the phase noise. The performance of the technique can then be improved by using it iteratively. The complete iterative phase-noise mitigation algorithm is depicted in Fig. 1.

Notice that for notational simplicity, the cyclic prefix is not considered present in the equations. However, as denoted by superscript (CP) in the signals depicted in Fig. 1, the cyclic prefix is indeed present in the corresponding signals in the phase-noise estimation part of the algorithm.

It should also be noted that if the channel estimation is done OFDM-symbol-by-OFDM-symbol, CPE estimation and removal is done during the channel estimation and equalization automatically. In Fig. 1 the blocks are however separate if, e.g. the channel is considered quasistatic and some advanced channel estimation method is used, as e.g. the one proposed in [10]. If desired, the channel estimation can be done only in the first iteration for computational simplicity. However, for improved performance, the structure allows to do the channel estimation again when the amount of phase noise has been lowered by the previous iterations. This again helps channel estimation reliability. The CPE estimation and removal are only done in the first iteration, because the proposed algorithm does not discriminate between CPE and ICI parts of the phase noise. Therefore, in every iteration of the algorithm, CPE and ICI are both mitigated, and hence separate CPE estimation and mitigation parts do not have any practical impact on the quality of the phase noise estimates in the latter iterations.

For the design of the low-pass filter, the considerations given in [11] also apply for the proposed algorithm. This

means that the used relatively selective, and thus long, digital low-pass filter causes a potential transient problem in the estimate. However, keeping the cyclic prefix present in the algorithm tackles the problem partially.

IV. Simulations and Performance Analysis

This section gives the used parameters and describes the simulator. It also gives the simulation results and compares the performance of the proposed phase noise mitigation algorithm to the performances of the state-of-the-art phase noise mitigation algorithms reported in [6], [7], [9] and [11]. The simulations are first run for all the reference techniques with perfect channel information. The best performing techniques are then compared in more practical channel estimation cases with imperfect channel information.

A. Parameters and Simulator

In the simulator we simulate OFDM communications system with 1024 subcarriers. 300 subcarriers on the both sides of the centre subcarrier are active, and the remaining subcarriers are null. The 600 active subcarriers are 16QAM subcarrier modulated. For perfect channel information case, 18 of the active subcarriers are used as pilot subcarriers, i.e., considered known at the receiver. In cases with channel estimation, every ninth subcarrier is considered a pilot, resulting in total of 66 pilot subcarriers. Furthermore, cyclic prefix of 63 samples is present in the system. Assuming 15 kHz subcarrier spacing, this maps to around 10 MHz total waveform bandwidth and 4.2 microsecond cyclic prefix.

The simulator first generates 16QAM symbols and OFDM modulates them. Then cyclic prefix is added and transmitter phase noise is applied. After this, communications channel is modelled. We use extended ITU-R Vehicular A (VEHA) multipath channel [14]. The channel is considered constant during one OFDM symbol, and it is generated independently for all the OFDM symbols, except for the case when advanced channel estimation technique of [10] is considered. For that case, channel is assumed quasistatic for the duration of 12 OFDM symbols. After the channel, at the receiver input, the additive noise is added to get the desired signal-to-noise ratio (SNR). Receiver phase noise is then modelled. At this point, the proposed algorithm is applied, or for the reference techniques, needed operations and algorithms are applied. The parameters of the state-of-the-art algorithms are chosen as in [9] and [11] (optimized empirically for the best estimation quality). For the proposed algorithm, the digital low-pass filter is designed with well-known Remez-algorithm. The order of the filter is 350 with passband width 0 Hz and normalized stopband edges at 0.04 and 1. For channel estimation cases, the channel estimation is done only in the first iteration for the proposed technique, and after the CPE mitigation for the reference techniques. Finally, the simulator computes the symbol-error rates (SER) from the detected signals.

Reported 3-dB bandwidth of the phase noise is the 3-dB bandwidth of the total phase noise including the transmitter and receiver phase noises. Both the phase noise processes are independent but with the same diffusion rate.

In the simulations the reference techniques for performance comparisons are denoted by Petrovic, Bittner, LI-TE and Previous for the techniques in [6], [8], [9] and [11], respectively. In Fig. 2, Fig. 3, Fig. 6 and Fig. 7, the techniques are iterated 3 times. In Fig. 4 and Fig. 5, the performance of the proposed technique is compared to the performance of the best performing reference technique (Previous from [11]) from the number of iterations perspective.

A. Simulation Results and Analysis

The simulation results as a function of received SNR and phase noise 3-dB bandwidth are given in Fig. 2 and Fig. 3, respectively. From the results, we see that the proposed technique gives noticeable performance improvement over the state-of-the-art techniques overall. From Fig. 2 for fixed β of 350 Hz, we see that the performance given by the proposed algorithm is very near to the no phase-noise case up until around 25-dB received SNR. After that it starts to floor, but at much lower level than the reference techniques. From Fig. 3 we can see that for fixed received SNR of 24 dB, the proposed

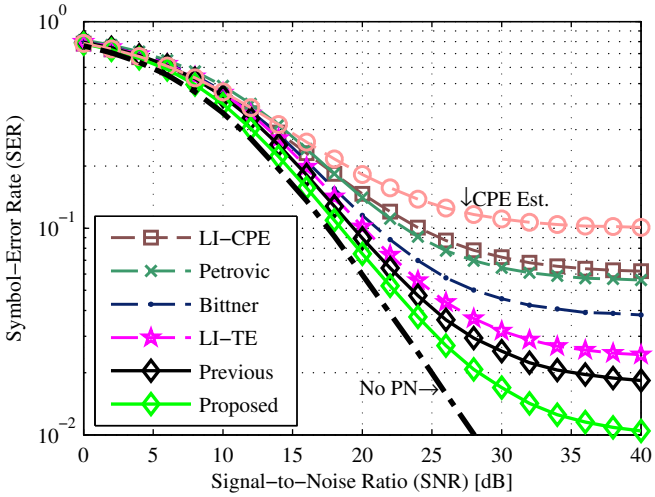

Fig. 2. SER as a function of received SNR. Phase noise 3-dB bandwidth (β) is fixed to 350 Hz.

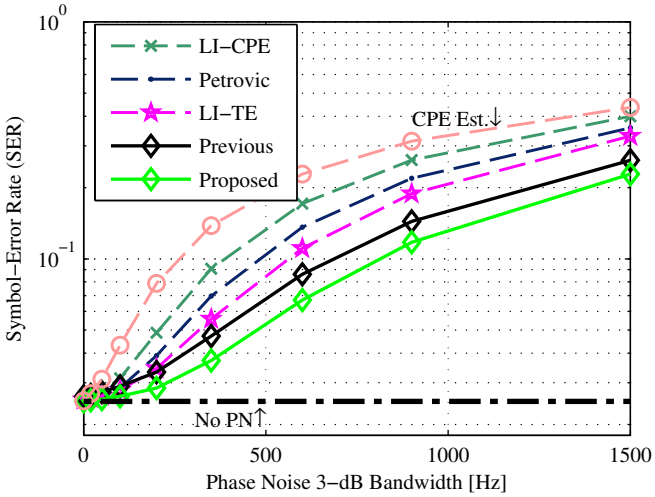

Fig. 3. SER as a function of phase noise 3-dB bandwidth (β). Received SNR is fixed to 24 dB.

algorithm performs very well over the whole studied phase noise 3-dB bandwidth region, and manages to clearly outperform the reference techniques. Altogether, the results also verify the used approximations in earlier signal modelling and in deriving the mitigation algorithm, since the transmission chain in the simulator does not use any approximations.

The simulation results from the amount of iteration perspective are shown in Fig. 4 and Fig. 5. As Fig. 4 shows, already three iterations of the proposed technique clearly outperforms the Previous technique in [11] for fixed β of 350 Hz over the whole studied SNR region. As Fig. 5 depicts, when phase noise gets more dominating, the previous technique gets a little better, but only hardly outperforms the three iterations of the proposed technique with five of its iterations. Overall, the proposed technique can still improve the performance greatly when number of iterations increases.

The simulations were also run for case of additive white Gaussian noise channel. As expected, improvements were seen in the performance compared to the technique of [11]. At SER of 10^{-2}, around 1 dB improvement was got at 350 Hz phase noise level compared to technique of [11]. Also the SER performance floor was lowered from around $6 \cdot 10^{-3}$ to around $5 \cdot 10^{-3}$ with the same phase noise level. The improvements were gained because the proposed algorithm structure enabled the exploitation of the cyclic prefix in the phase noise estimation process, so the filter transient problem of [11] was partly solved. The performance simulation curves were omitted from this paper for compactness of the presentation. Overall, the performance improvements in additive white Gaussian noise conditions were significant, but clearly smaller than in extended ITU-R Vehicular A multipath channel case.

The simulation results for cases with channel estimation are depicted in Fig. 6 and Fig. 7. In the figures, conventional channel estimation refers to channel estimation done by estimating channel at pilot subcarriers and linearly interpolating the results to get the other channel estimates. The advanced channel estimation refers to the technique proposed in [10]. The results with these channel estimation approaches are compared to the case with perfect channel information at

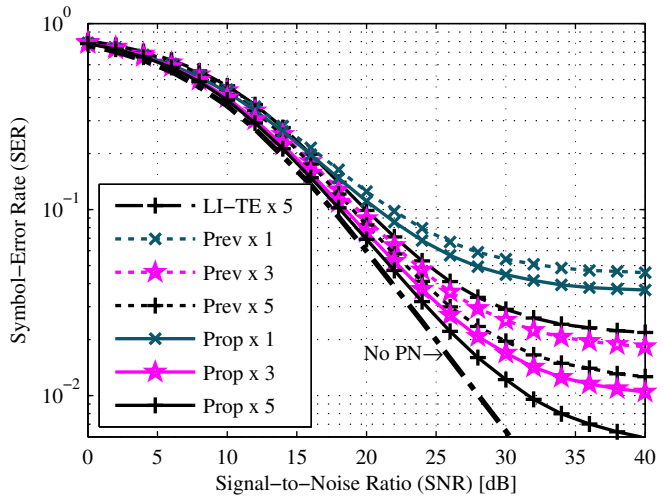

Fig. 4. SER as a functions of received SNR. Phase noise 3-dB bandwidth (β) is fixed to 350 Hz.

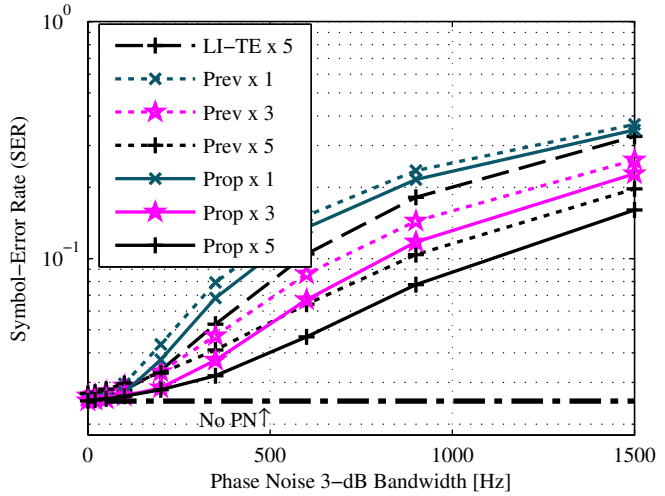

Fig. 5. SER as a function of phase noise 3-dB bandwidth (β). Received SNR is fixed to 24 dB.

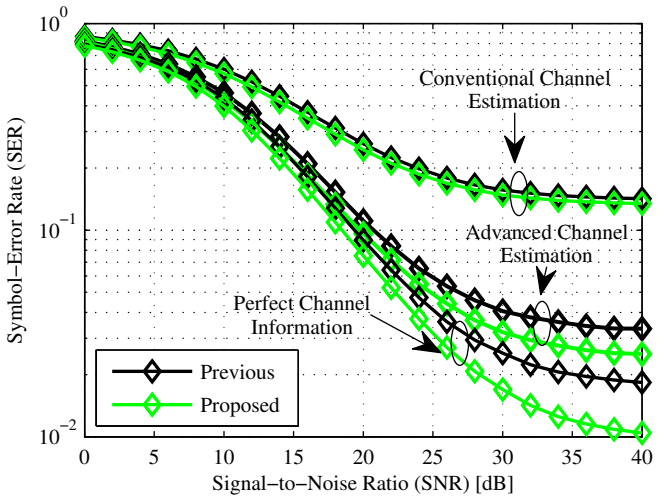

Fig. 6. SER as a functions of received SNR. Phase noise 3-dB bandwidth (β) is fixed to 350 Hz.

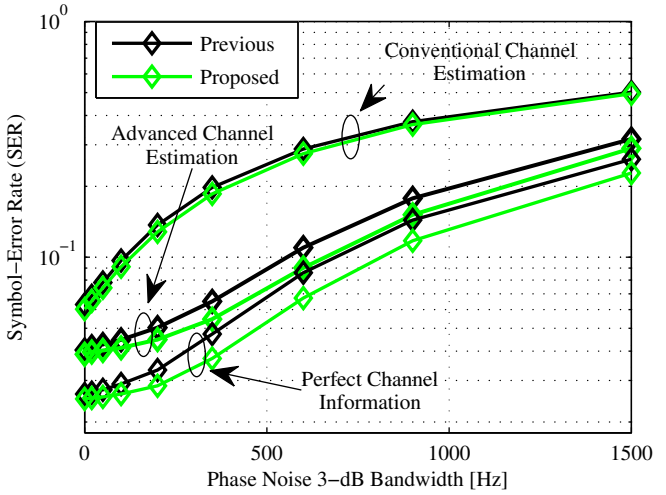

Fig. 7. SER as a function of phase noise 3-dB bandwidth (β). Received SNR is fixed to 24 dB.

the receiver. The results in Fig. 6 and Fig. 7 clearly demonstrate that the proposed technique outperforms the best performing reference technique of [11] also when different channel estimation approaches are used. Already very good performance is achieved with advanced channel estimation compared to the case with perfect channel information.

Overall superior performance of the proposed algorithm when compared to the performance of the algorithm of [11], in case of frequency-selective multipath-channel, is explained by the fact that the phase noise estimation is done before the channel equalization. This effectively means that the noise does not get amplified at some (channel dependent) frequencies in the signal from which the estimation is done (received signal with phase noise, $\mathbf{r}_m^{(CP)}$), as it does in algorithm of [11]. Of course the channel modelling on the reference signal (reconstructed received signal, $\hat{\mathbf{r}}_{m,noPN}^{(CP)}$) causes possible erroneous subcarriers to be amplified when the channel is strong. However, when channel is strong, also the subcarrier decisions are more likely true. Therefore, actually this amplifies the more probable subcarriers and gives less weight to more likely erroneous subcarriers. Therefore, the reference signal is also better. The improvement in additive white Gaussian noise case can be explained with the use of the cyclic prefix in the phase-noise estimation process.

V. CONCLUSION

Transmitter and receiver phase noises heavily affect the performance of an OFDM-based cognitive-radio link. This paper proposed a new received-side algorithm for joint transmitter and receiver phase-noise mitigation. The performance of the algorithm was compared to the performances of the state-of-the art algorithms. The proposed technique was seen to be able to give a clear performance improvement over the previous algorithms in the literature, when extended ITU-R Vehicular A multipath channel was assumed in the communications link. More generally, the results demonstrate that the signal distortion due to imperfect oscillators in multicarrier receivers can be efficiently suppressed. Such methods are seen essential in full deployment of dynamic spectrum access and cognitive radio, especially when the available and possible heavily scattered narrow spectral slices are used for secondary radio communications in the presence of strong neighbouring channels. Thus the DSP-enhanced RF hardware methods, like the one described in this article, are seen essential building blocks towards full-scale opportunistic spectrum access with practical RF circuits.

REFERENCES

[1] B. Wang and K. J. R. Liu, "Advances in cognitive radio networks: A survey," *IEEE Journal on Selected Topics in Signal Processing*, Vol. 5, No. 1, pp. 5-23, February 2011.

[2] M. Valkama, A. Springer, and G. Hueber, "Digital signal processing for reducing the effects of RF imperfections in radio devices – An overview," in *Proc. International Symposium on Circuits and Systems (ISCAS'10)*, Paris, France, May-June 2010, pp. 813-816.

[3] G. Fettweis, "Dirty-RF: A new paradigm," in *Proc. 16th International Symposium on Personal, Indoor and Mobile Radio Communications 2005 (PIMRC'05)*, Berlin, Germany, September 2005, pp. 2347-2355.

[4] B. Razavi, "Cognitive radio design challenges and techniques," *IEEE Journal on Solid-State Circuits*, Vol. 45, pp. 1542-1553, August 2010.

[5] S. Wu, and Y. Bar-Ness, "OFDM systems in the presence of phase noise: consequences and solutions," *IEEE Transactions on Communications*, Vol. 52, No. 11, pp. 1988-1997, November 2004.

[6] D. Petrovic , W. Rave, and G. Fettweis, "Effects of phase noise on OFDM systems with and without PLL: characterization and compensation," *IEEE Transactions on Communications*, Vol. 55, No. 8, pp. 1607-1616, August 2007.

[7] S. Bittner, W. Rave, and G. Fettweis, "Joint iterative transmitter and receiver phase noise correction using soft information," in *Proc. IEEE International Conference on Communications 2007 (ICC'07)*, Glasgow, Scotland, June 2007, pp. 2847-2852.

[8] S. Bittner, E. Zimmermann, and G. Fettweis, "Exploiting phase noise properties in the design of MIMO-OFDM receivers," in *Proc. IEEE Wireless Communications and Networking Conference 2008 (WCNC'08)*, Las Vegas, NV, March 2008, pp. 940-945.

[9] V. Syrjälä, M. Valkama, N. N. Tchamov, and J. Rinne, "Phase noise modelling and mitigation techniques in OFDM communications systems," in *Proc. Wireless Telecommunications Symposium 2009 (WTS'09)*, Prague, Czech Republic, April 2009.

[10] V. Syrjälä and M. Valkama, "Analysis and mitigation of phase noise and sampling jitter in OFDM radio receivers," *International Journal of Microwave and Wireless Technologies*, Vol. 2, No. 2, pp. 193-202, April 2010.

[11] V. Syrjälä and M. Valkama, "Receiver DSP for OFDM systems impaired by transmitter and receiver phase noise," in *Proc. IEEE International Conference on Communications 2011 (ICC'11)*, Kyoto, Japan, June 2011.

[12] T. Schenk, *RF Impairments in Multiple Antenna OFDM: Influence and Mitigation*, PhD dissertation, Technische Universiteit Eindhoven, 2006. ISBN 90-386-1913-8. 291 p.

[13] A. Goldsmith, *Wireless Communication*, Cambridge University Press, 2005, 672 p. ISBN 978-0521837163.

[14] T. B. Sorensen, P. E. Mogersen, and F. Frederiksen, "Extension of the ITU channel models for wideband (OFDM) systems," in Proc. IEEE Vehicular Technology Conference 2005 (VTC'05-Fall), Dallas, TX, September 2005, pp. 392-396.

Tampereen teknillinen yliopisto
PL 527
33101 Tampere

Tampere University of Technology
P.O.B. 527
FI-33101 Tampere, Finland

ISBN 978-952-15-2832-3
ISSN 1459-2045